Simultaneous Minimization of Arsenic Mobilization and N_2O Emission in Rice Paddy Soils

Dissertation

der Mathematisch-Naturwissenschaftlichen Fakultät
der Eberhard Karls Universität Tübingen
zur Erlangung des Grades eines
Doktors der Naturwissenschaften
(Dr. rer. nat.)

vorgelegt von
M.Sc. Hanna Madelaine Grimm, geb. Joß
aus Filderstadt

Tübingen
2024

Gedruckt mit Genehmigung der Mathematisch-Naturwissenschaftlichen Fakultät der Eberhard Karls Universität Tübingen.

Tag der mündlichen Qualifikation:	17.02.2025
Dekan:	Prof. Dr. Thilo Stehle
1. Berichterstatter:	Prof. Dr. Andreas Kappler
2. Berichterstatter:	Prof. Dr. Thomas Scholten

Acknowledgements

I strongly believe that science (and so many other things in life) is about sharing knowledge and ideas, about communication and collaboration. Therefore, I would like to thank all of the people who contributed to where I am today.

Starting with my family! Even though you stopped reading my scientific content after I finished my Bachelor´s, I still know that you support me in any way I can possibly imagine. Thank you, mum, for your unconditional love, thanks dad for your endless support, thanks Kathrin, Fredrik, Yannick and Adriana for being such a great family! And thanks to my beloved niece, Mariella, and nephew, Vincent. A big thank you also goes to my extended family Holger, Nadine, Ira and Lian and the best mum-in-law, Vlasta. Thanks for all your support and interest!

All of this of course would not have been possible without you supporting my scientific curiosity, Andreas! I came to Tübingen for my Master´s because I wanted to understand more about these tiny little organisms that affect our environment in so many ways. I was able to pursue this right from the beginning of my Master´s, after you approached me while walking in the Schönbuch during one of your courses. All of this started as a HiWi in your working group, to finishing and publishing my Master´s thesis, until starting my PhD in your group. It was a great and unforgettable experience being an integral part of your working group. Thanks for supporting me throughout those years, for giving me the freedom to pursue my interests and for trusting me. Your enthusiasm for science really is inspiring!

A big thank you also goes to you Christiane, for supporting me in every decision I made and guiding me through this new topic of numerical modelling. It is great to have someone so understanding as a supervisor, especially when it comes to balancing science and private life!

I would also like to thank Marie Mühe for very interesting discussions on all different kinds of topics, e.g. rice plants, arsenic, microbial ecology, etc. Your pool of knowledge is really incredible :) Thank you for always giving me tips when needed, constructive

comments on my manuscripts and already asking me the “big picture” and transfer questions early on in my PhD.

Another thank you goes to Thomas for being my second examiner and for his insights into soil science. Starting working with you in my Master´s on permafrost soil samples from the Tibetan Plateau was a great experience and fostered my interest in soil science.

Starting my PhD at the same time as Prachi started led to probably the shortest field trip abroad - a joint field trip to Italy with the goal to collect as many soil samples as possible in less than 48 hours in total :) Corona restrictions hit us hard, but we managed! Thanks for your help! But also, for the support throughout all the years, for always having an open door and discussions with me whenever I doubted something :) I wish you all the best on your future path!

A warm thank you also goes to Shun Li and Yong-Guan Zhu for their collaboration and for providing Chinese paddy soil samples. Unfortunately, I was unable to visit China and its paddy fields during my PhD due to Corona restrictions. Without the provided paddy soil samples culture HP would not exist. So, thanks a lot!

I would also like to thank Caroline for writing this PhD proposal, for telling me about this project and supporting me in my scientific career. Happy to have you as a neighbor in Lustnau :)

The Geomicrobiology working group was another reason supporting me in my decision to start a PhD, due to many, many great people that have worked there in all those years. It really feels like a small little family and luckily friendships lasted even beyond work. I don´t even start to count everyone on the list, but in my early days I enjoyed the company of Lea, Ulf, Monique, Markus, Anh, Sören, Verena, Christopher, Timm, Franziska, Anjela, Ellen… and during the last months I would have not wanted to miss out on Martina, Nora, Eva, Marie, Caro, Cris, Sigrid… Thanks for all the nice yard parties at our old institute, coffee breaks, breakfasts, after work activities, but also discussions on all the little aspects of my PhD :)

I am greatly thankful for all the students that have supported me over the years. A very special thanks goes to you, Paula, for staying with me for uncountable years in the lab, for being so independent and for starting this whole modelling within your BSc thesis. It was a great experience to guide you through the first experiments with culture HP, Jenny and having you also as a HiWi later on. Both your help was highly appreciated especially in times when baby diapers were my main focus :) Another big thank you goes to Sarah Keldenich, who was my first student 2 months after I have started myself. It was a lot of testing ideas and being a bit messy in the lab, but I had a fun time! And the best of it is to see all of you still in the Kappler Lab, now way more advanced than ever - I wish you a great future!

Following the tradition to save the best for last:
One thing I will miss the most is working with my best friend, my husband and father of my beloved kids. I enjoyed every little coffee break we had and will miss them deeply :) Thanks for the unconditional and endless support of yours, for always making me laugh, for really bringing out the best in me and always reminding me about the important things in live – you, us and our family!

Summary

Rice represents a major food source for billions of people worldwide. Traditional water-logged rice cultivation induces reducing conditions under which natural, toxic arsenic can accumulate in rice grains causing health issues for humankind. Under nitrogen (N) fertilization, microbial denitrification causes the formation of nitrite as intermediate and dinitrogen gas or nitrous oxide (N_2O), a potent greenhouse gas, as final reaction products. Iron(II) can react abiotically with nitrite during the process of chemodenitrification, leading to N_2O production. During both biotic iron(II) oxidation and chemodenitrification, iron(III) minerals form, which serve as highly reactive sorption templates for nutrients or contaminants, such as arsenic. The application of less or no N-fertilizer in waterlogged rice cultivation will shift redox conditions towards iron(III) reduction ultimately remobilizing arsenic.

In the framework of this dissertation, we identified conditions under which we have lowest arsenic mobilization and greenhouse gas emissions (i.e., N_2O and methane) to minimize health- and climate-related risks. In a microcosm study with paddy soil from Vercelli, Italy, that was carried out over 129 days, we applied nitrate fertilizer at different concentrations and timepoints. We found that arsenic was rapidly scavenged by iron(III) minerals after fertilizer application, yet, also rapidly mobilized after nitrate depletion. Only the highest rate of nitrogen application resulted in sustained, long-term retention of arsenic on iron minerals. At the same time, N_2O emissions were similarly high irrespective of fertilizer concentrations added. This illustrates that timing and frequency of fertilizer application is crucial for controlling arsenic mobility and N_2O emissions not only under lab settings, but also likely under more natural conditions. Under N fertilization, iron(III) mineral formation was caused by iron(II)-oxidizing microorganisms, such as *Gallionellaceae* that were more abundant under nitrate fertilization compared to non-fertilization.

By cultivation techniques, we were able to enrich a first lithoautotrophic nitrate-reducing, iron(II)-oxidizing culture from a paddy soil – called “culture HP” – which is dominated by *Gallionellaceae*. We quantified the extent of nitrate reduction, iron(II) oxidation and identified N_2O as the main product during denitrification. By combining

experimental data with environmental systems analysis, we were able to quantify that 99.5% of the produced N_2O was biologically derived and that enzymatic iron(II) oxidation accounted for 99.8% of the total iron(II) oxidation. Further, we were able to show that labile, bioavailable organic carbon sources (i.e., acetate) tremendously impacted the microbial community composition shifting the enrichment culture towards more mixotrophic or heterotrophic denitrifiers (*Dechloromonas* sp., *Acidovorax* sp., *Zoogloea* sp., and *Parvibaculum* sp.).

This study systematically investigated the dynamics of arsenic mobility and N_2O emissions under diverse nitrate fertilization regimes in rice paddy soils. By enriching microbial key players responsible for nitrate-dependent iron(II) oxidation in paddy soils, we provided insights into important microbial processes. Our findings underscore the significance of biotically derived N_2O emissions, emphasizing that these emissions cannot be overlooked in lab microcosm experiments, in microbial cultures and likely also in rice paddy soils. Through an interdisciplinary framework that integrated field sampling, laboratory experiments, molecular biology techniques, and numerical reaction modeling, we elucidated the intricate interplay of biotic and abiotic reactions, microbiome composition, and their collective impact on arsenic mobility and greenhouse gas dynamics in nitrate-fertilized paddy soils.

Zusammenfassung

Reis ist eine essentielle Nahrungsquelle für Milliarden von Menschen weltweit. Der traditionelle Anbau von Reis unter wassergesättigten Bedingungen schafft reduzierende Verhältnisse, die eine Anreicherung von toxischem, natürlich vorkommenden Arsen in den Reiskörnern begünstigen. Dies hat negative Auswirkungen auf die menschliche Gesundheit zur Folge. Die Stickstoffdüngung in Reisanbausystemen fördert mikrobiologische Denitrifikationsprozesse, bei denen Nitrit als Zwischenprodukt und molekularer Stickstoff (N_2) oder Lachgas (N_2O), ein klimawirksames Treibhausgas, als Endprodukte entstehen. Reduziertes Eisen (Eisen(II)) kann mit Nitrit während der Chemodenitrifikation abiotisch reagieren, wobei N_2O gebildet wird. Gleichzeitig können sich bei der biotischen Eisen(II) Oxidation und der Chemodenitrifikation Eisen(III) Minerale bilden, die als hochreaktive Sorptionsoberflächen für Nähr- und Schadstoffe, einschließlich Arsen, agieren. Ein Verzicht auf oder die Reduktion von Stickstoffdünger unter wassergesättigten Bedingungen kann die Redoxverhältnisse hin zur Eisen(III) Reduktion verschieben. Die Reduktion von Eisen(III) Mineralen führt zur Remobilisierung von zuvor gebundenem Arsen. In der vorliegenden Dissertation wurden systematisch die Bedingungen untersucht, unter denen die Mobilisierung von Arsen und die Emissionen von Treibhausgasen (N_2O und Methan) minimiert werden können, um sowohl Gesundheits- als auch Klimarisiken im Reisanbau zu reduzieren.

In einer 129-tägigen Mikrokosmenstudie mit Reisfeldböden aus Vercelli, Italien, wurde Nitratdünger in unterschiedlichen Konzentrationen und Zeitabständen hinzugegeben. Unsere Ergebnisse zeigen, dass Nitrat als Düngemittel zunächst eine rasche Immobilisierung von Arsen durch die Bildung von Eisen(III) Mineralen bewirkte. Nachdem das zugegebene Nitrat vollständig verbraucht war, wurde das Arsen jedoch schnell remobilisiert. Lediglich die höchste Stickstoffkonzentration führte zu einer langfristigen Arsenbindung an Eisenminerale. Gleichzeitig waren die N_2O Emissionen unabhängig von der Nitratkonzentration ähnlich hoch, was verdeutlicht, dass sowohl der Zeitpunkt als auch die Häufigkeit der Düngerausbringung entscheidende Faktoren für die Steuerung der Arsenmobilität und der Treibhausgasemissionen sind. Diese Ergebnisse sind wahrscheinlich nicht nur unter Laborbedingungen gültig, sondern

auch unter natürlichen Bedingungen im Feld. Die Stickstoffdüngung führte zur Bildung von Eisen(III) Mineralen durch Eisen(II)-oxidierende Mikroorganismen, wie beispielsweise *Gallionellaceae*, die unter Stickstoffdüngung in höherer Abundanz im Vergleich zu nicht gedüngtem Boden vorhanden waren.

Durch Kultivierungstechniken konnten wir in einem weiteren Projekt eine erste lithoautotrophe nitratreduzierende, Eisen(II)-oxidierende Kultur aus einem Reisboden - genannt „culture HP“ - anreichern, die von *Gallionellaceae* dominiert wird. Wir quantifizierten die Nitratreduktion und Eisen(II) Oxidation und identifizierten N_2O als Hauptprodukt der Denitrifikation. Durch die Kombination von experimentellen Daten mit prozessbasierter numerischer Modellierung konnten wir zeigen, dass 99,5% des produzierten N_2O biotischen Ursprungs waren und, dass die enzymatische Eisen(II) Oxidation zu 99,8% dominierte. Darüber hinaus zeigten unsere Experimente, dass die Zugabe von bioverfügbarem organischem Kohlenstoff (z.B. Acetat) die Zusammensetzung der mikrobiellen Gemeinschaft stark beeinflusste, indem mixotrophe und heterotrophe denitrifizierende Mikroorganismen wie *Dechloromonas* sp., *Acidovorax* sp., *Zoogloea* sp. und *Parvibaculum* sp. in der Kultur stärker angereichert wurden.

Zusammenfassend wurden in dieser Dissertation die komplexe Dynamik der Mobilität von Arsen und der N_2O Emissionen unter verschiedenen Bedingungen der Nitratdüngung in Reisfeldböden systematisch untersucht. Durch die Anreicherung und Charakterisierung mikrobieller Schlüsselakteure, die für die nitratabhängige Eisen(II) Oxidation verantwortlich sind, wurden wesentliche Einblicke in mikrobielle Prozesse und deren geochemische Auswirkungen gewonnen. Die Ergebnisse unterstreichen die Bedeutung biotisch abgeleiteter N_2O Emissionen und verdeutlichen, dass diese in Mikrokosmenexperimenten, in mikrobiellen Kulturen und wahrscheinlich auch in Feldstudien nicht vernachlässigt werden dürfen. Der interdisziplinäre Ansatz, der Feldproben, Laborexperimente, molekularbiologische Analysen und numerische Reaktionsmodelle integriert, ermöglicht ein fundiertes Verständnis der Wechselwirkungen zwischen biotischen und abiotischen Reaktionen, der mikrobiellen Gemeinschaft und deren kollektiver Wirkung auf die Arsenmobilität und die Treibhausgasdynamik in nitratgedüngten Reisfeldern.

Table of Contents

Summary ..... **I**

Zusammenfassung ..... **III**

Publications ..... **VII**

a) Published Manuscripts VII

b) Manuscripts in preparation for submission VII

1. Introduction **1**

1.1 Socio- and Environmental Relevance of Nitrogen-Fertilized Paddy Soils 3

1.2 Biogeochemical Processes in Paddy Soils 7

1.3 Microbial Key Players Involved in Iron and Nitrogen Cycling versus Abiotic Reactions in Paddy Soils 11

2. Objectives of This Study **13**

3. Discussion and Outlook **15**

3.1 Biogeochemical Processes under Nitrate Fertilization in Paddy Soils 17

3.2 Pinpointing Microbial Key Players under Nitrate Fertilization in Paddy Soils 21

3.3 Enrichment Cultures: A Tool for Unraveling Microbial Interactions in Paddy Soils 24

3.4 Unraveling Complexity: The Critical Role of Rice Plants in Paddy Soil Experiments 31

3.5 A Balancing Act: How Can We Simultaneously Reduce Nitrous Oxide Emissions and Arsenic Mobility in Paddy Soils? 33

References **35**

Statement of Personal Contribution **49**

Appendix **52**

Grimm et al. (2024a). Arsenic immobilization and greenhouse gas emission depend on quantity and frequency of nitrogen fertilization in paddy soil 53

Supporting Information 66

Grimm et al. (2024b). Nitrous oxide is the main product during nitrate reduction by a novel lithoautotrophic iron(II)-oxidizing culture from an organic-rich paddy soil .. 101

Supporting Information 121

Grimm et al. (in prep.). Acetate addition shifts community composition and extent of chemodenitrification in a lithoautotrophic nitrate-reducing microbial culture 145

Supporting Information 188

Publications

a) Published Manuscripts

Grimm, H.; Drabesch, S.; Nicol, A.; Straub, D.; Joshi, P.; Zarfl, C.; Planer-Friedrich, B.; Muehe, E. M.; Kappler, A. Arsenic Immobilization and Greenhouse Gas Emission Depend on Quantity and Frequency of Nitrogen Fertilization in Paddy Soil. *Heliyon* **2024**, *10* (16), e35706. https://doi.org/10.1016/j.heliyon.2024.e35706.

Grimm, H.; Lorenz, J.; Straub, D.; Joshi, P.; Shuster, J.; Zarfl, C.; Muehe, E. M.; Kappler, A. Nitrous Oxide Is the Main Product during Nitrate Reduction by a Novel Lithoautotrophic Iron(II)-Oxidizing Culture from an Organic-Rich Paddy Soil. *Appl. Environ. Microbiol.* **2024**, e01262-24. https://doi.org/10.1128/aem.01262-24.

b) Manuscripts in preparation for submission

Grimm, H.; Gscheidel, P.; Boeckmann, M.; Straub, D.; Fischer, S.; Kappler, A.; Zarfl, C. Acetate Addition Shifts Community Composition and Extent of Chemodenitrification in a Lithoautotrophic Nitrate-Reducing Microbial Culture. **in prep.**

1. Introduction

The global population continues to rise, with projections estimating nearly 10 billion people by 2050, and much of this growth occurring in developing countries.[1,2] Many developing countries are undergoing rapid economic growth, often accompanied by an increase in consumption and demand of resources.[3,4] This presents some major challenges, particularly in relation to climate change and global food demand.[5] Economic growth is frequently linked to higher greenhouse gas emissions, driven by industrialization, transportation, and energy generation.[6] Additionally, deforestation - often carried out to expand urban or agricultural areas - releases significant amounts of greenhouse gases and reduces the Earth´s capacity to scavenge greenhouse gases from the atmosphere.[7]

However, meeting the expected 30–62% rise in global food demand by 2050 will require the expansion of agricultural land.[8] This increase is not only driven by population growth, but also by shifting dietary preferences. However, agricultural yields are stagnating in many regions due to soil degradation, water scarcity, and climate-related challenges.[9–11] Climate change and agriculture are intricately linked: for instance, climate change exacerbates water shortages, threatening food production, while agriculture's high water demand intensifies this issue.[12]

Moreover, the widespread use of chemical fertilizers introduces excess nutrients like nitrate into groundwater, degrading water quality and soil health. Ultimately, it is humans who bear the consequences of the impacts of both climate change and unsustainable agricultural practices. In response to these challenges, the United Nations established the Sustainable Development Goals (SDGs) in 2015.[13] SDG 2 (zero hunger), 3 (good health, and well-being), 6 (clean water, and sanitation), and 12 (responsible consumption, and production) are directly affected by the dynamic interplay between climate change and agriculture. Scientific research is crucial in addressing these issues and in the future, it is essential to strengthen the connection between science and policy to ensure that research is effectively translated into meaningful action.

This PhD thesis provides research that aims to answer fundamental research questions related to agriculture and climate change, which can be in future the basis for more applied research that will be beneficial for understanding urgent environmental issues.

1.1 Socio- and Environmental Relevance of Nitrogen-Fertilized Paddy Soils

In 2021, wheat, rice, and maize accounted for over 90% of the total cereal production, with cereals making up 32% of the total crop production.[14] Rice is a versatile crop that grows in different regions (delta regions to highlands) under different management strategies on paddy soils. Worldwide, 75% of rice is grown on lowland, irrigated fields that are harvested one, two, or three times per year depending on the region.[15] About 90% of the rice is grown in Asia, with China (27%), India (25%), and Bangladesh (7%) accounting for the majority of the global rice production.[14] Rice provides the staple food for 3.5 billion people on earth, which is more than half of the world´s current population.[15] However, it is the main calorie uptake for the poor and undernourished people that have no access to more nutritious food. Problematically, increased levels of arsenic are often found in rice grains. Arsenic is a toxic metalloid, which has acute and chronic toxicity effects if encountering poisoning due to high uptake of arsenic.[16] Arsenic is either of geogenic origin or additionally supplied and accumulated via arsenic-contaminated irrigation water.[17] Its mobility and bioavailability are greatly influenced by iron redox cycling and sequestration by Fe(III) (oxyhydr)oxide minerals, that are also naturally abundant in paddy soils.[18] However, under reducing conditions due to waterlogging, the reductive dissolution of iron(III) minerals releases bound arsenic.[19,20] High concentrations of arsenic in the paddy soils was shown to limit rice yields,[21] also under future climatic conditions (elevated temperature and atmospheric CO_2).[22] Rice yields are normally highest under waterlogged, irrigated conditions, due to suppression of weed growth.[23] It is estimated that rice yields need to increase by 1.2 to 1.5% if expansion of land area is excluded.[15] In comparison, currently, rice yields are only increasing by around 0.8%.[24] Climate change poses another challenge on rice yields due to increasing arsenic mobility in the paddy soil, as it was shown under future climatic conditions.[22] In the past, rice yields increased worldwide from 1.86 to 4.66 t ha^{-1} between 1961 and 2019 due to the first green revolution.[25] The green revolution is characterized by an intensified use of chemical fertilizers (nitrogen-based) and by high-yielding rice varieties that respond better to chemical fertilizers especially in developing countries.[26] This reliance on chemical nitrogen (N)-based fertilizers that is

ongoing until today, ultimately leads to a loss in soil fertility, water pollution, and increased nitrous oxide (N_2O) emissions. N_2O is a climate active greenhouse gas, which has 273-times the global warming potential to carbon dioxide over 100 years.[27] N_2O emissions are often positively correlated with the use of N-based fertilizers. A fertilizer effect on N_2O emissions was shown by Guenet et al. (2021)[28], where it becomes visually apparent that particularly areas in South, and Southeast Asia (main rice producing areas) are greatly affected by fertilizer effects (Figure 1.1).

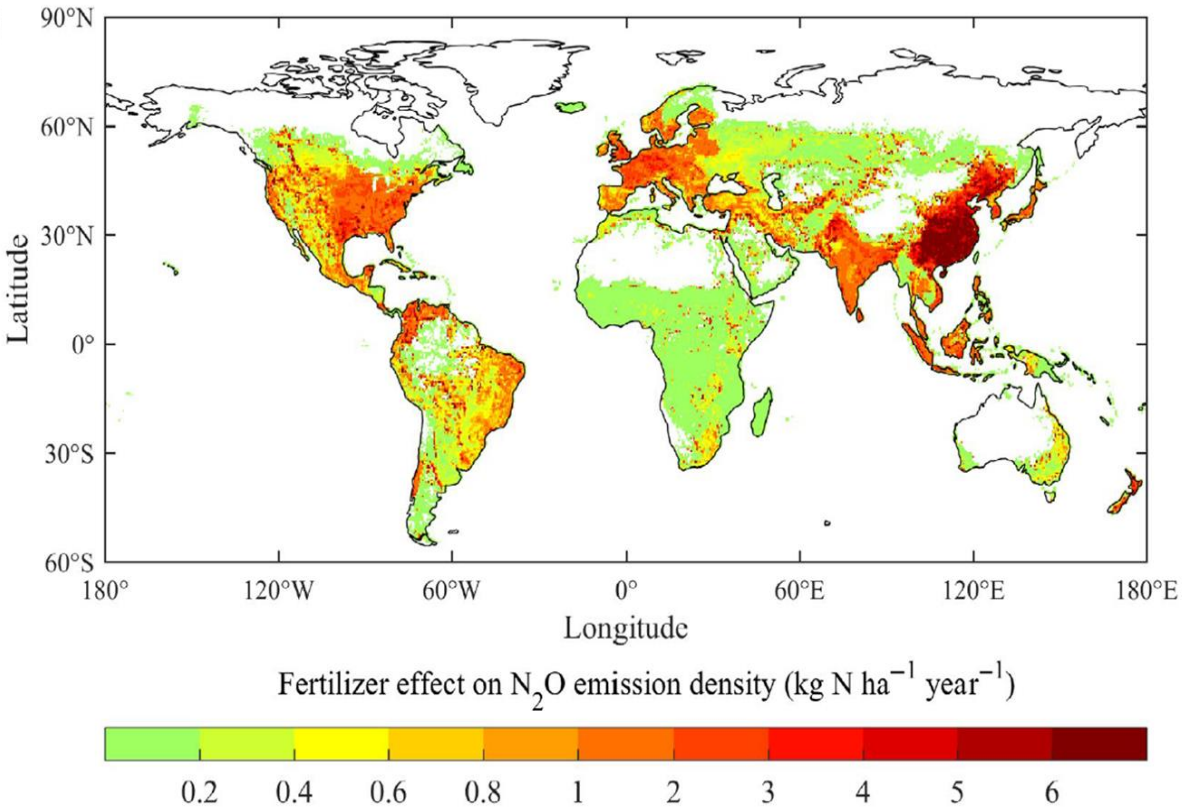

Figure 1.1. World map of the fertilizer effect on nitrous oxide emissions (modified after Guenet et al. (2021)[28]). Green colors represent little effects and dark red colors represent strong effects.

Paddy fields are also contributing to methane (CH_4) emission, accounting for around 48% of total cropland methane emissions,[29] even though rice paddies only incorporate 9% of the total cropland area.[30] Studies have shown a negative correlation between N_2O emissions and CH_4 emissions from paddy fields due to trade-offs in biogeochemical processes.[31] However, both, N_2O and CH_4 emissions outweigh the greenhouse gas mitigation potential of paddy soils to sequester organic carbon under waterlogged conditions.[30]

Due to the above-mentioned challenges, research has focused on paddy management strategies that should balance effects on rice yield and on greenhouse gas emissions. Zhao et al. (2019)[32] investigated the effects of different management strategies on changes of area-scaled global warming potentials, and on yield-scaled global warming potentials (GWP). New rice varieties, biochar, or herbicide applications were found to be promising in decreasing the yield-scaled GWP and simultaneously increasing rice yields (Figure 1.2). The use of N fertilizer, however, was also found to decrease the yield-scaled GWP and had the most positive effects on the rice yield.

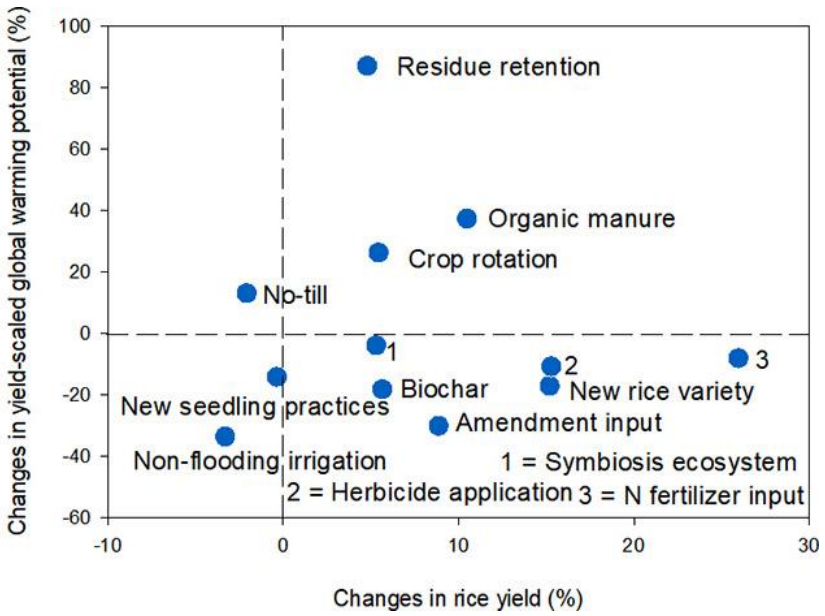

Figure 1.2. Yield-scaled global warming potential and changes in rice yield for different management strategies for rice cultivation (based on Zhao et al. (2019)[32]).

Studies focusing on nitrogen fertilization in paddy soils have either focused on arsenic mobility or on N_2O emission from paddy soils. Generally, nitrogen fertilization leads to an immobilization of arsenic and to an increase in N_2O emission, while limiting methane emissions.[31,33–39] To the best of our knowledge, only two studies investigated the effects of nitrogen fertilizer on both parameters simultaneously. Wang et al. (2023)[40] used nitrate and ammonia/nitrate fertilizer and observed that arsenic immobilization was greater under nitrate fertilization, but N_2O production was less in ammonia/nitrate fertilizer treatments. In a follow up study by Wang et al. (2024)[41], a combination of birnessite and nitrate fertilizer has proven to be most successful in immobilizing arsenic and limiting N_2O emissions over 8 days of incubation. In general, those experiments

were supplemented with arsenite and acetate and were only run over a short time (10 days). Thus, it remains open how arsenic and N_2O dynamics evolve under more natural conditions and over longer time periods that are more representative regarding rice cultivation periods. Also, the effect of different fertilizer concentrations and repeated addition of fertilizer on arsenic mobility and N_2O production remains to be investigated.

In the following, biogeochemical processes involved in the iron and nitrogen cycle are discussed in detailed, in addition to other biogeochemical processes at play.

1.2 Biogeochemical Processes in Paddy Soils

A range of biogeochemical processes occur in waterlogged, nitrogen-fertilized paddy soils. Waterlogging results in a rapid consumption of oxygen in the upper centimeters of the paddy soil. This leads to reducing, anoxic conditions in the paddy soil, which favors anaerobic microorganisms that utilize alternative electron donors such as nitrate (NO_3^-), sulfate, or iron(III) (Fe(III)).[42] Due to its reducing conditions, paddy soils are naturally rich in reduced compounds such as arsenite (As(III)), or iron(II) (Fe(II)).

Iron is ubiquitously abundant in paddy soils and is considered as the most redox-active metal in the earth´s crust.[43] In the environment, iron is present as dissolved ions or as iron-bearing minerals. Many iron(III) minerals are good adsorbents for negatively charged ions due to their high zero point of charge resulting in positively charged mineral surfaces at neutral pH.[44] These sorption mechanisms highly influence the mobility and bioavailability of nutrients or toxic metals, but also the fate of iron(III) (oxyhydr)oxides in the environment itself.[45]

In the paddy soil, iron is involved in various biotic and abiotic processes. Typically, rice plants are planted on the paddy soil and roots penetrate into the anoxic part of the soil. In a process called radial oxygen loss, rice roots exert oxygen into the surrounding area as a protective mechanism to prevent the plant from iron toxicity.[46–48] Released oxygen can abiotically react with iron(II) to form a so called iron plaque around the rice roots. Microaerophilic iron(II) oxidation (Figure 1.3) also contributes substantially to the formation of iron plaque,[49] which prevents not only the uptake of iron into the rice plant but also of toxic substances, such as arsenic.[50] In the reduced, anoxic part of the paddy soil, iron(III) can be reduced, which results in CO_2 emissions due to organic matter decomposition and to the formation of solid-phase iron(II) or high concentrations of dissolved iron(II). The reductive dissolution of iron(III) minerals thereby has tremendous impacts on contaminant mobility, such as arsenic, that is being released during iron(III) reduction. This, together with arsenate reduction under anaerobic conditions are the main drivers for mobilizing arsenic in paddy soils.

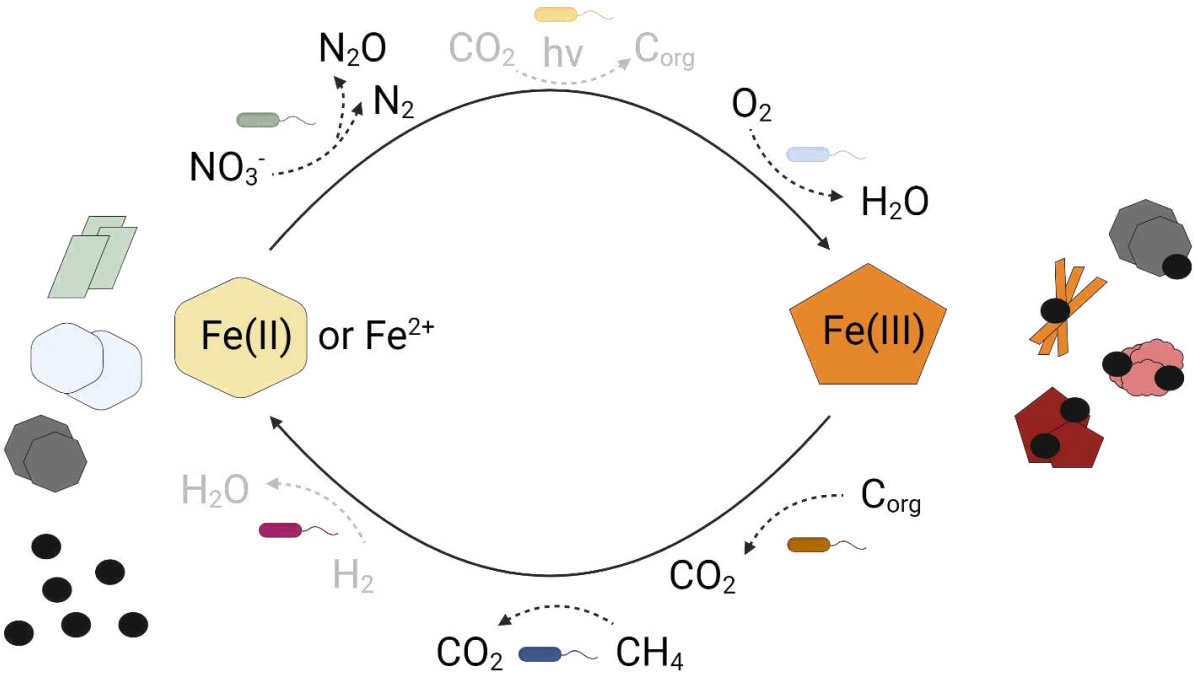

Figure 1.3. Schematic representation of the iron redox cycle. Relevant processes that are discussed more in detail in the text are displayed in black text. Other, less relevant processes that are included for completeness are highlighted in light grey. Black dots represent organic carbon, nutrients, or contaminants, other shapes represent different iron(II) or iron(III) minerals. Created with BioRender.com.

The iron redox cycle is closely intertwined with other elemental cycles, particularly carbon and nitrogen. On the reductive site, iron(III) reduction can be coupled to the oxidation of methane, which may originate from methanogenesis in deeper soil layers or ammonium (NH_4^+). Conversely, on the oxidative side iron(II) oxidation is often coupled to nitrate reduction (Figure 1.3), a process recognized as the dominant microbial pathway for iron(II) oxidation in paddy soils[51]. This interconnection highlights the importance of the nitrogen cycle, which plays a pivotal role in paddy soils. The following section further elaborates on the nitrogen cycle and its broader implications in these environments.

The nitrogen cycle is highly influenced by the addition of nitrogen fertilizer onto the paddy soil. For example, the fate of urea in paddy soils follows a well-defined pathway (Figure 1.4). After urea is applied, it undergoes hydrolysis, converting into NH_4^+ with some potential loss of ammonia (NH_3) to the atmosphere through volatilization. The remaining NH_3 dissolves in water where it further reacts to form NH_4^+, which becomes available for subsequent microbial processes. During nitrification in the oxic part of the paddy soil, NH_4^+ is converted to nitrite (NO_2^-) and finally to NO_3^-.

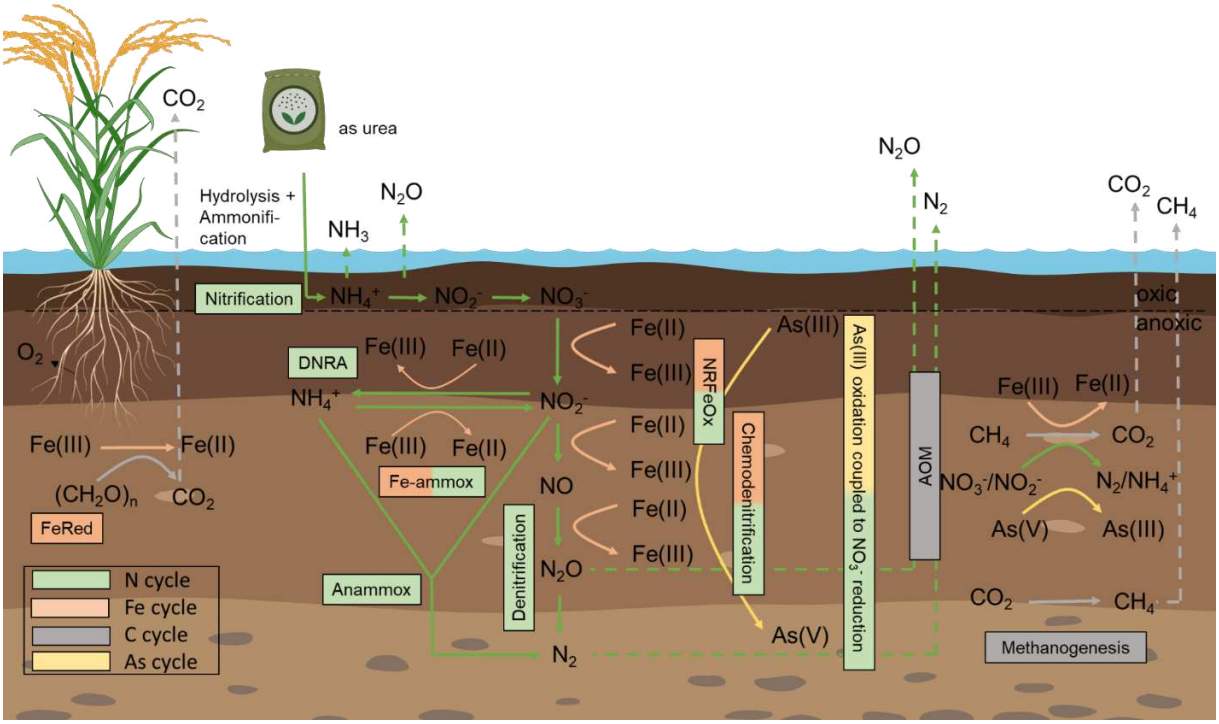

Figure 1.4. Overview of major biogeochemical processes in nitrogen-fertilized, waterlogged paddy soils. Biogeochemical cycles (N, Fe, C, As) are highlighted in different colors, acknowledging the fact that some elemental cycles (e.g., sulfur, manganese, etc.), and processes are left out (e.g., fermentation, etc.). Created with BioRender.com.

In the anoxic part of the paddy soil, nitrate can be converted to nitrite and further to ammonium during dissimilatory nitrate reduction to ammonium (DNRA). In another process, called anaerobic ammonium oxidation (Anammox), ammonium and nitrite can be converted to dinitrogen gas (N_2). Ammonium oxidation can furthermore be coupled to iron(III) reduction in a process called Fe-ammox, leading to nitrite, nitrate, or N_2 as the final N-product depending on the prevailing pH.[52] During denitrification, NO_3^- can be further reduced to other N-species, resulting in N_2O or N_2 as gaseous intermediates

or end products.[53] The reactive N-species during denitrification can abiotically react with iron(II) during chemodenitrification. Biotically, the reduction of nitrate can be coupled to the oxidation of organic carbon or to the oxidation of inorganic compounds, such as As(III) or iron(II) during denitrification. It was shown that different parameters like pH, sulfide concentrations, type, and complexity of electron donors together with the ratio of organic carbon to N influences the likelihood of denitrification or DNRA.[54] Typically, denitrification is the favored process for nitrate removal under lower organic carbon to N ratios.[55]

1.3 Microbial Key Players Involved in Iron and Nitrogen Cycling versus Abiotic Reactions in Paddy Soils

Soil is a hotspot for microbial life and provides a habitat for billions of microorganisms. A spatio-temporal variability of microbial abundance and community structure was observed in a paddy soil over the rice growing season, with numbers as high as ~1.7 $x10^9$ and $3x10^9$ cells per g soil in the bulk and rhizosphere soil, respectively.[56] The diversity of the paddy soil microbiome is crucial for maintaining ecosystem functions and services and for mediating biogeochemical processes.[57] In the following, microbial key players involved in the iron and nitrogen cycle are presented.

Iron(III) reduction has been considered an important process in paddy soils right after the first cultivation and isolation of iron(III)-reducing microorganisms.[58,59] *Shewanella* sp. and *Geobacter* sp. are two of the most prominent genera of iron(III) reducers that couple the oxidation of organic carbon (e.g., lactate, acetate), or hydrogen to the reduction of iron(III).[60] The reduction of iron(III) or nitrate can also be coupled to the oxidation of methane by archaea, more specifically ANME-2a[61] and ANME-2d (e.g., '*Candidatus* Methanoperedens').[62]

Ratering and Schnell (2001)[51] postulated that the metabolic capacity for nitrate reduction coupled to iron(II) oxidation (NRFeOx) is widespread in paddy soils. Denitrifying microorganisms can be classified as (i) heterotrophs, which require an organic carbon substrate for energy generation, (ii) mixotrophs, which can use both organic carbon and inorganic compounds, or (iii) lithoautotrophs, which only use inorganic compounds such as hydrogen, reduced sulfur compounds, arsenite, or iron(II).[63] Heterotrophic or mixotrophic nitrate-reducing, iron(II)-oxidizing microorganisms have been enriched or isolated from paddy soils before. *Ferrigenium kumadai* An22, a known microaerophilic iron(II)-oxidizer, has been isolated from a paddy soil[64] and microorganisms of the genus *Dechloromonas*, *Azospira*, *Zoogloea*, or *Pseudomonas* have been enriched in paddy soils after iron(II), nitrate, and organic carbon addition (e.g., lactate, acetate).[65–69] However, lithoautotrophic microorganisms have not been isolated or enriched in the past from paddy soil.

Different lithoautotrophic NRFeOx enrichment cultures exist (named KS, BP, AG), originating from sediment or a pyrite-rich aquifer.[70–72] Various N-intermediates can be formed during microbial nitrate reduction. It was long thought that these lithoautotrophic cultures perform complete denitrification leading to dinitrogen gas as the final product, however, it was shown that culture AG and KS produce significant amounts of N_2O,[70,73] following eq. 1.

$$2\ NO_3^- + 8\ Fe^{2+} + 19\ H_2O \rightarrow\ N_2O + 8\ Fe(OH)_3 + 14\ H^+ \qquad \text{eq. 1}$$

Meta'omics have shown that the '*Candidatus* ferrigenium' in culture KS, BP, and AG have the genetic potential to perform only certain steps of denitrification (NO_3^-, NO_2^-, NO, N_2O, and N_2), without the potential to reduce N_2O to N_2, but feature genes for iron(II) oxidation.[74] Besides enzymatic iron(II) oxidation, nitrite or other reactive intermediates (i.e., nitric oxide) can also abiotically react with iron(II) (eq. 2).

$$NO_2^- + 2\ Fe^{2+} + 4.5\ H_2O \rightarrow\ 0.5\ N_2O + 2Fe(OH)_3 + 3\ H^+ \qquad \text{eq. 2}$$

In the literature, N_2O emissions that were observed in the environment were often attributed to abiotic processes, however, recent results point towards a significant enzymatic contribution to N_2O emissions by nitrate-reducing, iron(II)-oxidizing microorganisms. However, experimentally it remains difficult to disentangle these processes and other methods, such as isotope fractionation and numerical modelling has to be applied.[75–80] In addition, it remains scarcely documented how different growth conditions, such as the ratio of electron donor (e.g., iron(II)) and electron acceptor (e.g., nitrate) or the type of electron donor (iron(II), or organic carbon) influence the intermediates during denitrification and the microbial community composition in such enrichment cultures.

2. Objectives of This Study

The above-mentioned processes highlight that iron, nitrogen, and arsenic can interact in various ways. In this thesis, we focused on certain processes that we considered to be most relevant in affecting arsenic mobility and N_2O emissions in paddy soils.

We hypothesize that (i) the addition of nitrate will prevent reductive dissolution of iron(III) minerals and with it the release of bound arsenic and the reduction of arsenate, thus, the mobilization of arsenic. In addition, (ii) enzymatic and abiotic iron(II) oxidation via nitrate-reducing, iron(II)-oxidizing microorganism and chemodenitrification, respectively, will lead to the formation of iron(III) minerals that can scavenge and thus, immobilize arsenic. On the other hand, (iii) enzymatic nitrate reduction and chemodenitrification will result in higher N_2O production, while simultaneously lowering CH_4 emissions from paddy soils. Ultimately, we hypothesize that (iv) by balancing the addition of nitrate to paddy soils we would find conditions under which arsenic mobilization and total greenhouse gas emissions are lowest. Thus, we investigated the effects of nitrogen fertilizer addition on N_2O emissions and the mobility of arsenic in a range of experimental approaches to answer the following research questions, which are outlined below.

Previous studies have investigated individual effects of N fertilizer addition on either arsenic mobility[20,22,23] or greenhouse gas emissions (i.e., N_2O, and CH_4)[24–26] in paddy soils. Optimized fertilizer application methods (timing, or matching crop demand) or split applications have been suggested in the past to decrease N_2O emissions.[81] Yet, the effects on arsenic mobility remain unresolved. Thus, in the first project addressed in **Grimm et al. (2024a)**[82], we wanted to determine the effects of different quantities and frequencies of N fertilizer application (as potassium nitrate) in paddy soils on

- the extent of nitrate reduction coupled to iron(II) oxidation,
- iron mineral formation and transformation,
- greenhouse gas formation (CO_2, CH_4, and N_2O) and emission,
- the mobilization of arsenic from iron minerals into the porewater,
- microbiome composition and activity.

In the second project, published in **Grimm et al. (2024b)**[83], we aimed to investigate the important role of lithoautotrophic nitrate-reducing, iron(II)-oxidizing microorganisms for arsenic mobility and greenhouse gas emissions in paddy soils. Thus, the objectives were to

- obtain a model culture of lithoautotrophic nitrate-reducing, iron(II)-oxidizing microorganisms from a paddy soil,
- identify microbial key players for NRFeOx using 16S rRNA gene amplicon sequencing,
- determine the extent of nitrate reduction, iron(II) oxidation, and N_2O production, and
- compare growth conditions influencing the performance of the enrichment culture.

In the third project, which is currently in preparation for publication **(Grimm et al. (in prep.)**[84]**)**, we cultivated the novel lithoautotrophic enrichment culture HP under autotrophic, mixotrophic, and heterotrophic conditions to

- identify and quantify shifts in the microbial community composition in the presence of iron(II) and/or nitrate, and/or acetate,
- determine differences in extent and rates of nitrate reduction and iron(II) oxidation,
- quantify main products during denitrification, i.e., nitrite and N_2O, and
- estimate the contribution of abiotic and biotic processes to iron(II) oxidation and N_2O production by applying kinetic modelling.

Ultimately, the results from **Grimm et al. (in prep.)**[84] will help us to understand how organic carbon affects the adaptability of autotrophic NRFeOx cultures and NRFeOx-mediated iron and nitrogen cycling, which can be translated to ecosystems where organic matter is prevalent (e.g., paddy soils).

3. Discussion and Outlook

The addition of nitrogen fertilizer in paddy soils and its effects on either arsenic mobility, nitrous oxide, or methane emissions has been intensively studied in the past.[31,33–36,39,85] Previous studies have focused on microcosm or pot experiments and used different types of fertilizer and paddy soils. However, studies have often added unrealistic amounts of nitrogen fertilizer,[41] arsenic,[40] or acetate[68] to their experiments, which poorly reflects environmental conditions. Additionally, the effects of nitrogen fertilizer on both arsenic mobility and nitrous oxide emissions remains scarcely described. Therefore, in this PhD study, we aimed to simulate different nitrogen fertilizer regimes in microcosm experiments to conclude on the mobility of arsenic, on nitrous oxide emissions, and total greenhouse gas emissions at the same time and to identify the microbial key players involved in nitrate reduction coupled to iron(II) oxidation in paddy soils (Figure 3.5, left).

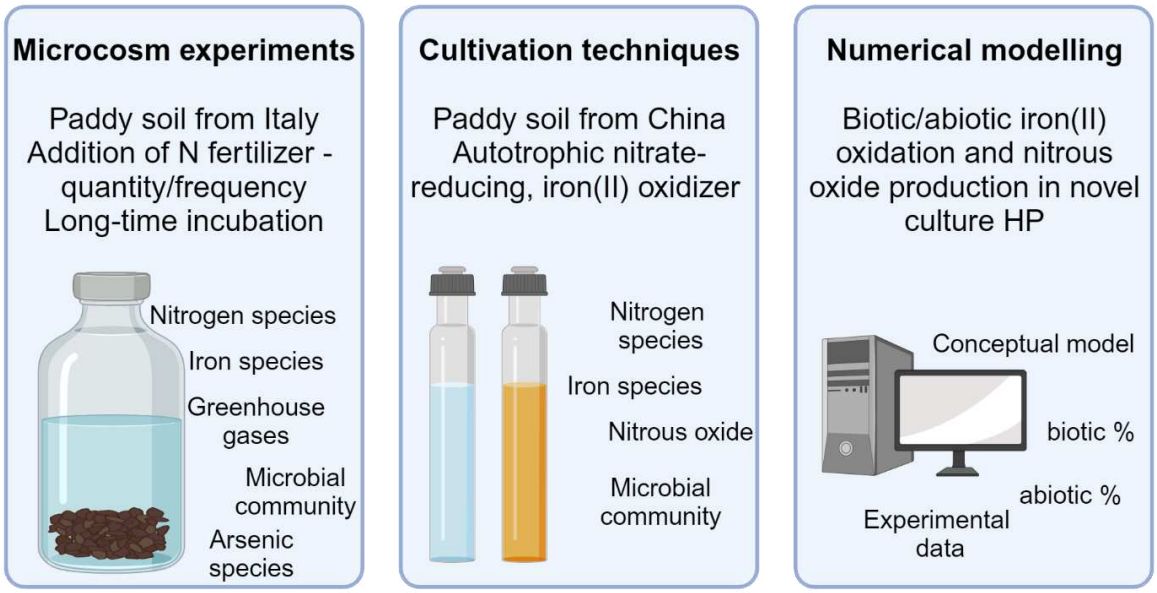

Figure 3.5. Overview of methodological approaches applied during this PhD thesis. Created with BioRender.com.

By cultivation techniques, we successfully enriched microbial key players involved in nitrate reduction coupled to iron(II) oxidation (Figure 3.5, middle), enabling us to study this metabolic process more in detail (e.g., changing growth conditions to determine effects on N_2O production). By applying numerical modelling, we were able to quantify contributions of abiotic and biotic processes on iron(II) oxidation and N_2O production (Figure 3.5, right). These results broaden our understanding of the factors influencing arsenic mobility, N_2O production, key microbial community members, and their interactions, as well as the relative contributions of abiotic and biotic processes to nitrate-dependent iron(II) oxidation.

The main outcomes of this PhD study and remaining open questions are discussed in the following.

3.1 Biogeochemical Processes under Nitrate Fertilization in Paddy Soils

In **Grimm et al. (2024a)**[82], we added different amounts of nitrate fertilizer at different timepoints to a paddy soil incubated in a microcosm setup over 129 days. We followed dissolved N-species, iron species, and arsenic species, extracted solid-phase iron minerals, and associated total arsenic, quantified greenhouse gas emissions (CO_2, CH_4, and N_2O), and identified the microbial community at certain timepoints. We found that the addition of nitrate fertilizer stimulates the oxidation of dissolved and solid-phase iron(II) (Figure 3.6). By this, most of the arsenic was immobilized (28 µg L^{-1}, within 3 days) from the porewater and bound to iron mineral phases as proven by solid-phase extractions. Nevertheless, complete nitrate consumption occurred rapidly (minimum: within 6 days), which was followed by microbial iron(III) reduction. The reductive dissolution of iron(III) minerals not only led to an increase in dissolved iron(II), but also to the formation of secondary iron(II) minerals of different crystallinity as shown by sequential chemical extractions. Arsenic was immobilized only on short-term and readily mobilized as soon as nitrate was depleted. Only when maintaining constant nitrate concentrations in the paddy soil porewater was arsenic retained on iron minerals (under high N fertilization treatment).

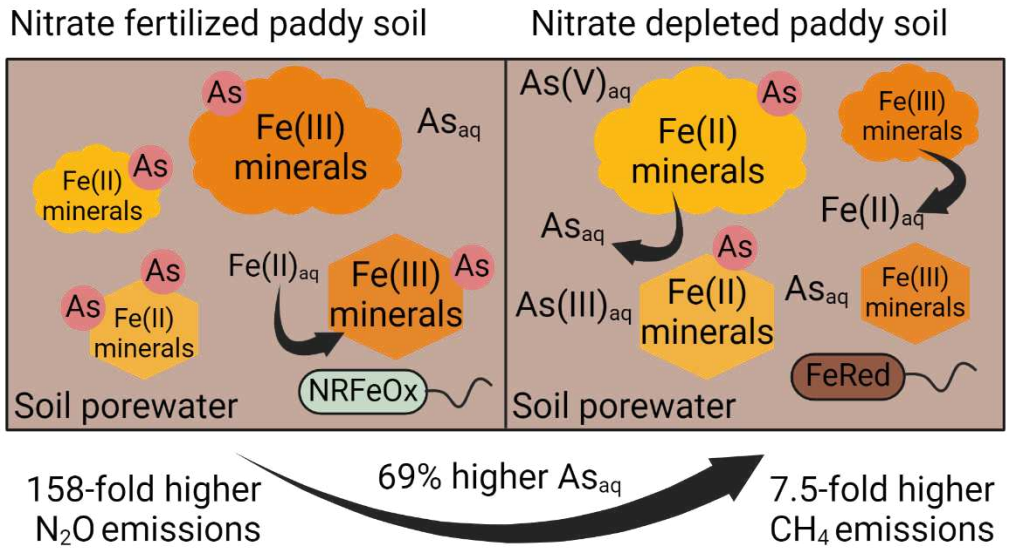

Figure 3.6. Overview of findings in Grimm et al. (2024a)[82]. Created with BioRender.com.

Regarding greenhouse gas emissions, nitrate fertilization led to increased N_2O emissions, irrespective of fertilizer concentration and lower CH_4 emissions, especially when supplied in higher concentrations (medium/high N treatment). We found similar N_2O emissions even when supplying nitrate in 2.5-times lower concentrations due to short-term peak emissions of N_2O. This observation occurred after supplying nitrate a second time to the paddy soil. Microbial community analysis at a time of greatest differences (day 37) between N fertilized treatment and the control revealed distinct community compositions. *Gallionellaceae*, *Comomonadaceae,* and *Rhodospirillales* were more abundant under nitrate fertilization indicating their key role in nitrate reduction and iron(II) oxidation.

The results from **Grimm et al. (2024a)**[82] suggest that arsenic mobility and N_2O emission can only be minimized if nitrate is supplied in very high concentrations compared to lower nitrate applications. Yet, this does not reflect economically practices, thus, further strategies to minimize N_2O and arsenic mobility need to be deployed. Alternate wetting, and drying (AWD) has been shown to maintain yield, reduce methane emissions from paddy soils, and arsenic concentrations in the porewater, ultimately limiting As uptake into the rice grain.[86] On the other side, the combination of AWD and nitrogen fertilization might even enhance N_2O emission due to combined denitrification and nitrification (under aerobic conditions).[87] Studies have not focused yet on the combined effects of AWD and N fertilizer on As mobility and greenhouse gas emissions. Thus, experiments could be performed that address the following research questions:

1) How does combined AWD and N fertilization affect N_2O and CH_4 emissions?
2) Can combined AWD and N fertilization even increase the immobilization of arsenic?
3) Does the combined application of AWD and N fertilization provide the best management practice to improve yield without compromises in GHG emissions or arsenic mobility?

Another determining factor influencing N_2O emissions and arsenic mobility is the dominance of denitrification or dissimilatory nitrate reduction to ammonia (DNRA).[34,40,88] The type of fertilizer or the ratio of C to N in a paddy soil can determine the likelihood of DNRA or denitrification.[89] For a better understanding of the impact of DNRA and denitrification on arsenic mobility and N_2O emissions, the following open research questions need to be addressed:

1) Which soil and geochemical parameters support DNRA or denitrification in paddy soils under N fertilization?
2) In which way do different fertilizers and different paddy soils influence the likelihood of DNRA or denitrification?
3) Can we identify a fingerprint geochemical parameter or microbial indicator (e.g., community composition) that can uniformly be applied to paddy soils to predict which dominant process takes place?

To answer the open questions and identify the dominant nitrogen pathways in various paddy soils, experiments can be conducted using a wide range of global paddy soils supplemented with ^{15}N-labelled fertilizer. By determining concentrations of $^{15}NO_3^-$, $^{15}NO_2^-$, and $^{15}NH_4^+$, we can gain insights into the prevailing pathways. Coupling these findings with geochemical and microbial community analyses, and employing statistical methods such as multiple regression, or principal component analysis, will help identify key structural fingerprints (e.g., C/N ratio thresholds) that predict the dominance of DNRA or denitrification.

Different types of fertilizer can be tested time effectively with an elegant tool, named MicroResp® assay, detecting CO_2 emissions from soil under standard operation. Modifying the traditional usage of the MicroResp® assay allows us to follow changes in microbial community composition, iron mineralogy, and arsenic mobility (see exemplary setup in Figure 3.7). Previous tests with the MicroResp® assay performed in the framework of this PhD work (during the B.Sc. thesis of Sarah Keldenich) proved promising by showing large differences between the type of nitrogen fertilizer (urea, ammonium nitrate, and nitrate), and between paddy soils (China, Italy). This work could be expanded in future by testing also slow release fertilizer, deep placement of urea or other combination of fertilizers with or without additives (e.g., straw, biochar, etc.).

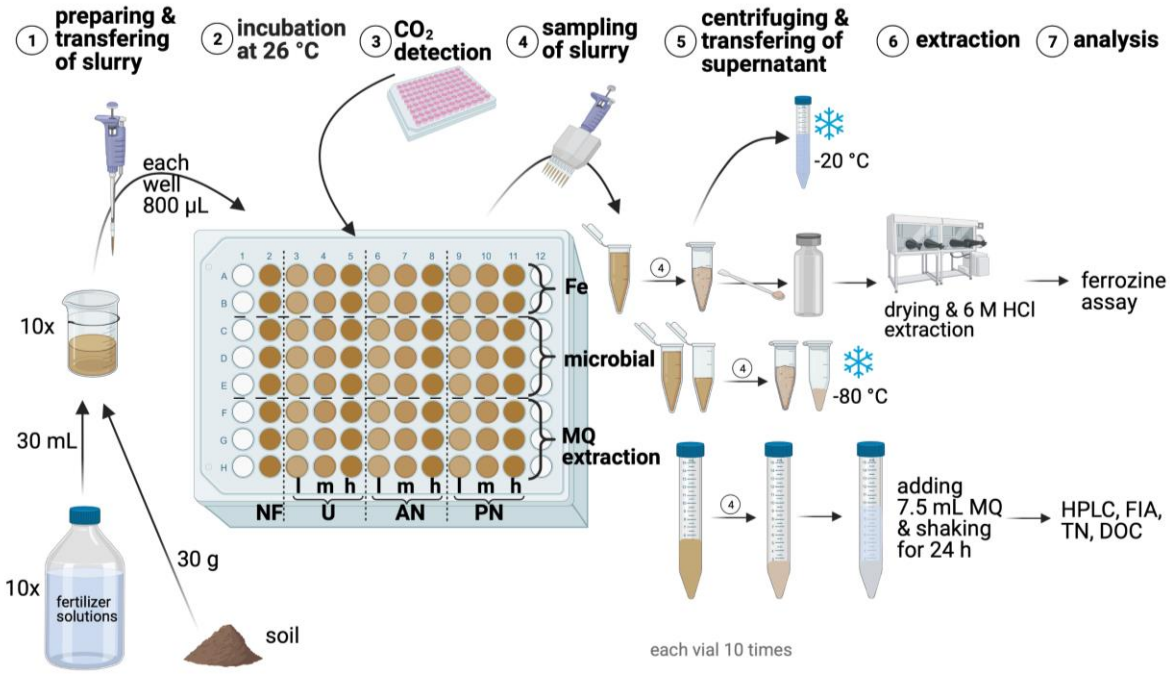

Figure 3.7. Schematic of a potential setup, and sampling procedure using the MicroResp® assay. Different treatments are labelled on the deep-well plate (NF: control with no fertilizer, U: urea, AN: ammonium nitrate, PN: potassium nitrate), and can be replaced by other fertilizers. Different fertilizer concentrations are highlighted in different color intensities, and indicated in small letters (l: low, m: medium, h: high). Created with BioRender.com by Sarah Keldenich.

3.2 Pinpointing Microbial Key Players under Nitrate Fertilization in Paddy Soils

During the microcosm experiment described in **Grimm et al. (2024a)**[82], we performed a variety of molecular biology analyses. By quantifying gene, and transcript 16S rRNA copy numbers, we were able to not only conclude on the abundance, but also on the activity of the whole microbial community at different timepoints. We only found significant differences in 16S rRNA copy numbers on a transcript level on day 37, indicating that nitrogen fertilizer positively affected microbial activity. We further quantified different functional and marker genes that are involved in the iron, nitrogen, and arsenic cycle, however, we could not find conclusive differences between the treatments. In a next step, we could further improve the interpretation of these results by calculating, i.e., transcript-to-gene ratios that have proven to be a valuable tool in other studies.[90,91] The transcript-to-gene ratio is suggested to be a more accurate measure for transcriptional activity than absolute abundances. A key challenge in comparing the activity of specific functional genes across different treatments is the variability in the absolute abundance of these genes. Therefore, conducting comparisons on a relative basis may provide insights, which microorganisms actively contribute to certain processes or if nitrogen fertilization alters gene regulation. Ultimately, this would enable us to conclude on microbial nitrogen utilization pathways across treatments (e.g., DNRA, denitrification, see section 5.1).

Through 16S rRNA gene amplicon sequencing, we identified which microorganisms became more abundant over time under nitrate fertilization, as described in **Grimm et al. (2024a)**[82]. Notably, *Gallionellaceae* showed increased abundance under nitrate fertilization, and were successfully enriched from paddy soil, as described in **Grimm et al. (2024b)**[83]. A systematic comparison of described isolates, or species in enrichment cultures from the literature, alongside an evaluation of their metabolic functionality, would provide valuable insights into their role in nitrate-dependent iron(II) oxidation in the environment. In **Grimm et al. (2024b)**[83], we conducted a maximum-likelihood analysis of *Gallionellaceae* species identified in paddy soils, revealing close phylogenetic relationships. However, since these analyses were based on short-read 16S rRNA gene sequences, further comparison using long-read 16S rRNA gene

sequencing is necessary to confirm these findings and provide a more comprehensive understanding.

Furthermore, applying a similar experimental approach as in **Grimm et al. (2024a)**[82] to various types, or origins of paddy soils, and different varieties of N-based fertilizer would enhance our understanding of microbial key players. The following open questions could be addressed in an additional experiment:

1) How do different fertilizer types (e.g., urea, ammonia-based, nitrate-based, mix of ammonia and nitrate, slow release fertilizer, etc.) affect the microbial community composition of paddy soils?
2) Do different paddy soils (different parent material, different origin, different management practices) react differently to N fertilizer input?
3) Can we derive a microbial fingerprint for different N fertilizers or different paddy soils?

To answer these open research questions, experiments could be conducted in glass vials that are filled with paddy soil, left open to the atmosphere, and incubated under waterlogged conditions over several weeks. Samples for 16S rRNA gene amplicon sequencing can be taken at the beginning and at the end of the incubation to compare changes in microbial community composition. By comparing different paddy soils and different N fertilizers, we would aim to identify unique microbial community compositions for either different N fertilizer types or different paddy soils that could be uniformly transferred to other paddy soils or fertilizers.

In **Grimm et al. (2024a)**[82], we attributed nitrate reduction to the oxidation of iron(II). In later times during the incubation we also observed CH_4 emissions at least from the control and the low N fertilized paddy soil. CH_4 is produced during methanogenesis in deeper soil layers under waterlogged conditions. However, there are also microbial processes limiting CH_4 emissions, such as CH_4 oxidation coupled to the reduction of nitrate or iron(III). Luo et al.(2021)[92] emphasized that both processes are relevant for CH_4 oxidation in paddy soils. CH_4 oxidation coupled to iron(III) reduction is a process that was first described in 2006 happening in marine sediments[93] and was also found in arsenic-contaminated aquifers in Asia, where it significantly contributed to limiting

CH_4 emission and increasing arsenic mobility due to the reductive dissolution of iron(III) minerals and the subsequent release of bound arsenic.[94] CH_4 oxidation coupled to nitrate reduction has been studied in the past decades and has been shown to limit CH_4 emission from N fertilized paddy soils.[95] In **Grimm et al. (2024a)**[82] we found that '*Candidatus* Methanoperedens' were more abundant in N fertilized setups and Vaksmaa et al. (2017)[96] successfully enriched '*Candidatus* Methanoperedens' from an Italian paddy soil. To investigate the role of methane oxidation in more detail, functional genes involved in methane oxidation (e.g., *mcrA*, *pmoA*), could be analyzed in DNA extracts of the experiment described in **Grimm et al. (2024a)**[82]. Additionally, to study the interplay between CH_4 oxidation coupled to nitrate or iron(III) reduction, enrichment cultures could be set up similar to **Grimm et al. (2024b)**[83]. Here, paddy soil would be incubated with CH_4 and nitrate (culture 1) and with CH_4 and iron(III) (culture 2), to obtain an enrichment culture or even a single strain by isolation techniques, which can be further studied in detail.

3.3 Enrichment Cultures: A Tool for Unraveling Microbial Interactions in Paddy Soils

Microorganisms typically exist within complex microbial communities, interacting with a diverse range of other community members.[97] Therefore, isolation sometimes proofs to be difficult for certain microorganisms, e.g., lithoautotrophic nitrate-reducing, iron(II)-oxidizing microorganisms. So far, autotrophic NRFeOx has only been unequivocally shown in enrichment cultures (culture KS, BP, AG).[71,72,98] These cultures share a common origin in organic-poor environments (such as sediment and aquifer), which is reasonable since these microorganisms do not rely on organic carbon for survival. Generally, autotrophic microorganisms are considered to be better adapted to thrive under redox fluctuations where substrate availability may be scarce[99] and could inhabit ecological niches with low organic carbon in paddy soils that are considered as rather organic-rich environments.[100] To date, it has remained unclear whether this metabolism also occurs in paddy soils. The successful enrichment of a lithoautotrophic NRFeOx culture from a paddy soil in China (Huilongpu Town, Hunan Province), as described in **Grimm et al. (2024b)**[83], strongly suggests that this metabolism likely plays a significant role in iron(II) oxidation, and nitrate reduction in paddy soils and may also influence other elemental cycles such as carbon and arsenic.

The novel lithoautotrophic nitrate-reducing, iron(II)-oxidizing culture HP is dominated by *Gallionella* sp., and a unique microbial flanking community. The culture reduces nitrate, and iron(II) within 4 days, resulting in a ratio of $nitrate_{reduced}$ to $iron(II)_{oxidized}$ of 0.2-0.3. Nitrite is only occasionally detected and does not accumulate in culture HP. We further identified N_2O as the main product during denitrification. During the majority of transfers, N_2O was not the sole product of denitrification, thus nitric oxide or dinitrogen gas (both could technically not be detected by the experimental setup) are also produced. Because nitric oxide is toxic, we hypothesize that the microbial flanking community further reduced N_2O to N_2, while being fed with organic carbon autotrophically produced by *Gallionella* sp. (Figure 3.8).

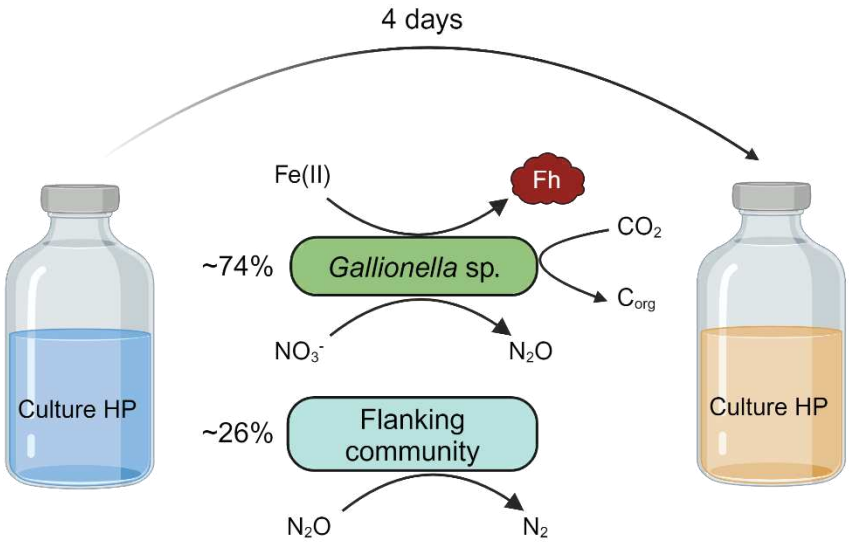

Figure 3.8. Overview of proposed nitrate transformation and iron(II) oxidation in culture HP, with *Gallionella* sp. being responsible for nitrate reduction till N_2O and the flanking community for further N_2O reduction. Created with BioRender.com.

In **Grimm et al. (in prep.)**[84], we quantified that 99.5% of the total N_2O in culture HP is biotically-derived, with the rest being of abiotic nature. The numerical reaction model also revealed that iron(II) oxidation in the lithoautotrophic culture HP is to 99.8% biotically driven. Under mixotrophic conditions (supplemented with acetate), the maximum contribution of chemodenitrification can reach up to 44%, but enzymatic processes accounted for 98.6% of the cumulative iron(II) oxidation and N_2O production.

By changing the growth conditions of culture HP in **Grimm et al. (in prep.)**[84], we were able to identify key players during autotrophic NRFeOx, mixototrophic, and heterotrophic NRFeOx that are potentially involved in different steps of denitrification. *Gallionella* sp. and *Dechloromonas* sp. were most abundant irrespective of their growth conditions. However, acetate addition influenced the flanking community boosting *Acidovorax* sp., *Zoogloea* sp., and *Parvibaculum* sp., highlighting their role in mixotrophic or heterotrophic nitrate reduction in culture HP. Further, we state that culture HP and its microbial community reacts sensitively towards changes in cultivation conditions, yet, the products of denitrification are similar between different conditions (except heterotrophic conditions: nitrite instead of N_2O).

In **Grimm et al. (2024b)**[83], culture HP was exposed to 100 µM arsenite in an experiment, which slowed down nitrate reduction and iron(II) oxidation. Additional 16S rRNA gene amplicon sequencing, not included in the manuscript published in *Applied and Environmental Microbiology*, revealed that *Macrococcus caseolyticus* was abundant (12%) in the first transfer at day 0 when nitrate, iron(II), and arsenite were supplied. This species was never observed in culture HP before, thus, it indicates its potential role in arsenite oxidation and nitrate reduction, however no supporting information is provided in the literature. Future studies should expose culture HP to more environmentally relevant concentrations of arsenite or arsenate to explore its potential for arsenic immobilization. Additionally, microbial enrichments could be designed to target microorganisms performing nitrate reduction coupled to arsenite oxidation, allowing for the investigation of competition between nitrate-dependent iron(II) oxidation and arsenite oxidation in paddy soils.

The fact that lithoautotrophic nitrate reduction coupled to iron(II) oxidation has been only unequivocally proven in enrichment cultures (culture KS; AG; BP, HP (enriched during this PhD thesis)), points towards the need of interspecies connections to perform iron(II) oxidation and nitrate reduction. It is speculated that heterotrophic community members rely on organic carbon from autotrophic community members. In an experiment, where culture HP was cultivated without any electron donor, 16S rRNA gene copy numbers increased and small amounts of nitrate were reduced, which was attributed to internally stored carbon or electrons in **Grimm et al. (2024b)**[83]. Follow up 16S rRNA gene amplicon sequencing that is not included in the published manuscript revealed that *Gallionella* sp. and *Noviherbaspirillum* sp. decreased in relative abundances (by 52% and 5%, respectively) and *Dechloromonas* sp., *Acidovorax* sp., *Azospira* sp., and *Ramlibacter* sp. increased in relative abundances (by 25%, 20%, 5%, and 3% respectively) over 7 days of incubation. This raises the question if those are the community members that are internally cross-fed by lithoautotrophic members, such as *Gallionella* sp. when grown under standard autotrophic conditions and highlights the need for follow up studies, such as metabolomics (e.g., in collaboration with Daniel Petras, University of California).

Some more open questions ought to be investigated regarding the lithoautotrophic NRFeOx culture HP. Surprisingly, the culture HP and other lithoautotrophic cultures such as culture KS, BP, and AG lead to N_2O emissions instead of showing complete nitrate reduction to N_2. In literature, it has been shown that biochar can enhance complete nitrate reduction by increasing the abundance and activity of *nosZ*, a bacterial functional gene involved in the reduction of N_2O to N_2.[101] Further, Sharma et al. (2022)[102] found that 10 to 300 nM of copper successfully enhanced the reduction of N_2O to N_2, due to the copper requirement of nitrous oxide reductase. Another factor that might influence denitrification rates or N_2O production is the pulsing frequency of, for example, nitrate fertilizer, which has been shown to affect denitrification in wetlands[103] and suggested as important through modeling for naphthalene-degrading cultures.[104] Therefore, experiments should be conducted to optimize the denitrification process and promote complete reduction of nitrogen species, ensuring full denitrification. The following research question should be answered in further experiments:

1) Can supplements, such as biochar or copper improve the denitrification process and lead to N_2 as the final or main product instead of N_2O?
2) Are low pulse-additions of the electron donor (i.e., iron(II)) or acceptor (nitrate) more successful in leading to complete denitrification rather than one-time high additions?

In the environment, iron(II) can be dissolved, adsorbed, complexed, and is often found in solid phases, such as in clays or iron(II) minerals.[105–107] Therefore, microorganisms likely possess the ability to oxidize solid-phase iron(II). However, this capability has only been demonstrated for cultures KS, capable of oxidizing various iron(II) minerals[108,109] and for culture AG, capable of oxidizing pyrite.[110] Future studies should systematically investigate the ability of various autotrophic NRFeOx cultures to oxidize different solid iron(II) phases, including both biogenic and abiogenic forms of minerals such as magnetite, siderite, and vivianite.

In literature, it was also shown that secondary iron(II) minerals are present as iron plaque at the rice roots.[111] Further, *Gallionellaceae* spp. are found in paddy soils and are often associated with the rice roots, thus, exposed to oxygen inputs.[112] Based on

the results in **Grimm et al. (2024a)**[82], we hypothesized that *Gallionellaceae* spp. could be in close proximity to rice roots and could switch their metabolism from microaerophilic iron(II) oxidation to nitrate-dependent iron(II) oxidation. Previously, cultivation in gradient tubes under microoxic conditions has not been successful for culture AG, BP, or HP. To further investigate the role of oxygen, additional experiments could be performed targeting the following research questions:

1) Can the lithoautotrophic culture HP and also other cultures such as KS, BP, or AG tolerate oxygen? If yes, where is the concentration threshold?
2) Can the cultures also switch back to nitrate-reducing, iron(II)-oxidizing conditions after being exposed to oxygen?

For this experiment, oxygen consumption could be followed with sensor foils (Presens, Germany) and nitrate, and iron(II) with standard techniques. The microbial community abundance, and activity can be followed by gene and transcript 16S rRNA, respectively. This would allow to conclude on the metabolic potential to switch between microaerophilic and nitrate-dependent iron(II) oxidation.

In **Grimm et al. (2024b)**[83] and **Grimm et al. (in prep.)**[84], the electron donor iron(II) was exchanged or other electron donors were supplied to the lithoautotrophic NRFeOx culture HP. We were able to show that native soil-extractable OC (10 mg L^{-1}) and arsenite (100 µM) could not be used as the sole electron donor for nitrate reduction. When soil-extractable OC or arsenite were supplied in addition to iron(II), the microbial performance was not affected in the case of OC or almost completely suppressed, especially with consecutive transfers under the given growth conditions, in the case of arsenic. It remains open:

1) If other electron donors such as hydrogen, sulfide, methane, or organic compounds like short-chain fatty acids (originating from fermenting bacteria), root-derived OC (by rice plants), etc. can be used by the culture HP?
2) If N_2O production differs depending on the electron donor?
3) How the microbial community composition is affected and changing when different electron donors are supplied?

Related work to this PhD thesis (Master thesis of Hayley Green) found out that culture HP is also capable to utilize glucose. The main focus was set on rice root exudates, however, the addition of natural root exudates collected from a rice plants did not lead to differences in geochemical performance, likely due to insufficient amounts supplied to culture HP. In a follow up experiment by the Master student, three common root exudates (pyruvic acid, sucrose, and serine, based on targeted GC-MS analysis from the natural root exudates) were added individually and in unison to culture HP. The addition of pyruvic acid and sucrose resulted in increased rates of iron oxidation, nitrate reduction, and N_2O production compared to the cultivation under standard, autotrophic conditions. The results on alteration in organic carbon content, cell growth, microbial community composition, and N_2O production are still being analyzed.

To date, lithoautotrophic NRFeOx cultures exist in laboratory settings but have never been exposed to more environmental settings. Introducing culture HP to paddy soils could provide insights into the biogeochemical interactions within the paddy soil and offer insights into nitrate removal, iron dynamics, and potential strategies for reducing greenhouse gas emissions, and remediating contaminants. Following research questions could be addressed in a follow up experiment:

1) Does the addition of culture HP to paddy soil lead to enhanced dissolved and solid-phase iron(II) oxidation, and consequently arsenic immobilization?
2) Does the addition of culture HP to paddy soil lead to higher N_2O emissions or will formed N_2O be further reduced by the native soil microbial community?
3) How does redox cycling affect the culture HP and does it have long term effects on fertilized paddy soil?

A previous experiment within the framework of this PhD (project seminar of Paula Gscheidel) has shown that the addition of culture HP to the native paddy soil has little effects if only supplied with nitrate. Thus, iron(II) should be supplemented in addition to nitrate and the inoculation of culture HP as cell suspension (concentrated cell culture) might be more promising. Alternatively, if experiments with modified conditions also do not show significant differences between native soil and culture HP-inoculated paddy soil, culture HP could be added to a rice plant grown in rhizotrons with a Gelrite-stabilized Hoagland solution (similar to Maisch et al. (2019)[49]). By knowing rates of

microaerophilic iron(II) oxidation and abiotic iron(II) oxidation from literature,[49,113] rates of nitrate-dependent iron(II) oxidation by culture HP could be quantified. Following this approach, the importance of NRFeOx in comparison with abiotic and microaerophilic iron(II) oxidation in close proximity to rice roots could be elaborated. To visualize the microbial community members in culture HP and their spatial distribution in the rhizotrons, fluorescence in-situ hybridization (FISH) probes designed for individual members of the community can be used. This approach would provide valuable insights into the local distribution of microorganisms involved in nitrate-dependent iron(II) oxidation in the environment. Additionally, metagenomic analysis of culture HP is necessary (and ongoing, in collaboration with Dr. Cristina Escudero) to obtain the complete genome, which will further enhance our understanding of the functional potential of the microbial community.

3.4 Unraveling Complexity: The Critical Role of Rice Plants in Paddy Soil Experiments

In this PhD thesis, we gained a mechanistic understanding of complex biogeochemical processes by simplifying the paddy soil system. As a consequence, we neglected plant-specific processes that could influence NRFeOx and thus arsenic mobility and N_2O production.

To address this issue, several different experimental approaches could be used that are outlined in the following. In soil cores (Figure 3.9), rhizonsamplers could be inserted as artificial roots (after Keiluweit et al. (2015)[114] or Sokol and Bradford (2019)[115]) to introduce oxygen and/or model root exudates (e.g. mix of amino acids, glucose, mannose, galactose, malic acids, citric acid, etc.) into the soil, to generate rhizosphere-like conditions. By this, the impact of either oxygen or root exudates (or both, if combined) on iron mineral (trans-)formation, arsenic (im-)mobilization, and N_2O emissions between rhizosphere and bulk soil will be identified. Furthermore, this soil core setup will allow us to identify vertical gradients within the paddy soil by applying microelectrode measurements and porewater sampling (via rhizonsampler) at different depths.

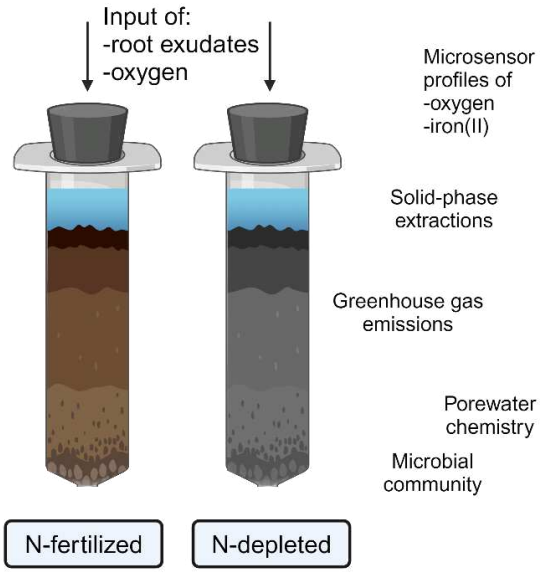

Figure 3.9. Schematics of future experiments in soil cores that aim to simulate and account for plant-specific processes and its impact on nitrate-dependent iron(II) oxidation and ultimately, arsenic mobility, and N_2O production.

In a follow-up experiment, plant pots could be used to reflect more natural paddy soil conditions and to include plant-induced processes. Here, rice plants can be grown over one cultivation period until harvest to identify crucial growth stages for arsenic mobilization and N_2O emissions (Figure 3.10). At the end or ideally at different growth stages, paddy soil and porewater samples will be taken and analyzed. Gas emission will be regularly followed to conclude on N_2O production and CH_4 emissions. After harvesting rice plants, arsenic will be determined in tissue and grains to estimate the health risk. In paddy soils, synchrotron-based XAS experiments on the As and Fe K-edge in combination with geochemical, mineralogical, and molecular biology analyses can be used to a) identify present and forming iron mineral phases, b) associated arsenic species and shifts in arsenic binding environment, and c) linked to microbial processes to mechanistically understand differences in the mobilization process of arsenic before, during, and after N fertilization (Figure 3.10).

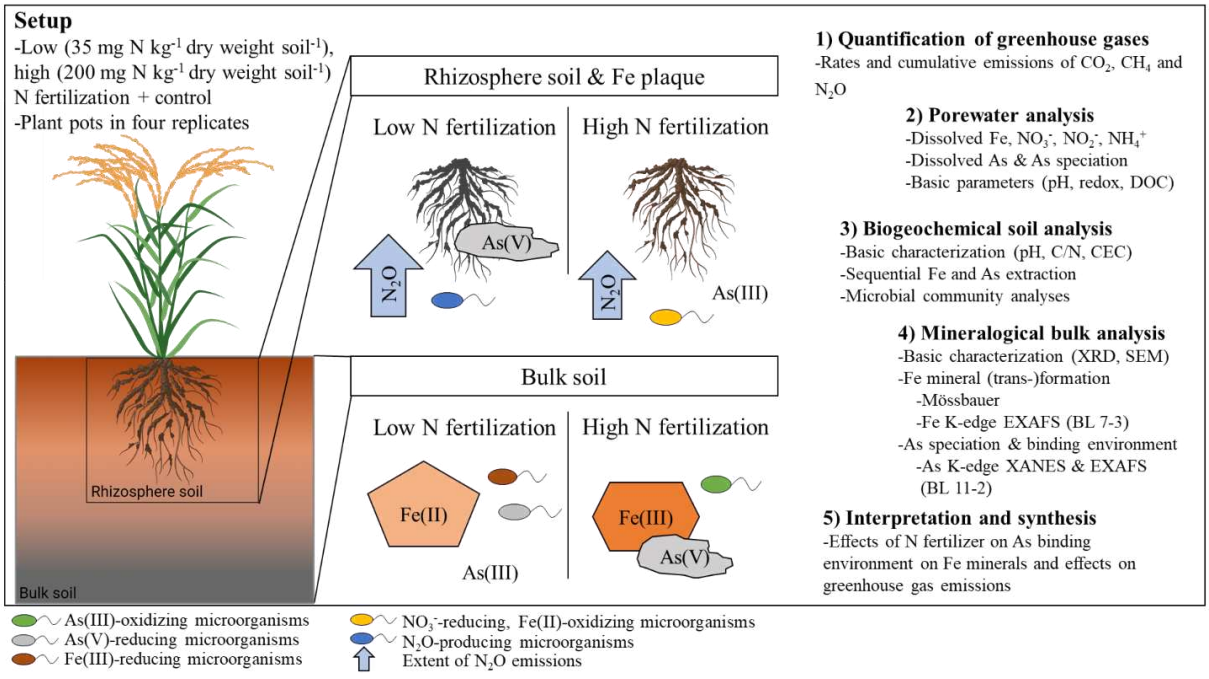

Figure 3.10. Experimental design of rice plant-based fertilization experiments linking greenhouse gas emissions (1) to biogeochemical (2, 3) and mineralogical analysis (4) to conclude on effects of nitrogen fertilization on arsenic mobility and greenhouse gas emissions (5). Created with BioRender.com.

3.5 A Balancing Act: How Can We Simultaneously Reduce Nitrous Oxide Emissions and Arsenic Mobility in Paddy Soils?

Within this PhD thesis, we gained valuable insights into the dynamics of arsenic and N_2O after nitrogen fertilization and the role of microorganisms. Based on the results, we hypothesize that autotrophic NRFeOx can occur in paddy soils, with *Gallionella* sp. being the microbial key players (Figure 3.11). However, *Dechloromonas* sp., *Acidovorax* sp. and *Zoogloea* sp. were found to play a great role in mixotrophic denitrification and thus, could play an important role in the paddy soil where organic carbon is available. In all of these processes iron(III) minerals are formed that can potentially scavenge arsenic from the paddy soil porewater and limit the uptake in rice plants.

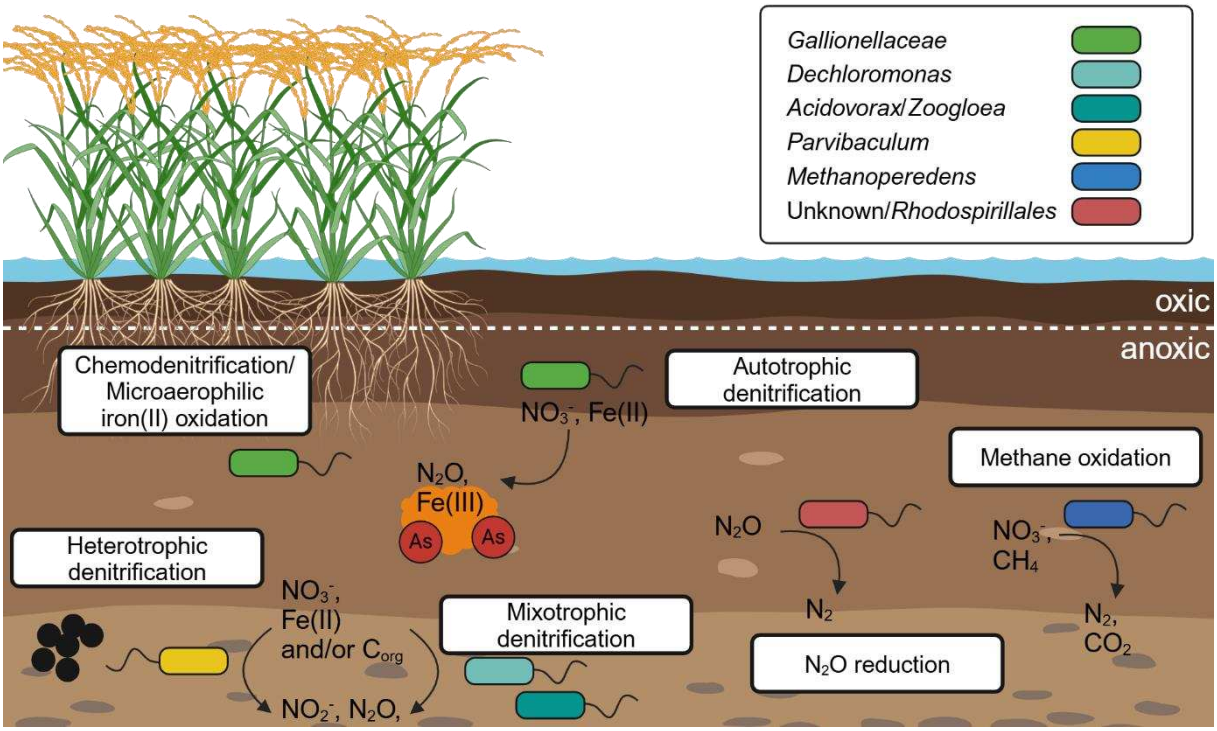

Figure 3.11. Schematic overview of ecological niches of different microorganisms relevant for nitrate reduction or iron(II) oxidation. Different microorganisms are highlighted in different colors and black dots represent organic carbon compounds. Iron minerals and their impact on arsenic scavenging are representatively shown for autotrophic denitrification.

In the case of iron(II) limitation or high availability of organic carbon, heterotrophic denitrifying bacteria, such as *Parvibaculum* sp. could be highly relevant for nitrate reduction in paddy soils (Figure 3.11). From the microcosm study in **Grimm et al. (2024a)**[82] we further conclude that microorganisms of the order *Rhodospirillales* could be relevant for N_2O reduction, however, unknown key players ought to be enriched or isolated. And last, *Methanoperedens* could also play an important role for nitrate reduction by coupling nitrate reduction and methane oxidation in paddy soils (Figure 3.11).

The findings in this PhD thesis have expanded our understanding of the effects of nitrogen fertilizer on arsenic mobility and N_2O production when applied at varying concentrations and times to paddy soil. We identified key microbial players involved in NRFeOx and successfully enriched these organisms in a culture that was further characterized (extent of nitrate reduction, iron(II) oxidation, N_2O production, microbial community composition, different growth conditions, etc.). Through numerical modeling, we quantified the contributions of abiotic and enzymatic processes influencing iron(II) oxidation and N_2O production under different growth conditions. With the presented results, we were not yet successful to simultaneously minimize N_2O production and arsenic mobility. We hypothesize that the interplay of microbial species, supplements such as biochar or root exudates, fertilizer type, quantity, and frequency, and the paddy soil influence this pressing issue. Several questions ought to be investigated, as NRFeOx and its impact on arsenic and N_2O production are highly soil-specific. A comprehensive understanding can only be achieved through the integration of diverse techniques including laboratory and field experiments, molecular biology approaches, and numerical modeling. This multidisciplinary approach is essential for predicting abiotic and biotic processes in the environment, which is crucial for assessing potential risks to human and environmental health. The results from the experiments and numerical modelling conducted in the framework of this PhD thesis, together with the results of the illustrated future experiments can be further used to feed a numerical reaction model that can ultimately answer the question, how we can simultaneously minimize N_2O emissions and arsenic mobilization in paddy soils.

References

(1) Searchinger, T.; Waite, R.; Hanson, C.; Ranganathan, J.; Dumas, P.; Matthews, E.; Klirs, C. Creating a Sustainable Food Future: A Menu of Solutions to Feed Nearly 10 Billion People by 2050. Final Report, 2019. https://agritrop.cirad.fr/593176/1/WRR_Food_Full_Report_0.pdf (accessed 2024-09-25).

(2) Alexandratos, N.; Bruinsma, J. World Agriculture towards 2030/2050: The 2012 Revision. **2012**.

(3) Rask, K. J.; Rask, N. Economic Development and Food Production–Consumption Balance: A Growing Global Challenge. *Food Policy* **2011**, *36* (2), 186–196.

(4) Delgado, C. L. Rising Consumption of Meat and Milk in Developing Countries Has Created a New Food Revolution. *J. Nutr.* **2003**, *133* (11), 3907S-3910S.

(5) Evans, A. The Feeding of the Nine Billion. *Glob. Food Secur. 21st Century Chatham House Rep. Www Chathamhouse Orgukfiles13179r0109 Accessed* **2009**, *8*.

(6) Nadeau, K. C.; Agache, I.; Jutel, M.; Annesi Maesano, I.; Akdis, M.; Sampath, V.; D'Amato, G.; Cecchi, L.; Traidl-Hoffmann, C.; Akdis, C. A. Climate Change: A Call to Action for the United Nations. *Allergy* **2022**, *77* (4), 1087–1090. https://doi.org/10.1111/all.15079.

(7) Karousakis, K. Incentives to Reduce GHG Emissions from Deforestation: Lessons Learned from Costa Rica and Mexico. *OECD Pap.* **2007**, *7* (1), 1–50. https://doi.org/10.1787/oecd_papers-v7-art1-en.

(8) van Dijk, M.; Morley, T.; Rau, M. L.; Saghai, Y. A Meta-Analysis of Projected Global Food Demand and Population at Risk of Hunger for the Period 2010–2050. *Nat. Food* **2021**, *2* (7), 494–501. https://doi.org/10.1038/s43016-021-00322-9.

(9) Aggarwal, P. K.; Singh, A. K. Implications of Global Climatic Change on Water and Food Security. In *Global Change: Impacts on Water and food Security*; Ringler, C., Biswas, A. K., Cline, S., Eds.; Water Resources Development and Management; Springer Berlin Heidelberg: Berlin, Heidelberg, 2010; pp 49–63. https://doi.org/10.1007/978-3-642-04615-5_3.

(10) Khedun, C. P.; Singh, V. P. Climate Change, Water, and Health: A Review of Regional Challenges. *Water Qual. Expo. Health* **2014**, *6* (1–2), 7–17. https://doi.org/10.1007/s12403-013-0107-1.

(11) Lal, R. Soil Degradation as a Reason for Inadequate Human Nutrition. *Food Secur.* **2009**, *1* (1), 45–57. https://doi.org/10.1007/s12571-009-0009-z.

(12) Brown, T. C.; Mahat, V.; Ramirez, J. A. Adaptation to Future Water Shortages in the United States Caused by Population Growth and Climate Change. *Earths Future* **2019**, *7* (3), 219–234. https://doi.org/10.1029/2018EF001091.

(13) UN General Assembly. Transforming Our World : The 2030 Agenda for Sustainable Development. **2015**, A/RES/70/1.

(14) FAO. Agricultural Production Statistics 2000–2021. **2022**. https://doi.org/10.4060/cc3751en.

(15) Seck, P. A.; Diagne, A.; Mohanty, S.; Wopereis, M. C. S. Crops That Feed the World 7: Rice. *Food Secur.* **2012**, *4* (1), 7–24. https://doi.org/10.1007/s12571-012-0168-1.

(16) Kapaj, S.; Peterson, H.; Liber, K.; Bhattacharya, P. Human Health Effects From Chronic Arsenic Poisoning–A Review. *J. Environ. Sci. Health Part A* **2006**, *41* (10), 2399–2428. https://doi.org/10.1080/10934520600873571.

(17) Kumarathilaka, P.; Seneweera, S.; Meharg, A.; Bundschuh, J. Arsenic Speciation Dynamics in Paddy Rice Soil-Water Environment: Sources, Physico-Chemical, and Biological Factors-a Review. *Water Res.* **2018**, *140*, 403–414.

(18) Muehe, E. M.; Kappler, A. Arsenic Mobility and Toxicity in South and South-East Asia – a Review on Biogeochemistry, Health and Socio-Economic Effects, Remediation and Risk Predictions. *Environ. Chem.* **2014**, *11* (5), 483. https://doi.org/10.1071/EN13230.

(19) Ponnamperuma, F. N. The Chemistry of Submerged Soils. *Adv. Agron.* **1972**, *24*, 29–96. https://doi.org/10.1016/S0065-2113(08)60633-1.

(20) Takahashi, Y.; Minamikawa, R.; Hattori, K. H.; Kurishima, K.; Kihou, N.; Yuita, K. Arsenic Behavior in Paddy Fields during the Cycle of Flooded and Non-Flooded Periods. *Environ. Sci. Technol.* **2004**, *38* (4), 1038–1044. https://doi.org/10.1021/es034383n.

(21) Huhmann, B. L.; Harvey, C. F.; Uddin, A.; Choudhury, I.; Ahmed, K. M.; Duxbury, J. M.; Bostick, B. C.; Van Geen, A. Field Study of Rice Yield Diminished by Soil Arsenic in Bangladesh. *Environ. Sci. Technol.* **2017**, *51* (20), 11553–11560. https://doi.org/10.1021/acs.est.7b01487.

(22) Muehe, E. M.; Wang, T.; Kerl, C. F.; Planer-Friedrich, B.; Fendorf, S. Rice Production Threatened by Coupled Stresses of Climate and Soil Arsenic. *Nat. Commun.* **2019**, *10* (1), 4985. https://doi.org/10.1038/s41467-019-12946-4.

(23) Ansar, M.; Ardiani, F.; Yusoff, S. F. Minimizing Weed Competition through Waterlogging in Rice (Oryza Sativa) under Various Soil Types. *Res. Crops* **2022**, *23* (4), 755–762.

(24) Van Nguyen, N.; Ferrero, A. Meeting the Challenges of Global Rice Production. *Paddy Water Environ.* **2006**, *4* (1), 1–9. https://doi.org/10.1007/s10333-005-0031-5.

(25) Bin Rahman, A. N. M. R.; Zhang, J. Trends in Rice Research: 2030 and Beyond. *Food Energy Secur.* **2023**, *12* (2), e390. https://doi.org/10.1002/fes3.390.

(26) Evenson, R. E.; Gollin, D. Assessing the Impact of the Green Revolution, 1960 to 2000. *Science* **2003**, *300* (5620), 758–762. https://doi.org/10.1126/science.1078710.

(27) Intergovernmental Panel on Climate Change (IPCC). The Physical Science Basis. Contribution of Working Group I to the Sixth Assessment Report of the Intergovernmental Panel on Climate Change. *Camb. Univ. Press* **2021**, 923–1054. https://doi.org/10.1017/9781009157896.

(28) Guenet, B.; Gabrielle, B.; Chenu, C.; Arrouays, D.; Balesdent, J.; Bernoux, M.; Bruni, E.; Caliman, J.-P.; Cardinael, R.; Chen, S.; Ciais, P.; Desbois, D.; Fouche, J.; Frank, S.; Henault, C.; Lugato, E.; Naipal, V.; Nesme, T.; Obersteiner, M.; Pellerin, S.; Powlson, D. S.; Rasse, D. P.; Rees, F.; Soussana, J.-F.; Su, Y.; Tian, H.; Valin, H.; Zhou, F. Can N2O Emissions Offset the Benefits from Soil Organic Carbon Storage? *Glob. Change Biol.* **2021**, *27* (2), 237–256. https://doi.org/10.1111/gcb.15342.

(29) Carlson, K. M.; Gerber, J. S.; Mueller, N. D.; Herrero, M.; MacDonald, G. K.; Brauman, K. A.; Havlik, P.; O'Connell, C. S.; Johnson, J. A.; Saatchi, S.; West,

P. C. Greenhouse Gas Emissions Intensity of Global Croplands. *Nat. Clim. Change* **2017**, *7* (1), 63–68. https://doi.org/10.1038/nclimate3158.

(30) Liu, Y.; Ge, T.; van Groenigen, K. J.; Yang, Y.; Wang, P.; Cheng, K.; Zhu, Z.; Wang, J.; Li, Y.; Guggenberger, G.; Sardans, J.; Penuelas, J.; Wu, J.; Kuzyakov, Y. Rice Paddy Soils Are a Quantitatively Important Carbon Store According to a Global Synthesis. *Commun. Earth Environ.* **2021**, *2* (1), 1–9. https://doi.org/10.1038/s43247-021-00229-0.

(31) Cai, Z.; Xing, G.; Yan, X.; Xu, H.; Tsuruta, H.; Yagi, K.; Minami, K. Methane and Nitrous Oxide Emissions from Rice Paddy Fields as Affected by Nitrogen Fertilisers and Water Management. *Plant Soil* **1997**, *196* (1), 7–14. https://doi.org/10.1023/A:1004263405020.

(32) Zhao, X.; Pu, C.; Ma, S.-T.; Liu, S.-L.; Xue, J.-F.; Wang, X.; Wang, Y.-Q.; Li, S.-S.; Lal, R.; Chen, F.; Zhang, H.-L. Management-Induced Greenhouse Gases Emission Mitigation in Global Rice Production. *Sci. Total Environ.* **2019**, *649*, 1299–1306. https://doi.org/10.1016/j.scitotenv.2018.08.392.

(33) Han, B.; Chen, W.-Q.; Jiao, Y.-Q.; Yang, R.; Niu, L.-L.; Chen, X.-R.; Ji, C.-Y.; Yin, D.-X. Effects of Nitrogen Fertilizer Application on Soil Properties and Arsenic Mobilization in Paddy Soil. *Sustainability* **2024**, *16* (13), 5565. https://doi.org/10.3390/su16135565.

(34) Liu, L.; Shen, R.-L.; Zhao, Z.-Q.; Ding, L.-J.; Cui, H.-L.; Li, G.; Yang, Y.-P.; Duan, G.-L.; Zhu, Y.-G. How Different Nitrogen Fertilizers Affect Arsenic Mobility in Paddy Soil after Straw Incorporation? *J. Hazard. Mater.* **2022**, *436*, 129135. https://doi.org/10.1016/j.jhazmat.2022.129135.

(35) Chen, X.-P.; Zhu, Y.-G.; Hong, M.-N.; Kappler, A.; Xu, Y.-X. Effects of Different Forms of Nitrogen Fertilizers on Arsenic Uptake by Rice Plants. *Environ. Toxicol. Chem.* **2008**, *27* (4), 881–887. https://doi.org/10.1897/07-368.1.

(36) Chen, G.; Du, Y.; Fang, L.; Wang, X.; Liu, C.; Yu, H.; Feng, M.; Chen, X.; Li, F. Distinct Arsenic Uptake Feature in Rice Reveals the Importance of N Fertilization Strategies. *Sci. Total Environ.* **2023**, *854*, 158801.

(37) Lin, Z.; Wang, X.; Wu, X.; Liu, D.; Yin, Y.; Zhang, Y.; Xiao, S.; Xing, B. Nitrate Reduced Arsenic Redox Transformation and Transfer in Flooded Paddy Soil-Rice System. *Environ. Pollut.* **2018**, *243*, 1015–1025.

(38) Nishimura, S.; Sawamoto, T.; Akiyama, H.; Sudo, S.; Yagi, K. Methane and Nitrous Oxide Emissions from a Paddy Field with Japanese Conventional Water Management and Fertilizer Application. *Glob. Biogeochem. Cycles* **2004**, *18* (2), 2003GB002207. https://doi.org/10.1029/2003GB002207.

(39) Hua, X.; Guangxi, X.; Cai, Z.-C.; Tsuruta, H. Nitrous Oxide Emissions from Three Rice Paddy Fields in China. *Nutr. Cycl. Agroecosystems* **1997**, *49* (1), 23–28. https://doi.org/10.1023/A:1009779514395.

(40) Wang, F.; Zhang, J.; Zeng, Y.; Wang, H.; Zhao, X.; Chen, Y.; Deng, H.; Ge, L.; Dahlgren, R. A.; Gao, H.; Chen, Z. Arsenic Mobilization and Nitrous Oxide Emission Modulation by Different Nitrogen Management Strategies in Flooded Ammonia-Enriched Paddy Soils. *Pedosphere* **2023**. https://doi.org/10.1016/j.pedsph.2023.09.008.

(41) Wang, F.; Zhang, J.; Hu, J.; Wang, H.; Zeng, Y.; Wang, Y.; Huang, P.; Deng, H.; Dahlgren, R. A.; Gao, H.; Chen, Z. Simultaneous Suppression of As Mobilization and N2O Emission from NH4+/As-Rich Paddy Soils by Combined Nitrate and Birnessite Amendment. *J. Hazard. Mater.* **2024**, *465*, 133451. https://doi.org/10.1016/j.jhazmat.2024.133451.

(42) Gao, S.; Tanji, K. K.; Scardaci, S. C.; Chow, A. T. Comparison of Redox Indicators in a Paddy Soil during Rice-Growing Season. *Soil Sci. Soc. Am. J.* **2002**, *66* (3), 805–817. https://doi.org/10.2136/sssaj2002.8050.

(43) Liu, L.; Zheng, N.; Yu, Y.; Zheng, Z.; Yao, H. Soil Carbon and Nitrogen Cycles Driven by Iron Redox: A Review. *Sci. Total Environ.* **2024**, *918*, 170660. https://doi.org/10.1016/j.scitotenv.2024.170660.

(44) Brooks, S. C.; Jardine, P. M.; Taylor, D. L. Thermodynamics of Bromide Exchange on Ferrihydrite: Implications for Bromide Transport. *Soil Sci. Soc. Am. J.* **1998**.

(45) Kappler, A.; Straub, K. Geomicrobiological Cycling of Iron. *Rev. Mineral. Geochem.* **2005**, *59* (1), 85–108. https://doi.org/10.2138/rmg.2005.59.5.

(46) Lai, W.-L.; Zhang, Y.; Chen, Z.-H. Radial Oxygen Loss, Photosynthesis, and Nutrient Removal of 35 Wetland Plants. *Ecol. Eng.* **2012**, *39*, 24–30.

(47) Colmer, T. D. Long-distance Transport of Gases in Plants: A Perspective on Internal Aeration and Radial Oxygen Loss from Roots. *Plant Cell Environ.* **2003**, *26* (1), 17–36. https://doi.org/10.1046/j.1365-3040.2003.00846.x.

(48) Li, H.; Ye, Z. H.; Wei, Z. J.; Wong, M. H. Root Porosity and Radial Oxygen Loss Related to Arsenic Tolerance and Uptake in Wetland Plants. *Environ. Pollut.* **2011**, *159* (1), 30–37.

(49) Maisch, M.; Lueder, U.; Kappler, A.; Schmidt, C. Iron Lung: How Rice Roots Induce Iron Redox Changes in the Rhizosphere and Create Niches for Microaerophilic Fe(II)-Oxidizing Bacteria. *Environ. Sci. Technol. Lett.* **2019**, *6* (10), 600–605. https://doi.org/10.1021/acs.estlett.9b00403.

(50) Wang, X.; Yao, H.; Wong, M. H.; Ye, Z. Dynamic Changes in Radial Oxygen Loss and Iron Plaque Formation and Their Effects on Cd and As Accumulation in Rice (Oryza Sativa L.). *Environ. Geochem. Health* **2013**, *35* (6), 779–788. https://doi.org/10.1007/s10653-013-9534-y.

(51) Ratering, S.; Schnell, S. Nitrate-Dependent Iron(II) Oxidation in Paddy Soil. *Environ. Microbiol.* **2001**, *3* (2), 100–109. https://doi.org/10.1046/j.1462-2920.2001.00163.x.

(52) Melton, E. D.; Swanner, E. D.; Behrens, S.; Schmidt, C.; Kappler, A. The Interplay of Microbially Mediated and Abiotic Reactions in the Biogeochemical Fe Cycle. *Nat. Rev. Microbiol.* **2014**, *12* (12), 797–808. https://doi.org/10.1038/nrmicro3347.

(53) Knowles, R. Denitrification. *Microbiol. Rev.* **1982**, *46* (1), 43–70. https://doi.org/10.1128/mr.46.1.43-70.1982.

(54) Rivett, M. O.; Buss, S. R.; Morgan, P.; Smith, J. W. N.; Bemment, C. D. Nitrate Attenuation in Groundwater: A Review of Biogeochemical Controlling Processes. *Water Res.* **2008**, *42* (16), 4215–4232. https://doi.org/10.1016/j.watres.2008.07.020.

(55) Kraft, B.; Tegetmeyer, H. E.; Sharma, R.; Klotz, M. G.; Ferdelman, T. G.; Hettich, R. L.; Geelhoed, J. S.; Strous, M. Nitrogen Cycling. The Environmental Controls That Govern the End Product of Bacterial Nitrate Respiration. *Science* **2014**, *345* (6197), 676–679. https://doi.org/10.1126/science.1254070.

(56) Schmidt, H.; Eickhorst, T. Spatio-Temporal Variability of Microbial Abundance and Community Structure in the Puddled Layer of a Paddy Soil Cultivated with Wetland Rice (*Oryza Sativa* L.). *Appl. Soil Ecol.* **2013**, *72*, 93–102. https://doi.org/10.1016/j.apsoil.2013.06.002.

(57) Wang, X.; Teng, Y.; Ren, W.; Li, Y.; Yang, T.; Chen, Y.; Zhao, L.; Zhang, H.; Kuramae, E. E. Variations of Bacterial and Diazotrophic Community Assemblies throughout the Soil Profile in Distinct Paddy Soil Types and Their Contributions to Soil Functionality. *mSystems* **2022**, *7* (2), e01047-21. https://doi.org/10.1128/msystems.01047-21.

(58) Lovley, D. R.; Stolz, J. F.; Nord, G. L.; Phillips, E. J. P. Anaerobic Production of Magnetite by a Dissimilatory Iron-Reducing Microorganism. *Nature* **1987**, *330* (6145), 252–254. https://doi.org/10.1038/330252a0.

(59) Lovley, D. R.; Phillips, E. J. P. Novel Mode of Microbial Energy Metabolism: Organic Carbon Oxidation Coupled to Dissimilatory Reduction of Iron or Manganese. *Appl. Environ. Microbiol.* **1988**, *54* (6), 1472–1480. https://doi.org/10.1128/aem.54.6.1472-1480.1988.

(60) Lovley, D. R. Microbial Fe(III) Reduction in Subsurface Environments. *FEMS Microbiol. Rev.* **1997**, *20* (3–4), 305–313. https://doi.org/10.1111/j.1574-6976.1997.tb00316.x.

(61) Aromokeye, D. A.; Kulkarni, A. C.; Elvert, M.; Wegener, G.; Henkel, S.; Coffinet, S.; Eickhorst, T.; Oni, O. E.; Richter-Heitmann, T.; Schnakenberg, A.; Taubner, H.; Wunder, L.; Yin, X.; Zhu, Q.; Hinrichs, K.-U.; Kasten, S.; Friedrich, M. W. Rates and Microbial Players of Iron-Driven Anaerobic Oxidation of Methane in Methanic Marine Sediments. *Front. Microbiol.* **2020**, *10*. https://doi.org/10.3389/fmicb.2019.03041.

(62) Ettwig, K. F.; Zhu, B.; Speth, D.; Keltjens, J. T.; Jetten, M. S. M.; Kartal, B. Archaea Catalyze Iron-Dependent Anaerobic Oxidation of Methane. *Proc. Natl. Acad. Sci.* **2016**, *113* (45), 12792–12796. https://doi.org/10.1073/pnas.1609534113.

(63) Di Capua, F.; Pirozzi, F.; Lens, P. N. L.; Esposito, G. Electron Donors for Autotrophic Denitrification. *Chem. Eng. J.* **2019**, *362*, 922–937. https://doi.org/10.1016/j.cej.2019.01.069.

(64) Khalifa, A.; Nakasuji, Y.; Saka, N.; Honjo, H.; Asakawa, S.; Watanabe, T. Ferrigenium Kumadai Gen. Nov., Sp. Nov., a Microaerophilic Iron-Oxidizing Bacterium Isolated from a Paddy Field Soil. *Int. J. Syst. Evol. Microbiol.* **2018**, *68* (8), 2587–2592. https://doi.org/10.1099/ijsem.0.002882.

(65) Hu, M.; Chen, P.; Sun, W.; Li, F.; Cui, J. A Novel Organotrophic Nitrate-Reducing Fe(Ii)-Oxidizing Bacterium Isolated from Paddy Soil and Draft Genome Sequencing Indicate Its Metabolic Versatility. *RSC Adv.* **2017**, *7* (89), 56611–56620. https://doi.org/10.1039/C7RA09328D.

(66) Li, S.; Li, X.; Li, F. Fe(II) Oxidation and Nitrate Reduction by a Denitrifying Bacterium, Pseudomonas Stutzeri LS-2, Isolated from Paddy Soil. *J. Soils Sediments* **2018**, *18* (4), 1668–1678. https://doi.org/10.1007/s11368-017-1883-1.

(67) Li, X.; Zhang, W.; Liu, T.; Chen, L.; Chen, P.; Li, F. Changes in the Composition and Diversity of Microbial Communities during Anaerobic Nitrate Reduction and Fe(II) Oxidation at Circumneutral pH in Paddy Soil. *Soil Biol. Biochem.* **2016**, *94*, 70–79. https://doi.org/10.1016/j.soilbio.2015.11.013.

(68) Pan, D.; Chen, P.; Yang, G.; Niu, R.; Bai, Y.; Cheng, K.; Huang, G.; Liu, T.; Li, X.; Li, F. Fe(II) Oxidation Shaped Functional Genes and Bacteria Involved in Denitrification and Dissimilatory Nitrate Reduction to Ammonium from Different Paddy Soils. *Environ. Sci. Technol.* **2023**, *57* (50), 21156–21167. https://doi.org/10.1021/acs.est.3c06337.

(69) Tong, H.; Li, J.; Chen, M.; Fang, Y.; Yi, X.; Dong, L.; Jiang, Q.; Liu, C. Iron Oxidation Coupled with Nitrate Reduction Affects the Acetate-Assimilating Microbial Community Structure Elucidated by Stable Isotope Probing in Flooded Paddy Soil. *Soil Biol. Biochem.* **2023**, *183*, 109059. https://doi.org/10.1016/j.soilbio.2023.109059.

(70) Jakus, N.; Blackwell, N.; Osenbrück, K.; Straub, D.; Byrne, J. M.; Wang, Z.; Glöckler, D.; Elsner, M.; Lueders, T.; Grathwohl, P.; Kleindienst, S.; Kappler, A. Nitrate Removal by a Novel Lithoautotrophic Nitrate-Reducing, Iron(II)-Oxidizing Culture Enriched from a Pyrite-Rich Limestone Aquifer. *Appl. Environ. Microbiol.* **2021**, *87* (16), e0046021. https://doi.org/10.1128/AEM.00460-21.

(71) Straub, K. L.; Benz, M.; Schink, B.; Widdel, F. Anaerobic, Nitrate-Dependent Microbial Oxidation of Ferrous Iron. *Appl. Environ. Microbiol.* **1996**, *62* (4), 1458–1460. https://doi.org/10.1128/aem.62.4.1458-1460.1996.

(72) Huang, Y.-M.; Straub, D.; Kappler, A.; Smith, N.; Blackwell, N.; Kleindienst, S. A Novel Enrichment Culture Highlights Core Features of Microbial Networks Contributing to Autotrophic Fe(II) Oxidation Coupled to Nitrate Reduction. *Microb. Physiol.* **2021**, *31* (3), 280–295. https://doi.org/10.1159/000517083.

(73) Huang, J.; Mellage, A.; Garcia, J. P.; Glöckler, D.; Mahler, S.; Elsner, M.; Jakus, N.; Mansor, M.; Jiang, H.; Kappler, A. Metabolic Performance and Fate of Electrons during Nitrate-Reducing Fe(II) Oxidation by the Autotrophic Enrichment Culture KS Grown at Different Initial Fe/N Ratios. *Appl. Environ. Microbiol.* **2023**, *89* (3), e00196-23. https://doi.org/10.1128/aem.00196-23.

(74) Huang, Y.-M.; Jakus, N.; Straub, D.; Konstantinidis, K. T.; Blackwell, N.; Kappler, A.; Kleindienst, S. “Candidatus Ferrigenium Straubiae” Sp. Nov., “Candidatus Ferrigenium Bremense” Sp. Nov., “Candidatus Ferrigenium Altingense” Sp. Nov., Are Autotrophic Fe(II)-Oxidizing Bacteria of the Family Gallionellaceae. *Syst. Appl. Microbiol.* **2022**, *45* (3), 126306. https://doi.org/10.1016/j.syapm.2022.126306.

(75) Jamieson, J.; Prommer, H.; Kaksonen, A. H.; Sun, J.; Siade, A. J.; Yusov, A.; Bostick, B. Identifying and Quantifying the Intermediate Processes during Nitrate-Dependent Iron(II) Oxidation. *Environ. Sci. Technol.* **2018**, *52* (10), 5771–5781. https://doi.org/10.1021/acs.est.8b01122.

(76) Dopffel, N.; Jamieson, J.; Bryce, C.; Joshi, P.; Mansor, M.; Siade, A.; Prommer, H.; Kappler, A. Temperature Dependence of Nitrate-Reducing Fe(II) Oxidation by Acidovorax Strain BoFeN1 - Evaluating the Role of Enzymatic vs. Abiotic Fe(II) Oxidation by Nitrite. *FEMS Microbiol. Ecol.* **2022**, *97* (12). https://doi.org/10.1093/femsec/fiab155.

(77) Chen, G.; Chen, D.; Li, F.; Liu, T.; Zhao, Z.; Cao, F. Dual Nitrogen-Oxygen Isotopic Analysis and Kinetic Model for Enzymatic Nitrate Reduction Coupled with Fe(II) Oxidation by Pseudogulbenkiania Sp. Strain 2002. *Chem. Geol.* **2020**, *534*, 119456. https://doi.org/10.1016/j.chemgeo.2019.119456.

(78) Chen, D.; Liu, T.; Li, X.; Li, F.; Luo, X.; Wu, Y.; Wang, Y. Biological and Chemical Processes of Microbially Mediated Nitrate-Reducing Fe(II) Oxidation by *Pseudogulbenkiania* Sp. Strain 2002. *Chem. Geol.* **2018**, *476*, 59–69. https://doi.org/10.1016/j.chemgeo.2017.11.004.

(79) Liu, T.; Chen, D.; Luo, X.; Li, X.; Li, F. Microbially Mediated Nitrate-Reducing Fe(II) Oxidation: Quantification of Chemodenitrification and Biological Reactions. *Geochim. Cosmochim. Acta* **2019**, *256*, 97–115. https://doi.org/10.1016/j.gca.2018.06.040.

(80) Buchwald, C.; Grabb, K.; Hansel, C. M.; Wankel, S. D. Constraining the Role of Iron in Environmental Nitrogen Transformations: Dual Stable Isotope Systematics of Abiotic NO2− Reduction by Fe(II) and Its Production of N2O. *Geochim. Cosmochim. Acta* **2016**, *186*, 1–12. https://doi.org/10.1016/j.gca.2016.04.041.

(81) Tian, H.; Xu, R.; Canadell, J. G.; Thompson, R. L.; Winiwarter, W.; Suntharalingam, P.; Davidson, E. A.; Ciais, P.; Jackson, R. B.; Janssens-Maenhout, G.; Prather, M. J.; Regnier, P.; Pan, N.; Pan, S.; Peters, G. P.; Shi, H.; Tubiello, F. N.; Zaehle, S.; Zhou, F.; Arneth, A.; Battaglia, G.; Berthet, S.; Bopp, L.; Bouwman, A. F.; Buitenhuis, E. T.; Chang, J.; Chipperfield, M. P.; Dangal, S. R. S.; Dlugokencky, E.; Elkins, J. W.; Eyre, B. D.; Fu, B.; Hall, B.; Ito, A.; Joos, F.; Krummel, P. B.; Landolfi, A.; Laruelle, G. G.; Lauerwald, R.; LI, W.; Lienert, S.; Maavara, T.; MacLeod, M.; Millet, D. B.; Olin, S.; Patra, P. K.; Prinn, R. G.; Raymond, P. A.; Ruiz, D. J.; van der Werf, G. R.; Vuichard, N.; Wang, J.; Weiss, R. F.; Wells, K. C.; Wilson, C.; Yang, J.; Yao, Y. A Comprehensive Quantification of Global Nitrous Oxide Sources and Sinks. *Nature* **2020**, *586* (7828), 248–256. https://doi.org/10.1038/s41586-020-2780-0.

(82) Grimm, H.; Drabesch, S.; Nicol, A.; Straub, D.; Joshi, P.; Zarfl, C.; Planer-Friedrich, B.; Muehe, E. M.; Kappler, A. Arsenic Immobilization and Greenhouse Gas Emission Depend on Quantity and Frequency of Nitrogen Fertilization in Paddy Soil. *Heliyon* **2024**, *10* (16), e35706. https://doi.org/10.1016/j.heliyon.2024.e35706.

(83) Grimm, H.; Lorenz, J.; Straub, D.; Joshi, P.; Shuster, J.; Zarfl, C.; Muehe, E. M.; Kappler, A. Nitrous Oxide Is the Main Product during Nitrate Reduction by a

Novel Lithoautotrophic Iron(II)-Oxidizing Culture from an Organic-Rich Paddy Soil. *Appl. Environ. Microbiol.* **2024**, e01262-24. https://doi.org/10.1128/aem.01262-24.

(84) Grimm, H.; Gscheidel, P.; Boeckmann, M.; Straub, D.; Fischer, S.; Kappler, A.; Zarfl, C. Acetate Addition Shifts Community Composition and Extent of Chemodenitrification in a Lithoautotrophic Nitrate-Reducing Microbial Culture. **in prep.**

(85) Song, Y.; Lin, Y.; Chen, Z. Effect of Nitrogen Fertilizer Level on Bacterial Community and N2O Emission in Paddy Soil. *Chin. J. Eco-Agric.* **2017**, *25* (9), 1266–1275.

(86) Carrijo, D. R.; Akbar, N.; Reis, A. F.; Li, C.; Gaudin, A. C.; Parikh, S. J.; Green, P. G.; Linquist, B. A. Impacts of Variable Soil Drying in Alternate Wetting and Drying Rice Systems on Yields, Grain Arsenic Concentration and Soil Moisture Dynamics. *Field Crops Res.* **2018**, *222*, 101–110.

(87) Soliman, E.; Azam, R.; Hammad, S. A.; Mosa, A. A.; Mansour, M. M. Impacts of Alternate Wetting and Drying Technology on Water Use and Soil Nitrogen Transformations for Sustainable Rice Production: A Review. *J. Soil Sci. Agric. Eng.* **2024**, *0* (0), 151–163. https://doi.org/10.21608/jssae.2024.291648.1228.

(88) Wang, M.; Hu, R.; Ruser, R.; Schmidt, C.; Kappler, A. Role of Chemodenitrification for N2O Emissions from Nitrate Reduction in Rice Paddy Soils. *ACS Earth Space Chem.* **2020**, *4* (1), 122–132. https://doi.org/10.1021/acsearthspacechem.9b00296.

(89) Rivett, M. O.; Buss, S. R.; Morgan, P.; Smith, J. W. N.; Bemment, C. D. Nitrate Attenuation in Groundwater: A Review of Biogeochemical Controlling Processes. *Water Res.* **2008**, *42* (16), 4215–4232. https://doi.org/10.1016/j.watres.2008.07.020.

(90) Freitag, T. E.; Prosser, J. I. Correlation of Methane Production and Functional Gene Transcriptional Activity in a Peat Soil. *Appl. Environ. Microbiol.* **2009**, *75* (21), 6679–6687. https://doi.org/10.1128/AEM.01021-09.

(91) Ma, K.; Conrad, R.; Lu, Y. Responses of Methanogen mcrA Genes and Their Transcripts to an Alternate Dry/Wet Cycle of Paddy Field Soil. *Appl. Environ. Microbiol.* **2011**, *2* (78). https://doi.org/10.1128/AEM.06934-11.

(92) Luo, D.; Meng, X.; Zheng, N.; Li, Y.; Yao, H.; Chapman, S. J. The Anaerobic Oxidation of Methane in Paddy Soil by Ferric Iron and Nitrate, and the Microbial Communities Involved. *Sci. Total Environ.* **2021**, *788*, 147773. https://doi.org/10.1016/j.scitotenv.2021.147773.

(93) Beal, E. J.; House, C. H.; Orphan, V. J. Manganese- and Iron-Dependent Marine Methane Oxidation. *Science* **2009**, *325* (5937), 184–187. https://doi.org/10.1126/science.1169984.

(94) Glodowska, M.; Stopelli, E.; Schneider, M.; Rathi, B.; Straub, D.; Lightfoot, A.; Kipfer, R.; Berg, M.; Jetten, M.; Kleindienst, S.; Kappler, A. Arsenic Mobilization by Anaerobic Iron-Dependent Methane Oxidation. *Commun. Earth Environ.* **2020**, *1* (1), 1–7. https://doi.org/10.1038/s43247-020-00037-y.

(95) Wang, J.; Yao, X.; Jia, Z.; Zhu, L.; Zheng, P.; Kartal, B.; Hu, B. Nitrogen Input Promotes Denitrifying Methanotrophs' Abundance and Contribution to Methane Emission Reduction in Coastal Wetland and Paddy Soil. *Environ. Pollut.* **2022**, *302*, 119090. https://doi.org/10.1016/j.envpol.2022.119090.

(96) Vaksmaa, A.; Guerrero-Cruz, S.; Van Alen, T. A.; Cremers, G.; Ettwig, K. F.; Lüke, C.; Jetten, M. S. M. Enrichment of Anaerobic Nitrate-Dependent Methanotrophic 'Candidatus Methanoperedens Nitroreducens' Archaea from an Italian Paddy Field Soil. *Appl. Microbiol. Biotechnol.* **2017**, *101* (18), 7075–7084. https://doi.org/10.1007/s00253-017-8416-0.

(97) Ratzke, C.; Barrere, J.; Gore, J. Strength of Species Interactions Determines Biodiversity and Stability in Microbial Communities. *Nat. Ecol. Evol.* **2020**, *4* (3), 376–383. https://doi.org/10.1038/s41559-020-1099-4.

(98) Jakus, N.; Blackwell, N.; Osenbrück, K.; Straub, D.; Byrne, J. M.; Wang, Z.; Glöckler, D.; Elsner, M.; Lueders, T.; Grathwohl, P.; Kleindienst, S.; Kappler, A. Nitrate Removal by a Novel Lithoautotrophic Nitrate-Reducing, Iron(II)-Oxidizing Culture Enriched from a Pyrite-Rich Limestone Aquifer. *Appl. Environ. Microbiol.* **2021**, *87* (16), e0046021. https://doi.org/10.1128/AEM.00460-21.

(99) Zhou, J.; Bruns, M. A.; Tiedje, J. M. DNA Recovery from Soils of Diverse Composition. *Appl. Environ. Microbiol.* **1996**, *62* (2), 316–322. https://doi.org/10.1128/aem.62.2.316-322.1996.

(100) Widijanto, H.; Amalia, R. S.; Syamsiyah, J.; Suntoro. A Comparison of the Dynamics and Carbon Stocks in Rice Fields with Different Management Systems and Soil Types. *J. Arid. Agric.* **2023**, 31–38. https://doi.org/10.25081/jaa.2023.v9.8065.

(101) Harter, J.; Krause, H.-M.; Schuettler, S.; Ruser, R.; Fromme, M.; Scholten, T.; Kappler, A.; Behrens, S. Linking N2O Emissions from Biochar-Amended Soil to the Structure and Function of the N-Cycling Microbial Community. *ISME J.* **2014**, *8* (3), 660–674. https://doi.org/10.1038/ismej.2013.160.

(102) Sharma, N.; Flynn, E. D.; Catalano, J. G.; Giammar, D. E. Copper Availability Governs Nitrous Oxide Accumulation in Wetland Soils and Stream Sediments. *Geochim. Cosmochim. Acta* **2022**, *327*, 96–115. https://doi.org/10.1016/j.gca.2022.04.019.

(103) Hernandez, M. E.; Mitsch, W. J. Denitrification in Created Riverine Wetlands: Influence of Hydrology and Season. *Ecol. Eng.* **2007**, *30* (1), 78–88. https://doi.org/10.1016/j.ecoleng.2007.01.015.

(104) Vogel, A. L.; Thompson, K. J.; Kleindienst, S.; Zarfl, C. Dosage Concentration and Pulsing Frequency Affect the Degradation Efficiency in Simulated Bacterial Polycyclic Aromatic Hydrocarbon-Degrading Cultures. *Environ. Sci. Pollut. Res.* **2023**, *30* (21), 59813–59825. https://doi.org/10.1007/s11356-023-26546-9.

(105) Zhao, L.; Dong, H.; Edelmann, R. E.; Zeng, Q.; Agrawal, A. Coupling of Fe(II) Oxidation in Illite with Nitrate Reduction and Its Role in Clay Mineral Transformation. *Geochim. Cosmochim. Acta* **2017**, *200*, 353–366. https://doi.org/10.1016/j.gca.2017.01.004.

(106) Zhang, L.; Dong, H.; Kukkadapu, R. K.; Jin, Q.; Kovarik, L. Electron Transfer between Sorbed Fe(II) and Structural Fe(III) in Smectites and Its Effect on Nitrate-Dependent Iron Oxidation by Pseudogulbenkiania Sp. Strain 2002. *Geochim. Cosmochim. Acta* **2019**, *265*, 132–147. https://doi.org/10.1016/j.gca.2019.08.042.

(107) Hansel, C. M.; Benner, S. G.; Neiss, J.; Dohnalkova, A.; Kukkadapu, R. K.; Fendorf, S. Secondary Mineralization Pathways Induced by Dissimilatory Iron Reduction of Ferrihydrite under Advective Flow. *Geochim. Cosmochim. Acta* **2003**, *67* (16), 2977–2992. https://doi.org/10.1016/S0016-7037(03)00276-X.

(108) Weber, K. A.; Picardal, F. W.; Roden, E. E. Microbially Catalyzed Nitrate-Dependent Oxidation of Biogenic Solid-Phase Fe(II) Compounds. *Environ. Sci. Technol.* **2001**, *35* (8), 1644–1650. https://doi.org/10.1021/es0016598.

(109) Shelobolina, E.; Xu, H.; Konishi, H.; Kukkadapu, R.; Wu, T.; Blöthe, M.; Roden, E. Microbial Lithotrophic Oxidation of Structural Fe(II) in Biotite. *Appl. Environ. Microbiol.* **2012**, *78* (16), 5746–5752. https://doi.org/10.1128/AEM.01034-12.

(110) Jakus, N.; Mellage, A.; Höschen, C.; Maisch, M.; Byrne, J. M.; Mueller, C. W.; Grathwohl, P.; Kappler, A. Anaerobic Neutrophilic Pyrite Oxidation by a Chemolithoautotrophic Nitrate-Reducing Iron(II)-Oxidizing Culture Enriched from a Fractured Aquifer. *Environ. Sci. Technol.* **2021**, *55* (14), 9876–9884. https://doi.org/10.1021/acs.est.1c02049.

(111) Maisch, M.; Lueder, U.; Kappler, A.; Schmidt, C. From Plant to Paddy—How Rice Root Iron Plaque Can Affect the Paddy Field Iron Cycling. *Soil Syst.* **2020**, *4* (2), 28. https://doi.org/10.3390/soilsystems4020028.

(112) Chan, C. S.; Dykes, G. E.; Hoover, R. L.; Limmer, M. A.; Seyfferth, A. L. Gallionellaceae in Rice Root Plaque: Metabolic Roles in Iron Oxidation, Nutrient Cycling, and Plant Interactions. *Appl. Environ. Microbiol.* **2023**, *89* (12), e00570-23. https://doi.org/10.1128/aem.00570-23.

(113) Maisch, M.; Lueder, U.; Laufer, K.; Scholze, C.; Kappler, A.; Schmidt, C. Contribution of Microaerophilic Iron(II)-Oxidizers to Iron(III) Mineral Formation. *Environ. Sci. Technol.* **2019**, *53* (14), 8197–8204. https://doi.org/10.1021/acs.est.9b01531.

(114) Keiluweit, M.; Bougoure, J. J.; Nico, P. S.; Pett-Ridge, J.; Weber, P. K.; Kleber, M. Mineral Protection of Soil Carbon Counteracted by Root Exudates. *Nat. Clim. Change* **2015**, *5* (6), 588–595. https://doi.org/10.1038/nclimate2580.

(115) Sokol, N. W.; Bradford, M. A. Microbial Formation of Stable Soil Carbon Is More Efficient from Belowground than Aboveground Input. *Nat. Geosci.* **2019**, *12* (1), 46–53. https://doi.org/10.1038/s41561-018-0258-6.

Statement of Personal Contribution

The work described in this PhD thesis was funded by the Deutsche Forschungsgesellschaft (DFG, German Research Foundation, project ID 431072007). The conceptual background of this PhD project was developed by Prof. Christiane Zarfl, Prof. Andreas Kappler and Dr. Caroline Schmidt, who left environmental science, and, thus, was not an official supervisor during this PhD thesis. Throughout this PhD, Prof. Andreas Kappler was the first supervisor and Prof. Christiane Zarfl the second supervisor. Prof. E. Marie Muehe co-supervised this PhD thesis and was mainly involved in experiments and projects including paddy soil and rice plants. Dr. Prachi Joshi also co-supervised this PhD thesis and was mainly involved in general discussion, experimental designs, discussion of results and co-supervision of B.Sc/M.Sc. students. Unless otherwise stated, the experiments were conceptualized by me and Prof. Andreas Kappler and performed by myself. The analysis, evaluation, interpretation and discussion of the obtained results, as well as writing of all manuscripts were conducted by myself, in collaboration with Prof. Andreas Kappler (**Grimm et al. (2024a and 2024b)**[82,83]) and Prof. Christiane Zarfl (**Grimm et al. (in prep.)** [84]). Prof. Britta Planer-Friedrich, Dr. Prachi Joshi, Prof. E. Marie Muehe, Soeren Drabesch, Alan Nicol, Dr. Daniel Straub and Prof. Christiane Zarfl were also involved in **Grimm et al. (2024a)**[82]. **Grimm et al. (2024b)**[83] was performed in collaboration with Jennifer Lorenz, Dr. Prachi Joshi, Prof. E. Marie Muehe, Dr. Daniel Straub, Dr. Jeremiah Shuster and Prof. Christiane Zarfl. **Grimm et al. (in prep.)**[84] was finalized in collaboration with Paula Gscheidel, Matthias Böckmann, Dr. Daniel Straub, Dr. Stefan Fischer and Prof. Andreas Kappler. The contributions of the above-mentioned people including myself for the individual publications are listed in detail below.

Field work: I planned the field trip to Italy in October 2020 and Dr. Prachi Joshi helped me collecting paddy soil in the field in Vercelli, Italy. Paddy soil samples in China were collected in collaboration with Dr. Shun Li and Prof. Dr. Yongguan Zhu.

Grimm et al. (2024a)[82]**:** Andreas Kappler and Christiane Zarfl formulated the original hypothesis. E. Marie Muehe, Andreas Kappler and myself designed the project. I collected paddy soil samples together with Prachi Joshi. Sören Drabesch performed total arsenic analysis from sequential extractions and was involved in gas measurements. Alan Nicol and Britta Planer-Friedrich performed arsenic speciation analysis. Daniel Straub processed the amplicon sequencing data and helped with interpretation of the microbial community results. I conducted analyses in the laboratory, data evaluation, and wrote the original draft of the manuscript. All authors were responsible for data interpretation. All authors discussed the data, reviewed, and edited the manuscript.

Grimm et al. (2024b)[83]**:** Andreas Kappler and Christiane Zarfl formulated the original hypothesis. Andreas Kappler and I designed the experimental project. Daniel Straub processed the amplicon sequencing data, constructed the maximum-likelihood tree, and helped with interpretation of the microbial community results. Jeremiah Shuster took scanning electron microscopy pictures. Jennifer Lorenz performed experiments with arsenite. I performed the main experiment, conducted analyses in the laboratory, data evaluation, and wrote the original draft of the manuscript. All authors were responsible for data interpretation and involved in the revision of the manuscript.

Grimm et al. (in prep.)[84]**:** Andreas Kappler and Christiane Zarfl formulated the original hypothesis. Andreas Kappler and I designed the experimental project. Paula Gscheidel, Christiane Zarfl and myself developed the numerical model with the help of Matthias Boeckmann. Daniel Straub processed the amplicon sequencing data and helped with interpretation of the microbial community results. Stefan Fischer performed SEM sample preparation and analysis. I performed the main experiment, conducted analyses in the laboratory, data evaluation, and wrote the original draft of the manuscript. All authors were responsible for data interpretation. All authors were responsible for data interpretation and involved in the revision of the manuscript.

I hereby state that I have neither plagiarized nor copied any of the text. **Grimm et al. (2024a)**[82] and **Grimm et al. (2024b)**[83] have been published in scientific journals. **Grimm et al. (in prep.)**[84] will be submitted to a scientific journal and might be published in a slightly modified version elsewhere in the future.

Appendix

The work presented in this thesis resulted in two published journal articles and one manuscript that was in preparation for publication when the thesis was submitted in December 2024. The first paper, **Grimm et al. (2024a)**[82] was published in *Heliyon* on August 1st, 2024 and the second paper **Grimm et al. (2025b)**[83] was published in *Applied an Environmental Microbiology* on December 6th, 2024. The respective articles together with the unpublished Manuscript **Grimm et al. (in prep.)**[84] and the corresponding supporting-information documents are presented in this appendix and listed in the following.

Grimm et al. (2024a). Arsenic immobilization and greenhouse gas emission depend on quantity and frequency of nitrogen fertilization in paddy soil

Heliyon 10 (2024) e35706

Contents lists available at ScienceDirect

Heliyon

journal homepage: www.cell.com/heliyon

Research article

Arsenic immobilization and greenhouse gas emission depend on quantity and frequency of nitrogen fertilization in paddy soil

Hanna Grimm [a], Soeren Drabesch [a,b,c], Alan Nicol [d], Daniel Straub [e], Prachi Joshi [a], Christiane Zarfl [f], Britta Planer-Friedrich [d], E. Marie Muehe [b,c], Andreas Kappler [a,g,*]

[a] Geomicrobiology, Department of Geosciences, University of Tübingen, Schnarrenbergstrasse 94-96, 72076 Tübingen, Germany
[b] Plant Biogeochemistry, Department of Applied Microbial Ecology, Helmholtz Centre for Environmental Research - UFZ, Permoserstrasse 15, 04318 Leipzig, Germany
[c] Plant Biogeochemistry, Department of Geosciences, University of Tübingen, Schnarrenbergstrasse 94-96, 72076 Tübingen, Germany
[d] Environmental Geochemistry, Bayreuth Center for Ecology and Environmental Research (BayCEER), University of Bayreuth, Germany
[e] Quantitative Biology Center (QBiC), University of Tübingen, Germany
[f] Environmental Systems Analysis, Department of Geosciences, University of Tübingen, Schnarrenbergstrasse 94-96, 72076 Tübingen, Germany
[g] Cluster of Excellence: EXC 2124: Controlling Microbes to Fight Infection, Tübingen, Germany

ARTICLE INFO

Keywords:
Nitrate reduction
Iron(II) oxidation
Ferrous iron
Nitrous oxide
Methane
Global warming potential

ABSTRACT

Nitrogen (N) fertilization in paddy soils decreases arsenic mobility and methane emissions. However, it is unknown how quantity and frequency of N fertilization affects the interlinked redox reactions of iron(II)-driven denitrification, iron mineral (trans-)formation with subsequent arsenic (im-)mobilization, methane and nitrous oxide emissions, and how this links to microbiome composition. Thus, we incubated paddy soil from Vercelli, Italy, over 129 days and applied nitrate fertilizer at different concentrations (control: 0, low: ~35, medium: ~100, high: ~200 mg N kg^{-1} $soil^{-1}$) once at the beginning and after 49 days. In the high N treatment, nitrate reduction was coupled to oxidation of dissolved and solid-phase iron(II), while naturally occurring arsenic was retained on iron minerals due to suppression of reductive iron(III) mineral dissolution. In the low N treatment, 40 µg L^{-1} of arsenic was mobilized into solution after nitrate depletion, with 69 % being immobilized after a second nitrate application. In the non-fertilized control, concentrations of dissolved arsenic were as high as 76 µg L^{-1}, driven by mobilization of 36 % of the initial mineral-bound arsenic. Generally, N fertilization led to 1.5-fold higher total GHG emissions (sum of CO_2, CH_4 and N_2O as CO_2 equivalents), 158-fold higher N_2O, and 7.5-fold lower CH_4 emissions compared to non-fertilization. On day 37, *Gallionellaceae*, *Comamonadaceae* and *Rhodospirillales* were more abundant in the high N treatment compared to the non-fertilized control, indicating their potential role as key players in nitrate reduction coupled to iron(II) oxidation. The findings underscore the dual effect of N fertilization, immobilizing arsenic in the short-term (low/medium N) or long-term (high N), while simultaneously increasing N_2O and lowering CH_4 emissions. This highlights the significance of both the quantity and frequency of N fertilizer application in paddy soils.

* Corresponding author. Geomicrobiology, Department of Geosciences, University of Tübingen, Schnarrenbergstrasse 94-96, 72076 Tübingen, Germany.
E-mail address: andreas.kappler@uni-tuebingen.de (A. Kappler).

https://doi.org/10.1016/j.heliyon.2024.e35706
Received 24 July 2024; Accepted 1 August 2024
Available online 3 August 2024

1. Introduction

Increases in global rice production are needed to meet the future food demand arising from a growing and developing population without simultaneously increasing harmful impacts on the climate [1]. Thus, paddy soil management strategies should balance rice yield and greenhouse gas emissions [2,3]. Paddy soils account for only 9 % of the total cropland area [4], but contribute 48 % to total cropland greenhouse gas emissions due to high methane (CH_4) emissions (global warming potential over 100 years: 27) [5,6]. Inorganic nitrogen (N) fertilizer application was found to decrease the global warming potential by 4.2 % per unit rice yield as it mitigates CH_4 emissions and increases rice yield [2]. Such benefits could be enhanced by using slow release fertilizer or optimized timing of N fertilizer addition [2]. However, in waterlogged, anoxic paddy soils, N fertilization stimulates denitrification accompanied by increased emissions of nitrous oxide (N_2O) (global warming potential over 100 years: 273) [6]. Nitrate reduction is mostly limited by the amount, bioavailability, and energy yield of electron donors [7–9]. In addition to organic carbon as electron donor for nitrate reduction under anoxic conditions, iron(II) (Fe(II)), which is generated at high concentrations by microbial iron(III) (Fe(III)) reduction, can serve as an electron donor for nitrate-reducing, Fe(II)-oxidizing microorganisms (autotrophic denitrification) [10]. Together with the abiotic oxidation of Fe(II) by reactive N species via chemodenitrification, both processes contribute to the emission of N_2O as well as to the formation of Fe(III) minerals [11]. Fe(III) minerals can serve as adsorption matrix for nutrients or contaminants, such as arsenic [12,13].

Arsenic is ubiquitously and naturally present in paddy soils and often found in groundwater used for irrigation. Thus, it is considered as the most important contaminant in paddy soils [14]. Its mobility and bioavailability are greatly influenced by Fe redox cycling and sequestration by Fe(III) (oxyhydr)oxide minerals [15]. Owing to waterlogged, anoxic conditions, arsenic is released during reductive Fe(III) mineral dissolution [16,17] and is reduced to its more toxic and mobile species arsenite [18]. Besides posing risks for humans by dietary uptake, accumulation of arsenic in rice plants also negatively affects plant growth and inhibits grain filling, ultimately reducing grain yield [19]. Arsenic mobility and toxicity is expected to be greatly influenced by the application of N fertilizers to paddy soils due to microbial nitrate reduction coupled to Fe(II) oxidation or chemodenitrification. These processes lead to the formation of Fe(III) minerals and provide adsorption sites for arsenic, reducing its mobility. The fate of arsenic can also be influenced by nitrate reduction coupled to arsenite oxidation, suppression of reductive dissolution of arsenic-bearing Fe(III) minerals by providing nitrate as a more favorable electron acceptor [20] or by the type of N fertilizer. Wang et al. (2023) [21] compared nitrate and ammonia-nitrate fertilizers in anoxic paddy soil microcosms and found less As immobilization for ammonia-nitrate fertilizers due to the presence of Feammox (ammonium-stimulated Fe(III) mineral reduction).

Even though the individual effects of N fertilizer addition on either arsenic mobility [20,22,23] or greenhouse gas emissions (i.e., N_2O and CH_4) [24–26] have been studied in paddy soils before, the effects of different quantities and frequencies of N fertilizer application on (1) nitrate reduction coupled to Fe(II) oxidation and on greenhouse gas formation and emission, (2) on Fe mineral formation and transformation, subsequently (3) on the mobility of arsenic, and (4) the link to microbiome composition and activity remain unresolved in paddy soils. Acknowledging the fact that mainly urea or ammonia-based fertilizers are applied to paddy fields, we supplied nitrate as a fertilizer to directly couple nitrate reduction to iron(II) oxidation by excluding confounding effects of ammonification and nitrification processes. This allows for a mechanistic understanding of the interplay between the N, Fe, As, and C cycles. In the following, N fertilization refers to fertilization with nitrate.

2. Materials & methods

2.1. Soil sampling and characterization

Paddy soil samples were collected in October 2020 in Vercelli, Italy, located in the Po river plain of Piedmont. The sampled paddy field is located on the Cascina Boraso research farm (45°19′26.0″ N 8°22′24.6″ E) at the international rice research institute (CREA-CI). It is intensively managed with LUNA-CL, a Long A grain rice cultivar (Clearfield®) under waterlogged conditions. Fertilizers are applied in excess in the region of Piedmont [27]. In 2020, a total of 279 kg N ha^{-1} (~105 mg N kg^{-1} $soil^{-1}$) were applied as urea at pre-sowing (24 %), as 1st (24 %) and 2nd (52 %) top dressing. Paddy soil samples were taken with a shovel after removal of the plant layer from the upper 20 cm and stored at 4 °C in the dark until further processing. Soil characterization comprised analyses of soil texture, bulk density, water content, pH, cation exchange capacity, total elemental content, total organic carbon and total N content, water-extractable organic carbon and inorganic N species and sequentially extractable Fe and arsenic (1 M sodium acetate, 0.5 M HCl, 6 M HCl) (Supporting methods S1, Table SI 1).

2.2. Incubation experiment

2.2.1. Setup and pre-incubation

For microcosm experiments, serum bottles (245 mL total volume) were washed with 1 M HCl (10 min), rinsed three times with deionized water and sterilized at 180 °C for 4.5 h. Fresh paddy soil (25 ± 0.05 g) was weighed into each serum bottle (in total 15 bottles) under sterile conditions and degassed with N_2 (for our experiments, no arsenic was added; only the naturally occurring arsenic content was considered). Sub-samples were taken in triplicates during filling of serum bottles and dried at 70 °C for 72 h to determine the soil moisture content. Artificial irrigation water (200 mL, Table SI 2) was added under N_2 atmosphere to each serum bottle and microcosms were pre-incubated without any addition of N fertilizer for 18 days at 25 °C in the dark to acclimate the paddy soil, to deplete soil-borne nitrate, and to build up dissolved Fe(II) (Fig. SI 1). To prevent accumulation of produced gases in the microcosms,

the headspace was continuously flushed through a sterile 0.22 μm filter (polyethersulfone membrane, Carl Roth GmbH + Co. KG, Germany) with pre-moistened N_2 gas to minimize evaporation and water loss (Fig. SI 1). Three serum bottles were sampled during the course of the pre-incubation, while the others were not disturbed.

2.2.2. Fertilization and re-fertilization

After 18 days of pre-incubation, microcosms were subjected to different N fertilization regimes in triplicates (control: no N addition, low: ~35 mg N kg^{-1} $soil^{-1}$, medium: ~100 mg N kg^{-1} $soil^{-1}$, high: ~200 mg N kg^{-1} $soil^{-1}$) by the addition of potassium nitrate (KNO_3, quality level: MQ300, Merck KGaA, Germany) and incubated under the same conditions as described earlier (Table SI 3). After 49 days of incubation, all microcosms were re-fertilized with KNO_3. Levels and timing of N fertilization reflect common practices in paddy soil management simulating single events of N fertilizer addition and total N fertilizer concentrations [28].

2.2.3. Sampling

The microcosms were sampled for greenhouse gas emissions (CO_2, N_2O, CH_4), aqueous geochemistry (N species, Fe species, arsenic species, dissolved organic carbon (DOC), pH), mineralogy (sequential chemical extractions), and microbial community analyses (Fig. SI 2). For gas sampling, the gas flow was stopped and 2–5 mL of headspace was collected in the beginning (t0) and after a 0.5–3 h period (t1). This was repeated two times. The gas samples were injected into helium-flushed exetainer® vials (12 mL, Labco Limited, United Kingdom). Sample volume and incubation time was adjusted within the course of the experiment to account for changes in headspace volume. For geochemical analyses, 2 mL of soil slurry were sampled under N_2 atmosphere and centrifuged (5 min, 13,400 rpm). The supernatant was diluted in anoxic 1 M HCl/40 mM sulfamic acid (to prevent oxidation of Fe(II) by nitrite) [29] for Fe and arsenic species analysis and in anoxic MQ water for N species analysis. The soil pellet was dried under anoxic conditions and used for sequential chemical extractions as described below. At several timepoints, samples were taken for pH, DOC, and microbial community analyses.

2.2.4. Sequential extraction

To quantify different Fe mineral phases and the associated arsenic, dried soil pellets were extracted using 0.5 M HCl, targeting poorly crystalline Fe(III) (oxyhydr)oxides and 6 M HCl to determine crystalline Fe minerals [30–32]. In contrast to the general soil characterization, a sodium acetate extraction was not performed, however, adsorbed Fe, Fe in amorphous sulfides and carbonates (as targeted by sodium acetate extraction), and associated arsenic were also extracted by 0.5 M HCl. Therefore, the 0.5 M HCl extraction used in the experiment is comparable to the sum of sodium acetate extractable and 0.5 M HCl extractable Fe and arsenic of the soil characterization. First, 2 mL of 0.5 M HCl/40 mM sulfamic acid were added to the dried soil pellet, the sample was well mixed and extracted under anoxic conditions for 2 h in the dark at room temperature. Sulfamic acid was added to eliminate the abiotic reaction of nitrite with Fe(II) during acidification [29]. Afterwards, the sample was centrifuged (5 min, 13,400 rpm), the supernatant diluted in 1 M HCl, and transferred and stored anoxically in the dark at 5 °C. Subsequently, 2 mL of 6 M HCl was added to the soil pellet and extracted anoxically for 24 h in the dark at room temperature. Finally, the sample was centrifuged (5 min, 13,400 rpm), the supernatant diluted in 1 M HCl, transferred and stored anoxically in the dark at 5 °C.

2.3. Geochemical analyses

Nitrate (NO_3^-), nitrite (NO_2^-), and ammonium (NH_4^+) were analyzed in the supernatant of the sampled and centrifuged soil slurry by a segmented flow analyzer (AutoAnalyzer3, SEAL Analytical, Germany), equipped with a dialysis membrane for Fe removal to prevent side reactions during analysis.

Total Fe and Fe(II) were determined in the supernatant of the sampled soil slurry and after sequential extractions using the ferrozine assay [33], following a revised protocol for nitrite-containing samples [29]. Samples were analyzed in triplicates at 562 nm on a spectrophotometer (Thermo Scientific™ Multiskan™ Go Microplate Spectrophotometer).

Samples for total arsenic after sequential extractions were analyzed by ICP-MS (Agilent 7900, USA) in argon with a helium flow of 1–3 mL min^{-1} (Table SI 4). The Agilent internal standard mix (product #5188–6525, 100 ± 5 %) and the Agilent Environmental Calibration Set (product #5183-4688) were used. Arsenic speciation in the supernatant was analyzed by ICP-MS/MS (Agilent 8900) as AsO^+ (m/z 91) using oxygen as reaction cell gas. Arsenic species were separated in a high-pressure liquid chromatograph (Agilent 1260 Infinity II) equipped with a PRP-X100 column (Hamilton, 20 mM $NH_4H_2PO_4$, flow rate 1 mL min^{-1}). Quantification was done via calibration with commercial standards for arsenite and arsenate (Honeywell Fluka™, USA) and quality was verified by recovery of certified reference material (TMDA 54.6, Environment Canada 100 ± 6 %). Arsenite and arsenate concentrations made up 94.8 ± 23.9 % of the total arsenic concentrations, methylated arsenic species (monomethylarsonic acid and dimethylarsinic acid) were not detected and thiolated arsenic species could not be analyzed due to sample acidification (Table SI 5).

The pH was measured in the soil slurry using a benchtop pH meter (SG2, Mettler-Toledo GmbH, Germany) equipped with a pH electrode (InLab Easy DIN, Mettler-Toledo GmbH, Germany). DOC from the sampled, centrifuged soil slurry was analyzed by combustion at 750 °C (Elemental analyzer, multi N/C 2100S, Analytik Jena GmbH, Germany).

2.4. Greenhouse gas analysis

Gas samples were analyzed on a TraceGC1300 (ThermoFisher Scientific, modified by S + HA analytics), in which the sample is split into two different column configurations each connected to a pulsed discharge detector (first configuration: 30 m long, 0.53 mm ID

TGBondQ column and 30 m long, 0.53 mm ID Molsieve column; second configuration: 30 m long, 0.53 mm ID TGBondQ column and a 30 m long 0.25 mm ID TGBondQ+ column (all ThermoFisher Scientific)) (Table SI 6). Gas emission rates were determined by performing linear regression analysis between gas concentrations and incubation times at three specific time points. The initial time point, t0, was calculated as the average of two initial gas measurements. The second time point, t1, corresponded to the end of the first incubation period. The third time point, t2, was derived by summing the end point measurements of both incubation periods. Cumulative emissions were then calculated from individual gas fluxes and the time intervals between measurements [34].

2.5. DNA- and RNA-based microbial community analysis

Soil samples were frozen in liquid N_2 and stored at −80 °C prior to extraction. Total RNA and DNA were co-extracted from soil samples using a phenol-chloroform extraction protocol [35]. Quality and quantity of extracted DNA and RNA were determined using NanoDrop (NanoDrop 1000, Thermo Scientific, Waltham, MA, USA), gel electrophoresis (8 out of 78 samples randomly selected), and Qubit (Life Technologies, Carlsbad, CA, USA), respectively. DNA was digested using the TURBO DNA-free™ Kit to obtain pure RNA samples with subsequent reverse transcription using SuperScript™ III Reverse Transcriptase to obtain complementary DNA (cDNA). Quantitative PCR for DNA and cDNA was performed for bacterial 16S rRNA genes and different marker and functional genes using SybrGreen® Supermix (5 μL per qPCR reaction, Bio-Rad Laboratories GmbH, Munich, Germany) in addition to dimethylsulfoxide (DMSO, 0.5 μL per qPCR reaction, Carl Roth) on the C1000 Touch thermal cycler (CFX96TM real time system). For 16S rRNA gene amplicon sequencing, the 16S rRNA gene was amplified using primers 515f (GTGYCAGCMGCCGCGGTAA) [36] and 806r (GGACTACNVGGGTWTCTAAT) [37] targeting the V4 region. Sequencing data was analyzed using the nf-core/ampliseq pipeline (v2.3.1), which encompasses all necessary analysis steps and software. The pipeline is publicly available [38,39], and was executed with Nextflow (v21.10.3) [40] and Singularity (v3.8.7) [41]. Details of quantitative PCR analysis and Illumina sequencing can be found in the Supporting methods S2 and Table SI 7.

2.6. Data analysis

A non-parametric Kruskal-Wallis test was applied using R (4.3.3) and its interface RStudio (2023.12.1 + 402) to estimate differences in total GWP, CO_2, CH_4 and N_2O emissions between treatments. A one-way analysis of variance (ANOVA) combined with a post-hoc test (Tukey test) was applied to identify differences in microbial community composition between soil treatments.

3. Results and discussion

3.1. Nitrogen fertilization stimulates nitrate reduction coupled to iron(II) oxidation

After pre-incubation of the paddy soil microcosms for 18 days, all initial soil-borne nitrate was depleted and dissolved Fe(II) was generated (Fig. SI 3 a, b). After applying nitrate at low, medium, and high N concentrations at the beginning of the incubation, 2.6 ± 0.1, 8.0 ± 0.2 and 15.6 ± 0.1 mg N L^{-1} were completely consumed (≤0.2 mg N L^{-1}) within 10, 16 and 37 days, respectively (Fig. 1a). In the second fertilization period (49–129 days), dissolved nitrate concentrations were generally higher compared to the first fertilization period (0–49 days) and declined within 6, 22 and 80 days (after the second fertilization at day 49) to below 0.1 mg N L^{-1} in the low, medium and high N treatment, respectively (Fig. 1a). In the non-fertilized control, dissolved nitrate concentrations stayed constantly below 0.2 ± 0.2 mg L^{-1} over the 129 days of incubation (Fig. 1a). We applied a pseudo-first-order kinetic model to the N fertilized treatments (Supporting methods S3, Table SI 8) and observed that at least the low and medium N treatment adhere to this model. The half-lives for nitrate reduction were higher in the medium N (0–16 days: $t_{1/2}$ = 2.98 days, 49–71 days: $t_{1/2}$ = 2.91 days) compared to the low N treatment (0–10 days: $t_{1/2}$ = 1.73 days, 49–55 days: $t_{1/2}$ = 0.92 days). A lower half-life time in the second fertilization period observed in the low N treatment likely indicates differences in for example Fe(II) concentrations and availability or microbial composition and activity compared to the first fertilization period. However, nitrate reduction in the high N treatment did not visually follow a pseudo-first-order kinetic model, indicating that nitrate is not the sole rate-determining factor at higher N application rates. This suggests that other factors, such as Fe(II) concentrations, organic carbon availability, or specific microbial activities, significantly influence the nitrate reduction process. These factors may interact in complex ways, leading to non-linear kinetics that a simple first-order model cannot capture.

Dissolved Fe(II) concentrations decreased simultaneously with nitrate concentrations. Within the first fertilization period, the greatest decrease in dissolved Fe(II) concentrations was observed in the medium N treatment (6.9 ± 0.8 mg L^{-1}, between days 0 and 13) and in the high N treatment (7.9 ± 0.8 mg L^{-1}, between days 0 and 30) and to a smaller extent in the low N treatment (1.8 ± 0.3 mg L^{-1}, 0–6 days) (Fig. 1b). In the second fertilization period, the decrease in dissolved Fe(II) was higher in the low and medium N treatment, but lower for the high N treatment compared to the first fertilization period, due to generally low concentrations of dissolved Fe(II) in the high N treatment (Fig. 1b). In the non-fertilized control, dissolved Fe(II) concentrations increased to a maximum of 33.6 ± 5.5 mg L^{-1} on day 85 and stayed relatively constant until the end of incubation (Fig. 1b). Generally, dissolved Fe(II) concentrations increased in all fertilized treatments as soon as nitrate was depleted, indicating microbial Fe(III) reduction. In the first fertilization period, dissolved Fe(II) concentrations increased to a similar extent in the low (12.1 ± 0 mg L^{-1}, 6–49 days) and medium (13.4 ± 0.4 mg L^{-1}, 13–49 days) N treatment and to a lower extent in the high N treatment (3.9 ± 1 mg L^{-1}, 30–49 days) (Fig. 1b). In the second fertilization period, the increase in dissolved Fe(II) concentrations after nitrate consumption was similar for the low and medium N treatment, but only minor for the high N treatment

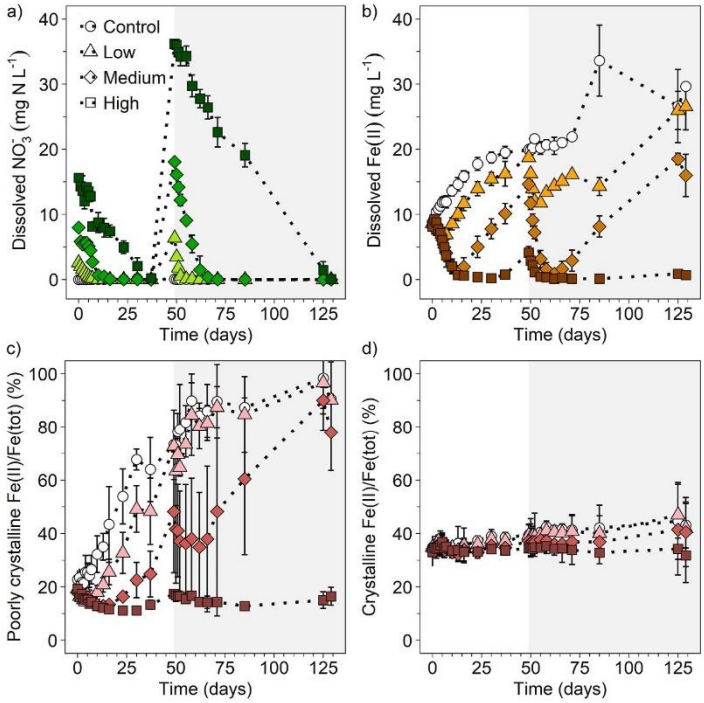

Fig. 1. Dissolved nitrate concentrations in mg N L^{-1} (a), dissolved Fe(II) concentrations in mg L^{-1} (b), Fe(II)/Fe(tot) ratio in % in poorly crystalline Fe mineral phases (0.5 M HCl extraction) (c) and Fe(II)/Fe(tot) ratio in % in crystalline Fe mineral phases (6 M HCl extraction) (d) for three different levels of nitrogen fertilizer applications and a non-fertilized control (control: white circles, low N: triangles, medium N: diamonds, high N: squares) over 129 days of incubation. Mean ± standard deviation is shown for biological triplicates and the mean ± range for the low N treatment in the second fertilization for biological duplicates. The white background illustrates the first (0–49 days) and the grey background the second (49–129 days) nitrate fertilization period. (For interpretation of the references to colour in this figure legend, the reader is referred to the Web version of this article.)

(0.8 ± 0.1 mg L^{-1}, 85–125 days).

To capture Fe mineral dynamics, sequential extractions of the paddy soil were performed. In the poorly crystalline Fe mineral fraction, the Fe(II)/Fe(tot) ratio increased from 8.7 ± 1.8 % to 28.4 ± 4.5 % within 18 days of pre-incubation (Fig. SI 4). In the first fertilization period, the Fe(II)/Fe(tot) ratios generally decreased in the poorly crystalline Fe mineral fraction for all fertilized treatments, to the greatest extent for the high N treatment from 19.2 ± 3.2 to 11.2 ± 0.6 % (Fig. 1c). Increasing Fe(II)/Fe(tot) ratios were observed after nitrate depletion, resulting in Fe(II)/Fe(tot) ratios of 72.7 ± 2.1 % (low N), 48.2 ± 22.9 % (medium N) and 17.5 ± 1.5 % (high N) at the end of the first fertilization period (49 days). In the second fertilization period, Fe(II)/Fe(tot) ratios first decreased, followed by an increase again after nitrate consumption leading to high Fe(II)/Fe(tot) ratios in the low (90.1 ± 1.4 %) and medium N treatment (78 ± 14.4 %) at the end of incubation (129 days). Increasing Fe(II)/Fe(tot) ratios point towards new, highly reactive, and bioavailable Fe(II) minerals formed by Fe(III) reduction. For the high N treatment, Fe(II)/Fe(tot) ratios stayed relatively constant at 13–17 % throughout the second fertilization period, which is likely caused by the lack of bioavailable Fe(II) minerals, as they had already been oxidized during the first phase of fertilization and were not recycled by Fe(III) reduction as in the other fertilized treatments. Fe(II)/Fe(tot) ratios in the poorly crystalline Fe mineral fraction of the non-fertilized control increased continuously from 22.8 ± 3.4 % to 90.5 ± 13.9 % over the 129 days of incubation (Fig. 1c). In the crystalline Fe mineral fraction, Fe(II)/Fe(tot) ratios stayed constant at ~35 % over 18 days of pre-incubation (Fig. SI 4). Within the first and second fertilization period, Fe(II)/Fe(tot) ratios in the crystalline mineral fraction were less prone to large changes compared to the poorly crystalline Fe mineral fraction (Fig. 1d). Yet, the ratio slowly increased constantly for the non-fertilized control (34.8 ± 4.3 % to 43.2 ± 8.6 %) as well as for the low (34.9 ± 3.6 % to 41.9 ± 9.3) and medium (34.2 ± 1.5 % to 40.5 ± 13 %) N treatment within 129 days of incubation, generating more crystalline Fe(II) minerals in the long-term. The constant level of Fe(II)/Fe(tot) ratios in the crystalline Fe mineral fraction might be attributed to less bioavailable Fe minerals, such as magnetite, Fe(II)-bearing silicates or sulfides [32], that are stable even under redox fluctuations [42,43]. In contrast to the medium and low N treatment, the Fe(II)/Fe(tot) ratio remained relatively stable for the high N treatment at 32–33 %.

Overall, nitrate fertilization led to a microbial coupling of nitrate reduction to Fe(II) oxidation [20,44–47], evidenced by the simultaneous decrease of nitrate and dissolved Fe(II) concentrations, as well as the decrease of the Fe(II)/Fe(tot) ratios in the poorly crystalline Fe mineral fraction after applying nitrate fertilizer. Based on the concentrations of dissolved nitrate and Fe(II), we calculated that the oxidation of dissolved Fe(II) was responsible for a maximum of 5.6 % of reduced nitrate (Table SI 9). The remainder was most likely caused by solid-phase Fe(II) pools, accounting for the larger proportion of Fe(II). Due to soil heterogeneity and the resulting variations in the total Fe and Fe(II) concentrations, calculations based on absolute values of oxidized solid-phase Fe(II) are not applicable. The decrease in Fe(II)/Fe(tot) ratio was likely caused by the oxidation of dissolved Fe(II), leading to the formation of Fe(III) minerals, and by the oxidation of solid-phase Fe(II) minerals coupled to nitrate reduction. The oxidation of solid-phase Fe(II) minerals (e.g., siderite, pyrite, green rust, reduced goethite, biotite) by nitrate-reducing, Fe(II)-oxidizers was also observed in other studies before [48–51]. Fe(II) was likely the major electron donor responsible for nitrate reduction as no other potential electron donor (e.g., organic carbon [52], ammonium [53], CH_4 [54], etc.) showed a clear relationship with nitrate concentrations (Fig. SI 5, 6, 7). Even though heterotrophic and autotrophic Fe(II)-driven denitrification can co-occur in paddy soils, we suggest that autotrophic Fe (II)-driven denitrification is the dominant process in our study, which is supported by decreasing dissolved Fe(II) concentrations, 0.5 M HCl extractable Fe(II)/Fe(tot) ratio, nitrate concentrations, and the lack of bioavailable fatty acids (representative samples analyzed by HPLC). Our data shows that as long as nitrate was present in solution, microbial Fe(III) mineral reduction was inhibited as nitrate is the thermodynamically more favorable electron acceptor relative to Fe(III) minerals [11,55,56]. Only after nitrate was completely consumed, Fe(III) reduction dominated and resulted in increasing dissolved Fe(II) concentrations and increasing Fe(II)/Fe (tot) ratios in the poorly crystalline Fe mineral fraction. Poorly crystalline Fe minerals were identified to be highly susceptible to redox changes induced by the application of N fertilizer, highlighting that crystallinity and bioavailability of Fe minerals impact the extent of Fe(II) oxidation.

3.2. *Arsenic immobilization by iron minerals formed by nitrogen fertilization*

We analyzed naturally occurring arsenic in the paddy soil to evaluate changes in arsenic mobility over the course of incubation. Total dissolved arsenic concentrations (calculated as the sum of arsenite and arsenate) stayed constantly low in the high N treatment between 0.4 ± 0.1 and 6 ± 3.7 μg L^{-1} over the 129 days of incubation (Fig. 2a). In the low and medium N treatment, total dissolved arsenic concentrations started to increase in both fertilization periods after nitrate was completely consumed. Dissolved arsenic concentrations reached 40.6 ± 3.1 μg L^{-1} (low N) and 26.5 ± 7.7 μg L^{-1} (medium N) at the end of the first fertilization period (after 49 days) and decreased by 27.8 ± 3.3 μg L^{-1} (low N) and by 21.1 ± 7.7 μg L^{-1} (medium N) within 3 days after the second N fertilizer application. At the end of incubation after 129 days, dissolved arsenic concentrations were lower in the medium N treatment (16 ± 7.4 μg L^{-1}) compared to the low N treatment (67 ± 12.5 μg L^{-1}). Total dissolved arsenic concentrations increased continuously in the non-fertilized control from 3.8 ± 0.5 μg L^{-1} to 62.6 ± 8.9 μg L^{-1} over the 129 days of incubation.

Arsenite initially constituted approximately 15–30 % of the total dissolved arsenic (70–85 % arsenate) and was removed completely from solution within 1 or 2 days after firstly applying N fertilizer (Fig. SI 8 a-d, Fig. SI 9). Even though absolute arsenate concentrations also decreased, arsenate accounted for 100 % of the remaining dissolved arsenic. After 10, 16 and 37 days, dissolved arsenite and arsenate concentrations started to increase in the low, medium and high N treatment, respectively, which correlated with the time of nitrate depletion. At the end of incubation (129 days), arsenite made up 48–67 % of total dissolved arsenic in the N fertilized treatments (33–52 % arsenate), with the highest proportion of arsenite observed in the high N treatment. After the second fertilizer application, the proportion of arsenite did not decline to the same extent as observed 1 or 2 days after the first fertilizer application.

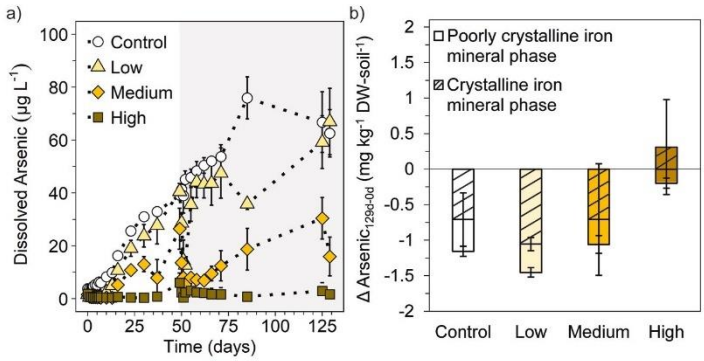

Fig. 2. Dissolved arsenic concentrations in μg L^{-1} (a), and difference in arsenic content associated with Fe mineral phases between day 0 and 129 in mg kg^{-1} DW-$soil^{-1}$ (b) in paddy soil with three different levels of nitrogen fertilizer applications (low, medium, high) compared to the non-fertilized control over 129 days of incubation. Mean ± standard deviation is shown for biological triplicates and the mean ± range for the low N treatment in the second fertilization for biological duplicates. The white background in (a) illustrates the first (0–49 days), and the grey background the second (49–129 days) nitrate fertilization period.

The non-fertilized control showed a gradual increase of dissolved arsenite and arsenate, with arsenite accounting for 30–40 % within the 129 days of incubation.

To investigate the role of Fe mineral phases for the mobility of arsenic, total arsenic concentrations associated with the poorly crystalline and crystalline Fe mineral phases were quantified (Fig. 2b). Over the 129 days of incubation, arsenic was lost for all treatments from the poorly crystalline Fe mineral phases in comparison to initial mineral-bound arsenic contents. The decline in bound arsenic was the greatest for the non-fertilized control (0.5 ± 0.1 mg kg^{-1} DW-$soil^{-1}$), low (0.4 ± 0.1 mg kg^{-1} DW-$soil^{-1}$) and medium N treatment (0.4 ± 0.1 mg kg^{-1} DW-$soil^{-1}$). The least arsenic was lost from poorly crystalline Fe minerals in the high N treatment (0.2 ± 0.1 mg kg^{-1} DW-$soil^{-1}$). The loss of arsenic from the crystalline Fe mineral fraction was about 2-fold greater for the non-fertilized control (0.7 ± 0.4 mg kg^{-1} DW-$soil^{-1}$), low (1.1 ± 0.1 mg kg^{-1} DW-$soil^{-1}$) and medium (0.7 ± 0.8 mg kg^{-1} DW-$soil^{-1}$) N treatment in comparison to the loss from the poorly crystalline phase. The high N treatment even exhibited an increase of 0.3 ± 0.7 mg kg^{-1} DW-$soil^{-1}$ in arsenic content in the crystalline Fe mineral phase.

These results illustrate that arsenic mobility is tightly linked to the fate of Fe minerals, and thus, susceptible to Fe redox changes [57]. When nitrate reduction coupled to Fe(II) oxidation dominates after N fertilizer application, dissolved arsenic can be scavenged within only a few days and retained on Fe mineral phases, even though only for a short time under low and medium N fertilizer applications. Liu et al. (2022) [20] observed that the retention of arsenic by Fe minerals is only of short-term duration (1–3 days) when applying KNO_3 as fertilizer. In contrast, the high N treatment successfully retained arsenic on Fe mineral phases limiting mobilization also over long term (129 days). When no nitrogen fertilizer was applied, 36 % of the total arsenic was mobilized from Fe mineral phases to the solution, which co-occurred with Fe(III) reduction. Even though the poorly crystalline Fe mineral phase was influenced to a greater extent by nitrogen fertilization, more arsenic was released from the crystalline Fe mineral phase. This might be due to the larger pool of Fe minerals in the crystalline fraction compared to the poorly crystalline fraction and generally higher amounts of arsenic being asssociated with the crystalline Fe mineral phase (Table SI 1).

Other mechanisms affecting arsenic mobility include nitrate reduction coupled to arsenite oxidation, which could be occurring under N fertilization [58]. This likely caused the strong decrease of the arsenite share on the total dissolved arsenic pool after N fertilization, pointing towards a greater removal of arsenite, especially in the first fertilization period. Dissolved arsenate concentrations decreased due to the preferential adsorption of arsenate to the newly formed Fe(III) (oxyhydr)oxides under given pH's (Fig. SI 10) [13,59]. In the second fertilization phase, a less pronounced oxidation effect of arsenite may be associated with generally elevated concentrations of both arsenite and arsenate, or it could be influenced by potential toxicity effects, thereby impeding microbial processes. As the binding of As to Fe(III) (oxyhydr)oxides is dependent on various parameters, such as mineral identity, properties, and structure, or pH, additional analysis would be required to elucidate the binding environment of As and Fe more in detail [59,60].

In summary, N fertilization successfully removed arsenite from solution and immobilized arsenic by adsorption onto newly formed Fe(III) minerals, even though the extent and efficiency depends on the amount of N fertilizer added. Reductive dissolution of Fe(III) minerals was responsible for arsenic mobilization, especially of arsenite, mainly from the crystalline mineral phase. However, redox cycling or type of binding of arsenic species also likely play a role for the mobilization of arsenic [61].

3.3. Greenhouse gas emissions depend on nitrogen fertilizer concentrations

To evaluate climate-related effects of N fertilizer application, CO_2, CH_4, and N_2O emissions were quantified over the course of incubation as CO_2 equivalents [6]. Total greenhouse gas emissions were similar for the low, medium and high N treatment (5.2 ± 0.2, 4.6 ± 0.4, 5.0 ± 0.1 g CO_2 eq. kg^{-1} DW-$soil^{-1}$ 125 $days^{-1}$, respectively) and higher than the non-fertilized control (3.2 ± 0.1 g CO_2 eq. kg^{-1} DW-$soil^{-1}$ 125 $days^{-1}$) (Fig. 3), although not significantly ($p = 0.06$, non-parametric Kruskal-Wallis test, Table SI 10).

The contributions of the individual greenhouse gases to the total emissions varied between the different treatments. CO_2 emissions were significantly different between the treatments ($p = 0.04$, non-parametric Kruskal-Wallis test, Table SI 10) and accounted for the largest proportion of total greenhouse gas emissions in the non-fertilized control (70.5 ± 3.4 %) compared to the N fertilized treatments (low: 50.1 ± 2.5 %, medium: 56 ± 6.3 %, high: 47.1 ± 1.6 %) (Fig. SI 11). CH_4 emissions were significantly different between treatments ($p = 0.02$, non-parametric Kruskal-Wallis test, Table SI 10) and only observed for the non-fertilized control and low N treatment, contributing 29 ± 4.7 % and 7.2 ± 0.5 % to the total greenhouse gas emissions, respectively (Fig. SI 12). CH_4 emissions were absent in the medium and high N treatment, even after nitrate was depleted. N_2O emissions were also significantly different between treatments ($p = 0.03$, non-parametric Kruskal-Wallis test, Table SI 10) and mainly observed for the fertilized treatments as long as nitrate was present in the soil (Fig. SI 13), without great differences between the amount of nitrate fertilizer added. In total, N_2O made up for 42.8 ± 4.1 % (low N), 44.0 ± 8.1 % (medium N) and 52.9 ± 3.1 % (high N) of the total greenhouse gas emissions. In contrast, only 0.5 ± 0.5 % were emitted as N_2O in the non-fertilized control (Fig. SI 13). However, it has to be noted that only gaseous N_2O concentrations are considered and might be underestimated as we left microcosms undisturbed before gas sampling.

N_2O and CH_4 emissions showed an inverse relationship, supporting prior studies that N fertilization suppresses methanogenesis [62,63]. In the control treatment, CH_4 emissions occurred after around 50 days of incubation. The timing likely represents conditions in the soil favoring methanogenesis, meaning that the soil was depleted in other, more favorable electron acceptors, i.e. nitrate, Fe(III), and sulfate. Due to the absence of nitrate, N_2O emissions were generally low. In contrast, N_2O was produced when nitrate was applied to the paddy soil, due to nitrate reduction coupled to Fe(II) or As(III) oxidation and other labile organic carbon sources or abiotic processes, i.e. chemodenitrification. CH_4 emissions were suppressed under N fertilization likely due to thermodynamic constraints (nitrate reduction being more favorable over methanogenesis), yet, nitrate reduction coupled to methane oxidation could have also limited CH_4 emissions [64]. It was estimated that methane oxidation coupled to nitrate reduction could offset 10–20 % of the global

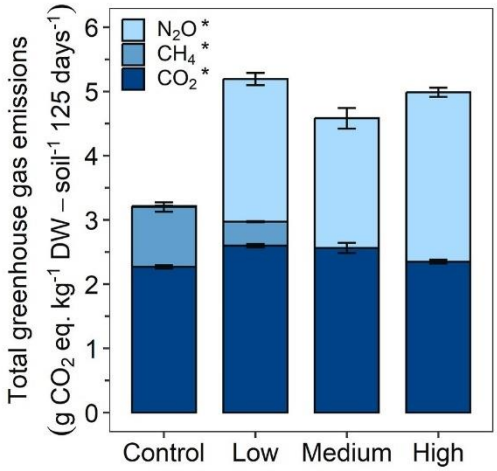

Fig. 3. Total greenhouse gas emissions in g CO_2 eq. kg^{-1} DW-$soil^{-1}$ 125 $days^{-1}$ from CO_2 (dark blue), CH_4 (blue), N_2O (light blue) emissions for the three different levels of nitrogen fertilizer application (low, medium, and high N) compared to the non-fertilized control. CO_2 equivalents of CH_4 and N_2O emissions were calculated by multiplication with the factors 27 and 273, respectively, which represent the global warming potential over 100 years [6]. Asterisks (*) represent significant differences ($p < 0.05$) of total CO_2, CH_4 and N_2O emissions between treatments. Mean ± standard deviation is shown for biological triplicates taking the mean ± range for the low N treatment in the second fertilization for biological duplicates into account. (For interpretation of the references to colour in this figure legend, the reader is referred to the Web version of this article.)

CH_4 emissions [65]. Vaksmaa et al. (2016) [66] showed that this process is contributing substantially to methane oxidation in an Italian paddy soil, from where our paddy soil also originates from. Together with relative abundances (based on 16S rRNA gene amplicon sequencing) of *Candidatus Methanoperedens* that are significantly higher (Welch *t*-test, $p = 0.005$, $df = 2.93$, $t = -7.63$, 95 % confidence interval = −0.31;-0.13) in the high N treatment (0.57 ± 0.04 %) compared to the control (0.35 ± 0.02 %) on day 37, methane oxidation coupled to nitrate reduction might have also limited CH_4 emissions in the N fertilized treatments in our study.

In general, N fertilization led to 1.5-fold greater total greenhouse gas emissions compared to the non-fertilized control, mainly due to overall greater N_2O emission. However, the extent of emissions was independent of the concentration of N fertilizer added, which might be due to the limited supply or bioavailability of electron donors [67] or in general the abundance and metabolic activity of the microorganisms present. When comparing different levels of N fertilization, we conclude that lower application quantities, but higher frequencies could even enhance total greenhouse gas emission (e.g., low compared to high N treatment), especially due to short-term peak emissions of N_2O [68].

3.4. Change in microbial community composition by nitrogen fertilization

In order to identify impacts of N fertilization on the microbiome, we quantified microbial community abundance, activity and composition. The 16S rRNA gene and transcript copy numbers generally varied between different timepoints during the incubation (Fig. SI 14, 15). The greatest differences between treatments were found on day 37 between the non-fertilized control and the high N treatment, when the greatest differences in geochemistry (i.e., dissolved Fe(II) and arsenic, solid-phase Fe) could also be observed. 16S rRNA transcript copy numbers were significantly lower for the non-fertilized control compared to the high N treatment on day 37 ($p = 0.0167$, Table SI 11, ANOVA). Abundances of functional and marker genes seemed to be similar to the general trends of 16S rRNA gene copy numbers. No significant differences in the abundances were found between the different N treatments on day 0, 16, 37, 49 or 129 for the marker and functional genes *narG*, *nosZ*, *aioA*, *arrA* and *Geobacter* spp. (Fig. SI 16 to 21). However, copies of genes involved in Fe or N cycling were generally higher for the medium and high N treatment compared to the low N treatment and the control on day 37, especially for *narG*, *nosZ* and *Geobacter* spp. Feng et al. (2023) [69] reported a higher abundance of the arsenite oxidase gene *aioA* in N fertilized paddy soils, yet, the similarity in *aioA* abundances between the non-fertilized control and N fertilized treatments suggests a minor role of microbial arsenite oxidation in our study. Stable trends in functional and marker genes suggest that the microbial community is resilient to nitrate fertilization, likely due to its composition being established over years of nitrogen fertilization. However, 16S rRNA gene amplicon sequencing on day 37 revealed differences in the microbial community composition on the phylum level between the non-fertilized control and the high N treatment (Fig. 4). The relative 16S rRNA gene sequence abundance of *Verrucomicrobiota* was significantly higher for the non-fertilized control (5.5 ± 0.5 %) compared to the high N treatment (4.5 ± 0.3 %) ($p = 0.044$, Table SI 11, one-way ANOVA), whereas *Proteobacteria* were present in greater relative abundance in the high N treatment (18.6 ± 0.1 %) compared to the non-fertilized control (14.1 ± 0.8 %) ($p = 1.5 \cdot 10^{-6}$, Table SI 11, one-way ANOVA). At the family level, *Pedosphaeraceae* belonging to *Verrucomicrobiota* were enriched in the non-fertilized control and have been found to be involved in the

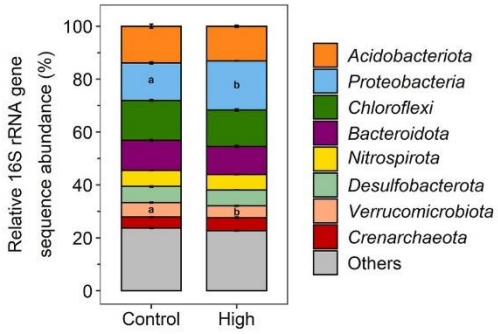

Fig. 4. Relative 16S rRNA gene sequence abundance in % on phylum level for the non-fertilized control and high N treatment on day 37. "Others" represent phyla with abundances below 3 % on average. Significant differences between non-fertilized control and high N treatment are indicated with a and b (*Verrucomicrobiota*: $p = 0.044$, *Proteobacteria*: $p = 1.5 \cdot 10^{-6}$, one-way ANOVA). Mean ± standard deviation is shown for biological triplicates.

CH_4-, N- and Fe-cycle (Fig. SI 22) [70]. They were also found in arsenic-contaminated soils, potentially involved in toxic metal resistance [71]. Moreover, *Pedosphaeraceae* likely play a role in methane oxidation, which could be coupled to Fe(III) reduction [72], impacting arsenic mobility and greenhouse gas emissions. Ratering and Schnell [44] revealed a widespread metabolic potential for nitrate reduction coupled to iron(II) oxidation among *Proteobacteria* in paddy soils. The families *Gallionellaceae*, *Comamonadaceae* and the order *Rhodospirillales* belonging to the *Proteobacteria* were enriched in the high N treatment on day 37 (Fig. SI 23). *Gallionellaceae* are typical microaerophilic Fe(II)-oxidizing microorganisms [73], yet some members are related to lithoautotrophic nitrate-reducing, Fe(II)-oxidizing microorganisms that have been successfully enriched in microbial cultures [74–78]. In paddy soils, members of the family *Gallionellaceae* were identified as potential key players for microbial nitrate reduction coupled to Fe(II) oxidation [79,80]. *Comamonadaceae* were found to be important decomposers in paddy soils [81] and are typically involved in the N-cycle mainly performing denitrification, which could potentially be linked to arsenite or Fe(II) oxidation [82–84]. *Rhodospirillales* are considered to play a role in N_2O reduction [85]. These results highlight that N fertilization changes the microbial community and favors N-cycling microorganisms.

3.5. Implications of nitrogen fertilization in paddy soils for arsenic mobility and greenhouse gas emissions

Our results showed that nitrate reduction coupled to Fe(II) oxidation was stimulated by the addition of N fertilizer to the paddy soil. This (1) led to the formation of Fe(III) minerals immobilizing a maximum of 28 μg L^{-1} of dissolved arsenic and (2) prevented the reductive dissolution of Fe(III) minerals and the simultaneous release of arsenic from Fe mineral phases into solution, which was most successful under the highest N fertilizer application. The formation of Fe(III) (oxyhydr)oxides was likely more important for arsenic immobilization than As(III) oxidation. This is supported by increasing Fe(III) levels, decreasing As(III) levels, a higher abundance of Fe (II)-oxidizers, and the lack of a significant increase in *aioA* gene abundance in the high N treatment. Although such high concentrations may not be directly applied to paddy soils as the common drinking water limit (50 mg L^{-1}) [86] for nitrate would be mostly exceeded, our data shows that constant nitrate concentrations, which could also be achieved by other methods such as applying slow release N fertilizer or different fertilization frequencies and quantities, could suppress Fe(III) reduction and prevent the mobilization of arsenic and limit methane emissions by suppression of methanogenesis. Whether the same mechanisms hold true if other common fertilizers, e.g., urea, ammonia, are applied to different paddy fields has to be investigated.

Minimizing arsenic concentrations in the porewater, in the rice plant and in the rice grain might become even more important in the future to counteract decreases in rice yield [19]. As it was shown that arsenic sequestration by Fe plaque or minerals is dependent on the growth stage of the rice plant, which is also critical for arsenic uptake by rice plants [57], our results could provide guidance for practical application. We showed that arsenic immobilization can occur quickly within just a few days and even long-term over 129 days, when KNO_3 was applied at higher concentrations. Thus, the frequency and amount of N fertilizer application becomes more important in future rice cultivation as it has a great potential in minimizing arsenic concentrations. Furthermore, the cultivation of microbial key players, such as *Gallionellaceae*, from paddy soils would enable us to study nitrate reduction coupled to Fe(II) oxidation in more detail with the goal to identify parameters that control rates of Fe(II) oxidation and nitrate reduction, and as a consequence, N_2O emissions and arsenic mobility.

In summary, our results showed that the highest N fertilizer application rate was most effective in retaining arsenic on Fe mineral phases and preventing the mobilization into solution, without increasing total greenhouse gas emissions compared to lower fertilizer application rates. These findings have enhanced our insight into how N fertilizer application influences the interconnected processes of the microbial Fe, N, and As cycles in paddy soils.

Data availability statement

Raw sequencing data was deposited into the Sequence Read Archive (SRA) at NCBI under the BioProject accession number PRJNA922084 (https://www.ncbi.nlm.nih.gov/bioproject/PRJNA922084). The dataset supporting the findings of this study is published on Zenodo and can be accessed via https://doi.org/10.5281/zenodo.10679656.

Funding sources

Deutsche Forschungsgemeinschaft (DFG, German Research Foundation, project ID 431072007).

CRediT authorship contribution statement

Hanna Grimm: Conceptualization, Methodology, Validation, Formal analysis, Investigation, Data curation, Visualization, Writing – Original Draft, Writing – review & editing. **Soeren Drabesch:** Formal analysis, Writing – review & editing. **Alan Nicol:** Formal analysis, Writing – review & editing. **Daniel Straub:** Formal analysis, Data curation, Writing – review & editing. **Prachi Joshi:** Validation, Writing – review & editing. **Christiane Zarfl:** Conceptualization, Resources, Supervision, Project administration, Funding acquisition, Writing – review & editing. **Britta Planer-Friedrich:** Validation, Writing – review & editing. **E. Marie Muehe:** Validation, Supervision, Writing – review & editing. **Andreas Kappler:** Conceptualization, Resources, Supervision, Project administration, Funding acquisition, Writing – review & editing.

Declaration of competing interest

The authors declare that they have no known competing financial interests or personal relationships that could have appeared to influence the work reported in this paper.

Acknowledgements

We thank Crea-CI for providing access to the paddy field for collection of soil samples. We thank Franziska Schädler for measurements of nitrogen species and for guidance during microbial community analyses and Ferdinand Hampl for XRF measurements. We are grateful for financial support from the Deutsche Forschungsgemeinschaft (DFG, German Research Foundation, project ID 431072007) and for infrastructural support by the DFG under Germany's Excellence Strategy, cluster of Excellence EXC2124 (project ID 390838134). We acknowledge support from the Open Access Publication Fund of the University of Tübingen. The graphical abstract was created using Biorender.com.

Appendix A. Supplementary data

Supplementary data to this article can be found online at https://doi.org/10.1016/j.heliyon.2024.e35706.

References

[1] M. van Dijk, T. Morley, M.L. Rau, Y. Saghai, A meta-analysis of projected global food demand and population at risk of hunger for the period 2010–2050, Nature Food 2 (7) (2021) 494–501, https://doi.org/10.1038/s43016-021-00322-9.
[2] X. Zhao, C. Pu, S.-T. Ma, S.-L. Liu, J.-F. Xue, X. Wang, Y.-Q. Wang, S.-S. Li, R. Lal, F. Chen, H.-L. Zhang, Management-induced greenhouse gases emission mitigation in global rice production, Sci. Total Environ. 649 (2019) 1299–1306, https://doi.org/10.1016/j.scitotenv.2018.08.392.
[3] J. Feng, C. Chen, Y. Zhang, Z. Song, A. Deng, C. Zheng, W. Zhang, Impacts of cropping practices on yield-scaled greenhouse gas emissions from rice fields in China: a meta-analysis, Agric. Ecosyst. Environ. 164 (2013) 220–228, https://doi.org/10.1016/j.agee.2012.10.009.
[4] Y. Liu, T. Ge, K.J. van Groenigen, Y. Yang, P. Wang, K. Cheng, Z. Zhu, J. Wang, Y. Li, G. Guggenberger, J. Sardans, J. Penuelas, J. Wu, Y. Kuzyakov, Rice paddy soils are a quantitatively important carbon store according to a global synthesis, Communications Earth & Environment 2 (1) (2021), https://doi.org/10.1038/s43247-021-00229-0.
[5] K.M. Carlson, J.S. Gerber, N.D. Mueller, M. Herrero, G.K. MacDonald, K.A. Brauman, P. Havlik, C.S. O'Connell, J.A. Johnson, S. Saatchi, P.C. West, Greenhouse gas emissions intensity of global croplands, Nat. Clim. Change 7 (1) (2017) 63–68, https://doi.org/10.1038/nclimate3158.
[6] IPCC, Climate Change 2021: the Physical Science Basis. Contribution of Working Group I to the Sixth Assessment Report of the Intergovernmental Panel on Climate Change, 2021, https://doi.org/10.1017/9781009157896.
[7] S.F. Korom, Natural denitrification in the saturated zone A review, Water Resour. Res. 28 (6) (1992) 1657–1668.
[8] B. Kelso, R.V. Smith, R.J. Laughlin, S.D. Lennox, Dissimilatory nitrate reduction in anaerobic sediments leading to river nitrite accumulation, Appl. Environ. Microbiol. 63 (12) (1997) 4679–4685, https://doi.org/10.1128/aem.63.12.4679-4685.1997.
[9] N. Bleyen, S. Smets, J. Small, H. Moors, N. Leys, A. Albrecht, P. de Cannière, B. Schwyn, C. Wittebroodt, E. Valcke, Impact of the electron donor on in situ microbial nitrate reduction in Opalinus Clay: results from the Mont Terri rock laboratory (Switzerland), Swiss J. Geosci. 110 (1) (2017) 355–374, https://doi.org/10.1007/s00015-016-0256-x.
[10] A. Kappler, C. Bryce, M. Mansor, U. Lueder, J.M. Byrne, E.D. Swanner, An evolving view on biogeochemical cycling of iron, Nat. Rev. Microbiol. 19 (6) (2021) 360–374, https://doi.org/10.1038/s41579-020-00502-7.
[11] M. Wang, R. Hu, R. Ruser, C. Schmidt, A. Kappler, Role of chemodenitrification for N2O emissions from nitrate reduction in rice paddy soils, ACS Earth Space Chem. 4 (1) (2020) 122–132, https://doi.org/10.1021/acsearthspacechem.9b00296.

[12] C. Hohmann, E. Winkler, G. Morin, A. Kappler, Anaerobic Fe(II)-oxidizing bacteria show as resistance and immobilize as during Fe(III) mineral precipitation, Environ. Sci. Technol. 44 (1) (2010) 94–101, https://doi.org/10.1021/es900708s.

[13] C. Hohmann, G. Morin, G. Ona-Nguema, J.-M. Guigner, G.E. Brown, A. Kappler, Molecular-level modes of as binding to Fe(III) (oxyhydr)oxides precipitated by the anaerobic nitrate-reducing Fe(II)-oxidizing Acidovorax sp. strain BoFeN1, Geochem. Cosmochim. Acta 75 (17) (2011) 4699–4712, https://doi.org/10.1016/j.gca.2011.02.044.

[14] S. Majumder, P. Banik, Geographical variation of arsenic distribution in paddy soil, rice and rice-based products: a meta-analytic approach and implications to human health, J. Environ. Manag. 233 (2019) 184–199, https://doi.org/10.1016/j.jenvman.2018.12.034.

[15] E.M. Muehe, A. Kappler, Arsenic mobility and toxicity in South and South-east Asia – a review on biogeochemistry, health and socio-economic effects, remediation and risk predictions, Environ. Chem. 11 (5) (2014) 483, https://doi.org/10.1071/EN13230.

[16] F.N. Ponnamperuma, The chemistry of submerged soils, Adv. Agron. 24 (1972) 29–96, https://doi.org/10.1016/S0065-2113(08)60633-1.

[17] Y. Takahashi, R. Minamikawa, K.H. Hattori, K. Kurishima, N. Kihou, K. Yuita, Arsenic behavior in paddy fields during the cycle of flooded and non-flooded periods, Environ. Sci. Technol. 38 (4) (2004) 1038–1044, https://doi.org/10.1021/es034383n.

[18] J. Zobrist, P.R. Dowdle, J.A. Davis, R.S. Oremland, Mobilization of arsenite by dissimilatory reduction of adsorbed arsenate, Environ. Sci. Technol. 34 (22) (2000) 4747–4753, https://doi.org/10.1021/es001068h.

[19] E.M. Muehe, T. Wang, C.F. Kerl, B. Planer-Friedrich, S. Fendorf, Rice production threatened by coupled stresses of climate and soil arsenic, Nat. Commun. 10 (1) (2019) 4985, https://doi.org/10.1038/s41467-019-12946-4.

[20] L. Liu, R.-L. Shen, Z.-Q. Zhao, L.-J. Ding, H.-L. Cui, G. Li, Y.-P. Yang, G.-L. Duan, Y.-G. Zhu, How different nitrogen fertilizers affect arsenic mobility in paddy soil after straw incorporation? J. Hazard Mater. 436 (2022) 129135 https://doi.org/10.1016/j.jhazmat.2022.129135.

[21] F. Wang, J. Zhang, Y. Zeng, H. Wang, X. Zhao, Y. Chen, H. Deng, L. Ge, R.A. Dahlgren, H. Gao, Z. Chen, Arsenic mobilization and nitrous oxide emission modulation by different nitrogen management strategies in flooded ammonia-enriched paddy soils, Pedosphere (2023), https://doi.org/10.1016/j.pedsph.2023.09.008.

[22] X. Wang, T. Liu, F. Li, B. Li, C. Liu, Effects of simultaneous application of ferrous iron and nitrate on arsenic accumulation in rice grown in contaminated paddy soil, ACS Earth Space Chem. 2 (2) (2018) 103–111, https://doi.org/10.1021/acsearthspacechem.7b00115.

[23] M.M. Hussain, I. Bibi, N.K. Niazi, M. Shahid, J. Iqbal, M.B. Shakoor, A. Ahmad, N.S. Shah, P. Bhattacharya, K. Mao, J. Bundschuh, Y.S. Ok, H. Zhang, Arsenic biogeochemical cycling in paddy soil-rice system: interaction with various factors, amendments and mineral nutrients, Sci. Total Environ. 773 (2021) 145040, https://doi.org/10.1016/j.scitotenv.2021.145040.

[24] M. Wang, R. Hu, J. Zhao, Y. Kuzyakov, S. Liu, Iron oxidation affects nitrous oxide emissions via donating electrons to denitrification in paddy soils, Geoderma 271 (2016) 173–180, https://doi.org/10.1016/j.geoderma.2016.02.022.

[25] Y. Furukawa, K. Inubushi, Effect of application of iron materials on methane and nitrous oxide emissions from two types of paddy soils, Soil Sci. Plant Nutr. 50 (6) (2004) 917–924, https://doi.org/10.1080/00380768.2004.10408554.

[26] E. Bolyen, J.R. Rideout, M.R. Dillon, N.A. Bokulich, C.C. Abnet, G.A. Al-Ghalith, H. Alexander, E.J. Alm, M. Arumugam, F. Asnicar, Y. Bai, J.E. Bisanz, K. Bittinger, A. Brejnrod, C.J. Brislawn, C.T. Brown, B.J. Callahan, A.M. Caraballo-Rodríguez, J. Chase, E.K. Cope, R. Da Silva, C. Diener, P.C. Dorrestein, G. M. Douglas, D.M. Durall, C. Duvallet, C.F. Edwardson, M. Ernst, M. Estaki, J. Fouquier, J.M. Gauglitz, S.M. Gibbons, D.L. Gibson, A. Gonzalez, K. Gorlick, J. Guo, B. Hillmann, S. Holmes, H. Holste, C. Huttenhower, G.A. Huttley, S. Janssen, A.K. Jarmusch, L. Jiang, B.D. Kaehler, K.B. Kang, C.R. Keefe, P. Keim, S.T. Kelley, D. Knights, I. Koester, T. Kosciolek, J. Kreps, M.G.I. Langille, J. Lee, R. Ley, Y.-X. Liu, E. Loftfield, C. Lozupone, M. Maher, C. Marotz, B.D. Martin, D. McDonald, L.J. McIver, A.V. Melnik, J.L. Metcalf, S.C. Morgan, J.T. Morton, A.T. Naimey, J.A. Navas-Molina, L.F. Nothias, S.B. Orchanian, T. Pearson, S.L. Peoples, D. Petras, M.L. Preuss, E. Pruesse, L.B. Rasmussen, A. Rivers, M.S. Robeson, P. Rosenthal, N. Segata, M. Shaffer, A. Shiffer, R. Sinha, S.J. Song, J.R. Spear, A. D. Swafford, L.R. Thompson, P.J. Torres, P. Trinh, A. Tripathi, P.J. Turnbaugh, S. Ul-Hasan, J.J.J. van der Hooft, F. Vargas, Y. Vázquez-Baeza, E. Vogtmann, M. von Hippel, W. Walters, Y. Wan, M. Wang, J. Warren, K.C. Weber, C.H.D. Williamson, A.D. Willis, Z.Z. Xu, J.R. Zaneveld, Y. Zhang, Q. Zhu, R. Knight, J. G. Caporaso, Reproducible, interactive, scalable and extensible microbiome data science using QIIME 2, Nat. Biotechnol. 37 (8) (2019) 852–857, https://doi.org/10.1038/s41587-019-0209-9.

[27] L. Zavattaro, M. Romani, D. Sacco, M. Bassanino, C. Grignani, Fertilization management of paddy fields in Piedmont (NW Italy), Ital. J. Agron. 3 (3) (2008) 201, https://doi.org/10.4081/ija.2008.201.

[28] J. Chen, Y. Huang, Y. Tang, Quantifying economically and ecologically optimum nitrogen rates for rice production in south-eastern China, Agric. Ecosyst. Environ. 142 (3–4) (2011) 195–204, https://doi.org/10.1016/j.agee.2011.05.005.

[29] F. Schaedler, A. Kappler, C. Schmidt, A revised iron extraction protocol for environmental samples rich in nitrite and carbonate, Geomicrobiol. J. 35 (1) (2018) 23–30, https://doi.org/10.1080/01490451.2017.1303554.

[30] U. Lueder, M. Maisch, K. Laufer, B.B. Jorgensen, A. Kappler, C. Schmidt, Influence of physical perturbation on Fe(II) supply in coastal marine sediments, Environ. Sci. Technol. 54 (6) (2020) 3209–3218, https://doi.org/10.1021/acs.est.9b06278.

[31] R.M. Cornell, U. Schwertmann, The Iron Oxides: Structure, Properties, Reactions, Occurrences and Uses, Wiley-Vch Verlag GmbH & Co. KGaA, 2003.

[32] G. Heron, C. Crouzet, A.C. Bourg, T.H. Christensen, Speciation of Fe(II) and Fe(III) in contaminated aquifer sediments using chemical extraction techniques, Environ. Sci. Technol. 28 (9) (1994) 1698–1705, https://doi.org/10.1021/es00058a023.

[33] L.L. Stookey, Ferrozine-a new spectrophotometric reagent for iron, Anal. Chem. 42 (7) (1970) 779–781, https://doi.org/10.1021/ac60289a016.

[34] Z. Yang, Y. Yu, R. Hu, X. Xu, J. Xian, Y. Yang, L. Liu, Z. Cheng, Effect of rice straw and swine manure biochar on N2O emission from paddy soil, Sci. Rep. 10 (1) (2020) 10843, https://doi.org/10.1038/s41598-020-67705-z.

[35] T. Lueders, M. Manefield, M.W. Friedrich, Enhanced sensitivity of DNA- and rRNA-based stable isotope probing by fractionation and quantitative analysis of isopycnic centrifugation gradients, Environ. Microbiol. 6 (1) (2004) 73–78, https://doi.org/10.1046/j.1462-2920.2003.00536.x.

[36] A.E. Parada, D.M. Needham, J.A. Fuhrman, Every base matters: assessing small subunit rRNA primers for marine microbiomes with mock communities, time series and global field samples, Environ. Microbiol. 18 (5) (2016) 1403–1414, https://doi.org/10.1111/1462-2920.13023.

[37] A. Apprill, S. McNally, R. Parsons, L. Weber, Minor revision to V4 region SSU rRNA 806R gene primer greatly increases detection of SAR11 bacterioplankton, Aquat. Microb. Ecol. 75 (2) (2015) 129–137, https://doi.org/10.3354/ame01753.

[38] P.A. Ewels, A. Peltzer, S. Fillinger, H. Patel, J. Alneberg, A. Wilm, M.U. Garcia, P. Di Tommaso, S. Nahnsen, The nf-core framework for community-curated bioinformatics pipelines, Nat. Biotechnol. 38 (3) (2020) 276–278, https://doi.org/10.1038/s41587-020-0439-x.

[39] D. Straub, N. Blackwell, A. Langarica-Fuentes, A. Peltzer, S. Nahnsen, S. Kleindienst, Interpretations of environmental microbial community studies are biased by the selected 16S rRNA (gene) amplicon sequencing pipeline, Front. Microbiol. 11 (2020) 550420, https://doi.org/10.3389/fmicb.2020.550420.

[40] P. Di Tommaso, M. Chatzou, E.W. Floden, P.P. Barja, E. Palumbo, C. Notredame, Nextflow enables reproducible computational workflows, Nat. Biotechnol. 35 (4) (2017) 316–319, https://doi.org/10.1038/nbt.3820.

[41] G.M. Kurtzer, V. Sochat, M.W. Bauer, Singularity: Scientific containers for mobility of compute, PLoS One 12 (5) (2017) e0177459, https://doi.org/10.1371/journal.pone.0177459.

[42] S. Peiffer, A. Kappler, S.B. Haderlein, C. Schmidt, J.M. Byrne, S. Kleindienst, C. Vogt, H.H. Richnow, M. Obst, L.T. Angenent, C. Bryce, C. McCammon, B. Planer-Friedrich, A biogeochemical–hydrological framework for the role of redox-active compounds in aquatic systems, Nat. Geosci. 14 (5) (2021) 264–272, https://doi.org/10.1038/s41561-021-00742-z.

[43] N. Chen, Q. Fu, T. Wu, P. Cui, G. Fang, C. Liu, C. Chen, G. Liu, W. Wang, D. Wang, P. Wang, D. Zhou, Active iron phases regulate the abiotic transformation of organic carbon during redox fluctuation cycles of paddy soil, Environ. Sci. Technol. 55 (20) (2021) 14281–14293, https://doi.org/10.1021/acs.est.1c04073.

[44] S. Ratering, S. Schnell, Nitrate-dependent iron(II) oxidation in paddy soil, Environ. Microbiol. 3 (2) (2001) 100–109, https://doi.org/10.1046/j.1462-2920.2001.00163.x.

[45] X. Li, W. Zhang, T. Liu, L. Chen, P. Chen, F. Li, Changes in the composition and diversity of microbial communities during anaerobic nitrate reduction and Fe(II) oxidation at circumneutral pH in paddy soil, Soil Biol. Biochem. 94 (2016) 70–79, https://doi.org/10.1016/j.soilbio.2015.11.013.

[46] T. Liu, D. Chen, X. Li, F. Li, Microbially mediated coupling of nitrate reduction and Fe(II) oxidation under anoxic conditions, FEMS Microbiol. Ecol. 95 (4) (2019), https://doi.org/10.1093/femsec/fiz030.

[47] X.-P. Chen, Y.-G. Zhu, M.-N. Hong, A. Kappler, Y.-X. Xu, Effects of different forms of nitrogen fertilizers on arsenic uptake by rice plants, Environ. Toxicol. Chem. 27 (4) (2008) 881–887.

[48] N. Jakus, A. Mellage, C. Höschen, M. Maisch, J.M. Byrne, C.W. Mueller, P. Grathwohl, A. Kappler, Anaerobic neutrophilic pyrite oxidation by a chemolithoautotrophic nitrate-reducing iron(II)-oxidizing culture enriched from a fractured aquifer, Environ. Sci. Technol. 55 (14) (2021) 9876–9884, https://doi.org/10.1021/acs.est.1c02049.

[49] K.A. Weber, F.W. Picardal, E.E. Roden, Microbially catalyzed nitrate-dependent oxidation of biogenic solid-phase Fe(II) compounds, Environ. Sci. Technol. 35 (8) (2001) 1644–1650, https://doi.org/10.1021/es0016598.

[50] E. Shelobolina, H. Xu, H. Konishi, R. Kukkadapu, T. Wu, M. Blöthe, E. Roden, Microbial lithotrophic oxidation of structural Fe(II) in biotite, Appl. Environ. Microbiol. 78 (16) (2012) 5746–5752, https://doi.org/10.1128/AEM.01034-12.

[51] C. Pantke, M. Obst, K. Benzerara, G. Morin, G. Ona-Nguema, U. Dippon, A. Kappler, Green rust formation during Fe(II) oxidation by the nitrate-reducing Acidovorax sp. strain BoFeN1, Environ. Sci. Technol. 46 (3) (2012) 1439–1446, https://doi.org/10.1021/es2016457.

[52] Y. Zhang, B. Xu, J. Han, L. Shi, Effects of drying-rewetting cycles on ferrous iron-involved denitrification in paddy soils, Water 13 (22) (2021) 3212, https://doi.org/10.3390/w13223212.

[53] Z. Wei, K. Jin, C. Li, M. Wu, J. Shan, X. Yan, Environmental factors controlling dissimilatory nitrate reduction to ammonium in paddy soil, J. Soil Sci. Plant Nutr. (2022) 1–8, https://doi.org/10.1007/s42729-022-01022-4.

[54] D. Luo, X. Meng, N. Zheng, Y. Li, H. Yao, S.J. Chapman, The anaerobic oxidation of methane in paddy soil by ferric iron and nitrate, and the microbial communities involved, Sci. Total Environ. 788 (2021) 147773, https://doi.org/10.1016/j.scitotenv.2021.147773.

[55] I. Kögel-Knabner, W. Amelung, Z. Cao, S. Fiedler, P. Frenzel, R. Jahn, K. Kalbitz, A. Kölbl, M. Schloter, Biogeochemistry of paddy soils, Geoderma 157 (1–2) (2010) 1–14, https://doi.org/10.1016/j.geoderma.2010.03.009.

[56] Y. Li, J. Ning, Q. Li, L. Li, N.S. Bolan, B.P. Singh, H. Wang, Effects of iron and nitrogen-coupled cycles on cadmium availability in acidic paddy soil from Southern China, J. Soils Sediments (2022), https://doi.org/10.1007/s11368-022-03328-3.

[57] H.-Y. Yu, X. Wang, F. Li, B. Li, C. Liu, Q. Wang, J. Lei, Arsenic mobility and bioavailability in paddy soil under iron compound amendments at different growth stages of rice, Environ. Pollut. 224 (2017) 136–147, https://doi.org/10.1016/j.envpol.2017.01.072.

[58] J. Zhang, W. Zhou, B. Liu, J. He, Q. Shen, F.-J. Zhao, Anaerobic arsenite oxidation by an autotrophic arsenite-oxidizing bacterium from an arsenic-contaminated paddy soil, Environ. Sci. Technol. 49 (10) (2015) 5956–5964, https://doi.org/10.1021/es506097c.

[59] S. Dixit, J.G. Hering, Comparison of arsenic(V) and arsenic(III) sorption onto iron oxide minerals: implications for arsenic mobility, Environ. Sci. Technol. 37 (18) (2003) 4182–4189, https://doi.org/10.1021/es030309t.

[60] Q. Zheng, S. Tu, Y. Chen, H. Zhang, W. Hartley, B. Ye, L. Ren, J. Xiong, W. Tan, A. Kappler, J. Hou, Micropore sites in ferrihydrite are responsible for its higher affinity towards As(III) relative to As(V), Geochem. Cosmochim. Acta 348 (2023) 27–40, https://doi.org/10.1016/j.gca.2023.03.007.

[61] N. Yamaguchi, T. Ohkura, A. Hikono, H. Yamaguchi, Y. Hashimoto, T. Makino, Effects of iron amendments on the speciation of arsenic in the rice rhizosphere after drainage, Soils 1 (1) (2017) 6, https://doi.org/10.3390/soils1010006.

[62] A.X. Hou, G.X. Chen, Z.P. Wang, O. van Cleemput, Jr Patrick, W. H, Methane and nitrous oxide emissions from a rice field in relation to soil redox and microbiological processes, Soil Sci. Soc. Am. J. 64 (2000) 2180–2186.

[63] H. Qin, Y. Tang, J. Shen, C. Wang, C. Chen, J. Yang, Y. Liu, X. Chen, Y. Li, H. Hou, Abundance of transcripts of functional gene reflects the inverse relationship between CH4 and N2O emissions during mid-season drainage in acidic paddy soil, Biol. Fertil. Soils 54 (8) (2018) 885–895, https://doi.org/10.1007/s00374-018-1312-7.

[64] M.F. Haroon, S. Hu, Y. Shi, M. Imelfort, J. Keller, P. Hugenholtz, Z. Yuan, G.W. Tyson, Anaerobic oxidation of methane coupled to nitrate reduction in a novel archaeal lineage, Nature 500 (7464) (2013) 567–570, https://doi.org/10.1038/nature12375.

[65] L. Fan, M.A. Dippold, T. Ge, J. Wu, V. Thiel, Y. Kuzyakov, M. Dorodnikov, Anaerobic oxidation of methane in paddy soil: role of electron acceptors and fertilization in mitigating CH4 fluxes, Soil Biol. Biochem. 141 (2020) 107685, https://doi.org/10.1016/j.soilbio.2019.107685.

[66] A. Vaksmaa, C. Lüke, T. van Alen, G. Valè, E. Lupotto, M.S.M. Jetten, K.F. Ettwig, Distribution and activity of the anaerobic methanotrophic community in a nitrogen-fertilized Italian paddy soil, FEMS (Fed. Eur. Microbiol. Soc.) Microbiol. Ecol. 92 (12) (2016), https://doi.org/10.1093/femsec/fiw181.

[67] M.O. Rivett, S.R. Buss, P. Morgan, J.W.N. Smith, C.D. Bemment, Nitrate attenuation in groundwater: a review of biogeochemical controlling processes, Water Res. 42 (16) (2008) 4215–4232, https://doi.org/10.1016/j.watres.2008.07.020.

[68] J.W. van Groenigen, D. Huygens, P. Boeckx, T.W. Kuyper, I.M. Lubbers, T. Rütting, P.M. Groffman, The soil N cycle: new insights and key challenges, SOIL 1 (1) (2015) 235–256, https://doi.org/10.5194/soil-1-235-2015.

[69] M. Feng, Y. Du, X. Li, F. Li, J. Qiao, G. Chen, Y. Huang, Insight into universality and characteristics of nitrate reduction coupled with arsenic oxidation in different paddy soils, Sci. Total Environ. 866 (2023) 161342, https://doi.org/10.1016/j.scitotenv.2022.161342.

[70] W. Chen, X. Yu, J. Huang, W. Zhao, J. Ju, J. Ye, H. Qin, Y. Long, The synergy of Fe(III) and NO2- drives the anaerobic oxidation of methane, Sci. Total Environ. 837 (2022) 155766, https://doi.org/10.1016/j.scitotenv.2022.155766.

[71] S.-J. Chun, Y.-J. Kim, Y. Cui, K.-H. Nam, Ecological network analysis reveals distinctive microbial modules associated with heavy metal contamination of abandoned mine soils in Korea, Environ. Pollut. 289 (2021) 117851, https://doi.org/10.1016/j.envpol.2021.117851.

[72] P.D. Martins, A. de Jong, W.K. Lenstra, N.A.G.M. van Helmond, C.P. Slomp, M.S.M. Jetten, C.U. Welte, O. Rasigraf, Enrichment of novel Verrucomicrobia, Bacteroidetes and Krumholzibacteria in an oxygen-limited, methane- and iron-fed bioreactor inoculated with Bothnian Sea sediments, Microbiology (Road Town, V. I. (Br.)) 10 (1) (2020) e1175, https://doi.org/10.1101/2020.09.22.307553.

[73] D. Emerson, E.K. Field, O. Chertkov, K.W. Davenport, L. Goodwin, C. Munk, M. Nolan, T. Woyke, Comparative genomics of freshwater Fe-oxidizing bacteria: implications for physiology, ecology, and systematics, Front. Microbiol. 4 (2013) 254, https://doi.org/10.3389/fmicb.2013.00254.

[74] Y.-M. Huang, N. Jakus, D. Straub, K.T. Konstantinidis, N. Blackwell, A. Kappler, S. Kleindienst, 'Candidatus ferrigenium straubiae' sp. nov., 'Candidatus ferrigenium bremense' sp. nov., 'Candidatus ferrigenium altingense' sp. nov., are autotrophic Fe(II)-oxidizing bacteria of the family Gallionellaceae, Syst. Appl. Microbiol. 45 (3) (2022) 126306, https://doi.org/10.1016/j.syapm.2022.126306.

[75] N. Jakus, N. Blackwell, D. Straub, A. Kappler, S. Kleindienst, Presence of Fe(II) and nitrate shapes aquifer-originating communities leading to an autotrophic enrichment dominated by an Fe(II)-oxidizing Gallionellaceae sp, FEMS (Fed. Eur. Microbiol. Soc.) Microbiol. Ecol. 97 (11) (2021), https://doi.org/10.1093/femsec/fiab145.

[76] Y.-M. Huang, D. Straub, A. Kappler, N. Smith, N. Blackwell, S. Kleindienst, A novel enrichment culture highlights core features of microbial networks contributing to autotrophic Fe(II) oxidation coupled to nitrate reduction, Microb. Physiol. 31 (3) (2021) 280–295, https://doi.org/10.1159/000517083.

[77] N. Jakus, N. Blackwell, K. Osenbrück, D. Straub, J.M. Byrne, Z. Wang, D. Glöckler, M. Elsner, T. Lueders, P. Grathwohl, S. Kleindienst, A. Kappler, Nitrate removal by a novel lithoautotrophic nitrate-reducing, iron(II)-oxidizing culture enriched from a pyrite-rich limestone aquifer, Appl. Environ. Microbiol. 87 (16) (2021) e0046021, https://doi.org/10.1128/AEM.00460-21.

[78] Y.-M. Huang, D. Straub, N. Blackwell, A. Kappler, S. Kleindienst, Meta-omics reveal Gallionellaceae and Rhodanobacter species as interdependent key players for Fe(II) oxidation and nitrate reduction in the autotrophic enrichment culture KS, Appl. Environ. Microbiol. 87 (15) (2021) e0049621, https://doi.org/10.1128/AEM.00496-21.

[79] T. Watanabe, N. Katayanagi, R. Agbisit, L. Llorca, Y. Hosen, S. Asakawa, Influence of alternate wetting and drying water-saving irrigation practice on the dynamics of Gallionella-related iron-oxidizing bacterial community in paddy field soil, Soil Biol. Biochem. 152 (2021) 108064, https://doi.org/10.1016/j.soilbio.2020.108064.

[80] T. Naruse, Y. Ban, T. Yoshida, T. Kato, M. Namikawa, T. Takahashi, M. Nishida, S. Asakawa, T. Watanabe, Community structure of microaerophilic iron-oxidizing bacteria in Japanese paddy field soils, Soil Sci. Plant Nutr. 65 (5) (2019) 460–470, https://doi.org/10.1080/00380768.2019.1671139.

[81] Y. Lu, D. Rosencrantz, W. Liesack, R. Conrad, Structure and activity of bacterial community inhabiting rice roots and the rhizosphere, Environ. Microbiol. 8 (8) (2006) 1351–1360, https://doi.org/10.1111/j.1462-2920.2006.01028.x.
[82] W. Sun, R. Sierra-Alvarez, L. Milner, R. Oremland, J.A. Field, Arsenite and ferrous iron oxidation linked to chemolithotrophic denitrification for the immobilization of arsenic in anoxic environments, Environ. Sci. Technol. 43 (17) (2009) 6585–6591, https://doi.org/10.1021/es900978h.
[83] P. Bao, G.-X. Li, Sulfur-driven iron reduction coupled to anaerobic ammonium oxidation, Environ. Sci. Technol. 51 (12) (2017) 6691–6698, https://doi.org/10.1021/acs.est.6b05971.
[84] A. Kappler, B. Schink, D.K. Newman, Fe(III) mineral formation and cell encrustation by the nitrate-dependent Fe(II)-oxidizer strain BoFeN1, Geobiology 3 (4) (2005) 235–245, https://doi.org/10.1111/j.1472-4669.2006.00056.x.
[85] S. Ishii, H. Ohno, M. Tsuboi, S. Otsuka, K. Senoo, Identification and isolation of active N2O reducers in rice paddy soil, ISME J. 5 (12) (2011) 1936–1945, https://doi.org/10.1038/ismej.2011.69.
[86] World Health Organization, Guidelines for drinking-water quality. Fourth Edition Incorporating the First Addendum, World Health Organization, 2017.

Supporting Information

Supporting information for

Arsenic immobilization and greenhouse gas emission depend on quantity and frequency of nitrogen fertilization in paddy soil

Hanna Grimm[1], Soeren Drabesch[1,2,3], Alan Nicol[4], Daniel Straub[5], Prachi Joshi[1], Christiane Zarfl[6], Britta Planer-Friedrich[4], E. Marie Muehe[2,3], Andreas Kappler[1,7*]

[1]*Geomicrobiology, Department of Geosciences, University of Tübingen, Schnarrenbergstrasse 94-96, 72076 Tübingen, Germany*

[2]*Plant Biogeochemistry, Department of Applied Microbial Ecology, Helmholtz Centre for Environmental Research - UFZ, Permoserstrasse 15, 04318 Leipzig, Germany*

[3]*Plant Biogeochemistry, Department of Geosciences, University of Tübingen, Schnarrenbergstrasse 94-96, 72076 Tübingen, Germany*

[4]*Environmental Geochemistry, Bayreuth Center for Ecology and Environmental Research (BayCEER), University of Bayreuth, Germany*

[5]*Quantitative Biology Center (QBiC), University of Tübingen, Germany*

[6]*Environmental Systems Analysis, Department of Geosciences, University of Tübingen, Schnarrenbergstrasse 94-96, 72076 Tübingen, Germany*

[7]*Cluster of Excellence: EXC 2124: Controlling Microbes to Fight Infection, Tübingen, Germany*

[*]Correspondence: andreas.kappler@uni-tuebingen.de

Table of Contents

Supplementary methods 3
Method S1: Soil characterization 3
Method S2: Microbial community analysis 5
Method S3: Pseudo-first-order kinetic model 6
Supplementary tables 7
Supplementary figures 13
References 33

Supplementary methods

Method S1: Soil characterization

Basic soil properties were analyzed in triplicates on soil samples after removal of plant debris and larger gravel. If not stated otherwise, analyses were performed at room temperature. For soil texture analysis, a soil dispersion was prepared by adding 25 mL of sodium pyrophosphate to 30 g of unsieved, fresh soil. After 30 min of stirring, the soil dispersion was filled up to a volume of 1000 mL and analyzed with a PARIO Soil Particle Analyzer (Meter Group, Germany).[1] After analysis, the soil was sieved (2 mm, 630 µm, 200 µm and 63 µm) to determine the sand and the fine fraction. Total loss of soil sample after sieving was below 5%. To determine the particle density, 20 g of dry soil was weighed into capillary pycnometer, filled up with deionized water and stepwise degassed before weight determination.[2] Bulk density was determined with a 100 cm^3 metal cylinder after drying fresh field soil at 105°C for 72 h.[3] Water contents from field fresh soil samples was determined by drying at 105°C for 72 h. Soil pH was determined by adding 10 mL of 0.01 M $CaCl_2$ to 2 g of field fresh soil samples (5:1, solution:soil) and measuring after 2 h and 24 h using a benchtop pH meter (SG2, Mettler-Toledo GmbH, Germany) equipped with a pH electrode (InLab Easy DIN, Mettler-Toledo GmbH, Germany).[4] The cation exchange capacity of the paddy soil was quantified in centrifuged samples after a 0.1 M $BaCl_2$ extraction (4 h, end-to-end shaker, 200 rpm), using 1.4 g of fresh soil (equivalent to ~1g of dry soil) and 25 mL of extraction solution, by microwave plasma atomic emission spectroscopy (4200 MP-AES, Agilent technologies, United States).[5] X-ray fluorescence (XRF) was used to determine total elemental contents of the dried paddy soil. To do so, glass beads were prepared by mixing 0.2333 g of dried and mortared sample with 3.9666 g of Fluxana FX-X65 (lithiumtetraborate:lithiummetaborate 66%:34%) and melted in a platinum crucible

using a Spetec Roto-Melt 2,0 µP at 0.45 for 6 min. Afterwards, the sample was poured into a platinum mold and loaded into a S8 Tiger (Bruker) prior to analysis. Total element concentrations were quantified using the calibration package GeoQuant (Bruker). The loss on ignition (LOI) was calculated as the percental weight difference between the dried (105°C for 24 h) and annealed sample powder (3000°C for 3 h) and is 6.06 wt%. The LOI and the total XRF sums add up to 99.93 wt%. Total soil carbon and nitrogen contents were analyzed for dry and mortared paddy soil samples by dry combustion (soliTOC cube, Elementar Analysensysteme GmbH, Germany). Water-extractable organic carbon and nitrogen species were determined in 0.45 µm filtered samples after extraction of 1 g dry weight soil with 5 mL of MQ (24 h, overhead shaker) by an elemental analyzer (multi N/C, 2100S, Analytik Jena GmbH) and segmented flow analysis (CFA, AutoAnalyzer 3, SEAL Analytical, Germany), respectively. To evaluate the presence of different Fe mineral phases and associated arsenic, sequential extractions were performed under anoxic conditions (rolling shaker or water bath). 1.3 g of fresh soil samples (equivalent to 1 g of dry soil) were extracted for 24 h with 10 mL of 1 M sodium acetate (pH 5, adjusted with acetic acid) targeting adsorbed Fe(II) and Fe in amorphous sulfide minerals (referred to as adsorbed Fe).[6,7] It is known that sodium acetate also extracts carbonates,[8] yet this is considered to play a minor role due to low total inorganic carbon contents and low pH (Table SI 1). This was followed by a 2 h extraction with 10 mL of 0.5 M HCl, extracting poorly crystalline Fe minerals and reduced Fe(II) minerals such as $FeCO_3$ and FeS (referred to as poorly crystalline Fe).[9] Lastly, samples were extracted for 24 h at 70°C with 10 mL of 6 M HCl for extraction of more crystalline Fe mineral phases and poorly reactive sheet silicate Fe or FeS species (referred to as crystalline Fe).[10]

Method S2: Microbial community analysis

Quantitative PCR (qPCR) was performed in technical triplicates for DNA and cDNA for bacterial 16S rRNA genes and for the *Geobacter* spp. marker gene. Due to low starting quantities of cDNA, only DNA analysis was performed for the functional genes *narG, nosZ, aioA* and *arrA*. A 7-fold standard dilution series was included in each qPCR assay. Data analysis was performed using the Bio-Rad CFX Maestro 1.1, software, version 4.1 (Bio-Rad, 2017). The qPCR primer sequences, gene-specific plasmid standards (pCR2.1®, Invitrogen, Darmstadt, Germany) and details of the thermal programs are given in Table SI 7. For 16S rRNA gene amplicon sequencing, Library preparation steps (Nextera, Illumina) and 250 bp paired-end sequencing with MiSeq (Illumina, San Diego, CA, USA) using v2 chemistry were performed by Microsynth AG (Balgach, Switzerland). Between 126,043 and 193,506 read pairs were obtained for each of the 6 samples (in total 930,001 read pairs). For data analysis, primers were trimmed, and untrimmed sequences were discarded (<6% per sample) with Cutadapt version 3.4.[11] Adapter and primer-free sequences were processed with DADA2 v1.22.0 to eliminate PhiX contamination, trim reads (before median quality drops below 35; forward reads were trimmed at 181 bp and reverse reads at 167 bp), correct errors, merge read pairs, and remove polymerase chain reaction (PCR) chimeras; ultimately, 6,891 amplicon sequencing variants (ASVs) were obtained across all samples.[12] Taxonomic classification was performed with DADA2 and the SILVA v138 database.[13] Intermediate results were imported into QIIME2 version 2021.8.0.[14] 208 ASVs classified as chloroplasts or mitochondria were removed, totaling <2% (average 0.86%) relative abundance per sample, and retaining 6,683 ASVs across all samples. Alpha rarefaction curves were produced with the QIIME2 diversity alpha-rarefaction plugin, which indicated that the richness of the samples had been fully observed.

Method S3: Pseudo-first-order kinetic model

Pseudo-first-order rate constants k for nitrate reduction were derived using eq. 1,

$$\ln\left(\frac{c_t}{c_0}\right) = -kt \quad (1)$$

with c_t: concentration of NO_3^- in mM at time t in days, c_0: initial concentrations of NO_3^- in mM, k: rate constant in day^{-1}. The model for pseudo-first-order kinetics was fitted to the experimental data with $y = \ln\left(\frac{c_t}{c_0}\right)$, $x = t$, where the slope corresponds to $-k$, fixing the y-intercept at 0. Half-life times were calculated using eq. 2,

$$t_{1/2} = \frac{\ln(2)}{k} \quad (2)$$

with $t_{1/2}$: half-life time in days and k: rate constant in day^{-1}.

Supplementary tables

Table SI 1 | Characterization of basic soil properties of paddy soil collected from Vercelli, Italy.

		Vercelli, Italy
Coordinates		45°19'26" N, 8°22'25" E
Parent material		River alluvium
Paddy management		rice
N Fertilizer - Urea	[kg N ha^{-1} $year^{-1}$]	279
Sampling depth	[cm]	0-20
Soil texture		
Sand	[%]	23.99 ± 2.17
Silt	[%]	58.00 ± 2.00
Clay	[%]	17.33 ± 3.21
CEC	[cmol kg^{-1}]	5.45 ± 0.04
pH_{CaCl2}		4.94 ± 0.05
Water content	[%]	23.88 ± 0.95
TOC	[%]	1.39 ± 0.10
TIC	[%]	0.05 ± 0.00
TN	[%]	0.12 ± 0.00
Adsorbed Fe*	[g kg^{-1}]	0.67 ± 0.07
Poorly crystalline Fe*	[g kg^{-1}]	2.23 ± 0.18
Crystalline Fe*	[g kg^{-1}]	18.03 ± 3.58
Total extractable Fe*	[g kg^{-1}]	20.93 ± 3.58
Adsorbed Fe-As*	[mg kg^{-1}]	3.90 ± 0.55
Poorly crystalline Fe-As*	[mg kg^{-1}]	0.63 ± 0.03
Crystalline Fe-As*	[mg kg^{-1}]	4.46 ± 0.92
Total extractable Fe-As*	[mg kg^{-1}]	8.99 ± 1.07
Na°	[g kg^{-1}]	16.039
Mg°	[g kg^{-1}]	17.212
Al°	[g kg^{-1}]	72.351
Si°	[g kg^{-1}]	302.73
P°	[g kg^{-1}]	0.55
S°	[g kg^{-1}]	0.48
K°	[g kg^{-1}]	16.03
Ca°	[g kg^{-1}]	17.27
Ti°	[g kg^{-1}]	5.36
V°	[g kg^{-1}]	0.07
Cr°	[g kg^{-1}]	0.23
Mn°	[g kg^{-1}]	0.49
Fe°	[g kg^{-1}]	33.29
Ni°	[g kg^{-1}]	0.24
Zn°	[g kg^{-1}]	0.05
Zr°	[g kg^{-1}]	0.16
Ba°	[g kg^{-1}]	0.04

Average and standard deviation are represented by triplicate measurements

*Obtained by sequentially extracting paddy soil samples with 1 M Na-acetate (adsorbed), 0.5 M HCl (poorly crystalline) and 6 M HCl (crystalline)

°Obtained by XRF analysis

Table SI 2 | Composition of artificial irrigation water used for microcosm incubation.

Artificial groundwater composition		
pH		6.2
electrical conductivity	µS cm^{-1}	550
$CaCl_2$	mmol L^{-1}	1.75
NaCl		0.44
$MgCl_2$		0.82
KCl		0.08

Table SI 3 | Volume of KNO_3 stock solution added to N fertilized microcosms.

Treatment	**KNO_3 stock**	**1st fertilization Volume added**	**2nd fertilization Volume added**
	mg N L^{-1}	mL	mL
Control	0	0	0
Low	777.81	0.83	0.86
Medium	2290.98	0.8	0.84
High	4610.98	0.8	0.83

Table SI 4 | Overview of ICP-MS parameters for total arsenic analysis from sequential extractions resembling Fe-bound arsenic.

Element	**Calibration range**	**Detection limit**	**Quality control 1**	**Quality control 2**	**Quality control 3**	**Instrument**
			ppb			
Arsenic	0-500	0.04	1.76 ± 0.24	2.40 ± 0.20	47.22 ± 2.55	Agilent 7900
		0.47	2.27 ± 0.5	66.75 ± 16.01		Agilent 7900

Table SI 5 | Recovery of total arsenic by comparing the sum of arsenite and arsenate obtained from arsenic speciation analysis with data from total arsenic analysis for representative samples.

Days	Treatment	Replicate	Arsenite	Arsenate	Total As (sum of species)	Total As (measured)	Recovery
			µg L^{-1}	µg L^{-1}	µg L^{-1}	µg L^{-1}	%
71	Control	2	27.03	26.99	54.02	54.94	98.33
71	Control	3	29.76	28.32	58.08	63.95	90.81
71	Low	3	31.42	25.58	57.00	59.65	95.54
85	Control	1	30.72	46.76	77.48	79.61	97.32
85	Control	2	39.81	43.14	82.95	92.60	89.57
85	Control	3	37.13	30.22	67.35	77.53	86.88
125	Control	1	30.11	31.53	61.64	64.53	95.52
125	Control	2	35.17	44.75	79.92	81.08	98.56
125	Control	3	31.06	27.65	58.71	58.63	100.14
125	Low	1	27.62	21.60	49.22	53.08	92.72
125	Low	3	38.62	30.53	69.15	72.92	94.83
129	Control	1	21.80	31.19	52.99	52.34	101.24
129	Control	2	26.70	37.28	63.98	67.37	94.98
129	Control	3	28.09	42.57	70.67	82.54	85.61
129	Low	1	27.78	26.67	54.46	51.76	105.22
129	Low	3	36.09	43.44	79.52	81.72	97.31

Recovery on average by 94.78±23.91%.

Table SI 6 | Calibration parameters of greenhouse gases CO_2, N_2O and CH_4.

Gas	Calibration range	Slope	Intercept	R^2	Detection limit	Quantification limit
	ppm				ppm	ppm
CO_2	0-200	34.98	-14.93	0.9985	-0.13	1.25
N_2O	0-3.5	26.18	0.01	0.9916	0.01	0.01
CH_4	0-2	26.87	-0.50	0.9902	0.08	0.29

Table SI 7 | Standards, primers and thermal profiles used in qPCR assays for different target genes.

Target gene	Standard	Primer	Primer sequence (5' -> 3')	Primer concentration (nM)	Thermal program	References
Bacterial 16S rRNA gene	*Thiomonas* sp.	515F	TCGTCGGCAGC GTCAGATGTGT AT	250	95°C - 3'; (95°C - 10''; 55°C - 30'') x 40; 95°C - 30''; 60-95°C - 5''	[15]
			AAGAGACAGGT GY			
			CAGCMGCCGCG GTA			
		806R	GTCTCGTGGGC TCGGAGATGTG T	250		
			ATAAGAGACAG GG			
			ACTACNVGGGT WTCTAAT			
Geobacter-aceae 16S rRNA gene	*Geobacter* sp.	Geo577F	GCGTGTAGGCG GTTTSTTAA	250	95°C - 3'; (95°C - 30''; 55°C - 20''; 72°C - 30'') x 40; 95°C - 2'; 60-95°C - 5''	modified after Stults et al.[16]
		Geo822R	TACCCGCRACA CCTAGTACT	250		
narG	*Pseudo-monas aeruginosa*	narG-F	TCGCCSATYCC GGCSATGTC	250	95°C - 3'; (95°C - 10''; 62°C - 20'') x 40; 95°C - 2'; 70-95°C - 5''	[17]
		narG-R	GAGTTGTACCA GTCRGCSGAYT CSG	250		
nosZ	*Ensifer meliloti 1021*	nosZ2F	CGCRACGGCAA SAAGGTSMSSG T	250	95°C - 3'; (95°C - 15''; 60°C - 25'') x 40; 95°C - 2'; 65-95°C - 5''	[18]
		nosZ2R	CAKRTGCAKSG CRTGGCAGAA	250		
aioA	clone Red_G05 As SF	aioA-1F	TGCATCGTSGG BTGYGGNTA	500	95°C - 3'; (95°C - 30''; 60°C - 30'') x 40; 95°C - 2'; 65-95°C - 5''	[19]
		aioA-1R	ACSACGCABTC YTTGTCSGG	500		
arrA	clone Red_A06 As SF	arrA-F	GGYSTGGGGC WSCGAYCC	500	95°C - 3'; (95°C - 30''; 62°C - 40'') x 40; 95°C - 2'; 65-95°C - 5''	[20]
		arrA-R	GGMASCCASTY GTGGGMCTT	500		

Table SI 8 | Rate constants and coefficient of determination of pseudo-first-order reaction kinetics for nitrate reduction in low, medium and high N treatment.

Treatment	Fertilization period	Time	Rate constant *k*	half-life time	R^2
		days	$days^{-1}$	days	
Low	1st	0-10	0.40	1.73	0.9507
	2nd	49-55	0.75	0.92	0.9877
Medium	1st	0-16	0.23	2.98	0.8567
	2nd	49-71	0.24	2.91	0.9095
High	1st	0-37	0.08	8.54	0.8171
	2nd	49-129	0.05	12.96	0.8158

Table SI 9 | Proportion of reduced nitrate by oxidized dissolved iron(II) based on theoretical stoichiometry ratio of 1:5 ($nitrate_{red.}$:$iron(II)_{ox.}$) during autotrophic nitrate reduction coupled to iron(II) oxidation for the low, medium and high N treatment during the 1st and 2nd fertilization period. Reduced nitrate and oxidized Fe(II) was calculated as the difference between day 49 and 0 and between day 49 and 129 for the first and second fertilization period, respectively.

Fertilization	Treatment	Dissolved $nitrate_{red.}$	Dissolved $Fe(II)_{ox.}$	Contribution of dissolved $Fe(II)_{ox.}$ to $nitrate_{red.}$
		mM	mM	%
1st period	Low	0.17 ± 0.01	0.03 ± 0.01	3.62 ± 1.74
	medium	0.53 ± 0.02	0.12 ± 0.02	4.61 ± 0.75
	High	0.97 ± 0.09	0.14 ± 0.01	2.95 ± 0.39
2nd period	Low	0.45 ± 0.02	0.12 ± 0.01	5.55 ± 0.57
	medium	1.18 ± 0.15	0.25 ± 0.02	4.16 ± 0.68
	High	2.58 ± 0.05	0.06 ± 0.02	0.48 ± 0.13

Table SI 10 | Results of a Kruskal Wallis test to identify differences in total global warming potential (GWP), CO_2, CH_4 and N_2O emissions between treatments. The p-value indicates significant differences among treatments at the 0.05 significance level.

Comparison	χ^2	df	p-value
Treatment vs total GWP	7.35	3	0.06158
Treatment vs CO_2	8.32	3	0.03987
Treatment vs CH_4	9.73	3	0.02101
Treatment vs N_2O	8.8	3	0.03203

Table SI 11 | Results of the ANOVA (a) and the post-hoc test (Tukey test) (b) across different treatments. The p-value indicates significant differences among treatments at the 0.05 significance level.

a) ANOVA

Comparison	Sum of squares (SS)	Degrees of Freedom (DF)	Mean square (MS)	F-value	p-value
Treatment vs Proteobacteria	54.52	5	10.905	44.13	$2.58*10^{-7}$
Treatment vs Verrucomicrobiota	2.701	5	0.5402	4.257	0.0185
Treatment vs 16S rRNA transcript	658.5	3	219.51	11.07	0.0032

b) Tukey Test

Parameter	Group	Timepoint	p-value
Proteobacteria	Control vs High	day 37	$1.5*10^{-6}$
Verrucomicrobiota	Control vs High	day 37	0.0444
16S rRNA transcript number	Control vs High	day 37	0.0167

Supplementary figures

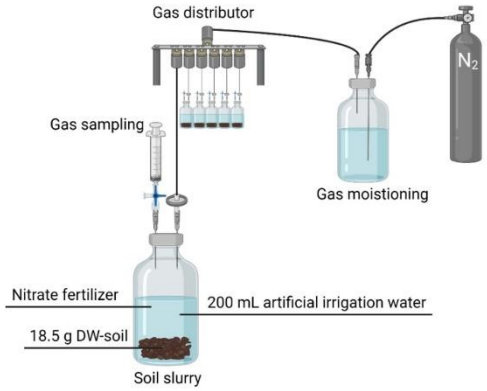

Figure SI 1 | Overview of experimental setup of microcosm experiment.

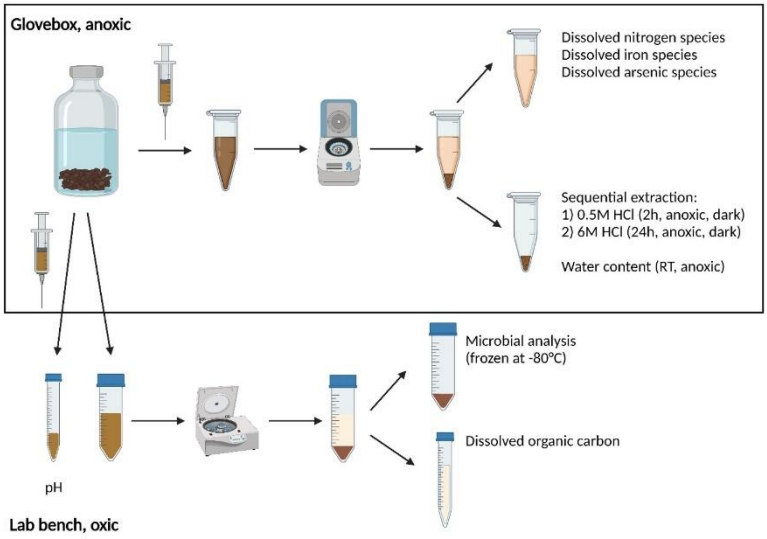

Figure SI 2 | Sampling overview, starting with a soil slurry sample taken in the glovebox for dissolved nitrogen species, Fe, arsenic and for water content. The dried soil was further sequentially extracted by 0.5 M HCl (2 h) and 6 M HCl (24 h). At selected timepoints a soil slurry sample was taken for pH, dissolved organic carbon and microbial analysis.

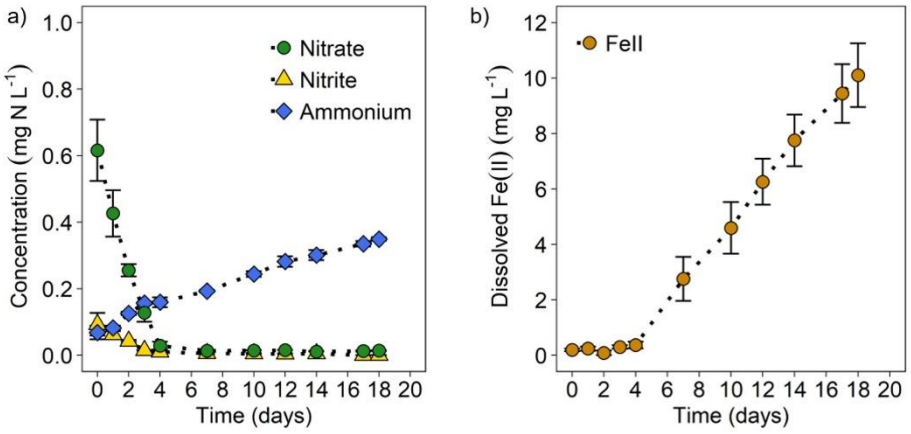

Figure SI 3 | Dissolved nitrate, nitrite and ammonium concentration in mg N L^{-1} (a) and dissolved Fe(II) in mg L^{-1} (b) during pre-incubation. Mean ± standard deviation is shown for biological triplicates.

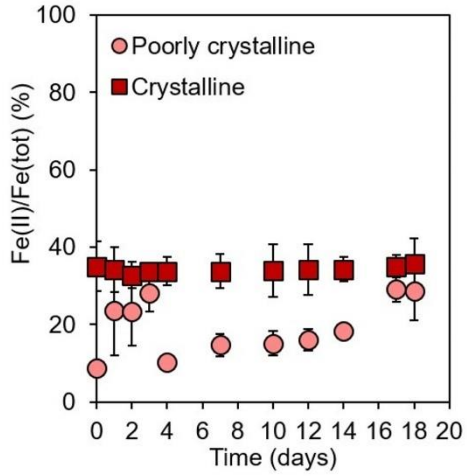

Figure SI 4 | Poorly crystalline and crystalline Fe(II)/Fe(tot) ratio in % during pre-incubation. Mean ± combined standard deviation from Fe(II) and Fe(tot) analysis is shown for biological triplicates.

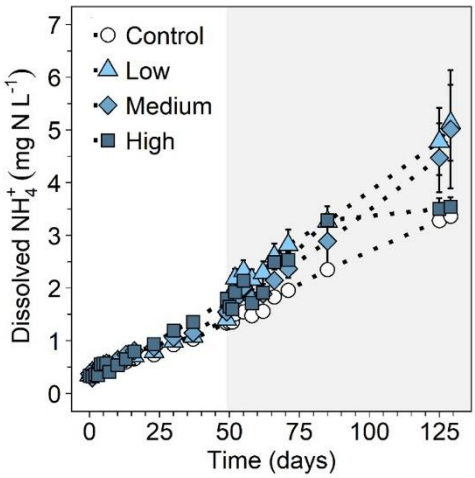

Figure SI 5 | Dissolved ammonium concentrations in mg N L^{-1} during the 129 days of incubation for the non-fertilized control and the N fertilized treatments (low N, medium N, high N). Mean ± standard deviation is shown for biological triplicates and the mean ± range for the low N treatment in the second fertilization for biological duplicates. The white background illustrates the first (0-49 days) and the grey background the second (49-129 days) nitrate fertilization period.

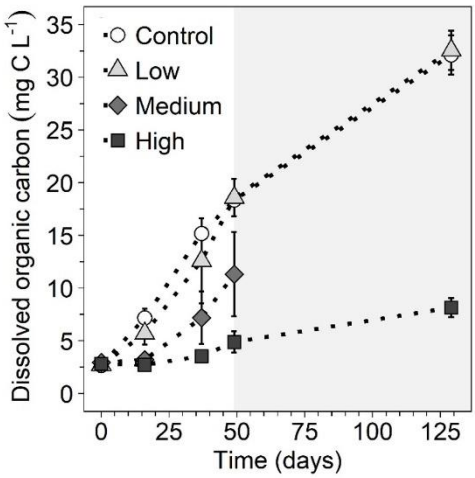

Figure SI 6 | Dissolved organic carbon in mg C L^{-1} during the 129 days of incubation for the non-fertilized control and the N fertilized treatments (low N, medium N, high N). Mean ± standard deviation is shown for biological triplicates and the mean ± range for the low N treatment in the second fertilization for biological duplicates. The white background illustrates the first (0-49 days) and the grey background the second (49-129 days) nitrate fertilization period. No measurement for dissolved organic carbon was possible on day 129 for the medium N treatment.

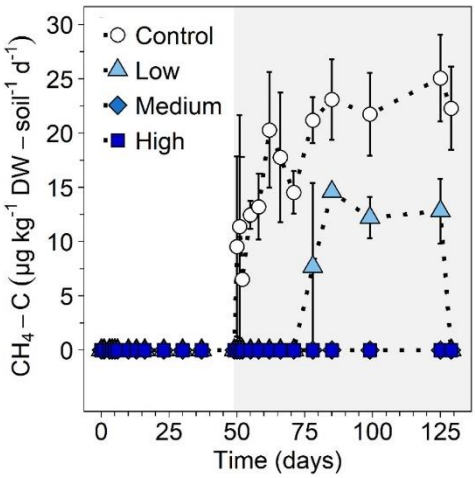

Figure SI 7 | Rates of CH_4-C emissions in µg kg^{-1} DW-$soil^{-1}$ d^{-1} during the 129 days of incubation for the non-fertilized control and the N fertilized treatments (low N, medium N, high N). Mean ± standard deviation is shown for biological triplicates and the mean ± range for the low N treatment in the second fertilization for biological duplicates. The white background illustrates the first (0-49 days) and the grey background the second (49-129 days) nitrate fertilization period.

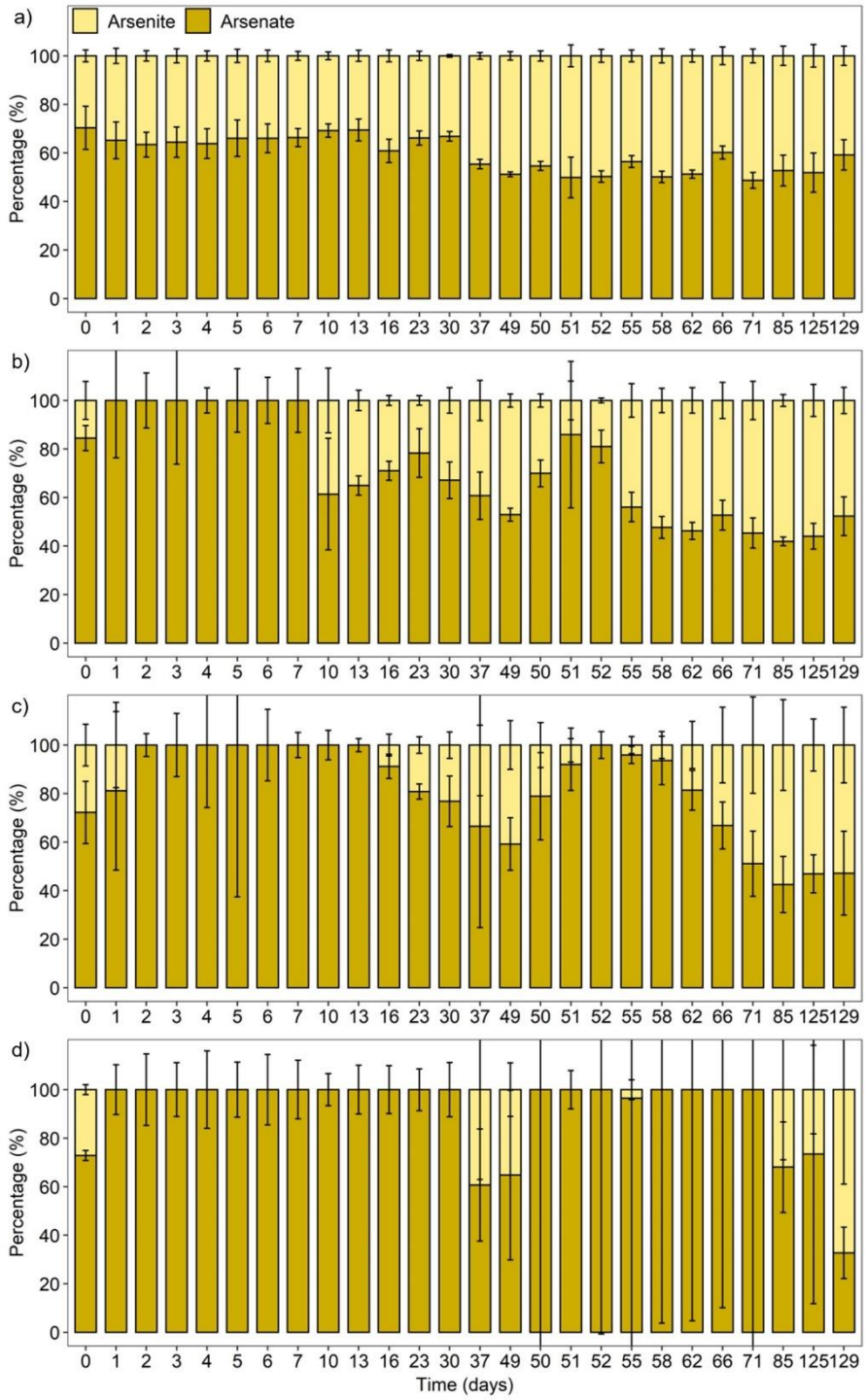
a)
Arsenite
Arsenate
b)
c)
d)
Percentage (%)
0
20
40
60
80
100
0 1 2 3 4 5 6 7 10 13 16 23 30 37 49 50 51 52 55 58 62 66 71 85 125 129
Time (days)

18

Figure SI 8 | Dissolved arsenite (dark) and arsenate (bright) percentages during the 129 days of incubation for the non-fertilized control (a), low N (b), medium N (c) and high N (d) fertilizer treatment. Mean ± standard deviation is shown for biological triplicates and the mean ± range for the low N treatment in the second fertilization for biological duplicates.

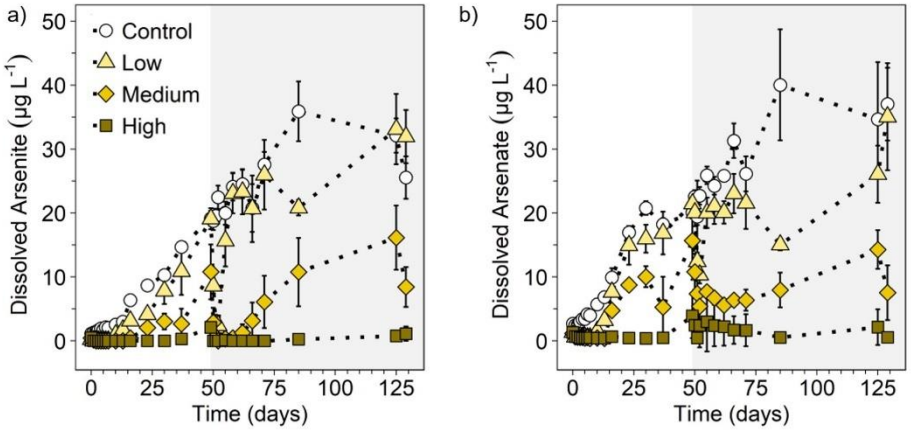

Figure SI 9 | Dissolved arsenite (a) and arsenate (b) concentrations in µg L^{-1} during the 129 days of incubation for the non-fertilized control and the N fertilized treatments (low N, medium N, high N). Mean ± standard deviation is shown for biological triplicates and the mean ± range for the low N treatment in the second fertilization for biological duplicates. The white background illustrates the first (0-49 days) and the grey background the second (49-129 days) nitrate fertilization period.

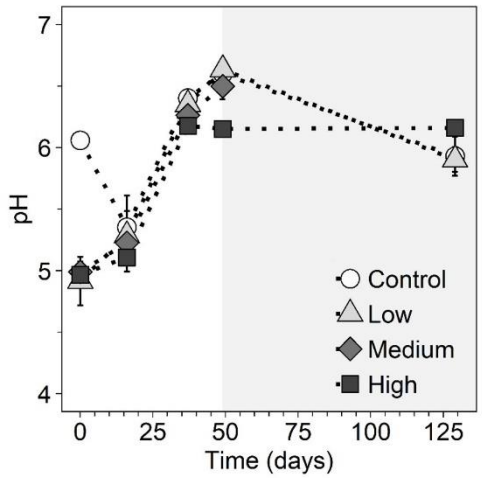

Figure SI 10 | pH of the soil slurry during the 129 days of incubation for the non-fertilized control and the N fertilized treatments (low N, medium N, high N). Mean ± standard deviation is shown for biological triplicates and the mean ± range for the low N treatment in the second fertilization for biological duplicates. The white background illustrates the first (0-49 days) and the grey background the second (49-129 days) nitrate fertilization period. No measurement for pH was possible on day 129 for the medium N treatment. Note that the y-axis spans pH values from 4 to 7.

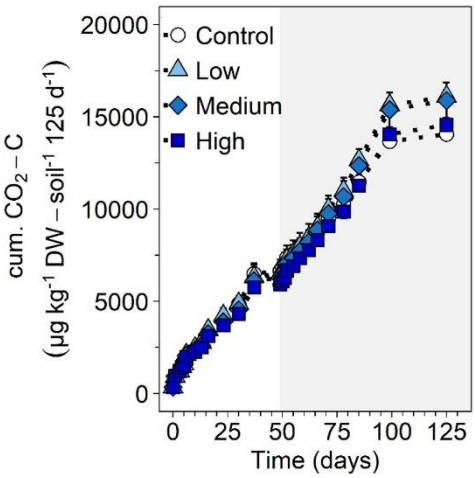

Figure SI 11 | Cumulative CO_2-C in µg kg^{-1} DW-$soil^{-1}$ 125 $days^{-1}$ during the 129 days of incubation for the non-fertilized control and the N fertilized treatments (low N, medium N, high N). Mean ± standard deviation is shown for biological triplicates and the mean ± range for the low N treatment in the second fertilization for biological duplicates. The white background illustrates the first (0-49 days) and the grey background the second (49-129 days) nitrate fertilization period.

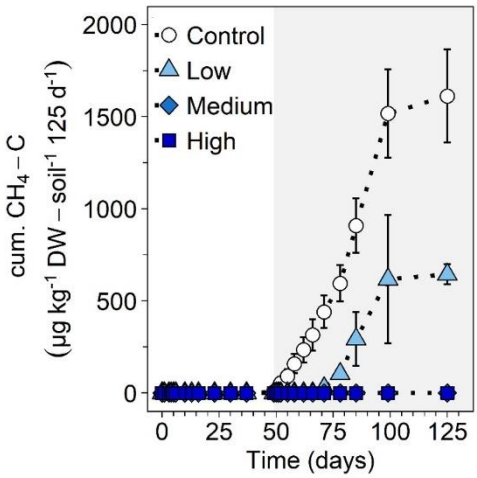

Figure SI 12 | Cumulative CH_4-C in µg kg^{-1} DW-$soil^{-1}$ 125 $days^{-1}$ during the 129 days of incubation for the non-fertilized control and the N fertilized treatments (low N, medium N, high N). Mean ± standard deviation is shown for biological triplicates and the mean ± range for the low N treatment in the second fertilization for biological duplicates. The white background illustrates the first (0-49 days) and the grey background the second (49-129 days) nitrate fertilization period.

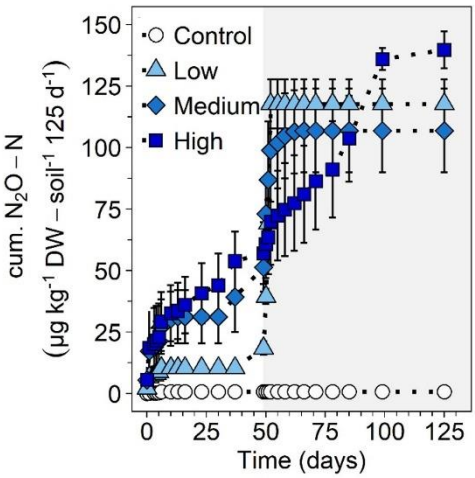

Figure SI 13 | Cumulative N_2O-N in µg kg^{-1} DW-$soil^{-1}$ 125 $days^{-1}$ during the 129 days of incubation for the non-fertilized control and the N fertilized treatments (low N, medium N, high N). Mean ± standard deviation is shown for biological triplicates and the mean ± range for the low N treatment in the second fertilization for biological duplicates. The white background illustrates the first (0-49 days) and the grey background the second (49-129 days) nitrate fertilization period.

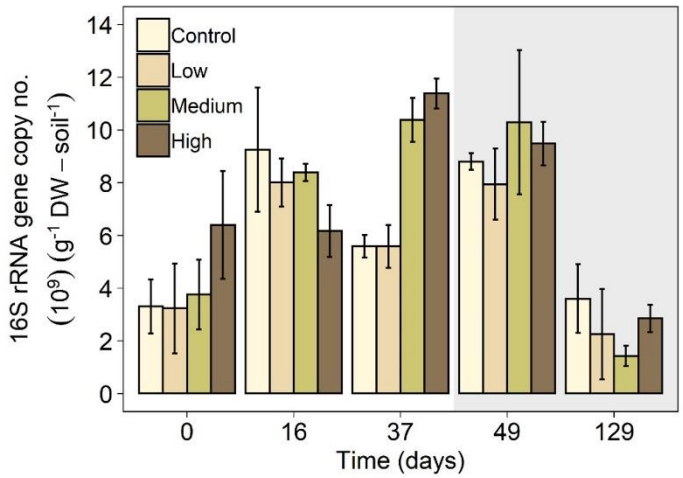

Figure SI 14 | 16S rRNA gene copy numbers (10^9) in g^{-1} DW-$soil^{-1}$ at different timepoints during the 129 days of incubation for the non-fertilized control and the N fertilized treatments (low N, medium N, high N). Mean ± standard deviation is shown for biological triplicates and the mean ± range for the low N treatment in the second fertilization for biological duplicates. The white background illustrates the first (0, 16, 37 days) and the grey background the second (49, 129 days) nitrate fertilization period.

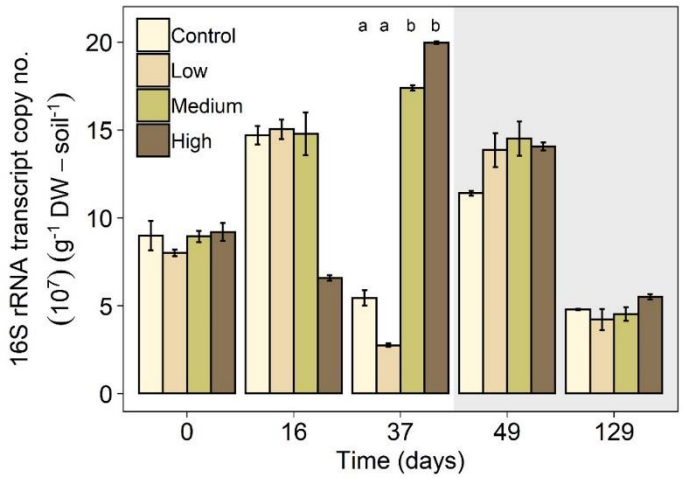

Figure SI 15 | 16S rRNA transcript copy numbers (10^7) in g^{-1} DW-$soil^{-1}$ at different timepoints during the 129 days of incubation for the non-fertilized control and the N fertilized treatments (low N, medium N, high N). Mean ± standard deviation is shown for biological triplicates and the mean ± range for the low N treatment in the second fertilization for biological duplicates. Small letters indicate significant differences on day 37 between treatments ($p<0.05$, one-way ANOVA). The white background illustrates the first (0, 16, 37 days) and the grey background the second (49, 129 days) nitrate fertilization period.

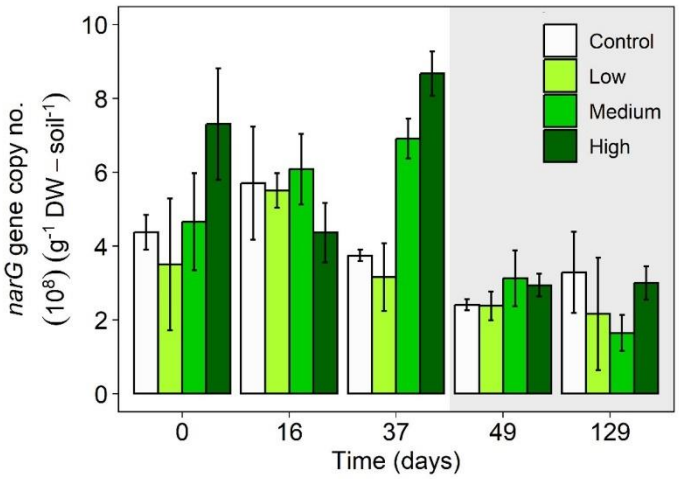

Figure SI 16 | Quantifying the potential for nitrate reduction with *narG* gene copy numbers (10^8) in g^{-1} DW-$soil^{-1}$ responsible for nitrate reduction at different timepoints during the 129 days of incubation for the non-fertilized control and the N fertilized treatments (low N, medium N, high N). The white background illustrates the first (0, 16, 37 days) and the grey background the second (49, 129 days) nitrate fertilization period.

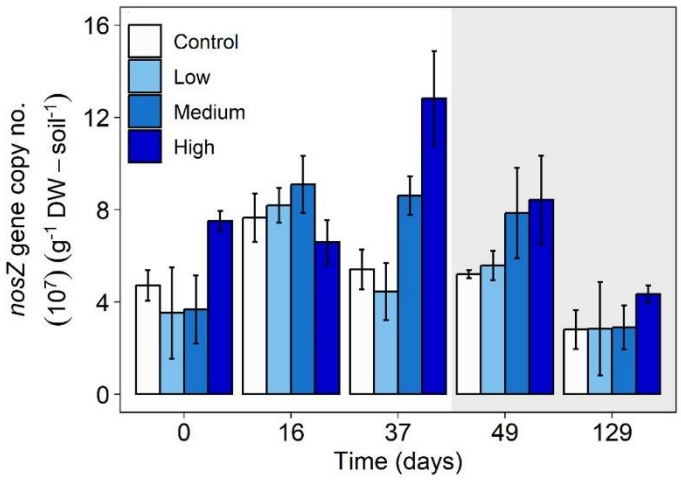

Figure SI 17 | Quantifying the potential for nitrous oxide reduction with *nosZ* gene copy numbers (10^7) in g^{-1} DW-$soil^{-1}$ at different timepoints during the 129 days of incubation for the non-fertilized control and the N fertilized treatments (low N, medium N, high N). The white background illustrates the first (0, 16, 37 days) and the grey background the second (49, 129 days) nitrate fertilization period.

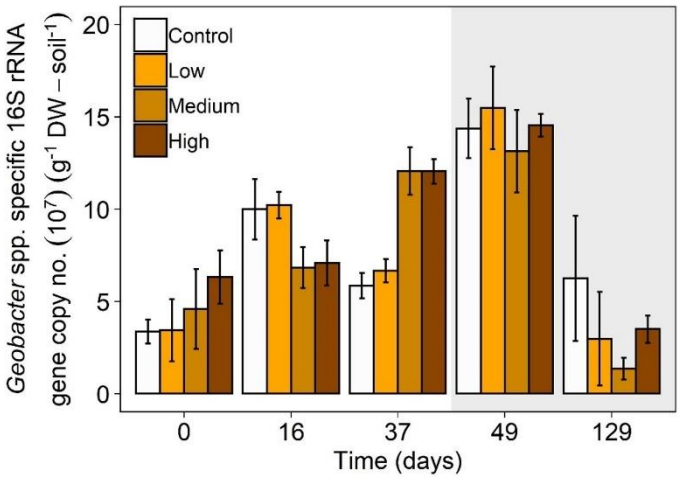

Figure SI 18 | Fe(III)-reducing bacterial numbers approximated by *Geobacter* spp. specific 16S rRNA gene copy numbers (10^7) in g^{-1} DW-$soil^{-1}$ at different timepoints during the 129 days of incubation for the non-fertilized control and the N fertilized treatments (low N, medium N, high N). The white background illustrates the first (0, 16, 37 days) and the grey background the second (49, 129 days) nitrate fertilization period.

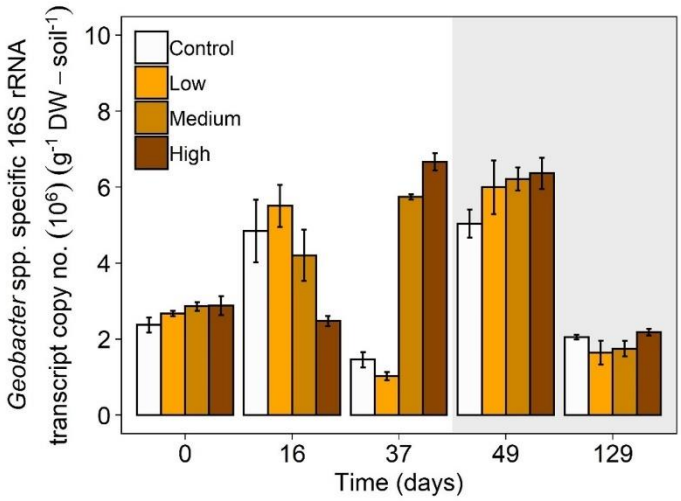

Figure SI 19 | Fe(III)-reducing bacterial activity approximated by *Geobacter* spp. specific 16S rRNA transcript numbers (10^6) in g^{-1} DW-$soil^{-1}$ at different timepoints during the 129 days of incubation for the non-fertilized control and the N fertilized treatments (low N, medium N, high N). The white background illustrates the first (0, 16, 37 days) and the grey background the second (49, 129 days) nitrate fertilization period.

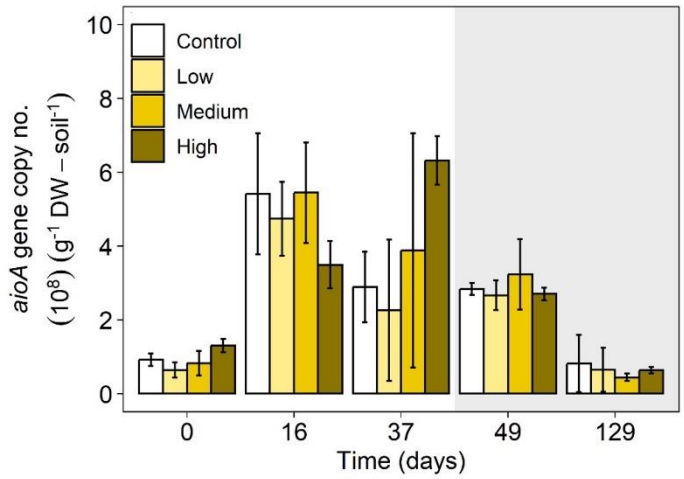

Figure SI 20 | Potential for arsenite oxidation quantified by *aioA* gene copy numbers (10^8) in g^{-1} DW-$soil^{-1}$ at different timepoints during the 129 days of incubation for the non-fertilized control and the N fertilized treatments (low N, medium N, high N). The white background illustrates the first (0, 16, 37 days) and the grey background the second (49, 129 days) nitrate fertilization period.

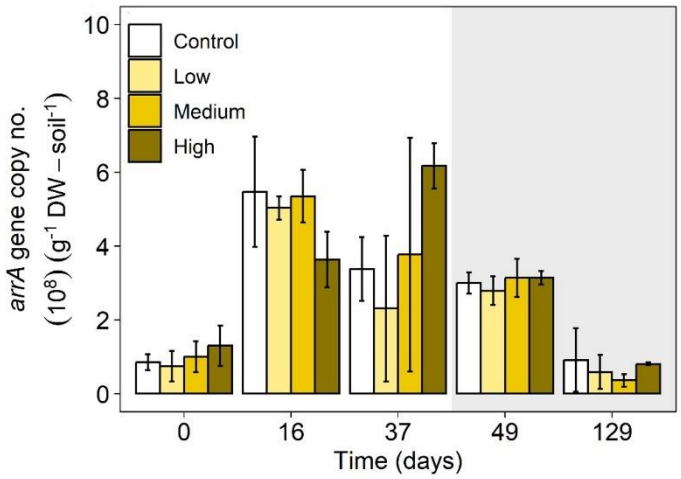

Figure SI 21 | Potential for arsenate reduction quantified by *arrA* gene copy numbers (10^8) in g^{-1} DW-$soil^{-1}$ at different timepoints during the 129 days of incubation for the non-fertilized control and the N fertilized treatments (low N, medium N, high N). The white background illustrates the first (0, 16, 37 days) and the grey background the second (49, 129 days) nitrate fertilization period.

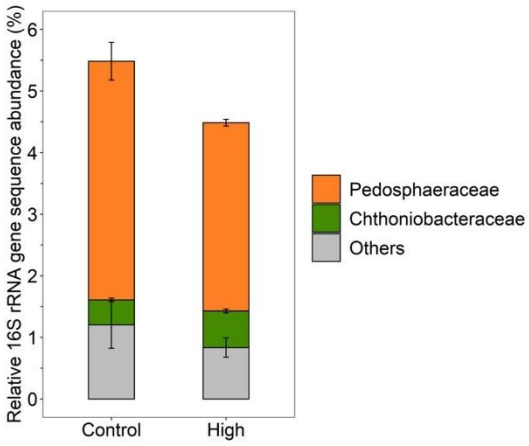

Figure SI 22 | Relative 16S rRNA gene sequence abundance in % on family level of the phyla *Verrucomicrobiota* for the control and high N treatment on day 37. "Others" represent families with abundances below 0.5% on average.

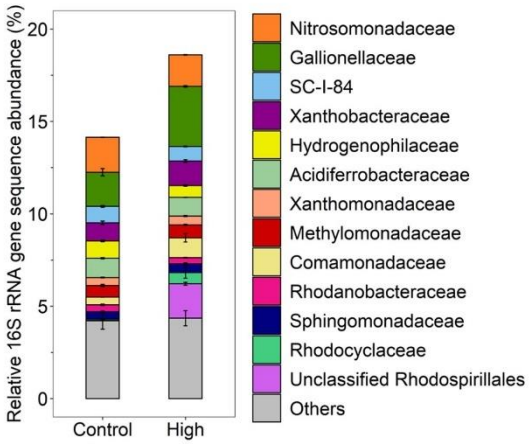

Figure SI 23 | Relative 16S rRNA gene sequence abundance in % on family level of the phyla *Proteobacteria* for the control and high N treatment on day 37. "Others" represent families with abundances below 0.5% on average.

References

(1) DIN 18123. Soil, investigation and testing - Determination of grain-size distribution **2011**.

(2) DIN 18124. Soil, investigation and testing - Determination of density of solid particles - Capillary pyknometer, wide mouth pycnometer, gas pycnometer **2011**.

(3) DIN EN ISO 17828. Solid biofuels - Determination of bulk density **2016**.

(4) ISO 10390. Soil, treated biowaste and sludge - Determination of pH **2021**.

(5) Muehe, E. M.; Wang, T.; Kerl, C. F.; Planer-Friedrich, B.; Fendorf, S. Rice production threatened by coupled stresses of climate and soil arsenic. *Nature communications* **2019**, *10* (1), 4985. DOI: 10.1038/s41467-019-12946-4.

(6) Roden, E. E.; Zachara, J. M. Microbial Reduction of Crystalline Iron(III) Oxides: Influence of Oxide Surface Area and Potential for Cell Growth. *Environmental Science & Technology* **1996**, *30* (5), 1618–1628. DOI: 10.1021/es9506216.

(7) Shannon, R. D.; White, J. R. The selectivity of a sequential extraction procedure for the determination of iron oxyhydroxides andiron sulfides in lake sediments. *Biogeochemistry* **1991**, *14* (3), 193–208. DOI: 10.1007/BF00000807.

(8) A. Tessier; P. G. C. Campbell; M. Bisson. Sequential extraction procedure for the speciation of particulate trace metals. *Analytical Chemistry* **1979**, *51* (7), 844–851.

(9) Heron, G.; Crouzet, C.; Bourg, A. C.; Christensen, T. H. Speciation of Fe(II) and Fe(III) in Contaminated Aquifer Sediments Using Chemical Extraction Techniques. *Environ. Sci. Technol.* **1994**, *28* (9), 1698–1705. DOI: 10.1021/es00058a023.

(10) Lueder, U.; Maisch, M.; Laufer, K.; Jorgensen, B. B.; Kappler, A.; Schmidt, C. Influence of Physical Perturbation on Fe(II) Supply in Coastal Marine Sediments. *Environmental Science & Technology* **2020**, *54* (6), 3209–3218. DOI: 10.1021/acs.est.9b06278.

(11) Martin, M. Cutadapt removes adapter sequences from high-throughput sequencing reads. *EMBnet j.* **2011**, *17* (1), 10. DOI: 10.14806/ej.17.1.200.

(12) Callahan, B. J.; McMurdie, P. J.; Rosen, M. J.; Han, A. W.; Johnson, A. J. A.; Holmes, S. P. DADA2: High-resolution sample inference from Illumina amplicon data. *Nature Methods* **2016**, *13* (7), 581–583. DOI: 10.1038/nmeth.3869.

(13) Quast, C.; Pruesse, E.; Yilmaz, P.; Gerken, J.; Schweer, T.; Yarza, P.; Peplies, J.; Glöckner, F. O. The SILVA ribosomal RNA gene database project: improved data processing and web-based tools. *Nucleic Acids Research* **2013**, *41* (Database issue), D590-6. DOI: 10.1093/nar/gks1219.

(14) Bolyen, E.; Rideout, J. R.; Dillon, M. R.; Bokulich, N. A.; Abnet, C. C.; Al-Ghalith, G. A.; Alexander, H.; Alm, E. J.; Arumugam, M.; Asnicar, F.; Bai, Y.; Bisanz, J. E.; Bittinger, K.; Brejnrod, A.; Brislawn, C. J.; Brown, C. T.; Callahan, B. J.; Caraballo-Rodríguez, A. M.; Chase, J.; Cope, E. K.; Da Silva, R.; Diener, C.; Dorrestein, P. C.; Douglas, G. M.; Durall, D. M.; Duvallet, C.; Edwardson, C. F.; Ernst, M.; Estaki, M.; Fouquier, J.; Gauglitz, J. M.; Gibbons, S. M.; Gibson, D. L.; Gonzalez, A.; Gorlick, K.; Guo, J.; Hillmann, B.; Holmes, S.; Holste, H.; Huttenhower, C.; Huttley, G. A.; Janssen, S.; Jarmusch, A. K.; Jiang, L.; Kaehler, B. D.; Kang, K. B.; Keefe, C. R.; Keim, P.; Kelley, S. T.; Knights, D.; Koester, I.; Kosciolek, T.; Kreps, J.; Langille, M. G. I.; Lee, J.; Ley, R.; Liu, Y.-X.; Loftfield, E.; Lozupone, C.; Maher, M.; Marotz, C.; Martin, B. D.; McDonald, D.; McIver, L. J.; Melnik, A. V.; Metcalf, J. L.; Morgan, S. C.; Morton, J. T.; Naimey, A. T.; Navas-Molina, J. A.; Nothias, L. F.; Orchanian, S. B.; Pearson, T.; Peoples, S. L.; Petras, D.; Preuss, M. L.; Pruesse, E.; Rasmussen, L. B.; Rivers, A.; Robeson, M. S.; Rosenthal, P.; Segata, N.; Shaffer, M.; Shiffer, A.; Sinha, R.; Song, S. J.; Spear, J. R.; Swafford, A. D.; Thompson, L. R.; Torres, P. J.; Trinh, P.; Tripathi, A.; Turnbaugh, P. J.; Ul-Hasan, S.; van der Hooft, J. J. J.; Vargas, F.; Vázquez-Baeza, Y.; Vogtmann, E.; Hippel, M. von; Walters, W.; Wan, Y.; Wang, M.; Warren, J.; Weber, K. C.; Williamson, C. H. D.; Willis, A. D.; Xu, Z. Z.; Zaneveld, J. R.; Zhang, Y.; Zhu, Q.; Knight, R.; Caporaso, J. G. Reproducible, interactive, scalable and extensible microbiome data science using QIIME 2. *Nature Biotechnology* **2019**, *37* (8), 852–857. DOI: 10.1038/s41587-019-0209-9.

(15) Caporaso, J. G.; Lauber, C. L.; Walters, W. A.; Berg-Lyons, D.; Lozupone, C. A.; Turnbaugh, P. J.; Fierer, N.; Knight, R. Global patterns of 16S rRNA diversity at a depth of millions of sequences per sample. *PNAS* **2011**, *108 Suppl 1* (Supplement 1), 4516–4522. DOI: 10.1073/pnas.1000080107.

(16) Stults, J. R.; Snoeyenbos-West, O.; Methe, B.; Lovley, D. R.; Chandler, D. P. Application of the 5' fluorogenic exonuclease assay (TaqMan) for quantitative ribosomal DNA and rRNA analysis in sediments. *Applied and Environmental Microbiology* **2001**, *67* (6), 2781–2789. DOI: 10.1128/AEM.67.6.2781-2789.2001.

(17) Bru, D.; Sarr, A.; Philippot, L. Relative abundances of proteobacterial membrane-bound and periplasmic nitrate reductases in selected environments. *Applied and Environmental Microbiology* **2007**, *73* (18), 5971–5974. DOI: 10.1128/AEM.00643-07.

(18) Henry, S.; Bru, D.; Stres, B.; Hallet, S.; Philippot, L. Quantitative detection of the nosZ gene, encoding nitrous oxide reductase, and comparison of the abundances of

16S rRNA, narG, nirK, and nosZ genes in soils. *Applied and Environmental Microbiology* **2006**, *72* (8), 5181–5189. DOI: 10.1128/AEM.00231-06.

(19) Sultana, M.; Vogler, S.; Zargar, K.; Schmidt, A.-C.; Saltikov, C.; Seifert, J.; Schlömann, M. New clusters of arsenite oxidase and unusual bacterial groups in enrichments from arsenic-contaminated soil. *Archives of Microbiology* **2012**, *194* (7), 623–635. DOI: 10.1007/s00203-011-0777-7.

(20) Song, B.; Chyun, E.; Jaffé, P. R.; Ward, B. B. Molecular methods to detect and monitor dissimilatory arsenate-respiring bacteria (DARB) in sediments. *FEMS Microbiology Ecology* **2009**, *68* (1), 108–117. DOI: 10.1111/j.1574-6941.2009.00657.x.

Grimm et al. (2024b). Nitrous oxide is the main product during nitrate reduction by a novel lithoautotrophic iron(II)-oxidizing culture from an organic-rich paddy soil

AMERICAN SOCIETY FOR MICROBIOLOGY | Applied and Environmental Microbiology

Check for updates

Environmental Microbiology | Full-Length Text

Nitrous oxide is the main product during nitrate reduction by a novel lithoautotrophic iron(II)-oxidizing culture from an organic-rich paddy soil

Hanna Grimm,[1] Jennifer Lorenz,[1] Daniel Straub,[2] Prachi Joshi,[1] Jeremiah Shuster,[1,3] Christiane Zarfl,[4] E. Marie Muehe,[5,6] Andreas Kappler[1,7]

AUTHOR AFFILIATIONS See affiliation list on p. 16.

ABSTRACT Microbial nitrate reduction coupled to iron(II) oxidation (NRFeOx) occurs in paddy soils due to high levels of dissolved iron(II) and regular application of nitrogen fertilizer. However, to date, there is no lithoautotrophic NRFeOx isolate or enrichment culture available from this soil environment. Thus, resulting impacts on greenhouse gas emissions during nitrate reduction (i.e., nitrous oxide [N_2O]) and on toxic metalloid (i.e., arsenic) mobility can hardly be investigated. We enriched a lithoautotrophic NRFeOx culture, culture HP (Huilongpu paddy, named after its origin), from a paddy soil (Huilongpu Town, China), which was dominated by *Gallionella* (71%). The culture reduced 0.45 to 0.63 mM nitrate and oxidized 1.76 to 2.31 mM iron(II) within 4 days leading to N_2O as the main N-product (62%–88% N_2O-N of total reduced NO_3^--N). Nitrite was present as an intermediate at a maximum of 0.16 ± 0.1 mM. Cells were associated with, but mostly not encrusted by, poorly crystalline iron(III) minerals (ferrihydrite). Culture HP performed best below an iron(II) threshold of 2.5–3.5 mM and in a pH range of 6.50–7.05. In the presence of 100 µM arsenite, only 0%–18% of iron(II) was oxidized. Due to low iron(II) oxidation, arsenite was not immobilized. However, the proportion of N_2O-N of total reduced NO_3^--N decreased from 77% to 30%. Our results indicate that lithoautotrophic NRFeOx occurs even in organic-rich paddy soils, resulting in denitrification and subsequent N_2O emissions. The obtained novel enrichment culture allows us to study the impact of lithoautotrophic NRFeOx on arsenic mobility and N_2O emissions in paddy soils.

IMPORTANCE Paddy soils are naturally rich in iron(II) and regularly experience nitrogen inputs due to fertilization. Nitrogen fertilization increases nitrous oxide emissions as it is an intermediate product during nitrate reduction. Microorganisms can live using nitrate and iron(II) as electron acceptor and donor, respectively, but mostly require an organic co-substrate. By contrast, microorganisms that only rely on nitrate, iron(II), and CO_2 could inhabit carbon-limited ecological niches. So far, no isolate or consortium of lithoautotrophic iron(II)-oxidizing, nitrate-reducing microorganisms has been obtained from paddy soil. Here, we describe a lithoautotrophic enrichment culture, dominated by a typical iron(II)-oxidizer (*Gallionella*), that oxidized iron(II) and reduced nitrate to nitrous oxide, negatively impacting greenhouse gas dynamics. High arsenic concentrations were toxic to the culture but decreased the proportion of nitrous oxide of the total reduced nitrate. Our results suggest that autotrophic nitrate reduction coupled with iron(II) oxidation is a relevant, previously overlooked process in paddy soils.

KEYWORDS culture HP, airborne microorganisms, greenhouse gas, arsenic, chemodenitrification, nitrogen, soil

Editor Arpita Bose, Washington University in St. Louis, St. Louis, Missouri, USA

Address correspondence to Andreas Kappler, andreas.kappler@uni-tuebingen.de.

The authors declare no conflict of interest.

See the funding table on p. 16.

Received 27 June 2024
Accepted 30 October 2024
Published 6 December 2024

Nitrogen (N) fertilization is a common practice in agriculture, for example, in rice cultivation worldwide. Typically, N is applied in excess to paddy soils (as urea, ammonium-, or nitrate-based fertilizer), which results in poor nitrate (NO_3^-) use efficiencies and leaching of nitrate into groundwater (1–3). Nitrogen fertilization also influences the microbial processes in the paddy soil by providing a favorable electron acceptor under anoxic conditions that prevail under waterlogged conditions. Under anoxic conditions, nitrate can be removed microbially during dissimilatory nitrate reduction to ammonium (DNRA) or by denitrification. Denitrifying microorganisms are classified as (i) heterotrophs, which require an organic carbon substrate for energy generation, (ii) mixotrophs, which can use both organic carbon and inorganic compounds, and (iii) lithoautotrophs, which only use inorganic compounds such as hydrogen, reduced sulfur compounds, arsenite, or iron(II) (4). It was shown that different parameters such as pH, sulfide concentrations, type, and complexity of electron donors together with the ratio of organic carbon (OC) to N influence the likelihood of denitrification or DNRA (5). Typically, denitrification is the favored process for nitrate removal under lower OC/N ratios (6). In paddy soils, concentrations of dissolved or solid-phase iron(II) are naturally high due to anoxic conditions stimulating iron(III) reduction. Thus, nitrate reduction coupled with iron(II) oxidation (NRFeOx) is considered to play an important role in paddy soils (7).

Nitrate reduction is thermodynamically favored over sulfate reduction, iron(III) reduction, and methanogenesis, thereby limiting methane emissions and suppressing the reductive dissolution of iron(III) minerals. Given the high scavenging potential of toxic metalloids, like arsenic, by the iron(III) minerals formed by microbial iron(II) oxidation (8), NRFeOx can also limit the mobility of arsenic. Arsenic-contaminated groundwater is often used for paddy field irrigation (9, 10), thus, introducing arsenic to the soil and potentially resulting in accumulation within rice plants and grains (11). Arsenic is mainly present in its inorganic forms, arsenate and arsenite, with the latter being more toxic and mobile (12). However, iron(III) (oxyhydr)oxides that form during iron(II) oxidation have been shown to successfully sequester arsenate and arsenite during iron(II) oxidation (13), which play a key role in arsenic mobility. Depending on the speciation and concentration, arsenic can also pose toxic effects on microorganisms, including nitrate-reducing, iron(II)-oxidizing microorganisms (8).

Several studies have isolated or enriched heterotrophic or mixotrophic nitrate-reducing, iron(II)-oxidizing microorganisms from paddy soils and followed changes in the microbial community composition and diversity after the addition of nitrate, iron(II), or organic carbon (e.g., lactate, acetate) (14–17). Ratering and Schnell (7) postulated that the metabolic capacity for NRFeOx is widespread in paddy soils; however, lithoautotrophic microorganisms have not been isolated or enriched in the past from paddy soil. In these rather organic-rich environments (18), such microorganisms could inhabit ecological niches with low organic carbon and are generally considered to be better adapted to thrive under redox fluctuations where substrate availability may be scarce (19).

Three enrichment cultures have been described so far that unequivocally perform lithoautotrophic NRFeOx, originating from ditch sediments (i.e., culture KS, culture BP) and a limestone aquifer (i.e., culture AG) (20–22). *Gallionellaceae* sp. are dominant in all three cultures and share many common features such as genes encoding for iron(II) oxidation (e.g., *cyc2*), denitrification (e.g., *narGHI*, *nirK/S*, *norBC*), and carbon fixation (*rbcL*). The *Gallionellaceae* sp. in these three mixed cultures, however, are only capable of partial denitrification until NO or N_2O, relying on a flanking community with other species such as *Rhodanobacter* sp. or *Bradyrhizobium* sp. for further nitrogen species removal (20, 23–25). Yet, 43%–96% and ~41% of the reduced nitrate accumulates as N_2O in culture KS (26) and AG (21), respectively.

To investigate the important role of lithoautotrophic nitrate-reducing, iron(II)-oxidizing microorganisms for arsenic mobility and greenhouse gas emissions in paddy soils, we aimed to (i) obtain a model culture of lithoautotrophic nitrate-reducing, iron(II)-oxidizing

microorganisms from paddy soil, (ii) identify microbial key players for NRFeOx using 16S rRNA gene amplicon sequencing, (iii) determine the extent of nitrate reduction, iron(II) oxidation, and N_2O production, and (iv) compare growth conditions influencing the performance of the enrichment culture. Our novel enrichment culture offers a unique opportunity to further study NRFeOx in paddy soils, thereby enhancing our understanding of their impact on biogeochemical cycling, arsenic mobility, and climate change.

RESULTS AND DISCUSSION

Microbial community composition of the lithoautotrophic nitrate-reducing, iron(II)-oxidizing enrichment culture

Lithoautotrophic nitrate-reducing, iron(II)-oxidizing microorganisms were enriched (Fig. 1a) by adding 1 g of paddy soil (Huilongpu Town, Hunan province, China) to 9 mL growth media containing 2 mM iron(II) and 1 mM nitrate (composition see Table S1). After observation of iron(II) oxidation and iron(III) mineral formation, indicated by a visual change from transparent to orange, 1 mL of the culture was transferred to 9 mL of fresh media. After 11 transfers under purely lithoautotrophic conditions by supplying 2 mM iron(II) as electron source and 1 mM nitrate as an electron acceptor, the microbial community composition of the NRFeOx culture was characterized by 16S rRNA gene amplicon sequencing (Fig. 1a). Two amplicon sequence variants (ASVs) classified as *Gallionella* (74.1±0.2%) dominated the microbial community of the successfully enriched NRFeOx culture HP (Huilongpu paddy, named after the origin of the soil, Fig. 1b). Members of *Gallionella* belong to the family *Gallionellaceae* of the order *Burkholderiales*. The more abundant *Gallionella* was present at 71.4% ± 0.3% and the other one at 2.7% ± 0.01% sharing 99.6% sequence identity (Fig. S1). Attempts to isolate the *Gallionella* species from the obtained NRFeOx culture involved different liquid or solid growth media (Table S2) with no success. The *Gallionella* did not grow under microoxic conditions in gradient tubes following the approach of Emerson and Floyd (27) (Table S2). In the native paddy soil, *Gallionella* accounted for 0.3% of the total microbial community (Table S3) and shared 94.4% sequence identity with the more abundant *Gallionella* in culture HP (Fig. S1).

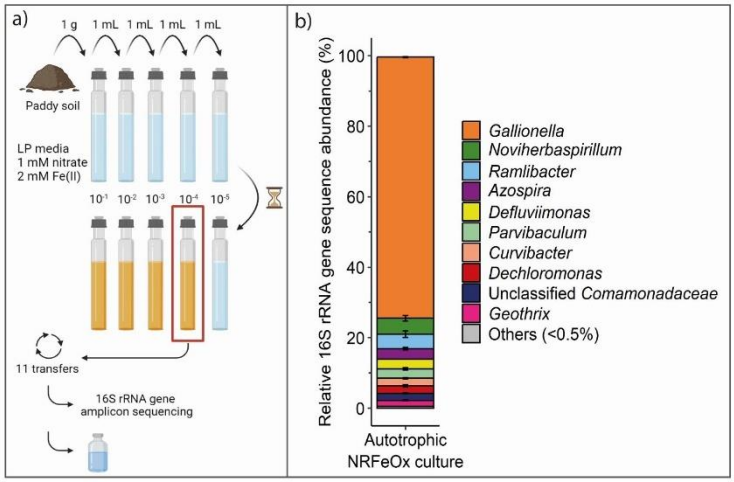

FIG 1 (a) Schematic of the enrichment and (b) microbial community composition at genus level of the lithoautotrophic nitrate-reducing, iron(II)-oxidizing enrichment culture HP from paddy soil. "Others" represent taxa with abundances below 0.5%. Error bars indicate the deviation from the mean of duplicate samples analyzed by 16S rRNA gene amplicon sequencing.

In the three other known lithoautotrophic NRFeOx enrichment cultures (20–22), *Gallionellaceae* were also found to be the dominant family. Abundances of *Gallionellaceae* are similarly high in culture KS (96%), BP (71%–78%) and AG (49%) (20, 21, 23), compared to the novel enrichment culture HP described here. Previously, members of the family *Gallionellaceae* were characterized as autotrophic, neutrophilic, and microaerophilic iron(II)-oxidizers (28–30). However, *"Candidatus* Ferrigenium straubiae" sp.nov., *"Candidatus* Ferrigenium bremense" sp.nov., and *"Candidatus* Ferrigenium altingense" sp.nov. (in cultures KS, BP, and AG, respectively) perform, in tandem with their associated flanking communities, partial denitrification coupled to iron(II) oxidation and carbon fixation and are, thus, considered lithoautotrophic nitrate-reducing, iron(II)-oxidizing microorganisms. The enrichment culture in this study is most similar to culture AG based on the geochemical growth conditions (culture AG: 2 mM nitrate, 2 mM iron(II), this culture: 1 mM nitrate, 2 mM iron(II)). Maximum likelihood analysis revealed that the most dominant *Gallionella* species in culture HP was most similar to *"Ca*. ferrigenium altingense" sp. nov. from culture AG (Fig. S1), sharing 100% sequence identity (251 bp overlap). Even though the comparison of sequence similarities on species levels based on short-read 16S rRNA gene sequence analysis needs to be taken with caution, this similarity indicates that the potential for lithoautotrophic NRFeOx likely exists in many environments and with the appropriate culture conditions, microorganisms possessing this metabolic capability can be enriched and studied. Meta'omics revealed that "*Ca*. ferrigenium altingense" sp. nov. possesses genes for iron(II) oxidation, carbon fixation, and almost all genes involved in denitrification except for *nosZ* (25), which gives rise to the assumption that the *Gallionella* in culture HP has a similar metabolic potential.

The second most abundant ASV (4.5% ± 1.6%) in our lithoautotrophic NRFeOx culture HP belongs to the order *Burkholderiales* but was affiliated with the family *Oxalobacteraceae* and the genus *Noviherbaspirillum* (Fig. 1b). *Noviherbaspirillum* was also found in the flanking community of culture BP (9%–15%) (20). Meta'omics revealed that *Noviherbaspirillum* in culture BP has the potential to perform iron(II) oxidation, carbon fixation, and complete denitrification, likely playing an important role in NRFeOx.

Almost equally abundant like the *Noviherbaspirillum* in culture HP was *Ramlibacter* (4.1% ± 1.8%), belonging to the family of *Comamonadaceae* of the order *Burkholderiales* (Fig. 1b). *Ramlibacter* sp. in culture BP is considered to be involved in iron(II) oxidation and denitrification (*norB* and *nosZ* genes) (20). Other flanking community members in culture HP showed relative abundances at or below 3% and comprised members of the family *Rhodocyclaceae* (*Azospira,* 3.0% ± 0.7% and *Dechloromonas*, 2.1% ± 0.7%), which account for 0.14% of the native paddy soil microbial community (Table S3), *Comamonadaceae* (*Curvibacter*, 2.2% ± 0.5% and 1 ASV with unclassified genus, 2.0% ± 0.1%), making up 1.14% of the native paddy soil microbial community (Table S3), *Parvibaculaceae* (*Parvibaculum*, 2.7% ± 0.3%), *Rhodobacteraceae* (*Defluviimonas*, 2.8% ± 0.0%), and *Holophagaceae* (*Geothrix*, 1.7% ± 0.2%), accounting for 0.2% of the native paddy soil microbial community (Table S3; Fig. 1b). In culture KS, BP, or AG, *Azospira* was not present in the flanking community and was likely specific to culture HP and potentially to NRFeOx communities in paddy soils in general. The addition of iron(II), nitrate, and organic carbon (e.g., lactate or acetate) to paddy soils was shown to enrich *Azospira* in several studies (16, 17), suggesting that it might play an important role in hetero- or mixotrophic denitrification. Other flanking community members present in culture HP (Fig. 1b) (e.g., *Dechloromonas*, *Curvibacter,* and *Geothrix*) were also suggested before to be involved in Fe- and/or N-cycling (31–36).

Nitrate removal and iron(II) oxidation under autotrophic growth conditions

Nitrate reduction and iron(II) oxidation were monitored in detail over three consecutive transfers each lasting 7 days. In biotic treatments, 0.53 ± 0.12 mM, 0.45 ± 0.03 mM, and 0.64 ± 0.13 mM nitrate was reduced and 1.06 ± 0.24 mM, 1.05 ± 0.31 mM, and 1.24 ± 0.09 mM of iron(II) was oxidized within 7 days of incubation during transfer 1, 2, and 3, respectively (Fig. 2; Table S4). Because iron(II) precipitated on the inside surface of the

glass serum bottles after the addition of $FeCl_2$, measured iron(II) concentrations were lower than the theoretical 2 mM. Iron that was precipitated and could not be accounted for during the experiment was retrieved after the experiment by adding 1 M HCl (37). The ratio of iron(II) to iron(tot) decreased from 87.3% ± 28.7% to 1.6% ± 0.2% in transfer 1, from 88.3% ± 37.2% to 2.4% ± 0.4% in transfer 2, and from 90.9% ± 10.3% to 2.8% ± 0.2% in transfer 3. In culture AG, approximately 90% of the total iron(II) was oxidized (21), whereas 16%–26% iron(II) remained in culture KS (38) and 20% in culture BP (24), which were cultivated at higher iron(II) concentrations. 16S rRNA gene copy numbers increased, although not significantly ($P = 0.12$, Table S5, non-parametric Wilcoxon signed-rank test), from $3.4 \times 10^3 \pm 1.6 \times 10^3$ mL^{-1} to $4.3 \times 10^5 \pm 2.5 \times 10^5$ mL^{-1} and from $6.2 \times 10^3 \pm 2.0 \times 10^3$ mL^{-1} to $1.2 \times 10^6 \pm 6.3 \times 10^5$ mL^{-1} from day 0 till day 7 during transfers 2 and 3, respectively.

To investigate intermediate and final N-products during denitrification, aqueous nitrite concentrations and nitrous oxide emissions were quantified. Aqueous nitrite concentrations were generally low in biotic treatments, reaching a maximum of 0.08 ± 0.16 mM (day 3), 0.02 ± 0.02 mM (day 1), and 0.16 ± 0.1 mM (day 2) during transfers 1, 2, and 3, respectively (Fig. S2a). N_2O production was determined by measuring gaseous concentrations and calculating dissolved concentrations based on Henry's constant which revealed that 72.3% ± 19.4%, 88.5% ± 4.6%, and 62.4% ± 16.0% of the total reduced NO_3^--N accumulated as N_2O-N at the end (7 days) of transfers 1, 2, and 3, respectively (Table S4). Thus, N_2O is the main product during lithoautotrophic NRFeOx in this culture. N_2O also accumulated over time in culture KS and AG and represented 43%–96% (26) and ~41% (21) of the total reduced nitrate, respectively.

For calculations of the $nitrate_{reduced}$ to $iron(II)_{oxidized}$ ratio, the retrieved iron was considered and summed up with the final iron(tot) concentrations to obtain the true total iron concentrations. Considering that 90% of the total iron was present as iron(II) (with about 10% iron(III) stemming from the inoculum), we calculated that ratios of

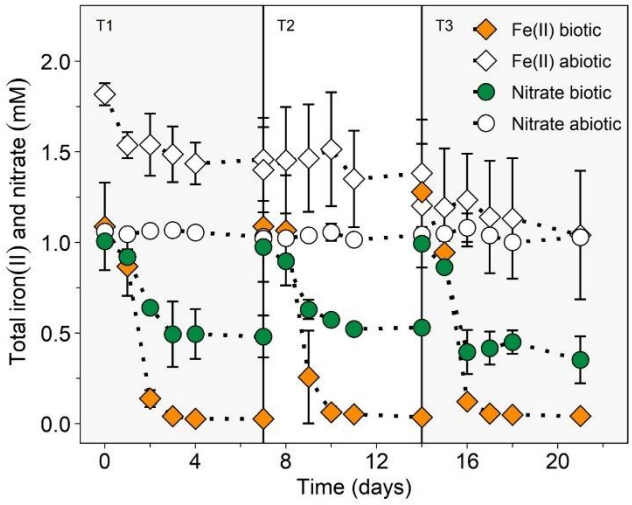

FIG 2 Total iron(II) (diamond) and nitrate (circle) concentrations over three consecutive transfers, each lasting over 7 days, of the lithoautotrophic nitrate-reducing, iron(II)-oxidizing enrichment culture HP from paddy soil. T1, T2, and T3 are visually separated by vertical lines and gray color and stand for transfer 1 (days 0–7), transfer 2 (days 7–14), and transfer 3 (days 14–21), respectively. Biotic treatments are represented as colored symbols and abiotic treatments are in white. Note that due to dilution by the microbial inoculum (10%, 2.5 mL), iron(II) concentrations were slightly lower in the biotic setups compared to abiotic setups. Mean ± standard deviation is shown of four replicates.

nitrate$_{reduced}$ to iron(II)$_{oxidized}$ were 0.23 ± 0.05, 0.23 ± 0.03, and 0.37 ± 0.08 in transfers 1, 2, and 3, respectively (Table S4). The higher ratio in transfer 3 was due to more reduced nitrate and less oxidized iron(II); however, the reason for this remains unidentified. Yet, the ratio in transfers 1 and 2 is close to the theoretical stoichiometry of 0.25, when assuming nitrate reduction to nitrous oxide (equation 1).

$$2\,NO_3^- + 8\,Fe^{2+} + 19\,H_2O \rightarrow N_2O + 8\,Fe(OH)_3 + 14\,H^+ \quad \text{Eq. (1)}$$

However, the ratio of nitrate$_{reduced}$ to iron(II)$_{oxidized}$ should probably be slightly lower (ca. 0.21) considering that ~15% of the electrons from iron(II) oxidation are needed for carbon fixation (39) (equation 2).

$$4\,Fe^{2+} + CO_2 + 11\,H_2O \rightarrow 4\,Fe(OH)_3 + CH_2O + 8\,H^+ \quad \text{Eq. (2)}$$

One explanation for a higher measured ratio than the theoretical ratio could be internally stored electrons or carbon leading to a greater nitrate reduction than theoretically possible under autotrophic conditions. Experiments without the addition of iron(II) showed a reduction of 0.05 ± 0.12 mM nitrate (Fig. S3). Considering this in the calculation of the nitrate$_{reduced}$ to iron(II)$_{oxidized}$ ratio, we achieved a ratio of 0.21, 0.20, and 0.34 for transfers 1, 2, and 3, respectively.

Without the addition of iron(II), 16S rRNA gene copy numbers increased from 2.5 × 10^4 ± 1.1 × 10^4 mL^{-1} (day 0) to 1.5 × 10^6 ± 1.5 × 10^6 mL^{-1} (day 7) (log2FC = 5.93, P = 0.25, Table S5, non-parametric Wilcoxon signed-rank test). The increase was similarly high as under standard conditions (log2FC = 6.65, 1.3 × 10^4 ± 9.5×10^3 mL^{-1} [day 0] to 1.3 × 10^6 ± 7.0 × 10^5 mL^{-1} [day 7], Table S6). Similar trends have been observed for the enrichment culture AG (21). When no iron(II) is supplied to the culture, biomass build-up could result from internally stored electrons or heterotrophic community members might be fueled by internally stored carbon. However, this underlines that 16S rRNA gene copy numbers alone have to be taken with caution when studying lithoautotrophic NRFeOx enrichment cultures or other cultures as well.

In abiotic treatments where no cells were added, nitrate concentrations stayed constant throughout the three transfers at around 1 mM (Fig. 2a). Iron(II) concentrations in the abiotic setups, however, decreased slowly within the 7 days of incubation (Fig. 2a). The decrease was strongest in the first transfer (1.82 ± 0.06 mM to 1.46 ± 0.23 mM) and less pronounced in the second and third transfers. This results from the precipitation of iron(II) minerals on the glass wall (37). The iron(II)/iron(tot) ratios stayed constant in the abiotic controls at 94.5% to 100%. Ammonium concentrations stemming from the growth media were constant throughout the three transfers at roughly 6 mM in biotic and abiotic treatments (Fig. S2b). The constant concentrations imply a minor role of DNRA or ammonium oxidation coupled to iron(III) reduction (Feammox).

Following the approach of Jakus et al. (21), 2 mM of iron(II) was re-spiked to culture HP after 7 days when all the initial iron(II) had been oxidized and nitrate had been reduced, to rule out that the lithoautotrophic NRFeOx enrichment culture HP grows on residual OC stemming from the MQ water. After re-spiking, iron(II) concentrations reached 1.71 ± 0.19 mM in the biotic treatments (Fig. S4). One day after the re-spike, 1.62 ± 0.19 mM of iron(II) was oxidized, corresponding to 95% of the re-spiked iron(II), and 0.38 ± 0.13 mM nitrate was reduced (less than 0.1 mM remaining nitrate) (Table S4). This corresponds to a molar ratio of nitrate$_{reduced}$ to iron(II)$_{oxidized}$ of 0.23 ± 0.08 (Table S4). Because precipitation of iron(II)-phosphate minerals at the glass wall did not occur in such a short timeframe, retrieved iron was not considered for the re-spike experiment. Due to very low nitrite concentrations, chemodenitrification likely plays a minor role, and iron(II) oxidation is assumed to be biotically catalyzed. 16S rRNA gene copy numbers were similar between day 0 and 7 days after the spike (day 0: 2.2 × 10^6 ± 1.4 × 10^6 mL^{-1}, day 7: 1.3 × 10^6 ± 6.1 × 10^6 mL^{-1}, P = 0.12, Table S5, non-parametric Wilcoxon signed-rank test). A 10 mM re-spike of iron(II) in culture KS also did not lead to a significant increase

in cell number (38); however, a two-time spike of 2 mM iron(II) in culture AG led to an increase in cell numbers (21). In summary, the fast oxidation of iron(II) after the re-spike underlines that culture HP performs lithoautotrophic NRFeOx.

Continuous cultivation under lithoautotrophic conditions (ca. 20 transfers within 1 year) and different experimental setups and microbial and geochemical analyses confirm that the novel NRFeOx enrichment culture HP from a paddy soil simultaneously reduces nitrate and oxidizes iron(II) in the absence of any organic carbon source. The simultaneous increase in cell numbers over time (log2FC of 6.76 and 7.64 in transfers 2 and 3, respectively) as a measure for growth and the continuous, stable cultivation since 3 years (>60 transfers) under autotrophic conditions verifies that at least three out of four criteria are being met to prove true lithoautotrophic behavior (28). The fixation of labeled CO_2 into biomass remains to be investigated. To the best of our knowledge, this is the first lithoautotrophic NRFeOx culture enriched from a soil environment, representing a rather organic-rich environment compared to the ditch sediment or aquifer material from which the lithoautotrophic NRFeOX cultures KS, AG, and BP have been enriched (20–22). Meta'omic analysis are needed in the future to determine the metabolic potential of culture HP and identify community members involved in iron(II) oxidation and certain steps of denitrification.

Cell-mineral interactions

Microbial nitrate reduction coupled with iron(II) oxidation in the novel enrichment culture HP led to the formation of iron(III) (oxyhydr)oxide minerals. ^{57}Fe-specific Moessbauer spectroscopy analysis identified a poorly crystalline iron(III) mineral phase (iron(III) oxyhydroxides) after 7 days of incubation (transfer 3) with hyperfine parameters similar to that of ferrihydrite (Table S7; Fig. S5).

Scanning electron microscopy (SEM) images revealed two dominant mineral structures, that is, mineral aggregates composed of either nanometer-scale particles (Fig. 3a) or nanometer- to micrometer-scale botryoidal-like particles (Fig. 3b). Energy dispersive spectroscopy analysis detected Fe, P, and O from these minerals (Fig. S6). Rod-shaped cells were closely associated with the newly formed iron(III) minerals (Fig. 3a). Only a few cells appeared encrusted by iron(III) minerals (Fig. 3b), whereas others were not encrusted or not in direct contact with iron(III) minerals (Fig. 3c). Light and fluorescence microscopy with LIVE/DEAD stain supported a close association of cells and iron(III) oxyhydroxides (Fig. 3d).

Autotrophic iron(II)-oxidizing microorganisms, i.e., nitrate-reducing, iron(II)-oxidizing microorganisms have been suggested to prevent cell encrustation during the precipitation of iron(III) minerals by excretion of iron(III)-complexing ligands, extracellular polymeric substances, modification of the cell surface charge or acidification of the microenvironment around the cell (40–43). In this study, SEM, fluorescence, and transmission light microscopy verified that most of the cells were free of encrustation irrespective of whether they were associated with the minerals or not. Only a few cells were partially or fully encrusted, which could resemble flanking community members that lack a prevention mechanism or dead cells that lost their ability to prevent encrustation (44, 45). However, Huang et al. (26) observed different degrees of encrustation in culture KS under varying nitrate-to-iron ratios with the degree of encrustation being lower when supplementing less iron. Yet, they did not find differences in mineral identity between different nitrate-to-iron ratios. The type of formed mineral was found to depend on growth conditions (46, 47) or metabolic processes (i.e., heterotroph vs. mixotroph vs. autotroph). Under heterotrophic or mixotrophic conditions, it was shown that abiotic iron(II) oxidation by nitrite (chemodenitrification) leads to the formation of goethite rather than poorly crystalline iron(III) (oxyhydr)oxides such as ferrihydrite (48–50). In the present study, the presence of a poorly crystalline iron(III) mineral phase (i.e., ferrihydrite) as identified by Moessbauer analysis and the low concentrations of nitrite point toward a minor role of chemodenitrification in this lithoautotrophic NRFeOx culture HP.

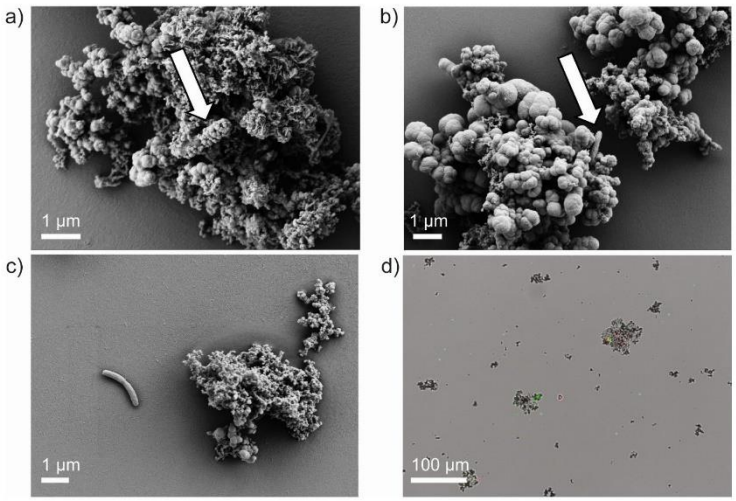

FIG 3 Scanning electron micrographs of the lithoautotrophic nitrate-reducing, iron(II)-oxidizing enrichment culture HP after 7 days (transfer 3) showing cell-mineral interactions of encrusted, mineral-associated (a), non-encrusted, mineral-associated (b), and non-encrusted (c) cells. Arrows point to cells. Overlay light micrograph of fluorescence and transmission light microscopic pictures (d). Cells were stained with the LIVE/DEAD stain (green, alive; red, dead).

Metabolic performance of the lithoautotrophic nitrate-reducing, iron(II)-oxidizing enrichment culture under various iron(II) concentrations and pH levels

In paddy soils, concentrations of dissolved iron(II) can vary greatly due to changes in redox conditions (51). Thus, we investigated the performance of the lithoautotrophic NRFeOx enrichment culture HP in the presence of different iron(II) concentrations. When providing 1, 2, and 3 mM iron(II), 0.74 ± 0.27, 1.71 ± 0.03, and 1.88 ± 0.9 mM iron(II) was oxidized within 7 days, respectively (Fig. 4a; Table S4). With increasing iron(II) concentrations, a lower extent of iron(II) oxidation was observed (4 mM iron(II): 0.45 ± 0.29 mM, 5 mM iron(II): 0.29 ± 0.35 mM) (Fig. 4a; Table S4). At the same time, the extent of nitrate reduction was greatest for the 2 mM and 3 mM iron(II) setup, with 0.46 ± 0.16 and 0.41 ± 0.21 mM nitrate being reduced, respectively (Fig. S7a; Table S4). The extent of nitrate reduction was lower at iron(II) concentrations of 1 mM (0.12 ± 0.07 mM), 4 mM (0.12 ± 0.08 mM), or 5 mM (0.08 ± 0.04 mM) (Fig. S7a; Table S4). The ratio of $nitrate_{reduced}$ to $iron(II)_{oxidized}$ ranged between 0.16 and 0.29 (Table S4), being lowest in the 1 mM iron(II) treatment and highest in the 5 mM iron(II) treatment. These results highlight that our NRFeOx culture performs best when 2 mM iron(II) is supplied with relatively less nitrate being reduced and iron(II) being oxidized the higher or lower the concentration of iron(II) is. It also emphasizes that iron(II) concentrations can be crucial for the success of enriching or isolating lithoautotrophic nitrate-reducing, iron(II)-oxidizing microorganisms from different environments, likely due to toxicity effects of high concentrations of iron(II) (52). However, other enrichment cultures are likely less susceptible to higher iron(II) concentrations, especially culture KS and BP, that are routinely cultivated with 10 mM of iron(II). Culture AG grew slower with 3 mM of iron(II), but still oxidized almost all iron(II) (21). Yet, it still remains open where the upper and lower limit of iron(II) for microbial growth, nitrate reduction, and iron(II) oxidation of the other lithoautotrophic enrichment cultures is set.

Fluctuations in pH are also typically common in paddy soil due to flooding and drainage (53, 54); thus, we wanted to explore the pH range for enzymatic iron(II)

oxidation by this enrichment culture. We found that the enrichment culture HP oxidized iron(II) from a pH of 6.50 to 7.05 without major differences in the extent but with differences in lag phases of iron(II) oxidation (Fig. 4b) or reduced nitrate (Fig. S7b). It has to be noted that the recovered initial iron(II) concentrations were slightly higher at lower pH values due to a larger extent of precipitation of iron(II) (at the glass wall) at higher pH values (55), which was also observed in the abiotic controls. Changes in pH between the beginning and the end of the experiment were minor (<0.1 pH unit, Table S8). Reduced nitrate ranged between 0.28 and 0.4 mM and oxidized iron(II) between 1.13 and 1.66 mM (Table S4). However, in all treatments, around 100% of iron(II) was oxidized. The ratio of $nitrate_{reduced}$ to $iron(II)_{oxidized}$ ranged between 0.22 and 0.25 (Table S4) and was well in line with the expected ratio of 0.25 or 0.21 when also considering biomass buildup. At a pH of 6.80, iron(II) oxidation and nitrate reduction were retarded by 1 day; however, at an even lower pH (pH 6.50), the culture HP behaved similarly to higher pH values. Different pH values could affect the contribution of chemodenitrification to iron(II) oxidation as shown by Zhu-Barker et al. (56). However, since nitrite was generally low and only observed for one treatment (pH 6.80) at day 1 (0.01 mM), we consider the contribution of chemodenitrification to iron(II) oxidation at all tested pH values as neglectable. Assuming a pH development during the rice growing season as modeled by Ding et al. (53) for paddy soils with an initial pH >6.5 (Table S9), where the pH slightly drops after flooding, stabilizes at pH 7 after around 30 days, and increases with decreasing moisture content, our results suggest that lithoautotrophic NRFeOx could occur throughout the rice-growing season. This indicates that the metabolic activity of these microorganisms is potentially sustained under the varying pH conditions typical of paddy soils.

Metabolic performance of the lithoautotrophic nitrate-reducing, iron(II)-oxidizing enrichment culture after arsenite addition

In paddy soils, waterlogged conditions are responsible for a reducing environment where the highly toxic and mobile arsenite is the dominant arsenic species in the porewater (57–60). In studies using bacterial cultures or isolates and in paddy soil microcosm studies, similar arsenite concentrations or even higher concentrations [5,000 µM arsenate (61) and 500 µM arsenite (62)] were used and shown to not affect

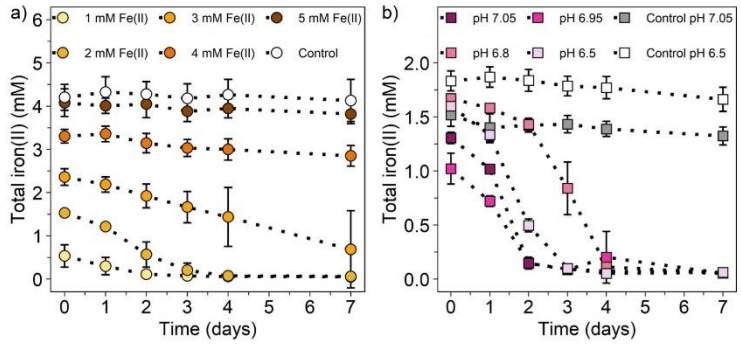

FIG 4 Total iron(II) concentrations for the lithoautotrophic nitrate-reducing, iron(II)-oxidizing enrichment culture HP from a paddy soil set up (a) with different iron(II) concentrations and (b) at different pH values over 7 days. Treatments in (a) were supplemented with 1 mM nitrate and different iron(II) concentrations, shown as circles with darker colors representing higher iron(II) concentrations. The control (white circles) represents abiotic conditions with 5 mM iron(II) and 1 mM nitrate. Treatments in (b) display different pH values as squares with darker colors representing higher pH values using 2 mM iron(II) and 1 mM nitrate. The controls represent abiotic conditions at pH 6.50 (white) and pH 7.05 (gray) using 2 mM iron(II) and 1 mM nitrate. Note that due to dilution by the microbial inoculum (10%, 2.5 mL), iron(II) concentrations were slightly lower in the biotic setups compared to abiotic setups. Mean ± standard deviation is shown of three replicates.

the metabolic capacity of the microorganisms (8, 61, 63–65). Thus, to allow comparison between previous studies on mixotrophic nitrate-reducing and phototrophic iron(II)-oxidizers (8), we supplemented 100 µM arsenite to culture HP, which allows us to better understand the limits and responses of the microbial community to arsenite toxicity, which would otherwise be more subtle or undetectable at lower concentrations.

We found that 13%–25% of nitrate was reduced when 100 µM arsenite was supplemented compared to 90%–98% without the presence of arsenite (Fig. S8a; Table S4). At the same time, 17.8% iron(II) was oxidized in the first transfer in the presence of arsenite and 0%–0.8% in transfers 2 and 3, which is lower compared to the setup without arsenite (62.5%–83.7% oxidized iron(II), Fig. S8b; Table S4). This points toward a toxic effect of arsenite on the lithoautotrophic NRFeOx enrichment culture HP. However, it remains open if the whole community in the culture or only specific community members were affected. Other iron(II)-oxidizing microorganisms, such as the mixotrophic strain BoFeN1, the lithoautotrophic culture KS, or phototrophic iron(II)-oxidizer *Rhodobacter ferrooxidans* strain SW2 were capable of thriving with a longer lag phase at the presence of 100 µM arsenite and even immobilized arsenite (initially: 50 µM arsenite) by newly formed iron(III) minerals (8). Thus, it remains to be investigated if arsenite still exerts toxicity effects under lower concentrations and if it can be successfully immobilized by iron(III) minerals formed during NRFeOx. Even though environmental concentrations of arsenite in the paddy soil are usually lower (58), our results suggest that the contribution of lithoautotrophic nitrate-reducing, iron(II)-oxidizing microorganisms in immobilizing arsenite in paddy soils might be lowered if initial concentrations of arsenite are as high as 100 µM, especially if the native microbial community is not adapted to high concentrations of arsenic in the paddy soil (here: 5 mg of 6 M HCl-extractable arsenic per kg soil, considerably low).

Variability of nitrous oxide production under different growth conditions

The percentages of N_2O-N of the total reduced NO_3^--N of different experimental setups were compared to identify differences in the extent of N_2O production (Fig. 5; Table S10). We found that N_2O production was significantly different between treatments ($P < 0.01$, Table S10a, non-parametric Kruskal-Wallis test). However, it was similar in treatments with different ratios of nitrate to iron(II) or different pH values. Under standard conditions (ratio N:Fe = 1:2, pH 6.95–7, $n = 15$), we calculated that on average 88.8% ± 26.6% of the reduced nitrate was converted to N_2O; however, values ranged from 50% to 110% N_2O-N of the total reduced NO_3^--N. Due to low concentrations of nitrite, we postulate that N_2O emissions are biologically derived and that chemodenitrification plays a minor role in the lithoautotrophic NRFeOx culture HP. Previously, N_2O emissions in paddy soils have been attributed partly to chemodenitrification (66). Wang et al. (67) calculated, based on chemodenitrification rates from mixotrophic NRFeOx cultures, that chemodenitrification accounted for 6.8% to 67.6% of the total N_2O emissions in two different paddy soils and postulated that the organic carbon content and iron(II) concentrations (determining the likelihood of DNRA or denitrification) are important for the contribution of chemodenitrification. However, our results suggest that lithoautotrophic NRFeOx leads almost exclusively to N_2O emissions. Thus, it remains open if biologically derived N_2O was previously underestimated in paddy soils. To better estimate the contribution of abiotic and biotic processes, the analysis of characteristic ^{15}N and ^{18}O fractionation patterns for chemodenitrification could be used (68) or kinetic modeling approaches similar to Jamieson et al. (69) and Liu et al. (50), including lithoautotrophic NRFeOx cultures, could be applied to disentangle the processes.

Growing culture HP under different pH values decreased the percentage of N_2O-N of the total reduced NO_3^--N only slightly to 85.3% ± 17.4% (pH 6.80, $n = 3$), 82% ± 9.7% (pH 7.05, $n = 3$) and 80% ± 17.6% (pH 6.50, $n = 3$). Thus, a potential inhibition of the *nosZ* gene due to lower pH values (70) can be excluded. Supplying culture HP with less nitrate (0.5 mM instead of 1 mM), which means that the electron acceptor is not in excess, also lowered the percentage of N_2O-N of the total reduced NO_3^--N to 76.8% ± 29.1%

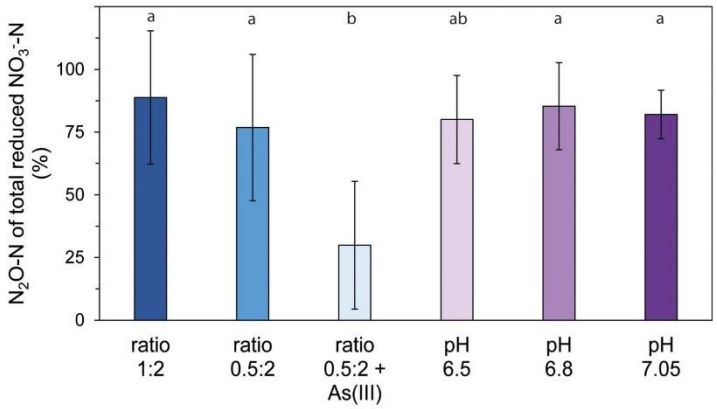

FIG 5 Relative N_2O-N of total reduced NO_3^--N of different experimental setups (different colors) of the lithoautotrophic nitrate-reducing, iron(II)-oxidizing enrichment culture HP from a paddy soil included different ratios of nitrate to iron(II), arsenite addition, and different pH values at standard conditions (nitrate to iron ratio of 1:2). Significant differences between treatments are indicated in small letters (significance level: $P < 0.05$, Table S10). Bars show the mean of replicates (ratio 1:2: $n = 15$, ratio 0.5:2: $n = 9$, ratio 0.5:2 + As(III): $n = 9$, pH 6.5: $n = 3$, pH 6.8: $n = 3$, pH 7.05: $n = 3$) and the error bars represent the standard deviation.

(ratio N:Fe = 0.5:2, pH 6.95–7, $n = 9$). In culture KS, N_2O emissions were also found to depend on the ratio of nitrate to iron, with lower N_2O under nitrate (electron acceptor) limitation (26). However, we only found a significant difference ($P < 0.05$, Table S10b, non-parametric Wilcoxon rank-sum test) when supplying 100 µM arsenite to culture HP, which lowered the percentage of N_2O-N of the total reduced NO_3^--N to 29.9% ± 25.5% ($n = 9$). With consecutive transfers of the culture on only nitrate and arsenite, less nitrate was reduced and mainly nitrite was the product of denitrification (Fig. S8c).

Implications for nitrate reduction coupled to iron(II) oxidation in paddy soils

In paddy soils, several studies have emphasized the importance of iron(II)-oxidizing microorganisms, especially of *Gallionellaceae* (71–75). Watanabe et al. (73) estimated that *Gallionella*-related iron(II)-oxidizers contribute 4.6% to iron(II) oxidation in paddy soils, mainly due to microaerophilic iron(II) oxidation. *Ferrigenium kumadai* An22, a known microaerophilic iron(II)-oxidizer, has been isolated from paddy soil (76) and microorganisms of the order *Dechloromonas*, *Azospira*, *Zoogloea,* or *Pseudomonas* have been enriched in paddy soils after iron(II), nitrate, and organic carbon addition (14–17). However, to our knowledge, no study has focused before on lithoautotrophic NRFeOx in paddy soils, despite its important role in other environments (28, 39). The successful enrichment of a lithoautotrophic nitrate-reducing, iron(II)-oxidizing culture highlights that this metabolism was previously overlooked, yet is potential of relevance in paddy soils. We suggest that paddy soils provide an ideal environment for lithoautotrophic nitrate-reducing, iron(II)-oxidizing microorganisms that could inhabit ecological niches formed due to fluctuating redox conditions creating microenvironments influenced by nitrogen fertilization and naturally rich in iron(II) and CO_2 (end product of organic matter decomposition). *Gallionellaceae* could be in close associations with roots, where oxygen concentrations vary depending on the growth stage of the plant (77), enabling it to switch from microaerophilic iron(II) oxidation to lithoautotrophic NRFeOx. (29) showed that *Gallionella* from a paddy soil rhizosphere possess *cyc2* for iron(II) oxidation, *nirK* for nitrite reductase, and *rbcL* for carbon fixation, giving rise to the assumption that *Gallionella* could perform lithoautotrophic NRFeOx, at least in interdependence with other microorganisms similar to culture BP and KS (20, 24). Whether

this metabolic flexibility occurs in the environment remains to be investigated. Based on our results, *Gallionella* would require other microorganisms that are capable of N_2O reduction. However, *Gallionella* and other lithoautotrophic nitrate-reducing, iron(II)-oxidizing microorganisms take up and sequester CO_2, thereby reducing the CO_2 concentration in the atmosphere (30), and in this way, could provide organic carbon for closely associated heterotrophic microorganisms, especially in times when organic carbon is limited. Further studies on lithoautotrophic NRFeOx in paddy soils, that is, with this novel culture HP, should focus on the metabolic potential of the dominant *Gallionella* and of the flanking community by meta'omics analysis.

The successful enrichment of lithoautotrophic nitrate-reducing, iron(II)-oxidizing microorganisms from paddy soil addresses several unresolved research questions. Specifically, it allows us to investigate the culture's capability to oxidize solid-phase iron(II), a process observed in other NRFeOx cultures or isolates (78–80). This could be particularly relevant in paddy soils rich in bioavailable and redox-sensitive iron(II) minerals (75, 81). In addition, it enables the study of the effects of other electron donors such as H_2, sulfide, methane, or organic compounds, like short-chain fatty acids (originating from fermenting bacteria), soil-derived OC (dissolved OC in porewater), or root-derived OC (by rice plants) on N_2O emissions and the microbial community composition. Ultimately, this novel lithoautotrophic NRFeOx enrichment culture HP provides a valuable basis for studying these processes in organic-rich environments.

MATERIALS AND METHODS

Field site, soil sampling, and soil characterization

Paddy soil samples were collected in September 2020 from a rice paddy field in Huilongpu Town, Hunan province, China (28°12′16″ N, 112°26′32″ E). The paddy soil is cultivated in a rice-rice cropping rotation and fertilized with 330 kg N ha^{-1} $year^{-1}$ using urea. Soil was sampled from the upper 20 cm and stored at 4°C in the dark until further processing. After the removal of plant debris and larger gravel, basic soil properties were analyzed in triplicates, comprising analyses of soil texture, water content, pH, cation exchange capacity, total elemental content, total organic carbon and total N content, water-extractable organic carbon and inorganic N-species, and sequentially extractable iron and arsenic (1 M sodium acetate, 0.5 M HCl, and 6 M HCl). Detailed information is reported in the Appendix (Soil characterization, Table S9). Briefly, the paddy soil contains around 14 mg kg^{-1} and 5 mg kg^{-1} extractable iron and arsenic, respectively, and has a TOC content of 3.5%.

Microbial enrichment

Microbial enrichments for lithoautotrophic nitrate-reducing, iron(II)-oxidizing microorganisms were set up in April 2021 by weighing 1 g of fresh paddy soil under sterile conditions into a sterile and anoxic Hungate tube. While continuously flushing the tube with N_2:CO_2 (90:10), 9 mL of anoxic, sterile modified low phosphate media (composition Table S1) supplemented with 1 mM nitrate (as KNO_3) and 2 mM iron(II) (as $FeCl_2$) was added and the tube was closed with a butyl stopper. By this, the electron donor, that is, nitrate, was present in excess (nitrate to iron ratio of 1:2). Afterwards, the Hungate tube was well mixed and a 10^{-5} dilution series into subsequent tubes was prepared by always transferring 1 mL into 9 mL of fresh growth media (82). The most positive dilution (based on color change from transparent to orange, indicating iron(II) oxidation) was always transferred into new Hungate tubes in a 10^{-5} dilution series as soon as color change appeared. This procedure was carried out over 11 transfers after which culture HP (Huilongpu paddy, named after the origin of the soil) was transferred into 25 mL serum bottles for further cultivation containing the same growth media and the same concentrations of iron(II) and nitrate. The culture HP was continuously transferred every 2–3 weeks and incubated at 25°C in the dark over roughly 10 months until culture HP was characterized.

Experimental setups

After 11 transfers, the extent of nitrate reduction, iron(II) oxidation, and nitrous oxide production were followed over three consecutive transfers in four replicates (experimental setup illustrated in Fig. S9). For this, growth media was supplemented with 1 mM nitrate (as KNO_3) and 2 mM iron(II) (as $FeCl_2$) and 10% (vol/vol) of culture HP of the previous transfer was inoculated (transfer 1). After 7 days, culture HP was transferred into fresh media, which was repeated two times (transfers 2 and 3). The supplements were always added a minimum of 1 day in advance, due to precipitation of iron(II)-phosphate minerals (i.e., vivianite) with phosphate stemming from the growth media (26).

To verify that culture HP is not using the traces of OC present in the MQ water, the NRFeOx culture was spiked with 2 mM iron(II) after one transfer (7 days) because any residual OC stemming from the water should be used up during the first transfer already (experimental setup illustrated in Fig. S10a). To account for nitrate reduction and cell growth due to usage of internally stored OC, culture HP was transferred onto growth media supplemented with only 1 mM nitrate (as KNO_3) (experimental setup illustrated in Fig. S10b).

For experiments testing arsenite toxicity effects and potential usage as an electron donor, 100 µM As(III) (as $NaAsO_2$) was supplemented to culture HP (experimental setup illustrated in Fig. S11). Here, the media was supplemented with 0.5 mM nitrate and 2 mM iron(II), lowering the ratio of nitrate to iron from 1:2 to 0.5:2.

To test optimum growth conditions of the NRFeOx culture, culture HP was incubated at standard conditions (growth media, 1 mM nitrate, 2 mM iron(II), pH 7) at different iron(II) concentrations (1, 2, 3, 4, and 5 mM iron(II); experimental setup illustrated in Fig. S12) and at different pH values (6.5, 6.8, 6.95, and 7.05) (experimental setup illustrated in Fig. S13).

Geochemical analyses

To determine iron redox speciation, 100 µL of a sample was fixed in 400 µL of a mixture of 1 M HCl/40 mM sulfamic acid and quantified using a modified ferrozine assay for nitrite-containing samples (83, 84). Briefly, 20 µL of the sample is mixed with 80 µL of 1 M HCl or with 80 µL of hydroxylamine hydrochloride followed by incubation for 30 min to quantify iron(II) and iron(tot), respectively. Afterwards, 100 µL of ferrozine solution is added, well mixed, and incubated for 5 min prior to spectrophotometric detection at 562 nm (Thermo Scientific Multiskan Go Microplate Spectrophotometer). Ferrozine measurements were conducted in technical triplicates.

To determine nitrogen species, 200 µL of the sample was diluted in 800 µL of MQ water for nitrate and nitrite and 50 µL of the sample was diluted in 950 µL of MQ water for ammonium prior to analysis by a segmented flow analyzer (AutoAnalyzer3, SEAL Analytical, Germany), which is equipped with a dialysis membrane for removal of iron to prevent side reactions during analysis.

The pH was measured in the culture suspension using a benchtop pH meter (SG2, Mettler-Toledo GmbH, Germany) equipped with a pH electrode (InLab Easy DIN, Mettler-Toledo GmbH, Germany).

Gas measurements

For gas measurements, 0.6 mL of headspace (total headspace volume between 25 and 30.4 mL) was withdrawn before liquid sampling and injected into helium-flushed headspace vials (total volume 12 mL). For the pH range experiment, nitrogen-flushed headspace vials were used. N_2O was quantified with a custom-built gas chromatograph (TRACEGC 1300, ThermoFisher Scientific, modified by S + HA analytics) on a pulsed discharge detector. The sample was split into two columns, one for N_2O with the following configurations: 30 m long, 0.53 mm ID TGBondQ column; 30 m long 0.25 mm ID TGBondQ+ column (ThermoFisher Scientific). Calibration was performed between 1 and 200 ppm N_2O, with helium or nitrogen background, depending on the experiment.

Since samples were only taken from the headspace, dissolved N_2O concentrations were calculated using the Henry constant (41.12 atm M^{-1}), thus accounting for equilibrium partitioning between liquid and gaseous phases. For calculating the amount of N_2O-N stemming from reduced NO_3^--N, both the gaseous (measured) and dissolved (calculated) N_2O concentrations were considered.

16S rRNA gene quantification, amplicon sequencing, and evolutionary analysis

After 11 transfers under lithoautotrophic conditions, two Hungate Tubes of culture HP were selected for analysis of the microbial community composition by 16S rRNA amplicon sequencing. For DNA extraction, 2 mL of sample was taken from culture HP and centrifuged (20,238 *g*, 5 min). The supernatant was discarded and the pellet was immediately frozen and stored at −20°C. The Power Soil DNA Kit was used for DNA extraction following standard procedures provided by the manufacturer (Qiagen, Germany). DNA was eluted in 50 µL DNase-free water and stored at −20°C. Quantitative polymerase chain reaction (qPCR) was performed for bacterial 16S rRNA genes using primers 341F (85) and 797R (86) in technical triplicates using SybrGreen Supermix (5 µL per qPCR reaction, Bio-Rad Laboratories GmbH, Munich, Germany) on a C1000 Touch thermal cycler (CFX96TM real-time system). As standards, plasmid vectors (pCR2.1, Invitrogen, Darmstadt, Germany) containing a cloned 16S rRNA gene fragment from *Thiomonas* sp. were used. A sevenfold standard dilution series and a negative control (RNase-free water) were included in each qPCR assay. Standard concentrations were quantified using Qubit (Life Technologies, Carlsbad, CA, USA). Finally, data analysis was performed using the Bio-Rad CFX Maestro 1.1, software, version 4.1 (Bio-Rad, 2017). For 16S rRNA gene amplicon sequencing, the 16S rRNA gene was amplified using primers 515F and 806R (87) targeting the V4 region. Detailed information on the primers, primer sequence, and thermal program used for qPCR and polymerase chain reaction (PCR) is listed in Table S11. Library preparation steps (Nextera, Illumina) and 250 bp paired-end sequencing with MiSeq (Illumina, San Diego, CA, USA) using v2 chemistry were performed by Microsynth AG (Balgach, Switzerland). 95,453 and 97,902 read pairs were obtained for two samples. Sequencing data were analyzed with nf-core/ampliseq v2.3.1, which includes all analysis steps and software and is publicly available (88, 89), with Nextflow v21.10.3 (90) and singularity v3.8.7 (91). Primers were trimmed, and untrimmed sequences were discarded (4% per sample) with Cutadapt version 3.4 (92). Adapter and primer-free sequences were processed with DADA2 v1.22.0 (93) to eliminate PhiX contamination, trim reads (before median quality drops below 35; forward reads were trimmed at 181 bp and reverse reads at 167 bp), correct errors, merge read pairs, and remove PCR chimeras; ultimately, 34 ASVs were obtained across both samples and 18 ASVs representing >99.9% abundance were found in both samples. Taxonomic classification was performed with DADA2 and the SILVA v138 database (94).

The evolutionary history was inferred using the Maximum Likelihood method and the Tamura-Nei model (95). The tree with the highest log likelihood (−462.61) is shown in Fig. S1. The percentage of trees in which the associated taxa clustered together is shown next to the branches. Initial tree(s) for the heuristic search were obtained automatically by applying Neighbor-Join and BioNJ algorithms to a matrix of pairwise distances estimated using the Tamura-Nei model and then selecting the topology with superior log likelihood value. The tree is drawn to scale, with branch lengths measured in the number of substitutions per site. This analysis involved 13 nucleotide sequences. All positions containing gaps and missing data were eliminated (complete deletion option). The final data set contained a total of 251 positions. Evolutionary analyses were conducted in MEGA X (96).

Cell-mineral interaction analysis by fluorescence and electron microscopy

Cell-mineral interactions were visually characterized after mixing 1 µL of stain (LIVE/DEAD BacLight Bacterial Viability and Counting Kit, molecular probes, ThermoFisher

Scientific, Waltham, MA, USA) and 6 µL of culture sample using combined fluorescence and transmission light microscopy (Leica DM5500 B microscope, Leica HCX PL S-APO 40×/0.75 objective, Leica DFC360 FX camera, Leica Microsystems LAS AF software). Additional samples were prepared for scanning electron microscopy (Zeiss Crossbeam 550L Focused Ion Beam SEM). For this, 1.11 mL of 25% electron microscopy-grade glutaraldehyde was added to sealable tubes containing 10 mL of culture HP. Samples were incubated overnight at 5°C to allow for thorough fixation. To rinse cells of any unreacted glutaraldehyde after incubation, samples were centrifuged (5 min, 7,000 *g*) to form a bacterial pellet. The supernatant was removed and 1 mL of DI water was added to each tube. The tubes were vortexed, to evenly distribute the cells in solution, and incubated at room temperature (ca. 21°C) for 15 min. After incubation, the tubes were re-centrifuged (1 min, 7,000 *g*) and the supernatant was removed. This procedure was repeated using 25%, 50%, and 75% ethanol to dehydrate the sample (i.e., replace water with an organic solvent for drying). A 25 µL aliquots of sample was pipetted onto separate poly-L-lysine coated glass slides, which were placed at the bottom of a well-plate. A lid was placed on top of the well-plate to prevent evaporation and the samples were incubated for 30 min allowing cells and minerals to settle onto the poly-L-lysine. A 1 mL volume of 100% ethanol was added to the well to completely submerse the glass slide, which was incubated for an additional 15 min with the lid on. After incubation, the ethanol was removed and replaced with "fresh" 100% ethanol with a 15-min incubation. This procedure was repeated a third time using 100% ethanol, once with 250 µL of 100% ethanol and 250 µL of hexamethyldisilazane (HMDS, Sigma-Aldrich, St. Louis, MO, USA) and finally with 100% HMDS. The lid of the well-plate was placed slightly ajar, allowing the HMDS to evaporate overnight. Once dry, the glass slides were attached to an aluminum stub using carbon adhesive tabs. The prepared samples were coated with a 10-nm-thick deposition of gold to prevent charging during analysis. Micrographs were taken in secondary electron (SE) mode using the SEM operating with an acceleration voltage of 2.0 kV. To identify the elemental composition of mineral precipitates, spot analysis of energy dispersive spectroscopy (EDS) was obtained from representative samples using an Oxford Instruments EDS detector and the SEM operating at 20 kV. Spectral data were analyzed using AZtec.

Mineral analysis

For Moessbauer spectroscopy analysis, 10 mL of suspension was filtered anoxically (0.45 µm, Millipore) after the third transfer from a randomly selected bottle. The filter was sealed between two layers of Kapton tape and stored under anoxic conditions at −20°C until analysis. Samples were inserted into a closed-cycle exchange gas cryostat (Janis cryogenics) under a helium gas flow to minimize air exposure. Transmission spectra were collected at 77 K and 5 K using a constant acceleration drive system (WissEL) in transmission mode with a ^{57}Co/Rh source. All spectra were calibrated against a 7 µm thick α-^{57}Fe foil that was measured at 295 K. Recoil (University of Ottawa) and the Voigt Based Fitting (VBF) routine (97) was applied for sample analysis. The half-width at half maximum was constrained to 0.134 mm s^{-1} during fitting.

Data analysis

A non-parametric Wilcoxon signed-rank test for paired samples, with the Benjamini-Hochberg *P*-adjustment method, was applied using R (4.3.3) and its interface RStudio (2023.12.1+402) to identify differences in 16S rRNA gene copy numbers between day 0 and day 7. A non-parametric Kruskal-Wallis test combined with a Wilcoxon rank-sum test, with the Benjamini-Hochberg *P*-adjustment method, was applied to estimate differences in N_2O production between treatments.

ACKNOWLEDGMENTS

We are thankful to Dr. Shun Li and Prof. Yong-Guan Zhou for sampling and providing paddy soil samples from China. We thank Franziska Schädler for measurements of nitrogen species and guidance and advice during microbial community analyses, Paula Gscheidel for her help in the laboratory, Markus Maisch and Eva Voggenreiter for Moessbauer analysis, and Ferdinand Hampl for XRF measurements. We gratefully acknowledge the Tübingen Structural Microscopy Core Facility (funded by the Excellence Strategy of the German Federal and State Governments) for their support and assistance in this work. We are grateful for financial support from the Deutsche Forschungsgemeinschaft (DFG, German Research Foundation, project ID 431072007) and for infrastructural support by the DFG under Germany's Excellence Strategy, cluster of Excellence EXC2124 (project ID 390838134).

A.K. and C.Z. formulated the original hypothesis. H.G. and A.K. designed the experimental project. D.S. processed the amplicon sequencing data, constructed the maximum-likelihood tree, and helped with the interpretation of the microbial community results. J.S. took scanning electron microscopy pictures. J.L. performed experiments with arsenite. H.G. performed the main experiment, conducted analyses in the laboratory, data evaluation, and wrote the original draft of the manuscript. All authors were responsible for data interpretation. All authors discussed the data, reviewed, and edited the manuscript, and have read and agreed to the published version of the manuscript.

Figure illustrations of the microbial enrichment (Fig. 1a) and of the experimental setups (Fig. S9 to S13) were constructed using Biorender.com.

AUTHOR AFFILIATIONS

[1]Geomicrobiology, Department of Geosciences, University of Tübingen, Tübingen, Germany
[2]Quantitative Biology Center (QBiC), University of Tübingen, Tübingen, Germany
[3]Tübingen Structural Microscopy Core Facility, University of Tübingen, Tübingen, Germany
[4]Environmental Systems Analysis, Department of Geosciences, University of Tübingen, Tübingen, Germany
[5]Plant Biogeochemistry, Department of Applied Microbial Ecology, Helmholtz Centre for Environmental Research - UFZ, Leipzig, Germany
[6]Plant Biogeochemistry, Department of Geosciences, University of Tübingen, Tübingen, Germany
[7]Cluster of Excellence: EXC 2124: Controlling Microbes to Fight Infection, Tübingen, Germany

PRESENT ADDRESS

Jeremiah Shuster, Department of Earth Sciences, Western University, London, Canada

AUTHOR ORCIDs

Hanna Grimm http://orcid.org/0000-0002-1285-544X
Daniel Straub http://orcid.org/0000-0002-2553-0660
Andreas Kappler http://orcid.org/0000-0002-3558-9500

FUNDING

Funder	Grant(s)	Author(s)
Deutsche Forschungsgemeinschaft (DFG)	project ID 431072007	Hanna Grimm Andreas Kappler
Deutsche Forschungsgemeinschaft (DFG)	project ID 390838134	Andreas Kappler

AUTHOR CONTRIBUTIONS

Hanna Grimm, Conceptualization, Data curation, Formal analysis, Investigation, Methodology, Validation, Visualization, Writing – original draft, Writing – review and editing | Jennifer Lorenz, Data curation | Daniel Straub, Data curation, Formal analysis, Supervision, Writing – original draft | Prachi Joshi, Formal analysis, Supervision, Writing – original draft | Jeremiah Shuster, Data curation, Supervision | Christiane Zarfl, Conceptualization, Formal analysis, Funding acquisition, Project administration, Resources, Supervision, Writing – original draft, Writing – review and editing | E. Marie Muehe, Methodology, Supervision, Writing – original draft | Andreas Kappler, Conceptualization, Formal analysis, Funding acquisition, Investigation, Methodology, Project administration, Resources, Supervision, Writing – original draft, Writing – review and editing

DATA AVAILABILITY

Raw sequencing data have been deposited at NCBI in the Sequence Read Archive (SRA) under BioProject accession number PRJNA1123617. The data set supporting the findings of this study can be accessed on Zenodo via https://doi.org/10.5281/zenodo.13683983.

ADDITIONAL FILES

The following material is available online.

Supplemental Material

Supplemental material (AEM01262-24-s0001.pdf). Figures S1 to S11; Tables S1 to S13.

REFERENCES

1. Chen K, Yu S, Ma T, Ding J, He P, Dai Y, Zeng G. 2022. Effects of water and nitrogen management on water productivity, nitrogen use efficiency and leaching loss in rice paddies. Water (Basel) 14:1596. https://doi.org/10.3390/w14101596
2. Dong Z, Wu L, Chai J, Zhu Y, Chen Y, Zhu Y. 2015. Effects of nitrogen application rates on rice grain yield, nitrogen-use efficiency, and water quality in paddy field. Commun Soil Sci Plant Anal 46:1579–1594. https://doi.org/10.1080/00103624.2015.1045595
3. Ye Q, Zhang H, Wei H, Zhang Y, Wang B, Xia K, Huo Z, Dai Q, Xu K. 2007. Effects of nitrogen fertilizer on nitrogen use efficiency and yield of rice under different soil conditions. Front Agric China 1:30–36. https://doi.org/10.1007/s11703-007-0005-z
4. Di Capua F, Pirozzi F, Lens PNL, Esposito G. 2019. Electron donors for autotrophic denitrification. Chem Eng J 362:922–937. https://doi.org/10.1016/j.cej.2019.01.069
5. Rivett MO, Buss SR, Morgan P, Smith JWN, Bemment CD. 2008. Nitrate attenuation in groundwater: a review of biogeochemical controlling processes. Water Res 42:4215–4232. https://doi.org/10.1016/j.watres.2008.07.020
6. Kraft B, Tegetmeyer HE, Sharma R, Klotz MG, Ferdelman TG, Hettich RL, Geelhoed JS, Strous M. 2014. Nitrogen cycling. The environmental controls that govern the end product of bacterial nitrate respiration. Science 345:676–679. https://doi.org/10.1126/science.1254070
7. Ratering S, Schnell S. 2001. Nitrate-dependent iron(II) oxidation in paddy soil. Environ Microbiol 3:100–109. https://doi.org/10.1046/j.1462-2920.2001.00163.x
8. Hohmann C, Winkler E, Morin G, Kappler A. 2010. Anaerobic Fe(II)-oxidizing bacteria show as resistance and immobilize as during Fe(III) mineral precipitation. Environ Sci Technol 44:94–101. https://doi.org/10.1021/es900708s
9. Dittmar J, Voegelin A, Roberts LC, Hug SJ, Saha GC, Ali MA, Badruzzaman ABM, Kretzschmar R. 2007. Spatial distribution and temporal variability of arsenic in irrigated rice fields in Bangladesh. 2. Paddy soil. Environ Sci Technol 41:5967–5972. https://doi.org/10.1021/es0702972
10. Gillispie EC, Sowers TD, Duckworth OW, Polizzotto ML. 2015. Soil pollution due to irrigation with arsenic-contaminated groundwater: current state of science. Curr Pollut Rep 1:1–12. https://doi.org/10.1007/s40726-015-0001-5
11. Muehe EM, Wang T, Kerl CF, Planer-Friedrich B, Fendorf S. 2019. Rice production threatened by coupled stresses of climate and soil arsenic. Nat Commun 10:4985. https://doi.org/10.1038/s41467-019-12946-4
12. Oremland RS, Stolz JF. 2005. Arsenic, microbes and contaminated aquifers. Trends Microbiol 13:45–49. https://doi.org/10.1016/j.tim.2004.12.002
13. Dixit S, Hering JG. 2003. Comparison of arsenic(V) and arsenic(III) sorption onto iron oxide minerals: implications for arsenic mobility. Environ Sci Technol 37:4182–4189. https://doi.org/10.1021/es030309t
14. Hu M, Chen P, Sun W, Li F, Cui J. 2017. A novel organotrophic nitrate-reducing Fe(II)-oxidizing bacterium isolated from paddy soil and draft genome sequencing indicate its metabolic versatility. RSC Adv 7:56611–56620. https://doi.org/10.1039/C7RA09328D
15. Li S, Li X, Li F. 2018. Fe(II) oxidation and nitrate reduction by a denitrifying bacterium, *Pseudomonas stutzeri* LS-2, isolated from paddy soil. J Soils Sediments 18:1668–1678. https://doi.org/10.1007/s11368-017-1883-1
16. Li X, Zhang W, Liu T, Chen L, Chen P, Li F. 2016. Changes in the composition and diversity of microbial communities during anaerobic nitrate reduction and Fe(II) oxidation at circumneutral pH in paddy soil. Soil Biol Biochem 94:70–79. https://doi.org/10.1016/j.soilbio.2015.11.013
17. Pan D, Chen P, Yang G, Niu R, Bai Y, Cheng K, Huang G, Liu T, Li X, Li F. 2023. Fe(II) oxidation shaped functional genes and bacteria involved in denitrification and dissimilatory nitrate reduction to ammonium from different paddy soils. Environ Sci Technol 57:21156–21167. https://doi.org/10.1021/acs.est.3c06337
18. Widijanto H, Amalia RS, Syamsiyah J, Suntoro. 2023. A comparison of the dynamics and carbon stocks in rice fields with different management systems and soil types. J Arid Agric:31–38. https://doi.org/10.25081/jaa.2023.v9.8065
19. Zhou J, Bruns MA, Tiedje JM. 1996. DNA recovery from soils of diverse composition. Appl Environ Microbiol 62:316–322. https://doi.org/10.1128/aem.62.2.316-322.1996
20. Huang Y-M, Straub D, Kappler A, Smith N, Blackwell N, Kleindienst S. 2021. A novel enrichment culture highlights core features of microbial

networks contributing to autotrophic Fe(II) oxidation coupled to nitrate reduction. Microb Physiol 31:280–295. https://doi.org/10.1159/000517083
21. Jakus N, Blackwell N, Osenbrück K, Straub D, Byrne JM, Wang Z, Glöckler D, Elsner M, Lueders T, Grathwohl P, Kleindienst S, Kappler A. 2021. Nitrate removal by a novel lithoautotrophic nitrate-reducing, iron(II)-oxidizing culture enriched from a pyrite-rich limestone aquifer. Appl Environ Microbiol 87:e0046021. https://doi.org/10.1128/AEM.00460-21
22. Straub KL, Benz M, Schink B, Widdel F. 1996. Anaerobic, nitrate-dependent microbial oxidation of ferrous iron. Appl Environ Microbiol 62:1458–1460. https://doi.org/10.1128/aem.62.4.1458-1460.1996
23. He S, Tominski C, Kappler A, Behrens S, Roden EE. 2016. Metagenomic analyses of the autotrophic Fe(II)-oxidizing, nitrate-reducing enrichment culture KS. Appl Environ Microbiol 82:2656–2668. https://doi.org/10.1128/AEM.03493-15
24. Huang Y-M, Straub D, Blackwell N, Kappler A, Kleindienst S. 2021. Meta-omics reveal *Gallionellaceae* and *Rhodanobacter* species as interdependent key players for Fe(II) oxidation and nitrate reduction in the autotrophic enrichment culture KS. Appl Environ Microbiol 87:e0049621. https://doi.org/10.1128/AEM.00496-21
25. Jakus N, Blackwell N, Straub D, Kappler A, Kleindienst S. 2021. Presence of Fe(II) and nitrate shapes aquifer-originating communities leading to an autotrophic enrichment dominated by an Fe(II)-oxidizing *Gallionellaceae* sp. FEMS Microbiol Ecol 97:fiab145. https://doi.org/10.1093/femsec/fiab145
26. Huang J, Mellage A, Garcia JP, Glöckler D, Mahler S, Elsner M, Jakus N, Mansor M, Jiang H, Kappler A. 2023. Metabolic performance and fate of electrons during nitrate-reducing Fe(II) oxidation by the autotrophic enrichment culture KS grown at different initial Fe/N ratios. Appl Environ Microbiol 89:e0019623. https://doi.org/10.1128/aem.00196-23
27. Emerson D, Floyd MM. 2005. Enrichment and isolation of iron-oxidizing bacteria at neutral pH. Meth Enzymol 397:112–123. https://doi.org/10.1016/S0076-6879(05)97006-7
28. Bryce C, Blackwell N, Schmidt C, Otte J, Huang Y-M, Kleindienst S, Tomaszewski E, Schad M, Warter V, Peng C, Byrne JM, Kappler A. 2018. Microbial anaerobic Fe(II) oxidation – Ecology, mechanisms and environmental implications. Environ Microbiol 20:3462–3483. https://doi.org/10.1111/1462-2920.14328
29. Chan CS, Dykes GE, Hoover RL, Limmer MA, Seyfferth AL. 2023. Gallionellaceae in rice root plaque: metabolic roles in iron oxidation, nutrient cycling, and plant interactions. Appl Environ Microbiol 89:e00570–23. https://doi.org/10.1128/aem.00570-23
30. Kappler A, Bryce C, Mansor M, Lueder U, Byrne JM, Swanner ED. 2021. An evolving view on biogeochemical cycling of iron. Nat Rev Microbiol 19:360–374. https://doi.org/10.1038/s41579-020-00502-7
31. Weber KA, Achenbach LA, Coates JD. 2006. Microorganisms pumping iron: anaerobic microbial iron oxidation and reduction. Nat Rev Microbiol 4:752–764. https://doi.org/10.1038/nrmicro1490
32. Weber KA, Urrutia MM, Churchill PF, Kukkadapu RK, Roden EE. 2006. Anaerobic redox cycling of iron by freshwater sediment microorganisms. Environ Microbiol 8:100–113. https://doi.org/10.1111/j.1462-2920.2005.00873.x
33. Coby AJ, Picardal F, Shelobolina E, Xu H, Roden EE. 2011. Repeated anaerobic microbial redox cycling of iron. Appl Environ Microbiol 77:6036–6042. https://doi.org/10.1128/AEM.00276-11
34. He S, Barco RA, Emerson D, Roden EE. 2017. Comparative genomic analysis of neutrophilic iron (II) oxidizer genomes for candidate genes in extracellular electron transfer. Front Microbiol 8:1584. https://doi.org/10.3389/fmicb.2017.01584
35. Hassan Z, Sultana M, Westerhoff HV, Khan SI, Röling WFM. 2016. Iron cycling potentials of arsenic contaminated groundwater in Bangladesh as revealed by enrichment cultivation. Geomicrobiol J 33:779–792. https://doi.org/10.1080/01490451.2015.1111471
36. Gülay A, Çekiç Y, Musovic S, Albrechtsen H-J, Smets BF. 2018. Diversity of iron oxidizers in groundwater-fed rapid sand filters: evidence of Fe(II)-dependent growth by *Curvibacter* and *Undibacterium* spp. Front Microbiol 9:2808. https://doi.org/10.3389/fmicb.2018.02808
37. Notini L, Byrne JM, Tomaszewski EJ, Latta DE, Zhou Z, Scherer MM, Kappler A. 2019. Mineral defects enhance bioavailability of goethite toward microbial Fe(III) reduction. Environ Sci Technol 53:8883–8891. https://doi.org/10.1021/acs.est.9b03208
38. Tominski C, Heyer H, Lösekann-Behrens T, Behrens S, Kappler A. 2018. Growth and population dynamics of the anaerobic Fe(II)-oxidizing and nitrate-reducing enrichment culture KS. Appl Environ Microbiol 84:e02173-17. https://doi.org/10.1128/AEM.02173-17
39. Laufer K, Røy H, Jørgensen BB, Kappler A. 2016. Evidence for the existence of autotrophic nitrate-reducing Fe(II)-oxidizing bacteria in marine coastal sediment. Appl Environ Microbiol 82:6120–6131. https://doi.org/10.1128/AEM.01570-16
40. Hegler F, Posth NR, Jiang J, Kappler A. 2008. Physiology of phototrophic iron(II)-oxidizing bacteria: implications for modern and ancient environments: physiology of phototrophic iron(II)-oxidizing bacteria. FEMS Microbiol Ecol 66:250–260. https://doi.org/10.1111/j.1574-6941.2008.00592.x
41. Kappler A, Newman DK. 2004. Formation of Fe(III)-minerals by Fe(II)-oxidizing photoautotrophic bacteria 1. Geochim Cosmochim Acta 68:1217–1226. https://doi.org/10.1016/j.gca.2003.09.006
42. Kluegleln N, Zeitvogel F, Stierhof Y-D, Floetenmeyer M, Konhauser KO, Kappler A, Obst M. 2014. Potential role of nitrite for abiotic Fe(II) oxidation and cell encrustation during nitrate reduction by denitrifying bacteria. Appl Environ Microbiol 80:1051–1061. https://doi.org/10.1128/AEM.03277-13
43. Schädler S, Burkhardt C, Hegler F, Straub KL, Miot J, Benzerara K, Kappler A. 2009. Formation of cell-iron-mineral aggregates by phototrophic and nitrate-reducing anaerobic Fe(II)-oxidizing bacteria. Geomicrobiol J 26:93–103. https://doi.org/10.1080/01490450802660573
44. Hegler F, Schmidt C, Schwarz H, Kappler A. 2010. Does a low-pH microenvironment around phototrophic FeII-oxidizing bacteria prevent cell encrustation by FeIII minerals? FEMS Microbiol Ecol 74:592–600. https://doi.org/10.1111/j.1574-6941.2010.00975.x
45. Saini G, Chan CS. 2013. Near-neutral surface charge and hydrophilicity prevent mineral encrustation of Fe-oxidizing micro-organisms. Geobiology 11:191–200. https://doi.org/10.1111/gbi.12021
46. Cheng B, Wang Y, Hua Y, Heal KV. 2021. The performance of nitrate-reducing Fe(II) oxidation processes under variable initial Fe/N ratios: the fate of nitrogen and iron species. Front Environ Sci Eng 15. https://doi.org/10.1007/s11783-020-1366-2
47. Larese-Casanova P, Haderlein SB, Kappler A. 2010. Biomineralization of lepidocrocite and goethite by nitrate-reducing Fe(II)-oxidizing bacteria: effect of pH, bicarbonate, phosphate, and humic acids. Geochim Cosmochim Acta 74:3721–3734. https://doi.org/10.1016/j.gca.2010.03.037
48. Chen D, Liu T, Li X, Li F, Luo X, Wu Y, Wang Y. 2018. Biological and chemical processes of microbially mediated nitrate-reducing Fe(II) oxidation by *Pseudogulbenkiania* sp. strain 2002. Chem Geol 476:59–69. https://doi.org/10.1016/j.chemgeo.2017.11.004
49. Kappler A, Schink B, Newman DK. 2005. Fe(III) mineral formation and cell encrustation by the nitrate - dependent Fe(II) - oxidizer strain BoFeN1. Geobiology 3:235–245. https://doi.org/10.1111/j.1472-4669.2006.00056.x
50. Liu T, Chen D, Luo X, Li X, Li F. 2019. Microbially mediated nitrate-reducing Fe(II) oxidation: quantification of chemodenitrification and biological reactions. Geochim Cosmochim Acta 256:97–115. https://doi.org/10.1016/j.gca.2018.06.040
51. Winkler P, Kaiser K, Thompson A, Kalbitz K, Fiedler S, Jahn R. 2018. Contrasting evolution of iron phase composition in soils exposed to redox fluctuations. Geochim Cosmochim Acta 235:89–102. https://doi.org/10.1016/j.gca.2018.05.019
52. Carlson HK, Clark IC, Melnyk RA, Coates JD. 2012. Toward a mechanistic understanding of anaerobic nitrate-dependent iron oxidation: balancing electron uptake and detoxification. Front Microbiol 3:57. https://doi.org/10.3389/fmicb.2012.00057
53. Ding C, Du S, Ma Y, Li X, Zhang T, Wang X. 2019. Changes in the pH of paddy soils after flooding and drainage: modeling and validation. Geoderma 337:511–513. https://doi.org/10.1016/j.geoderma.2018.10.012
54. Lu H-L, Li K-W, Nkoh JN, He X, Xu R-K, Qian W, Shi R-Y, Hong Z-N. 2022. Effects of pH variations caused by redox reactions and pH buffering capacity on Cd(II) speciation in paddy soils during submerging/draining alternation. Ecotoxicol Environ Saf 234:113409. https://doi.org/10.1016/j.ecoenv.2022.113409

55. Das GK, Li J. 2023. Iron removal as goethite from synthetic laterite leach solutions. ACS Omega 8:11931–11940. https://doi.org/10.1021/acsomega.2c07595
56. Zhu-Barker X, Cavazos AR, Ostrom NE, Horwath WR, Glass JB. 2015. The importance of abiotic reactions for nitrous oxide production. Biogeochemistry 126:251–267. https://doi.org/10.1007/s10533-015-0166-4
57. Bhattacharya P, Welch AH, Stollenwerk KG, McLaughlin MJ, Bundschuh J, Panaullah G. 2007. Arsenic in the environment: Biology and Chemistry. Sci Total Environ 379:109–120. https://doi.org/10.1016/j.scitotenv.2007.02.037
58. Lin Z, Wang X, Wu X, Liu D, Yin Y, Zhang Y, Xiao S, Xing B. 2018. Nitrate reduced arsenic redox transformation and transfer in flooded paddy soil-rice system. Environ Pollut 243:1015–1025. https://doi.org/10.1016/j.envpol.2018.09.054
59. Roberts LC, Hug SJ, Voegelin A, Dittmar J, Kretzschmar R, Wehrli B, Saha GC, Badruzzaman ABM, Ali MA. 2011. Arsenic dynamics in porewater of an intermittently irrigated paddy field in Bangladesh. Environ Sci Technol 45:971–976. https://doi.org/10.1021/es102882q
60. Stollenwerk KG, Breit GN, Welch AH, Yount JC, Whitney JW, Foster AL, Uddin MN, Majumder RK, Ahmed N. 2007. Arsenic attenuation by oxidized aquifer sediments in Bangladesh. Sci Total Environ 379:133–150. https://doi.org/10.1016/j.scitotenv.2006.11.029
61. Ohtsuka T, Yamaguchi N, Makino T, Sakurai K, Kimura K, Kudo K, Homma E, Dong DT, Amachi S. 2013. Arsenic dissolution from Japanese paddy soil by a dissimilatory arsenate-reducing bacterium *Geobacter* sp. OR-1. Environ Sci Technol 47:6263–6271. https://doi.org/10.1021/es400231x
62. Zhang J, Zhao S, Xu Y, Zhou W, Huang K, Tang Z, Zhao F-J. 2017. Nitrate stimulates anaerobic microbial arsenite oxidation in paddy soils. Environ Sci Technol 51:4377–4386. https://doi.org/10.1021/acs.est.6b06255
63. Muehe EM, Scheer L, Daus B, Kappler A. 2013. Fate of arsenic during microbial reduction of biogenic versus Abiogenic As-Fe(III)-mineral coprecipitates. Environ Sci Technol 47:8297–8307. https://doi.org/10.1021/es400801z
64. Li X, Qiao J, Li S, Häggblom MM, Li F, Hu M. 2020. Bacterial communities and functional genes stimulated during anaerobic arsenite oxidation and nitrate reduction in a paddy soil. Environ Sci Technol 54:2172–2181. https://doi.org/10.1021/acs.est.9b04308
65. Feng M, Du Y, Li X, Li F, Qiao J, Chen G, Huang Y. 2023. Insight into universality and characteristics of nitrate reduction coupled with arsenic oxidation in different paddy soils. Sci Total Environ 866:161342. https://doi.org/10.1016/j.scitotenv.2022.161342
66. Tang Y, Su X, Wen T, McBratney AB, Zhou S, Huang F, Zhu Y. 2024. Soil properties shape the heterogeneity of denitrification and N_2O emissions across large - scale flooded paddy soils. Glob Change Biol 30:e17176. https://doi.org/10.1111/gcb.17176
67. Wang M, Hu R, Ruser R, Schmidt C, Kappler A. 2020. Role of chemodenitrification for N_2O emissions from nitrate reduction in rice paddy soils. ACS Earth Space Chem 4:122–132. https://doi.org/10.1021/acsearthspacechem.9b00296
68. Jones LC, Peters B, Lezama Pacheco JS, Casciotti KL, Fendorf S. 2015. Stable isotopes and iron oxide mineral products as markers of chemodenitrification. Environ Sci Technol 49:3444–3452. https://doi.org/10.1021/es504862x
69. Jamieson J, Prommer H, Kaksonen AH, Sun J, Siade AJ, Yusov A, Bostick B. 2018. Identifying and quantifying the intermediate processes during nitrate-dependent iron(II) oxidation. Environ Sci Technol 52:5771–5781. https://doi.org/10.1021/acs.est.8b01122
70. Bergaust L, Mao Y, Bakken LR, Frostegård A. 2010. Denitrification response patterns during the transition to anoxic respiration and posttranscriptional effects of suboptimal pH on nitrogen oxide reductase in *Paracoccus denitrificans*. Appl Environ Microbiol 76:6387–6396. https://doi.org/10.1128/AEM.00608-10
71. Naruse T, Ban Y, Yoshida T, Kato T, Namikawa M, Takahashi T, Nishida M, Asakawa S, Watanabe T. 2019. Community structure of microaerophilic iron-oxidizing bacteria in Japanese paddy field soils. Soil Sci Plant Nutr 65:460–470. https://doi.org/10.1080/00380768.2019.1671139
72. Watanabe T, Kato K, Kawaguchi K, Oga T, Ban Y, Otoidobiga CH, Sawadogo A, Wonni I, Ouedraogo LS, Zongo JD, Dianou D, Asakawa S. 2023. Investigation of iron-reducing and iron-oxidizing bacterial communities in the rice rhizosphere of iron-toxic paddy field: a case study in Burkina Faso, West Africa. Soil Sci Plant Nutr 69:283–293. https://doi.org/10.1080/00380768.2023.2259426
73. Watanabe T, Katayanagi N, Agbisit R, Llorca L, Hosen Y, Asakawa S. 2021. Influence of alternate wetting and drying water-saving irrigation practice on the dynamics of *Gallionella*-related iron-oxidizing bacterial community in paddy field soil. Soil Biol Biochem 152:108064. https://doi.org/10.1016/j.soilbio.2020.108064
74. Xiao W, Ye X, Ye Z, Zhang Q, Zhao S, Chen D, Gao N, Huang M. 2022. Responses of microbial community composition and function to biochar and irrigation management and the linkage to Cr transformation in paddy soil. Environ Pollut 304:119232. https://doi.org/10.1016/j.envpol.2022.119232
75. Grimm H, Drabesch S, Nicol A, Straub D, Joshi P, Zarfl C, Planer-Friedrich B, Muehe EM, Kappler A. 2024. Arsenic immobilization and greenhouse gas emission depend on quantity and frequency of nitrogen fertilization in paddy soil. Heliyon 10:e35706. https://doi.org/10.1016/j.heliyon.2024.e35706
76. Khalifa A, Nakasuji Y, Saka N, Honjo H, Asakawa S, Watanabe T. 2018. *Ferrigenium kumadai* gen. nov., sp. nov., a microaerophilic iron-oxidizing bacterium isolated from a paddy field soil. Int J Syst Evol Microbiol 68:2587–2592. https://doi.org/10.1099/ijsem.0.002882
77. Zhang J, Wu H, Hu Z, Liang S, Fan J. 2014. Examination of oxygen release from plants in constructed wetlands in different stages of wetland plant life cycle. Environ Sci Pollut Res 21:9709–9716. https://doi.org/10.1007/s11356-014-2905-9
78. Jakus N, Mellage A, Höschen C, Maisch M, Byrne JM, Mueller CW, Grathwohl P, Kappler A. 2021. Anaerobic neutrophilic pyrite oxidation by a chemolithoautotrophic nitrate-reducing iron(II)-oxidizing culture enriched from a fractured aquifer. Environ Sci Technol 55:9876–9884. https://doi.org/10.1021/acs.est.1c02049
79. Shelobolina E, Xu H, Konishi H, Kukkadapu R, Wu T, Blöthe M, Roden E. 2012. Microbial lithotrophic oxidation of structural Fe(II) in biotite. Appl Environ Microbiol 78:5746–5752. https://doi.org/10.1128/AEM.01034-12
80. Weber KA, Picardal FW, Roden EE. 2001. Microbially catalyzed nitrate-dependent oxidation of biogenic solid-phase Fe(II) compounds. Environ Sci Technol 35:1644–1650. https://doi.org/10.1021/es0016598
81. Yu H-Y, Li F-B, Liu C-S, Huang W, Liu T-X, Yu W-M. 2016. Chapter five - iron redox cycling coupled to transformation and immobilization of heavy metals: implications for paddy rice safety in the red soil of South Chinap 279–317. In Sparks DL (ed), Advances in agronomy. Academic Press.https://doi.org/10.1016/bs.agron.2015.12.006
82. Melton ED, Swanner ED, Behrens S, Schmidt C, Kappler A. 2014. The interplay of microbially mediated and abiotic reactions in the biogeochemical Fe cycle. Nat Rev Microbiol 12:797–808. https://doi.org/10.1038/nrmicro3347
83. Schaedler F, Kappler A, Schmidt C. 2018. A revised iron extraction protocol for environmental samples rich in nitrite and carbonate. Geomicrobiol J 35:23–30. https://doi.org/10.1080/01490451.2017.1303554
84. Stookey LL. 1970. Ferrozine---a new spectrophotometric reagent for iron. Anal Chem 42:779–781. https://doi.org/10.1021/ac60289a016
85. Muyzer G, de Waal EC, Uitterlinden AG. 1993. Profiling of complex microbial populations by denaturing gradient gel electrophoresis analysis of polymerase chain reaction-amplified genes coding for 16S rRNA. Appl Environ Microbiol 59:695–700. https://doi.org/10.1128/aem.59.3.695-700.1993
86. Nadkarni MA, Martin FE, Jacques NA, Hunter N. 2002. Determination of bacterial load by real-time PCR using a broad-range (universal) probe and primers set. Microbiol (Reading, Engl) 148:257–266. https://doi.org/10.1099/00221287-148-1-257
87. Caporaso JG, Lauber CL, Walters WA, Berg-Lyons D, Lozupone CA, Turnbaugh PJ, Fierer N, Knight R. 2011. Global patterns of 16S rRNA diversity at a depth of millions of sequences per sample. Proc Natl Acad Sci U S A 108 Suppl 1:4516–4522. https://doi.org/10.1073/pnas.1000080107
88. Ewels PA, Peltzer A, Fillinger S, Patel H, Alneberg J, Wilm A, Garcia MU, Di Tommaso P, Nahnsen S. 2020. The nf-core framework for community-curated bioinformatics pipelines. Nat Biotechnol 38:276–278. https://doi.org/10.1038/s41587-020-0439-x
89. Straub D, Blackwell N, Langarica-Fuentes A, Peltzer A, Nahnsen S, Kleindienst S. 2020. Interpretations of environmental microbial

community studies are biased by the selected 16S rRNA (gene) amplicon sequencing pipeline. Front Microbiol 11:550420. https://doi.org/10.3389/fmicb.2020.550420
90. Di Tommaso P, Chatzou M, Floden EW, Barja PP, Palumbo E, Notredame C. 2017. Nextflow enables reproducible computational workflows. Nat Biotechnol 35:316–319. https://doi.org/10.1038/nbt.3820
91. Kurtzer GM, Sochat V, Bauer MW. 2017. Singularity: scientific containers for mobility of compute. PLoS One 12:e0177459. https://doi.org/10.1371/journal.pone.0177459
92. Martin M. 2011. Cutadapt removes adapter sequences from high-throughput sequencing reads. EMBnet J 17:10. https://doi.org/10.14806/ej.17.1.200
93. Callahan BJ, McMurdie PJ, Rosen MJ, Han AW, Johnson AJA, Holmes SP. 2016. DADA2: high-resolution sample inference from Illumina amplicon data. Nat Methods 13:581–583. https://doi.org/10.1038/nmeth.3869
94. Quast C, Pruesse E, Yilmaz P, Gerken J, Schweer T, Yarza P, Peplies J, Glöckner FO. 2013. The SILVA ribosomal RNA gene database project: improved data processing and web-based tools. Nucleic Acids Res 41:D590–D596. https://doi.org/10.1093/nar/gks1219
95. Tamura K, Nei M. 1993. Estimation of the number of nucleotide substitutions in the control region of mitochondrial DNA in humans and chimpanzees. Mol Biol Evol 10:512–526. https://doi.org/10.1093/oxfordjournals.molbev.a040023
96. Kumar S, Stecher G, Li M, Knyaz C, Tamura K. 2018. MEGA X: molecular evolutionary genetics analysis across computing platforms. Mol Biol Evol 35:1547–1549. https://doi.org/10.1093/molbev/msy096
97. Rancourt DG, Ping JY. 1991. Voigt-based methods for arbitrary-shape static hyperfine parameter distributions in Mössbauer spectroscopy. Nucl Instrum Methods Phys Res Sect B Beam Interact Mater 58:85–97. https://doi.org/10.1016/0168-583X(91)95681-3

Supporting Information

Appendix of

Nitrous oxide is the main product during nitrate reduction by a novel lithoautotrophic iron(II)-oxidizing culture from an organic-rich paddy soil

Hanna Grimm[1], Jennifer Lorenz[1], Daniel Straub[2], Prachi Joshi[1], Jeremiah Shuster[1,3*], Christiane Zarfl[4], E. Marie Muehe[5,6], Andreas Kappler[1,7#]

[1]Geomicrobiology, Department of Geosciences, University of Tübingen, Tübingen, Germany

[2]Quantitative Biology Center (QBiC), University of Tübingen, Germany

[3]Tübingen Structural Microscopy Core Facility, University of Tübingen, Tübingen, Germany

[4]Environmental Systems Analysis, Department of Geosciences, University of Tübingen, Tübingen, Germany

[5]Plant Biogeochemistry, Department of Applied Microbial Ecology, Helmholtz Centre for Environmental Research - UFZ, Leipzig, Germany

[6]Plant Biogeochemistry, Department of Geosciences, University of Tübingen, Tübingen, Germany

[7]Cluster of Excellence: EXC 2124: Controlling Microbes to Fight Infection, Tübingen, Germany

*Present address: Jeremiah Shuster, Department of Earth Sciences, Western University, London, Canada

#Address correspondence to Andreas Kappler, andreas.kappler@uni-tuebingen.de

Appendix: Soil characterization

Basic soil properties were analyzed in triplicates on soil samples after removal of plant debris and larger gravel. For soil texture analysis, a soil dispersion was prepared by adding 25 mL of sodium pyrophosphate to 30 g of non-sieved, fresh soil. After 30 min of stirring, the soil dispersion was filled up to a volume of 1000 mL and analyzed with a PARIO Soil Particle Analyzer (Meter Group, Germany) (1). After analysis, the soil was sieved (2 mm, 630 µm, 200 µm and 63 µm) to determine the sand and the fine fraction. Total loss of soil sample after sieving was below 5%. To determine the particle density, 20 g of dry soil was weighed into capillary pycnometer, filled up with deionized water and stepwise degassed before weight determination (2). Water content was determined by drying paddy soil at 105°C for 72 h. Soil pH was determined by adding 2.5 mL MQ water to 1 g of soil sample (2.5:1, solution:soil) and measuring after 2 h and 24 h using a benchtop pH meter (SG2, Mettler-Toledo GmbH, Germany) equipped with a pH electrode (InLab Easy DIN, Mettler-Toledo GmbH, Germany) (3).The cation exchange capacity of the paddy soil was quantified with a 0.1 M $BaCl_2$ extraction (4 h) by microwave plasma atomic emission spectroscopy (4200 MP-AES, Agilent technologies, United States) (4). X-ray fluorescence was used to determine total elemental content of the paddy soil. Glass beads were prepared by mixing 0.2333 g of dried and mortared sample with 3.9666 g of Fluxana FX-X65 (lithium tetraborate:lithium metaborate 66%:34%) and melted in a platinum crucible using a Spetec Roto-Melt 2,0 µP at 0.45 for 6 min. Afterwards, the sample was poured into a platinum mold and loaded into a S8 Tiger (Bruker) prior to analysis. Total element concentrations were quantified using the calibration package GeoQuant (Bruker). The loss on ignition (LOI) was calculated as the percental weight difference between the dried (105°C for 24 h) and annealed sample powder (3000°C for

3 h) and is 6.06 wt%. The LOI and the total XRF sums add up to 99.93 wt%. Total soil carbon and nitrogen contents were analyzed for dry and mortared paddy soil samples by dry combustion (soliTOC cube, Elementar Analysensysteme GmbH, Germany). Water-extractable organic carbon and nitrogen species were determined after extraction of 1 g dry weight soil with 5 mL of MQ by an elemental analyzer (multi N/C, 2100S, Analytik Jena GmbH) and segmented flow analysis (CFA, AutoAnalyzer 3, SEAL Analytical, Germany), respectively. To evaluate the presence of different iron mineral phases and associated arsenic, sequential extractions were performed under anoxic conditions. Soil samples were extracted for 24 h with 1 M sodium acetate (pH 5, adjusted with acetic acid) targeting adsorbed iron(II) and iron in amorphous sulfide minerals (referred to as adsorbed Fe) (5, 6). It is known that sodium acetate also extracts carbonates (7), yet this is considered to play a minor role due to low total inorganic carbon contents and low pH (Table A9). This was followed by 2 h extraction with 0.5 M HCl, extracting poorly crystalline iron minerals and reduced iron(II) minerals such as $FeCO_3$ and FeS (referred to as poorly crystalline Fe) (8). Lastly, samples were extracted for 24 h with 6 M HCl for extraction of more crystalline iron mineral phases and poorly reactive sheet silicate iron or FeS species (referred to as crystalline Fe) (9).

3

Appendix: Tables

Table A1. Composition of growth media for lithoautotrophic nitrate-reducing, iron(II)-oxidizing microorganisms.

Chemical	Concentration	Molar mass	Concentration	Reference
	mg L^{-1}	g mol^{-1}	mM	
KH_2PO_4	0.14	136.09	1.03	
NaCl	0.20	58.44	3.42	
NH_4Cl	0.30	53.49	5.61	
$MgSO_4 \cdot 7\ H_2O$	0.50	246.47	2.03	
$CaCl_2 \cdot 2\ H_2O$	0.10	147.01	0.68	
$NaHCO_3$	1.85	84.01	22.02	
Trace elements SL10	1.00			(10)
7 vitamine solution	1.00			(11)
Selenite/tungstate solution	0.10			(12)

Table A2. Attempts to isolate the relevant nitrate-reducing, iron(II)-oxidizing strain in the NRFeOx culture.

Isolation attempts	Condition	Description	Success
Growth media with nitrate+acetate	anoxic	Backtransfer to liquid growth medium containing nitrate+iron(II)	no
LB plates	oxic	Picking of single colonies with repetitive streaking on LB plates, backtransfer to liquid growth medium containing nitrate+iron(II)	no
	microoxic		no
Plates with growth media with nitrate+iron(II)	anoxic	picking of single colonies with repetitive streaking on LB plates, backtransfer to liquid growth media containing nitrate+iron(II)	no
Gradient tubes	microoxic		no

Table A3. Relative 16S rRNA gene sequence abundance in native paddy soil from which lithoautotrophic NRFeOx culture was enriched.

Taxa	Relative abundance
	%
Gallionella	0.30
Comamonadaceae	1.46
Rhodocyclaceae	0.14
Holophagaceae	0.20

5

Table A4. Extent and stoichiometric ratio of reduced nitrate and oxidized iron(II), percentage of N_2O-N of total reduced NO_3^--N and start and end 16S rRNA gene copy numbers for different experiments. 'T' stands for transfer.

		Nitrate reduced	Iron(II) oxidized*	Ratio $nitrate_{red.}$:$iron(II)_{ox.}$	N_2O-N of total reduced NO_3^--N
		mM	mM		%
Main experiment	T1	0.53 ± 0.12	2.29 ± 0.16	0.23 ± 0.05	72.29±19.38
	T2	0.45 ± 0.03	1.95 ± 0.20	0.23 ± 0.03	88.46±4.61
	T3	0.64 ± 0.13	1.72 ± 0.14	0.37 ± 0.08	62.38±16.00
Spike		0.38 ± 0.13	1.62 ± 0.19	0.23 ± 0.08	
No Fe(II) addition		0.05 ± 0.12	0		
Arsenite	Standard+As(III), T1	0.10 ± 0.05	0.51 ± 0.17	0.20 ± 0.12	39.78±19.92
	Standard+As(III), T2	0.15 ± 0.07	0.15 ± 0.18	1.02 ± 1.34	24.30±6.79
	Standard+As(III), T3	0.06 ± 0.03	0.22 ± 0.25	0.28 ± 0.34	25.66±14.36
Fe(II) concentrations	1 mM	0.12 ± 0.07	0.74 ± 0.27	0.16 ± 0.11	
	2 mM	0.46 ± 0.16	1.71 ± 0.03	0.27 ± 0.10	
	3 mM	0.41 ± 0.21	1.88 ± 0.90	0.22 ± 0.15	
	4 mM	0.12 ± 0.08	0.45 ± 0.29	0.27 ± 0.25	
	5 mM	0.08 ± 0.04	0.29 ± 0.35	0.29 ± 0.38	
pH range	pH 7.05	0.32 ± 0.03	1.41 ± 0.05	0.23 ± 0.02	82.02±9.65
	pH 6.95	0.28 ± 0.06	1.13 ± 0.14	0.25 ± 0.06	103.16±7.29
	pH 6.8	0.40 ± 0.02	1.66 ± 0.01	0.24 ± 0.01	85.32±17.36
	pH 6.5	0.34 ± 0.04	1.56 ± 0.09	0.22 ± 0.03	80.04±17.55

*considers retrieved iron and initially 90% iron(II) present

Table A5. 16S rRNA gene copy numbers as a measure for microbial growth at the beginning and end of a transfer or experiment. Log2FC displays the log 2-fold change of 16S rRNA gene copy numbers between day 0 and day 7. The results of a non-parametric Wilcoxon signed-rank test for paired samples, with the Benjamini-Hochberg p-adjustment method (FDR: false discovery rate), are summarized. 'T' stands for transfer.

		Start (day 0)	End (day 7)	Log2FC	n	W	FDR (adjusted p-value)	Effect size
		16S rRNA gene copy no. mL^{-1}						
Main experiment	T2	$3.98\times10^{3}\pm1.58\times10^{3}$	$4.31\times10^{5}\pm2.46\times10^{5}$	6.76	4	-1.15	0.12	0.54
	T3	$6.15\times10^{3}\pm2.02\times10^{3}$	$1.23\times10^{6}\pm6.28\times10^{5}$	7.64	4	-1.15	0.12	0.54
spike		$2.20\times10^{6}\pm1.40\times10^{6}$	$1.29\times10^{6}\pm6.09\times10^{5}$	-0.77	4	-1.15	0.12	0.54
no Fe(II) addition		$2.49\times10^{4}\pm1.05\times10^{4}$	$1.52\times10^{6}\pm1.45\times10^{6}$	5.93	3	-1.15	0.25	0.47
Arsenite	Standard+As(III), T1	$6.27\times10^{3}\pm1.41\times10^{3}$	$5.68\times10^{4}\pm1.44\times10^{4}$	3.18	3	-1.15	0.25	0.47
	Standard+As(III), T3	$6.74\times10^{3}\pm8.00\times10^{2}$	$4.03\times10^{4}\pm3.58\times10^{4}$	2.58	3	-1.15	0.25	0.47

Table A6. 16S rRNA gene copy numbers at day 0 (start) and day 7 (end) in different treatments. 1 mM nitrate, 2 mM Fe(II) reflect standard conditions and 1 mM nitrate setups the absence of an electron donor.

Day	16S rRNA gene copy no. mL^{-1}	
	1 mM nitrate, 2 mM Fe(II)	1 mM nitrate
0	1.32E+04 ± 9.48E+03	2.49E+04 ± 1.05E+04
7	1.33E+06 ± 6.95E+05	1.52E+06 ± 1.45E+06

Table A7. Moessbauer spectra hyperfine parameters for the mineral phase produced by the lithoautotrophic NRFeOx culture after 7 days of incubation (transfer 3).

Temperature	Phase	Iron mineral phase	CS	ΔE_Q	ε	B_{hf}	Pop	χ2
K			mm s^{-1}	mm s^{-1}	mm s^{-1}	T	%	
77	Db	Fe(III)	0.48	0.84			100	0.65
5	Sxt1	Fe(III), Fh	0.52		-0.05	42.03	57.1	0.76
	Sxt2	Fe(III), Fh	0.34		0.04	34.59	42.9	

Db: doublet, Sxt: sextet, Iron mineral phase - Fe(III): ferric Fe, Fh: ferrihydrite, CS: center shift, ΔE_Q: quadrupole splitting, ε: quadrupole shift, B_{hf}: hyperfine field, Pop: relative abundance, χ2: goodness of fit.

Table A8. pH values at day 0 (start) and day 7 (end) in different treatments during the pH range experiment.

Treatment	pH value	
	Day 0	Day 7
pH 7.05	7.06 ± 0.01	7.07 ± 0.00
pH 6.95	6.95 ± 0.01	6.97 ± 0.01
pH 6.8	6.82 ± 0.00	6.76 ± 0.01
pH 6.5	6.55 ± 0.04	6.47 ± 0.02
Control pH 7.05	7.09 ± 0.01	7.08 ± 0.01
Control pH 6.5	6.52 ± 0.03	6.49 ± 0.01

15 Table A9. Basic soil properties of paddy soil collected from Huilongpu Town, Hunan province, China.

		Huilongpu, China
Coordinates		28°12′16″ N, 112°26′32″ E
Parent material		River alluvium
Paddy management		rice-rice
Soil texture		
Sand	(%)	16.91 ± 0.08
Silt		60.00 ± 6.00
Clay		19.33 ± 5.51
CEC	(cmol kg^{-1})	14.09 ± 0.06
pH_{MQ}		7.31 ± 0.15
Water content	(%)	44.84 ± 1.33
TOC	(g kg^{-1})	35.47 ± 2.53
TIC		0.54 ± 0.37
TN		3.30 ± 0.31
Water-extractable OC	(g kg^{-1})	0.09 ± 0.02
Water-extractable N		0.02 ± 0.00
Adsorbed Fe*	(g kg^{-1})	0.75 ± 0.12
Poorly crystalline Fe*		1.94 ± 0.20
Crystalline Fe*		11.64 ± 1.22
Total extractable Fe*		14.34 ± 1.24
Adsorbed Fe-As*	(mg kg^{-1})	0.00 ± 0.00
Poorly crystalline Fe-As*		1.15 ± 0.27
Crystalline Fe-As*		3.91 ± 0.33
Total extractable Fe-As*		5.06 ± 0.43
Na°	(g kg^{-1})	2.05
Mg°		2.94
Al°		57.91
Si°		323.93
P°		0.71
S°		0.87
K°		13.83
Ca°		6.27
Ti°		5.60
V°		0.06
Cr°		0.05
Mn°		0.22
Fe°		21.09
Ni°		0.13
Zn°		0.02
Zr°		0.08
Ba°		0.04

Average and standard deviation are represented by triplicate measurements
*Obtained by sequentially extracting paddy soil samples with 1 M Na-acetate (adsorbed), 0.5 M HCl (poorly crystalline) and 6 M HCl (crystalline)
°Obtained by XRF analysis

16

9

Table A10. Results of a) Kruskal-Wallis test and b) Wilcoxon rank-sum test with Benjamini-Hochberg-adjusted p-values (FDR, false discovery rate) to identify differences in N_2O production of different treatments.

a) Kruskal-Wallis test.

Comparison	χ^2	df	p-value
Treatment vs N_2O	18.966	5	0.001951

b) Wilcoxon rank-sum test, Benjamini-Hochberg adjusted p-values (FDR).

	N_2O-N of total reduced NO_3^--N	n	Comparison with	FDR (adjusted p-value)
	%			
Ratio N:Fe, 1:2 (Standard conditions)	88.77 ± 26.57	15	Ratio N:Fe, 0.5:2	1
			Ratio N:Fe, 0.5:2 + As(III)	0.00044
			pH 7.05	1
			pH 6.8	1
			pH 6.5	1
Ratio N:Fe, 0.5:2	76.83 ± 29.14	9	Ratio N:Fe, 0.5:2 + As(III)	0.00123
			pH 7.05	1
			pH 6.8	1
			pH 6.5	1
Ratio N:Fe, 1:0.5 + As(III)	29.48 ± 25.48	9	pH 7.05	0.03409
			pH 6.8	0.03409
			pH 6.5	0.05455
pH 7.05	80.04 ± 17.55	3	pH 6.8	1
pH 6.8	85.32 ± 17.36	3	pH 6.5	1
pH 6.5	82.02 ± 9.65	3	pH 6.5	1

Table A11. Detailed information of qPCR and PCR analysis for 16S rRNA gene copy numbers and amplicon sequencing, respectively.

Target gene	Standard	Primer	Primer sequence (5' -> 3')	Primer concentration	Thermal program	References
				nM		
Bacterial 16S rRNA gene	*Thiomonas* sp.	341F	CCTACGGGAGGCAGCAG	250	95°C - 5'; (95°C - 10"; 60°C - 15") x 40; 95°C - 30"; 65-95°C - 5"	(13, 14)
		797R	GGACTACCAGGGTATCTAATCCTGTT	250		
Bacterial 16S rRNA gene amplicon sequencing	*Thiomonas* sp.	515F	TCGTCGGCAGCGTCAGATGTGTATAAGAGACAGGTGYCAGCMGCCGCGGTA	250	94°C - 3'; (94°C - 30"; 55°C - 30";72°C - 30") x 25; 72°C - 8'; 4°C	(15)
		806R	GTCTCGTGGGCTCGGAGATGTGTATAAGAGACAGGGACTACNVGGGTWTCTAAT	250		

Appendix: Figures

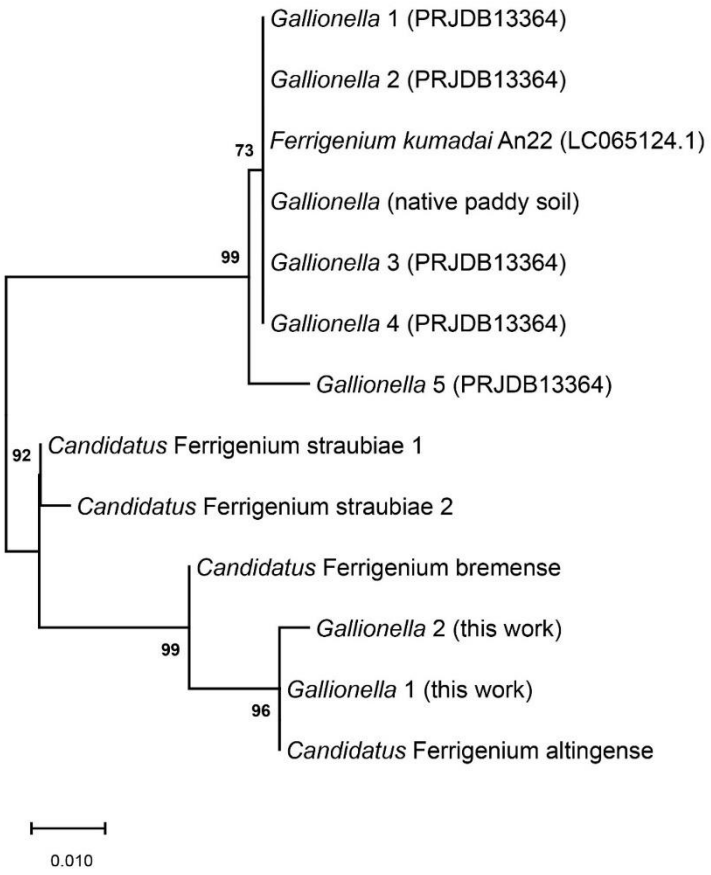

Figure A1. Maximum-likelihood phylogenetic tree of *Gallionella* species in lithoautotrophic nitrate-reducing, iron(II)-oxidizing enrichment cultures and paddy soils. In the enrichment culture obtained in this study, two *Gallionella* species were enriched; Gallionella 1 (71.39±0.3% relative abundance) and Gallionella 2 (2.69±0.01% relative abundance). The tree was constructed using the maximum-likelihood method based on 16S rRNA gene sequences with a total of 251 positions in the final dataset. The percentage of trees in which the associated taxa clustered together is shown next to the branches. The scale bar represents the number of substitutions per site.

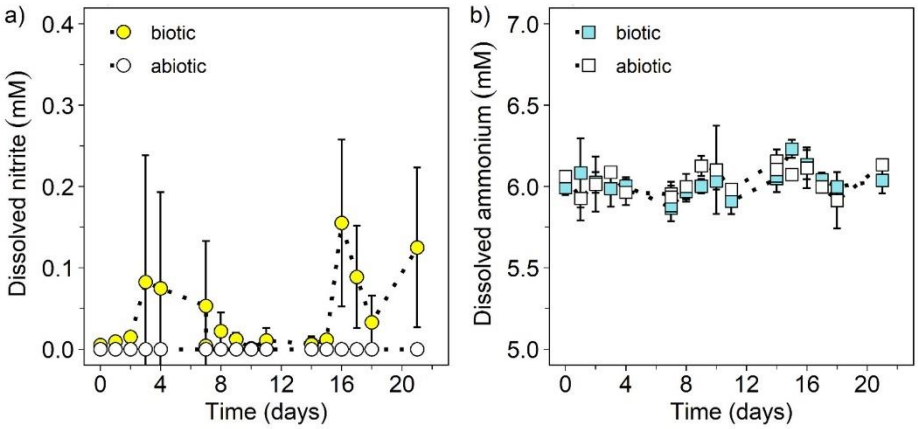

Figure A2. Nitrite (a) and ammonium (b) concentrations over three consecutive transfers each lasting 7 days (Transfer 1: 0-7 days, Transfer 2: 7-14 days and Transfer 3: 14-21 days. Nitrite (a) is displayed as yellow circles and ammonium (b) as blue squares, abiotic treatments in white. Note that the y-axis in b) ranges from 5 to 7 mM. Mean ± standard deviation is shown of four replicates.

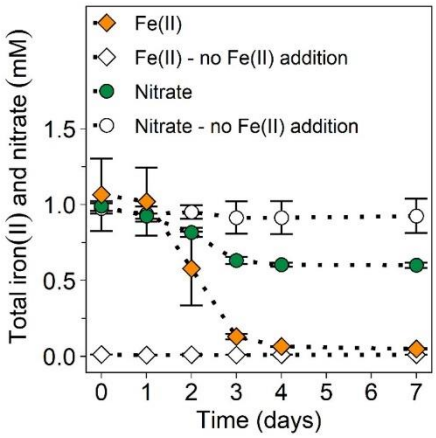

Figure A3. Total iron(II) (diamonds) and nitrate (circles) concentrations over 7 days in biotic treatments. Treatments with supplemented Fe(II) are represented as colored symbols (ratio N:Fe=1:2, pH 7), treatments without Fe(II) addition in white (ratio N:Fe=1:0, pH 7). Mean ± standard deviation is shown of three replicates.

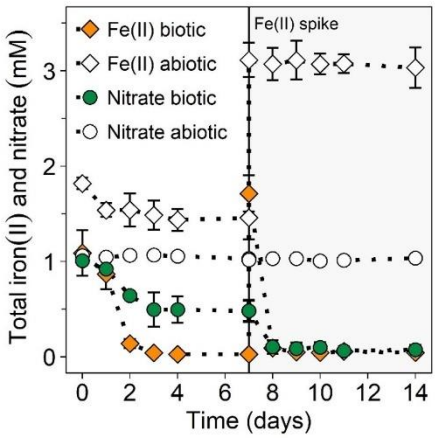

Figure A4. Total iron(II) (diamond) and nitrate (circle) concentrations over 14 days. 2 mM of Fe(II) was spiked after 7 days, visually separated by lines and color. Biotic treatments are represented as colored symbols, abiotic treatments in white. Mean ± standard deviation is shown of four replicates.

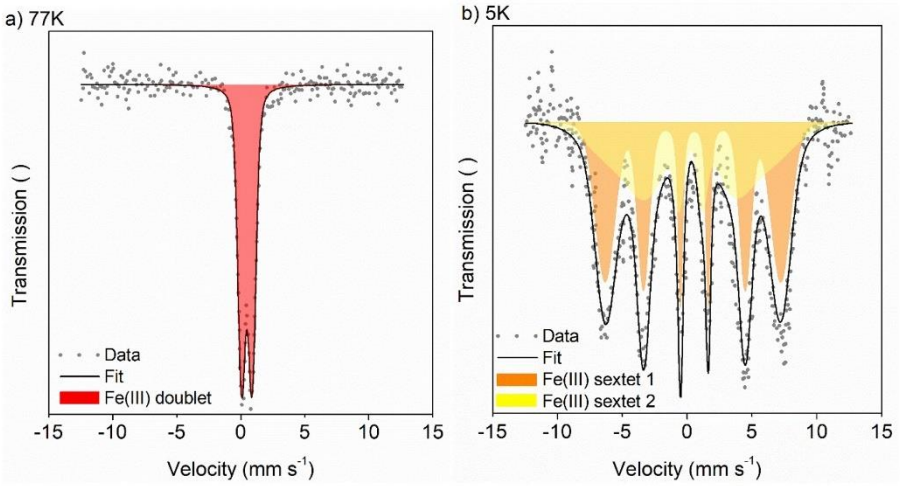

Figure A5. Moessbauer spectra collected at 77 K (a) and 5 K (b) of the mineral phase formed by the lithoautotrophic NRFeOx enrichment culture after 7 days of incubation. The spectra illustrates the data (grey dots), the fitted data (black solid line) and the different mineral phases (iron(III) doublet: red, iron(III) sextet 1: orange, iron(III) sextet 2: yellow). Grey dots represent data points, black solid lines the fitted data, and the colored areas the fitted mineral phases. Hyperfine parameters can be taken from Table A7.

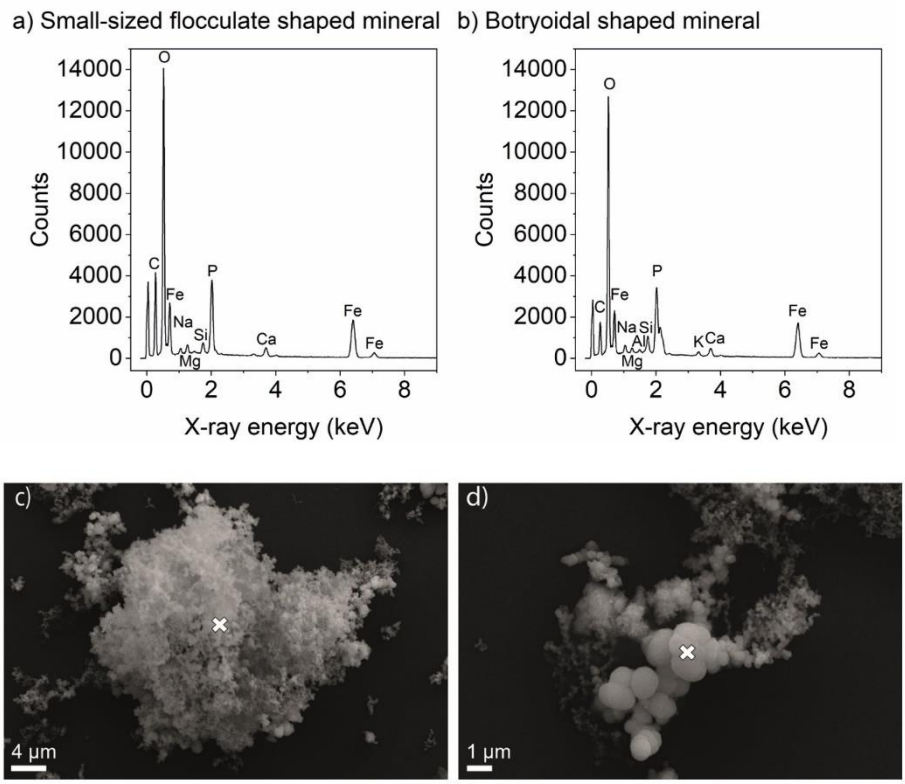

Figure A6. EDS spectra collected from a small-sized flocculate shaped mineral (a) and a botryoidal shaped mineral (b) from the lithoautotrophic NRFeOx culture after 7 days (Transfer 3). Corresponding SEM pictures of collected EDS spectra of a small-sized flocculate shaped mineral (c) and a botryoidal shaped mineral (d). The cross indicates the point of measurement.

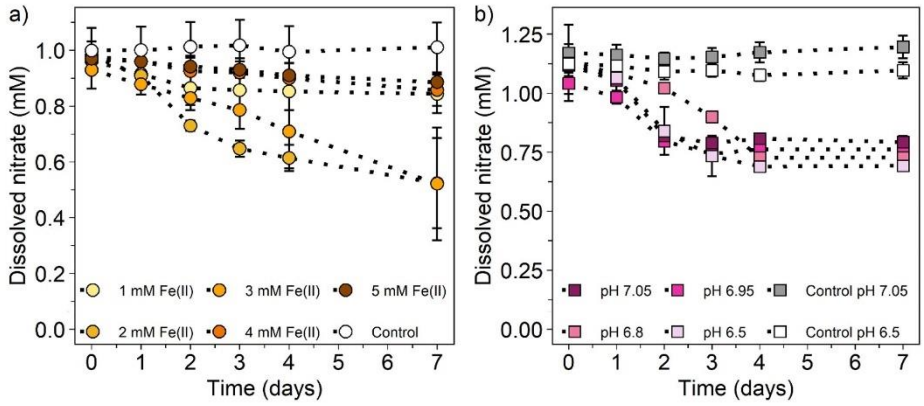

Figure A7. Nitrate concentrations (a) for cultures set up with different Fe(II) concentrations and (b) for cultures set up at different pH values over 7 days. Treatments in a) are showing different iron concentrations as circles with darker colors representing higher iron concentrations. The control (white) represents abiotic conditions using 5 mM iron(II) and 1 mM nitrate. Treatments in b) are displaying different pH values as squares with darker colors representing higher pH values. The controls represent abiotic conditions at pH 6.50 (white) and pH 7.05 (grey) using 2 mM iron(II) and 1 mM nitrate. Mean ± standard deviation is shown of three replicates.

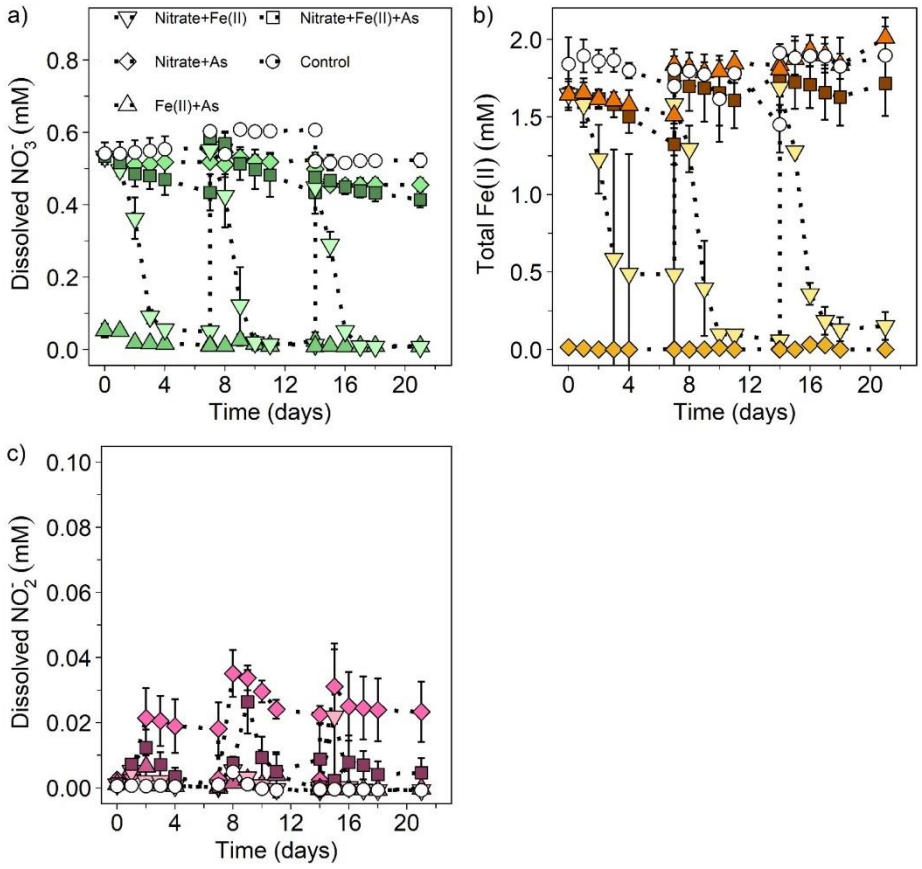

Figure A8. Dissolved nitrate (a), total Fe(II) (b) and dissolved nitrite (c) concentrations over three consecutive transfers (each 7 days) for four different biotic setups (upside down triangle: 0.5 mM nitrate, 2 mM Fe(II); diamond: 0.5 mM nitrate, 100 µM arsenite); triangle: 2 mM Fe(II), 100 µM arsenite; square: 0.5 mM nitrate, 2 mM Fe(II), 100 µM arsenite) and one abiotic control (circle). Mean ± standard deviation is shown of three replicates.

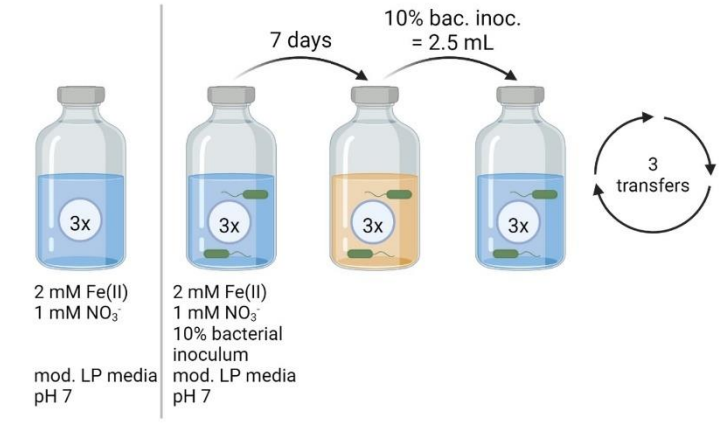

Figure A9. Experimental setup for growing the NRFeOx culture under autotrophic conditions over three consecutive transfers. Grey line separates and provides information of the media composition of abiotic (left) and biotic (right) setups.

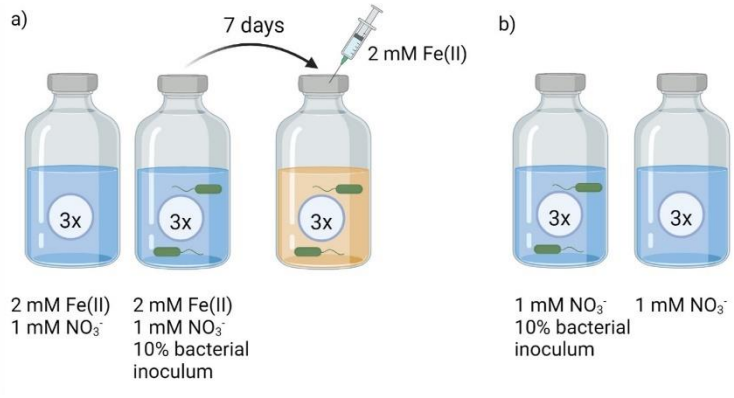

Figure A10. Experimental setup for examining the use of residual OC stemming from the MQ water (a) and of internally stored OC (b) by the NRFeOx culture.

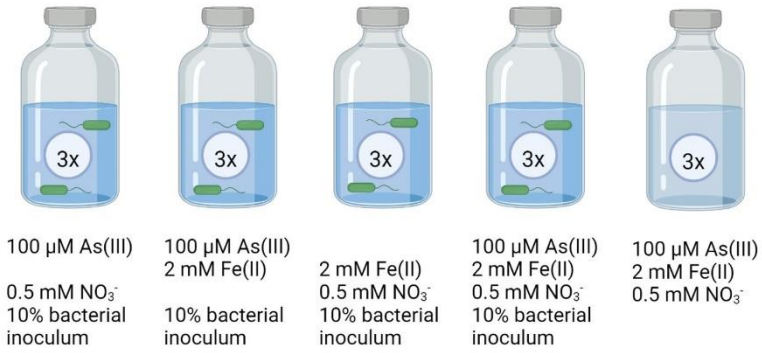

79

80 Figure A11. Experimental setup for testing arsenite toxicity and the potential of arsenite as electron donor

81 for the lithoautotrophic NRFeOx culture.

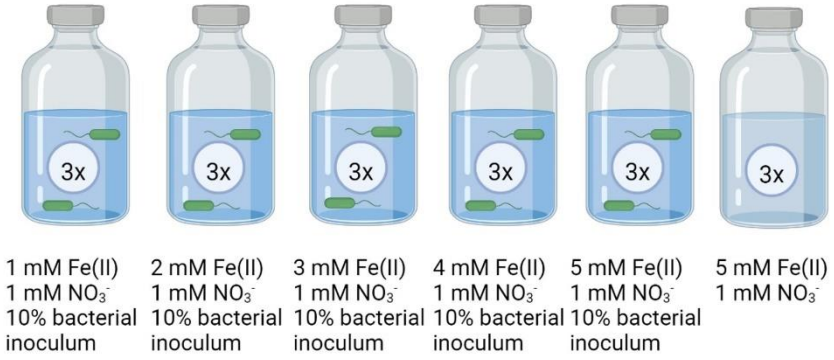

82

83 Figure A12. Experimental setup for using different concentrations of Fe(II) by the lithoautotrophic NRFeOx

84 culture.

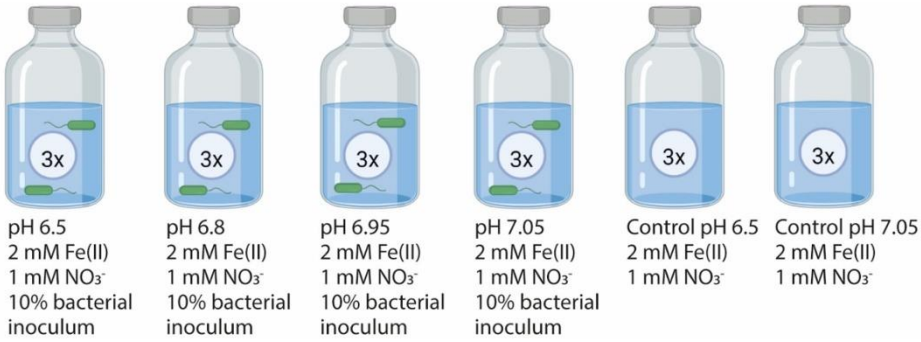

Figure A13. Experimental setup for testing different pH values for cultivation of the lithoautotrophic NRFeOx culture.

References

1. DIN 18123. 2011. Soil, investigation and testing - Determination of grain-size distribution.

2. DIN 18124. 2011. Soil, investigation and testing - Determination of density of solid particles - Capillary pyknometer, wide mouth pycnometer, gas pycnometer.

3. ISO 10390. 2021. Soil, treated biowaste and sludge - Determination of pH.

4. Muehe EM, Wang T, Kerl CF, Planer-Friedrich B, Fendorf S. 2019. Rice production threatened by coupled stresses of climate and soil arsenic. Nature communications 10:4985.

5. Roden EE, Zachara JM. 1996. Microbial Reduction of Crystalline Iron(III) Oxides: Influence of Oxide Surface Area and Potential for Cell Growth. Environ Sci Technol 30:1618–1628.

6. Shannon RD, White JR. 1991. The selectivity of a sequential extraction procedure for the determination of iron oxyhydroxides andiron sulfides in lake sediments. Biogeochemistry 14:193–208.

7. Tessier A, Campbell PGC, Bisson M. 1979. Sequential extraction procedure for the speciation of particulate trace metals. Anal Chem 51:844–851.

8. Heron G, Crouzet C, Bourg AC, Christensen TH. 1994. Speciation of Fe(II) and Fe(III) in Contaminated Aquifer Sediments Using Chemical Extraction Techniques. Environ Sci Technol 28:1698–1705.

9. Lueder U, Maisch M, Laufer K, Jorgensen BB, Kappler A, Schmidt C. 2020. Influence of Physical Perturbation on Fe(II) Supply in Coastal Marine Sediments. Environ Sci Technol 54:3209–3218.

10. Widdel F, Kohring G-W, Mayer F. 1983. Studies on dissimilatory sulfate-reducing bacteria that decompose fatty acids: III. Characterization of the filamentous gliding Desulfonema limicola gen. nov. sp. nov., and Desulfonema magnum sp. nov. Arch Microbiol 134:286–294.

11. Widdel F, Pfennig N. 1981. Studies on dissimilatory sulfate-reducing bacteria that decompose fatty acids. I. Isolation of new sulfate-reducing bacteria enriched with acetate from saline environments. Description of Desulfobacter postgatei gen. nov., sp. nov. Arch Microbiol 129:395–400.

12. Jakus N, Blackwell N, Osenbrück K, Straub D, Byrne JM, Wang Z, Glöckler D, Elsner M, Lueders T, Grathwohl P, Kleindienst S, Kappler A. 2021. Nitrate Removal by a Novel Lithoautotrophic Nitrate-Reducing, Iron(II)-Oxidizing Culture Enriched from a Pyrite-Rich Limestone Aquifer. Applied and environmental microbiology 87:e0046021.

13. Muyzer G, De Waal EC, Uitterlinden AG. 1993. Profiling of complex microbial populations by denaturing gradient gel electrophoresis analysis of polymerase chain reaction-amplified genes coding for 16S rRNA. Appl Environ Microbiol 59:695–700.

14. Nadkarni MA, Martin FE, Jacques NA, Hunter N. 2002. Determination of bacterial load by real-time PCR using a broad-range (universal) probe and primers set. Microbiology 148:257–266.

15. Caporaso JG, Lauber CL, Walters WA, Berg-Lyons D, Lozupone CA, Turnbaugh PJ, Fierer N, Knight R. 2011. Global patterns of 16S rRNA diversity at a depth of millions of sequences per sample. PNAS 108 Suppl 1:4516–4522.

Grimm et al. (in prep.). Acetate addition shifts community composition and extent of chemodenitrification in a lithoautotrophic nitrate-reducing microbial culture

Acetate addition shifts community composition and extent of chemodenitrification in a lithoautotrophic nitrate-reducing microbial culture

Hanna Grimm[1], Paula Gscheidel[1], Matthias Boeckmann[1], Daniel Straub[2], Stefan Fischer[3], Andreas Kappler[1,4], Christiane Zarfl [1,#]

[1]Department of Geosciences, University of Tübingen, Tübingen, Germany

[2]Quantitative Biology Center (QBiC), University of Tübingen, Germany

[3]Tübingen Structural Microscopy Core Facility, University of Tübingen, Tübingen, Germany

[4]Cluster of Excellence: EXC 2124: Controlling Microbes to Fight Infection, Tübingen, Germany

#Address correspondence to Christiane Zarfl, christiane.zarfl@uni-tuebingen.de

Abstract

Lithoautotrophic nitrate-reducing, iron(II)-oxidizing (NRFeOx) cultures have been shown to react sensitively to organ carbon additions by changing their microbial community composition towards mixotrophic or heterotrophic denitrifiers, thereby changing intermediates and products during denitrification. It remains unknown how organic carbon affects nitrous oxide emissions and chemodenitrification of lithoautotrophic NRFeOx cultures in general and the microbial community composition of the lithoautotrophic culture HP. Therefore, we cultivated it under autotrophic (iron, nitrate), mixotrophic (iron, nitrate, acetate) and heterotrophic (nitrate, acetate) conditions over three consecutive transfers (each 7 days). 16S rRNA gene amplicon sequencing revealed that *Gallionella* sp. and *Dechloromonas* sp. were most abundant irrespective of their growth conditions. However, acetate addition influences the flanking community boosting *Acidovorax* sp., *Zoogloea* sp., and *Parvibaculum* sp., highlighting their role in mixotrophic or heterotrophic nitrate reduction in culture HP. The extent of nitrate was highest under mixotrophic and heterotrophic conditions, however most Fe(II) was oxidized under autotrophic conditions. Nitrous oxide emissions were lower under mixotrophic conditions compared to autotrophic conditions (69% and 100%, respectively). Under heterotrophic conditions, nitrate was reduced until nitrite only. By a process-based reaction model, we quantified that biotic processes accounted for 99.75% and 98.56% of the total oxidized Fe(II) and 99.51% and 98.55% of the total produced N_2O under autotrophic and mixotrophic conditions, respectively. Our results demonstrate that organic carbon significantly influences microbial population dynamics and N_2O emissions, while having minimal impact on enzymatic processes and chemodenitrification in the lithoautotrophic NRFeOx culture HP.

Graphical abstract

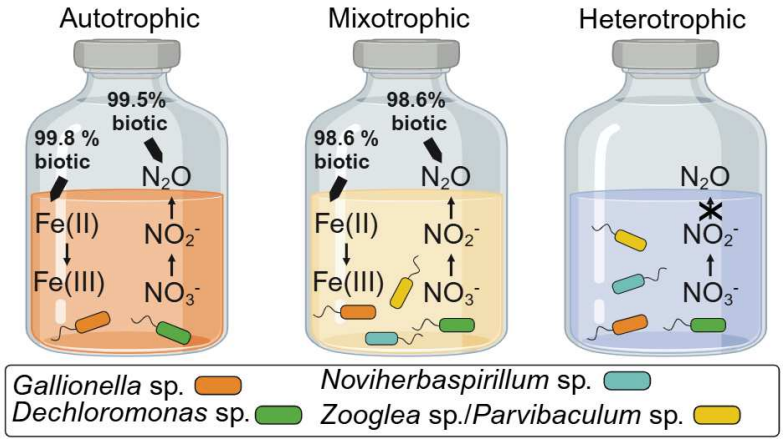

Introduction

Biogeochemical cycling of iron (Fe) is important for many environmental processes, such as organic carbon (OC) preservation, greenhouse gas emissions and the mobility of toxic metalloids in soils and groundwater, such as arsenic.[1,2] Microorganisms that harvest energy from iron redox transformations can couple various elemental cycles, i.e., Fe and nitrogen (N). Nitrate-reducing, iron(II)-oxidizing microorganisms can effectively be used for bioremediation[3–5] and removal of nitrate from e.g., groundwater.[6,7] Microorganisms that perform nitrate reduction coupled to iron(II) oxidation (NRFeOx) can be classified as autotrophs, mixotrophs, or chemodenitrifiers.[8] Autotrophic nitrate-reducing, iron(II)-oxidizing microorganisms do not require any organic carbon, but fix CO_2 for biomass build-up. Mixotrophic nitrate-reducing, iron(II)-oxidizing microorganisms reduce nitrate and oxidize Fe(II), however, they require an organic carbon co-substrate. Chemodenitrifiers are metabolically capable to reduce nitrate by the oxidation of organic carbon and indirectly oxidize Fe(II) by reactive N-intermediates such as nitrite (NO_2^-), a process called chemodenitrification and occurring under heterotrophic conditions. Chemodenitrifiers and mixotrophic strains have been isolated from various environments[9–13], but autotrophic

NRFeOx has only been unequivocally shown for *Gallionellaceae* in microbial enrichment cultures that originate from freshwater sediments (culture KS, BP)[14,15], an aquifer (culture AG)[6] and a paddy soil (culture HP).[16] Even though the environmental origin of these cultures is diverse, they are performing only partial denitrification, with nitrous oxide (N_2O) as the main product. Because N_2O is a very potent greenhouse gas,[17,18] it is important to understand which factors influence its production (e.g., organic carbon availability). Previously, it was believed that N_2O could serve as an indicator to differentiate between abiotic and biotic Fe(II) oxidation.[19] However, recent findings indicate that N_2O is the primary product during Fe(II)-driven denitrification in enrichment cultures KS,[20] AG,[6] and HP.[16] It remains challenging to disentangle abiotic and biotic processes for NRFeOx. Isotopic analysis of N_2O along with the identification of formed Fe(III) minerals have been conducted to distinguish abiotic and biotically-derived N_2O.[21,22] Further, kinetic modelling was applied to disentangle abiotic and biotic Fe(II) oxidation in mixotrophic NRFeOx strains[23–26], and was combined with dual N-O isotope analysis to also conclude on abiotic/biotic contributions of N_2O by *Acidovorax* sp. strain BoFeN1.[27] Until now, abiotic Fe(II) oxidation was generally omitted in studies about lithoautotrophic NRFeOx cultures[14,15,20,28,29], however, it remains open if the absence of nitrite is sufficiently supporting this assumption. This underlines the need for further investigation into the role of abiotic processes in autotrophic NRFeOx cultures, where interactions between chemical species are important[28,30] and peaks of nitrite have been observed (up to 0.23 mM in culture KS[31], <0.1 mM in culture AG[32], up to 0.16 mM in culture HP.[16]

Previous studies have shown that the microbial community composition reacts sensitively to changes in cultivation conditions. Tominski et al. (2018)[29] and Huang et al. (2021)[15]

supplemented acetate to culture KS and BP, respectively, and observed that the microbial community shifted from *Gallionellaceae* to *Bradyrhizobium* (culture KS) or *Rhodoferax (*culture BP)[15] being most abundant in the cultures. However, it remains unknown how the microbial community of culture HP reacts to organic carbon input and generally, if nitrous oxide production is affected by the addition of organic carbon. By modifying the cultivation conditions, the role of individual community members of the flanking community in autotrophic NRFeOx cultures can be identified and compared to environmental conditions.

In this study, we cultivated the novel enrichment culture HP under autotrophic, mixotrophic and heterotrophic conditions to i) identify and quantify shifts in the microbial community composition in the presence of Fe(II) and/or nitrate and/or acetate (representative for organic carbon) , ii) determine differences in extent and rates of nitrate reduction and Fe(II) oxidation, iii) quantify main products during denitrification, i.e., nitrite and nitrous oxide, and iv) estimate the contribution of abiotic and biotic processes to iron(II) oxidation and nitrous oxide production by analyzing the experimental data with a kinetic model under different cultivation conditions. Ultimately, the results will help us to understand how organic carbon affects the adaptability of autotrophic NRFeOx cultures and NRFeOx-mediated iron and nitrogen cycling, which can be translated to ecosystems like paddy soils where organic matter is prevalent.

Materials & Methods

Field site and sampling

Paddy soil samples were collected in September 2020 from a rice paddy field in Huilongpu, Hunan province, China (28°12′16″ N, 112°26′32″ E). Soil was sampled from the upper 20 cm and stored at 4°C in the dark until further processing. Details of further characterization and soil properties can be found in Grimm et al. (2024).[16]

Microbial enrichment

Microbial enrichment for autotrophic nitrate-reducing, iron(II)-oxidizing microorganisms have been described in detail in Grimm et al. (2024).[16] Briefly, 1 g of fresh paddy soil was mixed under sterile conditions with 9 mL of anoxic modified low phosphate medium, containing 1 mM NO_3^- and 2 mM Fe(II) and a 10^{-5} dilution series was prepared.[33] The most positive dilution was always transferred as soon as color change appeared. After 10 transfers, the culture was transferred into 25 mL serum bottles for further cultivation.

Experimental setup and sampling

Growth media were prepared by filling 25 mL of modified low phosphate medium (composition see Grimm et al. (2024)[16]) in 50 mL serum bottles using the Widdle flask. Serum bottles were supplemented with 1 mM nitrate, 2 mM Fe(II) (autotrophic), 1 mM nitrate, 2 mM Fe(II), 0.2 mM acetate (mixotrophic) and 1 mM nitrate, 0.2 mM acetate (heterotrophic) to set up different growth conditions. The supplements were always added minimum one day in advance, due to precipitation of Fe(II) phosphate minerals (i.e. vivianite) at the glass wall.[16,34] To start the first transfer, 10% (vol:vol) of a pre-culture that was grown autotrophically was inoculated to the serum bottles in triplicates and incubated

for 7 days. For the second and third transfer, 10% (vol:vol) inoculum of the previous transfer was transferred to fresh growth media.

Geochemical analyses

To determine iron speciation in the sample, 100 µL of sample was fixed in 400 µL of 1 M HCl/40 mM sulfamic acid and determined using a modified ferrozine assay for nitrite containing samples [35,36]. Briefly, 20 µL of sample are mixed with 80 µL of 1 M HCl or with 80 µL of hydroxylamine hydrochloride followed by incubation for 30 min to quantify iron(II) and iron(tot), respectively. Afterwards, 100 µL of ferrozine solution are added, well mixed and incubated for 5 min prior to spectrophotometric detection at 562 nm (Thermo Scientific™ Multiskan™ Go Microplate Spectrophotometer). Ferrozine measurements were conducted in technical triplicates.

To determine nitrogen species, 200 µL of sample were diluted in 800 µL of MQ water for nitrate and nitrite and 50 µL of sample were diluted in 950 µL of MQ water for ammonium prior to analysis by segmented flow analysis (AutoAnalyzer3, SEAL Analytical, Germany).

High Performance Liquid Chromatography (HPLC, LC-20 AT liquid chromatograph, Shimadzu, Japan) was used to analyze acetate in mixotrophic, heterotrophic and abiotic control treatments with standards ranging from 0.1 to 1 mM. Prior to analysis, 200 µL supernatant of the centrifuged slurry sample were pipetted into HPLC vials with small glass inlets. For analysis, the sample was injected into a mobile phase stream (5 mM H2SO4) and passed a stationary phase (Aminex HPX-87HION exclusion column from BioRad). Temperature was maintained at 40°C using a CTO-10 AS VP column oven. Acetate was identified at a specific retention time by a photo array detector (RID-20A

refractive index detector, Shimadzu, Japan) due to changes in light absorption and appeared as a peak on the chromatogram.

Gas measurements

Gas measurement and calculation of produced N_2O was performed as described in Grimm et al. (2024).[16] Briefly, 0.6 mL of headspace was withdrawn before liquid sampling and injected into helium-flushed headspace vials (total volume 12 mL). N_2O was measured on the front pulsed discharge detector of a custom-built gas chromatograph (TRACE 1310, Thermo Fisher Scientific, USA). Calibration of N_2O was performed between 0.05 and 380 ppm and dissolved N_2O was accounted for using the Henry´s constant.

Microbial community analysis

For DNA extraction, 2 mL of sample were taken from the NRFeOx culture and centrifuged (20,238 g, 5 min). The supernatant was discarded and the pellet was immediately frozen and stored at -20°C. The Power Soil® DNA Kit (Qiagen, Germany) was used for DNA extraction, DNA was eluted in 50 µl DNase-free water and stored at -20°C until analysis. Quantitative polymerase chain reaction (qPCR) was used to determine bacterial 16S rRNA genes using primers 515F and 806R.[37] Samples were analyzed in technical triplicates on a C1000 Touch thermal cycler (CFX96TM real time system) using SybrGreen® Supermix (50% per reaction, Bio-Rad Laboratories GmbH, Munich, Germany). A 7-fold standard dilution series (plasmid vectors containing a cloned 16S rRNA gene fragment from *Thiomonas* sp., pCR2.1®, Invitrogen, Darmstadt, Germany) was included on each qPCR assay in addition to one negative control (DNase-free water). Standard concentrations were quantified using Qubit (Life Technologies, Carlsbad, CA,

USA). Finally, data analysis was performed using the Bio-Rad CFX Maestro 1.1, software, version 4.1 (Bio-Rad, 2017). For 16S rRNA gene amplicon sequencing, the 16S rRNA gene was amplified by polymerase chain reaction using the iProof HF Master Mix (50% per reaction, Bio-Rad Laboratories GmbH, Munich, Germany), dimethylsulfoxide (DMSO, 2% per reaction, Carl Roth) and primers 515F and 806R (0.2 µM per reaction)[37], targeting the V4 region. Due to low DNA concentrations, the PCR products were purified using the Wizard® SV gel and PCR clean-up system (Promega, USA), with a modified final volume of 30 µL instead of 50 µL. Detailed information on the primers, primer sequences and thermal program used for qPCR and PCR is provided in Table A1.

Library preparation steps (Nextera, Illumina) and 250 bp paired-end sequencing with MiSeq (Illumina, San Diego, CA, USA) using v2 chemistry were performed by the Institute for Medical Microbiology and Hygiene (MGM) of the University of Tübingen. 9,910,078 read pairs were obtained for 54 samples (47,518 to 530,641 read pairs per sample) in two sequencing runs. Data processing, including quality control, reconstruction of sequences and taxonomic annotation was done using nf-core/ampliseq v2.11.0 of the nf-core collection of workflows[38,39]. nf-core/ampliseq was executed with Nextflow v24.04.4[40] and singularity v3.8.7[41]. Primers were trimmed, and untrimmed sequences were discarded (6-92% per sample, average 23%) with Cutadapt version 4.6[42]. Adapter and primer-free sequences were processed pooled with DADA2 v1.30.0[43] to eliminate PhiX contamination, trim reads (before median quality drops below 35; forward reads were trimmed at 95 bp and reverse reads at 200 bp), discard reads with >2 expected errors, correct errors, merge read pairs, and remove polymerase chain reaction (PCR) chimeras. Ultimately, 1,006 amplicon sequencing variants (ASVs) were obtained across all samples.

Taxonomic classification was performed with DADA2 and the SILVA v138.1 database[44]. Using QIIME2 version 2023.7.0,[45] 488 ASVs with 5,699 to 331,813 counts (total 6,773,280 counts) that were not classified as mitochondria or chloroplasts (deemed off-targets), occurred in at least two samples (less likely spurious sequences), and were between 240 and 270 bp in length (>95% of ASVs were expected to be between 250 and 256bp long)[39] were selected as final result.

Cell-mineral interactions

Samples for scanning electron microscopy (SEM) were fixed in 2.5% glutaraldehyde over night at 4°C by adding 100 µL of a 25% glutaraldehyde solution to 900 µL of centrifuged cell suspension in growth medium. After fixation, the samples were centrifuged (1 min, 20,238 g) to concentrate the cells, and 900 µL of supernatant were removed, and replaced with MQ water to wash out the glutaraldehyde. This washing step was repeated twice. Afterwards, 50 µL of sample were placed onto a poly-L-lysine coated cover glass slide (coated with 0.01% poly-L-lysine solution (PLANO, Wetzlar, item 18026)) in a 12-well plate, and left for 30 minutes to settle. In the following, the samples were dehydrated using a graded ethanol series (25%, 50%, 75%, 95% for 15 min each, followed by 100% ethanol twice for 30 min). The samples were then immersed in hexamethyldisilazane (HMDS). First, they were incubated in a 1:1 ratio of 100% ethanol and HMDS (30 min), followed by a second step in 100% HMDS (30 min). Finally, the HMDS was replaced by 250 µL of fresh HMDS and the lid of the well-plate was placed slightly ajar, allowing the HMDS to evaporate slowly over night. The dry cover glass slides were mounted on aluminum stubs using carbon tape (PLANO, Wetzlar, items G301 & G3347) and coated with 8 nm platinum using a BAL-TEC SCD 005 sputter coater. SEM imaging was performed at a Crossbeam

550L FIB-SEM (Zeiss, Oberkochen, Germany), operating with an acceleration voltage of 2.0 kV, using the SESI detector and a working distance of 5 mm.

Development of the chemical reaction model

Based on the geochemical and molecular biology results, a process-based numerical model was developed to derive rates of nitrate reduction, Fe(II) oxidation, and to determine the contribution of abiotic and biotic Fe(II) oxidation and N_2O production under autotrophic and mixotrophic growth conditions of the autotrophic NRFeOx culture HP from the available experimental data. For this, autotrophic denitrification was considered as a two-step process separated into the reduction of nitrate to nitrite (Eq. 1) and nitrite to nitrous oxide (Eq. 2).

$$2\,NO_3^- + 8\,Fe^{2+} + 19\,H_2O \rightarrow N_2O + 8\,Fe(OH)_3 + 14\,H^+ \quad \text{Eq. 1}$$

$$NO_2^- + 2\,Fe^{2+} + 4.5\,H_2O \rightarrow 0.5\,N_2O + 2Fe(OH)_3 + 3\,H^+ \quad \text{Eq. 2}$$

Based on previous results by Grimm et al. (2024)[16], ferrihydrite was assumed as the formed Fe(III) mineral during Fe(II) oxidation and N_2O instead of dinitrogen gas (N_2) was considered to be the product during denitrification. Because Fe(II) can also abiotically react with nitrite, chemodenitrification (equivalent to Eq. 2) was also considered in the biogeochemical model. Under mixotrophic conditions, in addition to autotrophic processes, nitrate reduction to nitrite coupled to the oxidation of acetate was also considered (Eq. 3). This assumption is based on observations under heterotrophic growth conditions, where nitrite was the main product during denitrification.

$$4\,NO_3^- + CH_3COO^- + H^+ \rightarrow 4\,NO_2^- + CO_2 + HCO_3^- + H_2O \quad \text{Eq. 3}$$

Based on these chemical reactions, two model alternatives were developed (Figure 1). The first model structure represents processes under autotrophic conditions, where biological reduction of nitrate to nitrite and nitrite to nitrous oxide, together with chemodenitrification is considered (Eq. 1 & 2). The second model structure was developed for mixotrophic conditions, where nitrate is reduced solely by acetate (Eq. 3), in addition to enzymatic and abiotic nitrite reduction (Eq. 2).

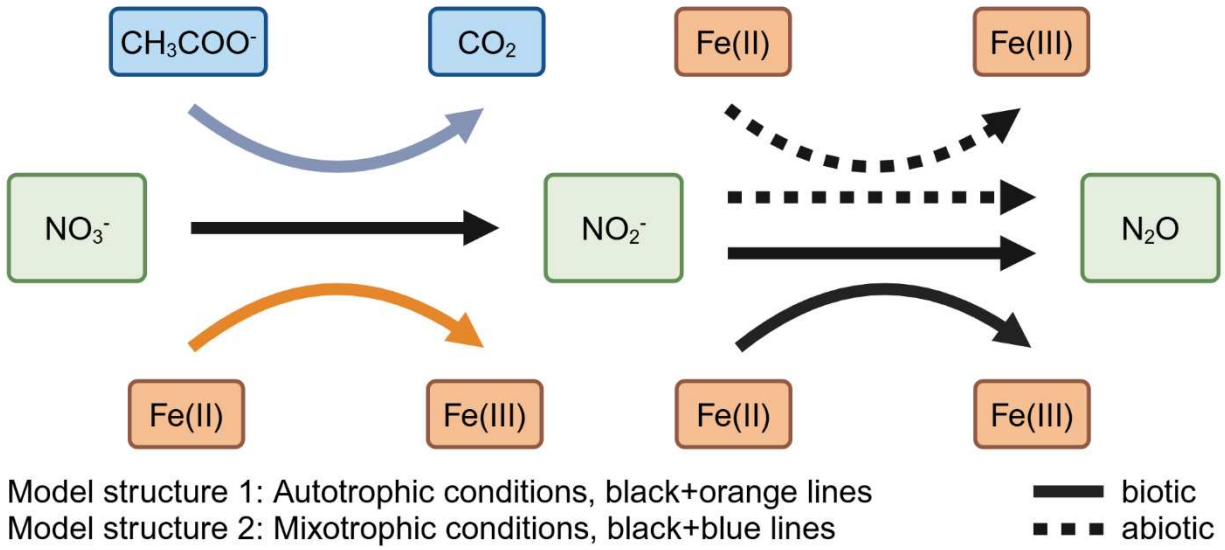

Figure 12. Conceptual figure showing nitrate reduction as a simplified two-step process (nitrate to nitrite and nitrite to nitrous oxide). Model alternative 1 (black+orange lines) considers biotic and abiotic processes relevant for nitrate-dependent iron(II) oxidation. Model alternative 2 (black+blue lines) represents processes considered for mixotrophic conditions. Solid lines regardless of color resemble biotic processes, dashed lines resemble abiotic processes (i.e., chemodenitrification). Detailed systems of the two underlying ordinary differential equations are given in the SI.

Dual-substrate Monod kinetics was considered for Eq. 1, 2, and 3, resulting in the following rate equations for biotic reactions.

$$r_{auto\_bio\_1} = \frac{r_{auto\_bio\_1}^{max}}{Y}\left(\frac{C_{Fe(II)}}{K_{Fe(II)} + C_{Fe(II)}}\right) \cdot \left(\frac{C_{NO_3^-}}{K_{NO_3^-} + C_{NO_3^-}}\right) \quad \text{Eq. 4}$$

$$r_{hetero\_bio\_1} = \frac{r_{hetero\_bio\_1}^{max}}{Y}\left(\frac{C_{acetate}}{K_{acetate} + C_{acetate}}\right) \cdot \left(\frac{C_{NO_3^-}}{K_{NO_3^-} + C_{NO_3^-}}\right) \quad \text{Eq. 5}$$

$$r_{auto\_bio\_2} = \frac{r_{auto\_bio\_2}^{max}}{Y}\left(\frac{C_{Fe(II)}}{K_{Fe(II)} + C_{Fe(II)}}\right) \cdot \left(\frac{C_{NO_2^-}}{K_{NO_2^-} + C_{NO_2^-}}\right) \quad \text{Eq. 6}$$

where $r_{auto\_bio\_1}^{max}$, $r_{auto\_bio\_2}^{max}$ and $r_{hetero\_bio\_1}^{max}$ (s^{-1}) are the maximum specific rate constants for each step of enzymatic denitrification, Y a biomass yield coefficient (cells mol^{-1} $Fe(II)^{-1}$), C_{FeII}, $C_{NO_3^-}$ and $C_{NO_2^-}$ (mol L^{-1}) represent the substrate concentrations and K_{FeII}, $K_{NO_3^-}$ and $K_{NO_2^-}$ (mol L^{-1}) the Monod half-saturation constants of dissolved Fe(II), NO_3^- and NO_2^-.

Chemodenitrification was described as a second-order rate law, based on Jamieson et al. (2019)[24] (eq. 7).

$$r_{abio} = k_{abio} \cdot C_{Fe(II)} \cdot C_{NO_2^-} \quad \text{Eq. 7}$$

with k_{abio} (mol L^{-1} s^{-1}) as the rate constant, $C_{Fe(II)}$ and $C_{NO_2^-}$ (mol L^{-1}) as substrate concentrations.

Based on the reaction rate expressions, the biogeochemical model was formalized into two systems of governing ordinary differential equations that represent autotrophic (Eq. 8 to 13) vs. mixotrophic (Eq. 14 to 20) growth conditions. Even though biomass was only quantified at the beginning and end of each transfer, biomass was considered explicitly in the model equations (Eq. 8 to 20).

$$\frac{\mathrm{dB}}{\mathrm{dt}} = w_1^{max} \frac{C_{NO_3^-}}{K_{NO_3^-} + C_{NO_3^-}} \cdot \frac{C_{Fe(II)}}{K_{Fe(II)} + C_{Fe(II)}} + w_2^{max} \frac{C_{NO_2^-}}{K_{NO_2^-} + C_{NO_2^-}} \cdot \frac{C_{Fe(II)}}{K_{Fe(II)} + C_{Fe(II)}} \quad \text{Eq. 8}$$

$$\frac{\mathrm{dFe(II)}}{\mathrm{dt}} = -2\ B\ r_{auto\_bio\_1} - 2\ B\ r_{auto\_bio\_2} - 2\ r_{abio} \quad \text{Eq. 9}$$

$$\frac{\mathrm{dFe(III)}}{\mathrm{dt}} = 2\ B\ r_{auto\_bio\_1} + 2\ B\ r_{auto\_bio\_2} + 2\ r_{abio} \quad \text{Eq. 10}$$

$$\frac{\mathrm{d}NO_3^-}{\mathrm{dt}} = -B\ r_{auto\_bio\_1} \quad \text{Eq. 11}$$

$$\frac{\mathrm{d}NO_2^-}{\mathrm{dt}} = \mathrm{B}\ r_{auto\_bio\_1} - B\ r_{auto\_bio\_2} - r_{abio} \quad \text{Eq. 12}$$

$$\frac{\mathrm{d}N_2O}{\mathrm{dt}} = 0.5\ \mathrm{B}\ r_{auto\_bio\_2} + 0.5\ r_{abio} \quad \text{Eq. 13}$$

$$\frac{\mathrm{dB}}{\mathrm{dt}} = \left(w_2^{max} \frac{C_{NO_2^-}}{K_{NO_2^-} + C_{NO_2^-}} \cdot \frac{C_{Fe(II)}}{K_{Fe(II)} + C_{Fe(II)}} \right) + \left(w_3^{max} \frac{C_{NO_3^-}}{K_{NO_3^-} + C_{NO_3^-}} \cdot \frac{C_{acetate}}{K_{acetate} + C_{acetate}} \right) \quad \text{Eq. 14}$$

$$\frac{\mathrm{dFe(II)}}{\mathrm{dt}} = -2\ B\ r_{auto\_bio\_2} - 2\ r_{abio} \quad \text{Eq. 15}$$

$$\frac{\mathrm{dFe(III)}}{\mathrm{dt}} = 2\ B\ r_{auto\_bio\_2} + 2\ r_{abio} \quad \text{Eq. 16}$$

$$\frac{\mathrm{d}NO_3^-}{\mathrm{dt}} = -4\ B\ r_{hetero} \quad \text{Eq. 17}$$

$$\frac{\mathrm{d}NO_2^-}{\mathrm{dt}} = 4\ B\ r_{hetero} - B\ r_{auto\_bio\_2} - r_{abio} \quad \text{Eq. 18}$$

$$\frac{\mathrm{d}N_2O}{\mathrm{dt}} = 0.5\ \mathrm{B}\ r_{auto\_bio\_2} + 0.5\ r_{abio} \quad \text{Eq. 19}$$

$$\frac{\mathrm{d}acetate}{\mathrm{dt}} = -\ B\ r_{hetero} \quad \text{Eq. 20}$$

with w being the specific growth rate constant in d^{-1}, B as biomass in cells L^{-1}, $r_{auto\_bio\_1}$, $r_{auto\_bio\_2}$, and $r_{hetero\_bio\_1}$ in mmol cells^{-1} d^{-1} and r_{abio} in mmol L^{-1} d^{-1}.

Relative contributions (%) of biotic and abiotic Fe(II) oxidation (Eq. 21, 22) and N_2O production (Eq. 23, 24) under autotrophic conditions were calculated according to previous studies.[23] For mixotrophic conditions, the biotic reaction to N_2O under autotrophic conditions (as reflected in $r_{auto\_bio\_1}$) was neglected (Eq. 21-24).

$$\text{Biotic Fe(II) } oxidation = \frac{2\text{B } r_{auto\_bio\_1} + 2\text{B } r_{auto\_bio\_2}}{2\text{B } r_{auto\_bio\_1} + 2\text{B } r_{auto\_bio\_2} + 2\ r_{abio}} \quad \text{Eq. 21}$$

$$\text{Abiotic Fe(II) } oxidation = \frac{2\ r_{abio}}{2\text{B } r_{auto\_bio\_1} + 2\text{B } r_{auto\_bio\_2} + 2\ r_{abio}} \quad \text{Eq. 22}$$

$$\text{Biotic } N_2O \text{ } production = \frac{0.5\text{B } r_{auto\_bio\_2}}{0.5\text{B } r_{auto\_bio\_2} + 0.5 r_{abio}} \quad \text{Eq. 23}$$

$$\text{Abiotic } N_2O \text{ } production = \frac{0.5\ r_{abio}}{0.5\text{B } r_{auto\_bio\_2} + 0.5 r_{abio}} \quad \text{Eq. 24}$$

The systems of ordinary differential equations were numerically solved with MATLAB (2024b, Prerelease Update 1) using the in-built solver *ode15s*. The parameters in the process-based models (Table 1) were calibrated by fitting the model equations (Eq. 8 to 13 or 14 to 20) to the obtained experimental data. Fitting was performed using MATLAB's *surrogate* optimization function to minimize the deviation (sum of squared errors) between model simulations and experimental data. Lower and upper boundaries were set for all parameters before the calibration procedure. Normalized root-mean-square error (NRMSE) was used as indicator to estimate the goodness-of-fit of the models.

Model assumptions

To model the different biotic and abiotic processes, certain simplifications and assumptions have been made. We considered autotrophic denitrification as a two-step process with first nitrate to nitrite and secondly nitrite to nitrous oxide. Acetate oxidation

coupled to nitrate reduction leads solely to nitrite, which is based on observations under heterotrophic conditions. In the mixotrophic model, we assumed that nitrate reduction to nitrite was driven solely by heterotrophs. This decision was based on reaction stoichiometry from the experimental data and comparable extent of nitrate reduction under heterotrophic and mixotrophic conditions. We experienced unstable modelling results when also considering autotrophic nitrate reduction, further supporting this assumption. The chemodenitrification rate constant was calibrated within a set range of 0 to 0.3 L $mmol^{-1}$ d^{-1}.

For calculating biomass based on 16S rRNA gene copy numbers per mL, the number of 16S copies was estimated based on the microbial community composition, thus we assumed that the initial microbial community remained constant over time.

The initial, bioavailable fraction of Fe(II) on day 0 was calibrated in the model due to difficulties in determining the exact Fe(II) concentrations in bicarbonate systems due to precipitation of Fe(II) on the glass wall.

Nordhoff et al. (2017)[28] suggested that nitrate-reducing, iron(II)-oxidizing microorganisms can prevent cell encrustation due to enzymatic Fe(II) oxidation. In contrast, indirect Fe(II) oxidation, i.e. during chemodenitrification leads to cell encrustation as microorganisms lack prevention mechanisms to avoid encrustation. The mixotrophic strain BoFeN1 excretes EPS to prevent cell encrustation[46] and other studies found out that encrustation is generally lower if less iron(II) is supplied to culture KS.[20,28] Scanning electron microscopy showed no evidence for cell encrustation by iron(III) minerals under autotrophic conditions, thus, we did not include an inhibition term in the process-based

reaction model. Under mixotrophic conditions, SEM imaging revealed that cells showed different degrees of encrustation, even though, an inhibition term in the model did not improve the model fit. Thus, it was appropriate in this case to assume that cells showing encrustation in the SEM either lost their mechanism to prevent encrustation due to death or starvation (SEM imaging after seven days of inoculation) or did not play a relevant role in ongoing processes.

Statistical analysis

To test for significant differences between abundances of genera at different timepoints, a non-parametric Wilcoxon signed-rank test for paired samples using the Benjamini-Hochberg p-adjustment method was applied using R (4.3.3) and its interface RStudio (2023.12.1+402). For differences in 16S rRNA gene copy numbers per mL at day 0 and day 7, a pairwise comparisons using the Wilcoxon signed rank exact test was applied.

Results

Acetate shifts the microbial community composition in culture HP

We exposed the lithoautotrophic NRFeOx culture HP to different growth conditions, i.e. autotrophic (nitrate+Fe(II)), mixotrophic (nitrate+Fe(II)+acetate), and heterotrophic (nitrate+acetate) conditions over three consecutive transfers. We found that total abundances of 16S copies were different between the growth conditions and generally increased from start of the experiment to after 7 days. Microbial 16S rRNA gene copy numbers per mL increased to the smallest extent under mixotrophic conditions (114-fold, $\log_2$FC of 6.8) from $8.7\pm5.4\text{x}10^3$ to $1.0\text{x}10^6\pm1.1\text{x}10^5$ (Table A2). Under autotrophic conditions, microbial 16S rRNA gene copy numbers per mL increased from $2.5\pm1.8\text{x}10^3$ to $4.3\pm5.0\text{x}10^5$, corresponding to a $\log_2$ fold change of 7.5 (175-fold change, Table A2). The increase in microbial 16S rRNA gene copy numbers was greatest under heterotrophic conditions with a $\log_2$ fold change of 8.2 (~290-fold, $2.0\pm2.0\text{x}10^4$ to $5.8\pm4.1\text{x}10^6$, Table A2). By combining results from qPCR with 16S rRNA gene sequencing, we calculated 16S copies per microbial community member (Figure 2a). On day 0, *Gallionella* sp. was only most abundant under autotrophic ($4.0\text{x}\pm4.7\text{x}10^4$) conditions, closely followed by *Dechloromonas* sp. ($2.3\pm2.6\text{x}10^4$). Under mixotrophic and heterotrophic conditions, *Dechloromonas* sp. accounted for the greatest absolute abundance ($1.0\text{x}10^5\pm8.7\text{x}10^4$ and $3.7\pm4.1\text{x}10^5$, respectively) and *Gallionella* sp. was less abundant ($6.8\pm4.1\text{x}10^4$ and $6.0\pm7.9\text{x}10^4$, respectively), yet with higher absolute abundances than under autotrophic conditions. In the course of incubation, all microbial community members were increasing in abundance (Figure 2b), with *Dechloromonas* sp. increasing by a $\log_2$ fold change of ~6.6 (autotrophic, mixotrophic) and 8.7 (heterotrophic) and *Gallionella* sp. by a $\log_2$ fold change of 4.6 to 4.9 similarly under all growth conditions (Figure 2b).

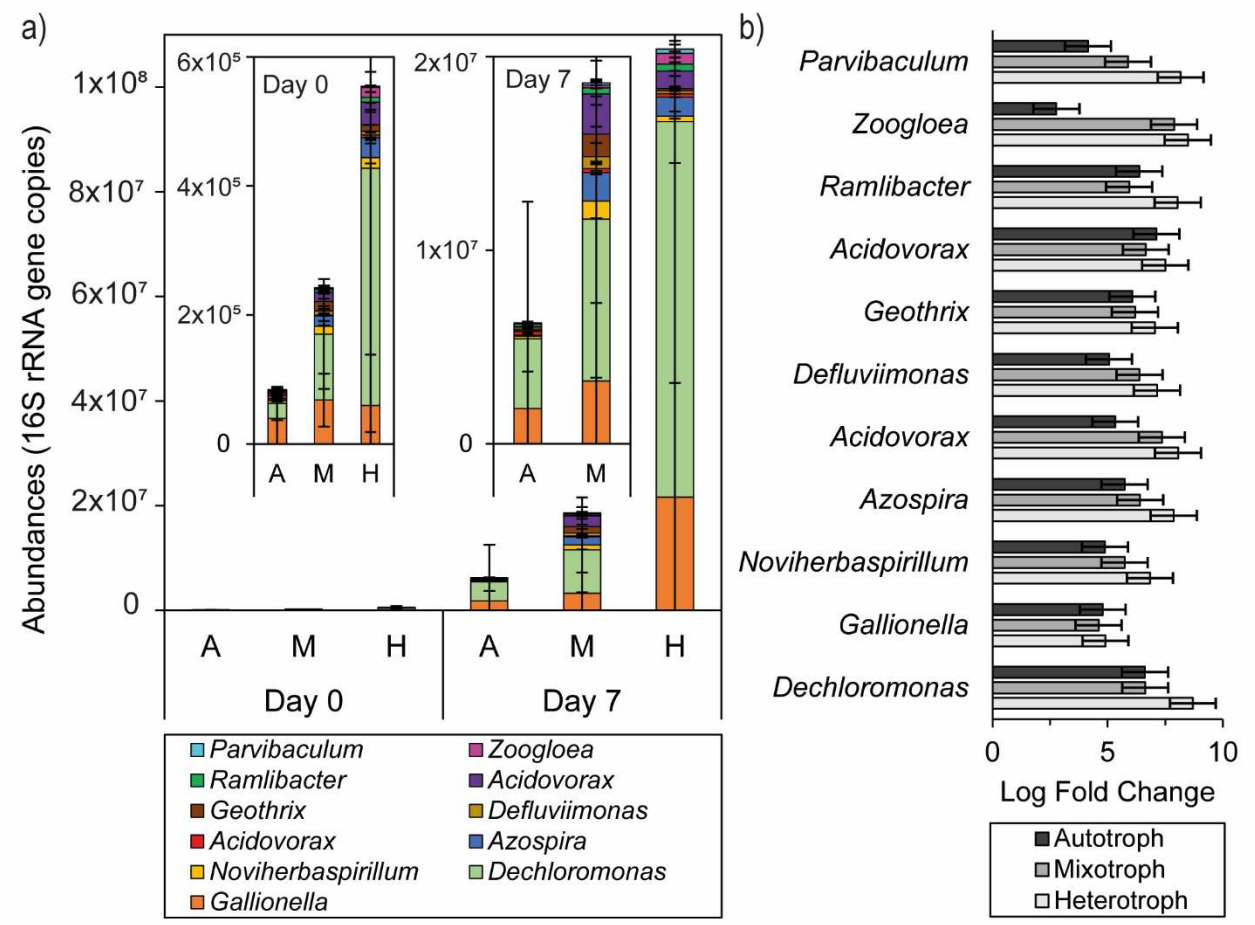

Figure 13. (a) Absolute abundances of different microbial community members in culture HP at day 0 and day 7 under different growth conditions (autotrophic, A; mixotrophic, M; heterotrophic, H). Inner panels zoom in on day 0 or day 7 (for autotrophic and mixotrophic). (b) Log fold changes of absolute abundance from day 0 till day 7 for the different microbial community members of culture HP for the three different growth conditions (autotrophic, mixotrophic, heterotrophic). Bars represent the average of eight (autotrophic) or nine (mixotrophic and heterotrophic) replicates and the error bar is showing the standard deviation (a) or the standard mean error (b).

The flanking community was dominated by *Noviherbaspirillum* sp. and *Acidovorax* sp. in all growth conditions, yet, the flanking community members increased to a different extent.

Acidovorax ASV-1 increased less under autotrophic (log_2FC of 5.3) than mixotrophic (log_2FC of 7.4) or heterotrophic (log_2FC of 8.1) conditions. This trend was similar for most of the flanking community members (Figure 2b). The log_2 fold change was significantly different between growth conditions (Table A3a, non-parametric Kruskal-Wallis test) for *Zoogloea* sp. (p=0.03) and *Parvibaculum* sp. (p=0.01). The log_2 fold change of *Zoogloea* sp. was significantly higher under heterotrophic than under autotrophic conditions (log_2FC of 2.8 and 7.9, respectively, adjusted p=0.04, non-parametric Wilcoxon sign-rank sum test, Table A3b). The log_2 fold change of *Parvibaculum* sp. was also significantly higher in heterotrophic conditions (log_2FC 8.2) compared to mixotrophic (log_2FC 5.9, adjusted p=0.04, non-parametric Wilcoxon sign-rank sum test, Table A3b) or autotrophic conditions (log_2FC 4.1, adjusted p=0.02, non-parametric Wilcoxon sign-rank sum test, Table A3b).

The lack of carbon: Geochemical performance of culture HP under lithoautotrophic conditions

Under lithoautotrophic growth conditions (1 mM nitrate, 2 mM Fe(II), 10% v:v bacterial inoculum), 0.4±0.1 mM nitrate was reduced within 4 days and at the same time, 1.0±0.2 mM iron(II) were oxidized (Figure 3a). The kinetic model estimated rate constants of 0.7 and 8.5 mM for nitrate and iron(II), respectively (Table 1). Considering iron(II) that precipitated at the glass wall at the end of the experiment as described in Grimm et al. (2024)[16], we calculated that the ratio of $nitrate_{reduced}$ to $iron(II)_{oxidized}$ was 0.25±0.07 on average. Nitrite reached a maximum of 0.1±0.1 mM on day 1 and was completely reduced on day 4 (Figure 3a), with estimated rate constants of 0.03 mM and 0.05 L $mmol^{-1}$ d^{-1} for enzymatic nitrite reduction and chemodenitrification, respectively (Table 1). Ultimately, N_2O was produced (0.2±0.1 mM, Figure 3a) and accounted for 100% of the total reduced NO_3^--N in all transfers. Ammonium concentrations in the autotrophic biotic treatment were

stable over time (range of 5.0 to 5.1 mM, Figure A1). In the abiotic control, ammonium, nitrate, iron(II), and acetate were also constant over time and nitrite and nitrous oxide were not detected (Figure A2b).

By scanning electron microscopy, we visualized cell-mineral interactions at the end of transfer 3 (Figure A3a) and found two distinct mineral structures under autotrophic conditions. The first was characterized by nanometer-scale and the other by nanometer- to micrometer-scale botryoidal-like particles (Figure A3a). Rod-shaped cells (~1-2 µm) were in close association with both types of mineral particles and were always found to be free of encrustation with Fe(III) minerals.

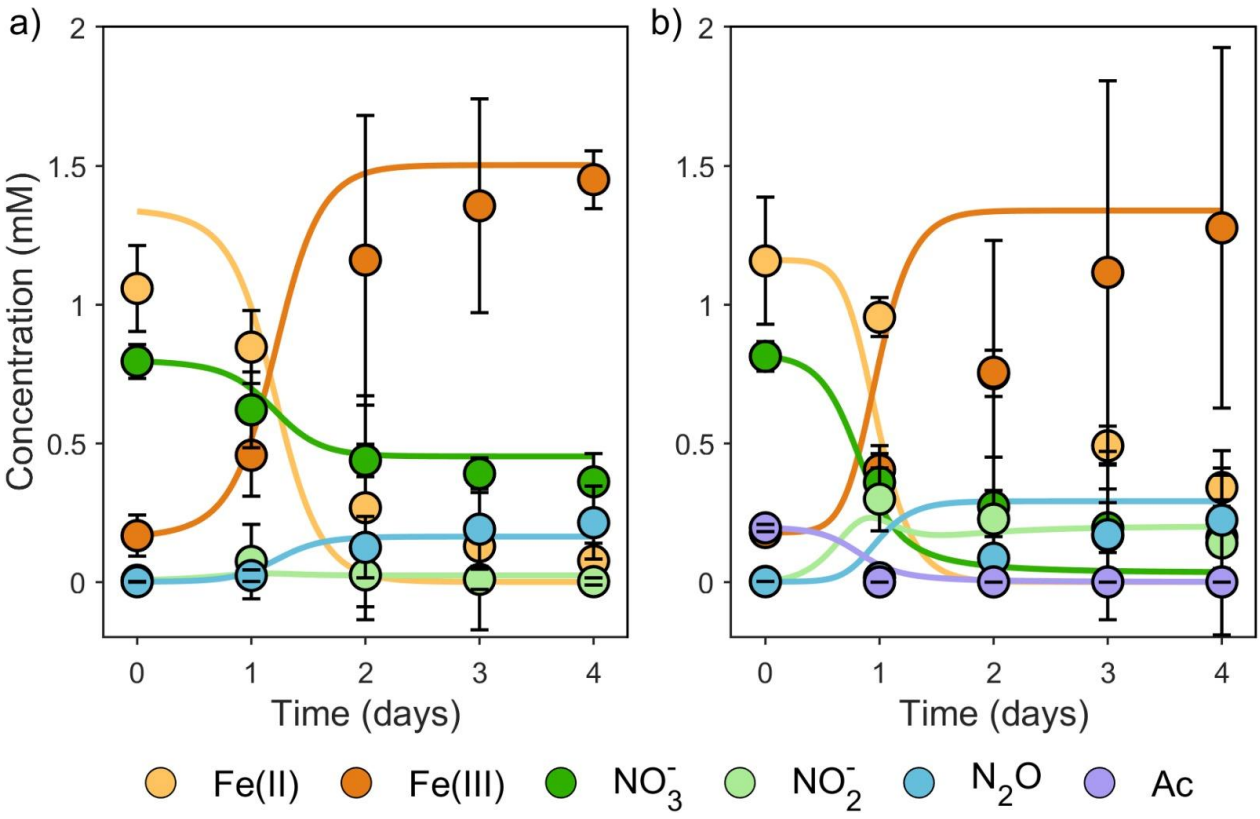

Figure 14. Geochemical results of the nitrate-reducing, iron(II)-oxidizing culture HP under (a) autotrophic and (b) mixotrophic growth conditions. Symbols represent measured data

points and solid lines represent modelling results. Average and standard deviation of three consecutive transfers is shown of eight (autotrophic) or nine (mixotrophic) replicates. Ac: acetate.

Feeding carbon: Geochemical performance of culture HP under mixotrophic and heterotrophic conditions

Under mixotrophic conditions, we supplied acetate to culture HP (1 mM nitrate, 2 mM iron(II), 0.2 mM acetate) and observed that 0.2±0.0 mM of acetate was quickly oxidized within one day (estimated rate constant of 0.27 mM, Table 1, Figure 3b). The extent of nitrate reduction (0.7±0.1 mM) was greater than under autotrophic conditions, but less Fe(II) was oxidized (0.8±0.8 mM) over time (Figure 3b). Fitting the kinetic model to the experimental data resulted in estimated rate constants for nitrate reduction (0.5 mM) and iron(II) oxidation (1.0 mM) being lower than under autotrophic conditions (Table 1). For iron(II) oxidation, we observed high variations between replicates and transfers. The ratio of $nitrate_{reduced}$ to $Fe(II)_{oxidized}$ was at 0.46±0.28, however, iron(II) was not the sole electron donor for nitrate reduction under mixotrophic conditions. Under mixotrophic conditions, nitrite concentrations also reached its maximum on day 1 (0.3±0.1 mM, Figure 3b), accounting for 64% of the reduced NO_3^--N. Afterwards, nitrite gradually decreased, however, 0.1 mM nitrite still remained after 4 days. The production of N_2O constantly increased over time, reaching around 0.2±0.2 mM of total N_2O after 4 days (Figure 3b). However, N_2O made up a smaller part of the total reduced NO_3^--N under mixotrophic (69±31% of reduced NO_3^--N) compared to autotrophic conditions. Scanning electron microscopy showed the same mineral particles as under autotrophic conditions, however, rod-shaped cells (~1-2 µm) seemed more bulbous (Figure A3b). Cells were also tightly

associated with mineral particles, yet, showed various degrees of encrustation by mineral particles (Figure A3b).

Table 1. Calibrated model parameters under autotrophic and mixotrophic conditions for culture HP.

Model parameter	**Autotrophic**	**Mixotrophic**
Monod half-saturation constant $K_{Fe(II)}$ (mM)	8.54	1.00
Monod half-saturation constant $K_{NO_3^-}$ (mM)	0.71	0.48
Monod half-saturation constant $K_{NO_2^-}$ (mM)	0.03	0.76
Monod half-saturation constant $K_{acetate}$ (mM)	-	0.27
Chemodenitrification rate k_{abio} (L mmol^{-1} d^{-1})	0.05	0.07
Yield coefficient $Y_{Fe(II)}$ (cells mmol^{-1} oxidized Fe(II)$^{-1}$)	5.33x10^8	9.95x10^8
Yield coefficient $Y_{acetate}$ (cells mmol^{-1} oxidized acetate^{-1})	-	1.50x10^9
Specific growth rate w_1 (d^{-1})	22.68	-
Specific growth rate w_2 (d^{-1})	51.98	1.59
Specific growth rate w_3 (d^{-1})	-	20.55
Maximum specific rate constant $r^{max}_{auto\_bio\_1}$ (d^{-1})	99.97	-
Maximum specific rate constant $r^{max}_{auto\_bio\_2}$ (d^{-1})	100.00	51.85
Maximum specific rate constant $r^{max}_{hetero\_bio\_1}$ (d^{-1})	-	20.00
Normalized root mean square error (%)	32.83	53.31

Under heterotrophic conditions, acetate was also completely consumed within one day (0.2±0.0 mM) and the extent of nitrate reduction (0.6±0.3 mM) was similar to mixotrophic conditions (Figure A2a). Nitrite concentrations were increasing and also reaching its peak on day 1 (0.5±0.2 mM, Figure A2a), accounting for around 90% of the reduced NO_3^--N. In contrast to autotrophic and mixotrophic conditions, nitrite stayed similarly high till the end of incubation under heterotrophic conditions (Figure A2a). However, variations between biological replicates were high. No considerable N_2O production was observed under heterotrophic conditions in contrast to mixotrophic or autotrophic conditions (Figure A2a).

Determining abiotic and biotic processes under different growth conditions

A kinetic model was applied to quantify the contributions of biotic (enzymatic) and abiotic (chemodenitrification) processes on iron(II) oxidation and N_2O production over time. The rates $r_{auto\_bio\_1}$, $r_{auto\_bio\_2}$, and r_{abio}were assumed to contribute to iron(II) oxidation under autotrophic conditions and rates $r_{auto\_bio\_2}$ and r_{abio} were taken into account for iron(II) oxidation under mixotrophic conditions and N_2O production in general. Under autotrophic conditions, nitrate reduction till nitrite was more dominant (76.1%) with nitrite reduction till N_2O becoming dominant after roughly 1 day with 51.2% (Figure 4a). The relative share between these two processes remained stable afterwards. We further found that the relative contribution of chemodenitrification to iron(II) oxidation was higher under mixotrophic than autotrophic conditions (maximum of 44.0 and 2.2% on day 0, respectively, Figure 4a,b), yet, in both cases, the abiotic contribution to the overall iron(II) oxidation decreased continuously afterwards. The cumulative iron(II) oxidation revealed minor differences between growth conditions with enzymatic processes accounting for 99.8 and 98.6% under autotrophic and mixotrophic conditions, respectively. We further found that abiotic processes were more important for N_2O production compared to iron(II) oxidation under autotrophic conditions with a maximum contribution of 9.3% (day 0). Under mixotrophic conditions, the relative contribution for N_2O production was similar to iron(II) oxidation due to the same underlying rates. Here, a maximum of 44.0% was attributed to abiotic processes (day 0). Considering cumulative N_2O production, biotic processes accounted for almost all of the N_2O with minor differences between autotrophic (99.5%) and mixotrophic (98.6%) conditions.

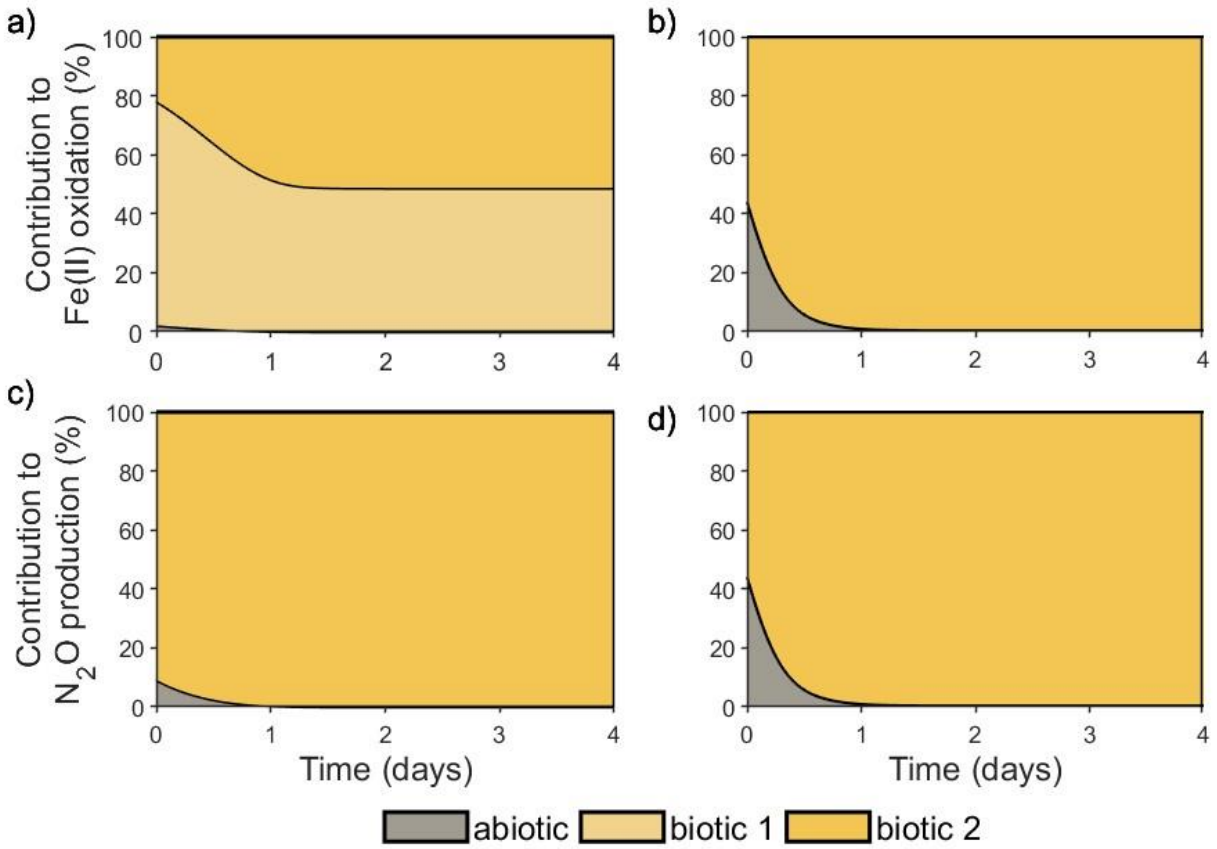

Figure 15. Relative contribution of abiotic and biotic processes to Fe(II) oxidation (a, b) and N_2O production (c, d) under autotrophic (left) and mixotrophic (right) growth conditions in the nitrate-reducing, iron(II)-oxidizing culture HP. Abiotic: chemodenitrification; biotic 1: enzymatic nitrate reduction till nitrite; biotic 2: enzymatic nitrite reduction till nitrous oxide.

Discussion

Identifying key microbial players under different growth conditions

By cultivating culture HP under varying growth conditions and simulating the input of organic carbon relevant to environmental settings, we observed that specific microbial community members increased in dominance with the addition of organic carbon (here: acetate). *Dechloromonas* sp. increased most in abundance under heterotrophic conditions, but also over time in the mixotrophic and autotrophic setup. *Dechloromonas* sp. has been studied intensively as a perchlorate reducer, but was also proposed as a nitrate reducer capable of iron(II) oxidation, yet, only in the presence of acetate and not capable of autotrophic growth.[8,12] This highlights its potential role in mixotrophic NRFeOx in culture HP. Because of its high abundance also under autotrophic conditions, we propose that *Dechloromonas* sp. is likely internally fed by organic carbon produced by autotrophic members (e.g., *Gallionella* sp.). *Acidovorax* sp. also increased over time, with some species performing mixotrophic NRFeOx, such as BoFeN1,[9] *A. delafieldii* strain 2AN,[11] or *A. ebreus* strain TPSY.[47] However, two *Acidovorax* ASV´s were identified to be important in culture HP, thus, meta´omics are needed in future to identify their individual metabolic potential. Another microbial community member that was increasing in abundance when acetate was supplied was *Zoogloea* sp., which was found in paddy soils to become also enriched after nitrate and lactate addition.[48] Further, *Parvibaculum* sp. has increased in abundance under heterotrophic conditions, even to a greater extent than under mixotrophic conditions. In literature, *Parvibaculum* sp. has been described as a heterotrophic nitrate reducer, without evidence to be involved in iron(II) oxidation.[49] Interestingly, the proposed autotrophic NRFeOx member of culture HP, *Gallionella* sp., increased to a similar extent under autotrophic, mixotrophic, and heterotrophic conditions,

which is in accordance to previous observations in culture KS.[28] However, relative abundances of *Gallionella* sp. were highest under autotrophic conditions (48% in the beginning and 31% after 7 days). In general, acetate shifted the microbial community towards mixotrophic or heterotrophic denitrifiers, yet, it was not dominated by only one genus or species. In comparison, culture KS or BP were dominated by *Bradyrhizobium* spp. (up to 83%)[29] or *Rhodoferax* sp. (84 to 94%),[15] when cultivated under heterotrophic conditions, whereas *Dechloromonas* sp. accounted for 78% on average on day 7 in culture HP when cultivated with nitrate and acetate only. Tominski et al (2018)[29] observed a lag phase of 6 days until acetate oxidation, whereas culture HP oxidized all the supplied acetate already within one day. In summary, we conclude that the diversity of the microbial community was preserved, pointing towards a relatively stable community composition even under different substrate availability. It ought to be investigated if culture HP is able to grow back on autotrophic conditions after being exposed to acetate or other organic carbon sources.

Extent of nitrate reduction, iron(II) oxidation, and intermediates during denitrification depends on growth conditions

Acetate addition influenced the metabolic activity of culture HP. The extent of nitrate reduction was greater under mixotrophic and heterotrophic conditions compared to autotrophic conditions, as acetate served as an additional electron donor for nitrate reduction. Based on reaction stoichiometry, 0.4 and 1.2 mM nitrate could be reduced with either only 2 mM Fe(II) or in addition with 0.2 mM acetate, yet, we observed less nitrate reduction than theoretically possible under mixotrophic conditions, which led us to the assumption that the first step of denitrification (nitrate till nitrite) was solely controlled by acetate and not by iron(II). A lower rate constant, yet a higher extent of nitrate reduction

as observed under mixotrophic conditions indicates the presence of a more efficient electron donor (here: acetate instead of Fe(II)) that enhances the overall reduction of nitrate despite slower kinetics.[50]

The addition of acetate led to relatively less N_2O production, even though absolute production was similar. In other lithoautotrophic NRFeOx cultures, N_2O production has not been monitored after changing growth conditions, thus it remains open if the addition of organic carbon influences intermediates or products during denitrification in other NRFeOx cultures. Nitrite was found to accumulate under mixotrophic and heterotrophic conditions suggesting that if electron donors (such as acetate) are limited, microbial nitrite reduction could be hindered, thereby increasing the role of chemodenitrification. Nitrite concentrations were also found to be higher and to accumulate under heterotrophic conditions when supplying acetate to culture BP, [15] but no nitrite was detected in culture KS after acetate addition.[29] Growing culture HP without iron(II) (heterotrophic conditions), N_2O was not detected and nitrate reduction almost completely stopped at nitrite as indicated by the N mass balance. Translating this to environmental conditions, heterotrophic microorganisms would provide large amounts of nitrite that could potentially react with Fe(II) abiotically. However, in a follow up experiment, we observed that nitrite was further reduced under heterotrophic conditions after acetate was supplied a second time (data not shown), indicating that the amount of electron donor/electron acceptor seems to be governing the intermediates during denitrification. It ought to be investigated if culture HP can also use other short-chain fatty acids or rice root exudates from rice plants that often contain bioavailable C substances in addition to N-rich compounds, such as amino acids.[51]

Our results have broader implications for wastewater treatment, especially when managing low-C/N ratio wastewater where heterotrophic denitrifiers are commonly used but require substantial organic carbon. Although mixotrophic microorganisms have been employed in such systems to achieve comparable performance, their long-term efficacy is hindered by encrustation with iron(III) minerals.[52–54] In contrast, autotrophic microorganisms capable of nitrate reduction coupled with iron(II) oxidation could offer a more sustainable alternative, as they do not depend on organic carbon and possess enzymatic mechanisms that prevent mineral encrustation. This study suggests that adding organic carbon to the autotrophic NRFeOx culture HP does not significantly alter its microbial community composition or promote dominance by any single species, as in previous findings for other NRFeOx cultures.[15,29] This stability highlights culture HP as a promising candidate for the autotrophic remediation of nitrate-rich water sources, including industrial wastewater and groundwater.

The role of abiotic and biotic processes under autotrophic and mixotrophic growth conditions

The recent observation that lithoautotrophic NRFeOx enrichment cultures, such as HP, KS, and AG, lead to significant amounts of N_2O during nitrate reduction raises the question on the contribution of abiotic and biotic processes. For a long time, biotic nitrate reduction was primarily considered to produce N_2 as its end product, however, up to 100% can end up as N_2O in such cultures.[16] N_2O production in the environment is often thought to be of abiotic nature, thus, disentangling these processes in microbial enrichment cultures is crucial to understand the underlying processes. Besides isotope fractionation experiments,[55] numerical reaction modelling can provide insights into the contribution of abiotic and biotic processes. Jamieson et al. (2018)[24] and Liu et al. (2019)[23] applied

numerical modelling for mixotrophic NRFeOx strains (e.g., BoFeN1, strain 2002) and found that abiotic Fe(II) oxidation played a more important role than biotic Fe(II) oxidation. However, the contribution of abiotic and biotic processes is different between microbial strains. Our results demonstrate that the autotrophic NRFeOx culture HP predominantly performs enzymatic Fe(II) oxidation. Even when the initially autotrophic culture is cultivated under mixotrophic conditions with added acetate, enzymatic Fe(II) oxidation remains the primary pathway for Fe(III) mineral formation.

Chemodenitrification rates are crucial for calculating the contribution of abiotic and biotic processes in NRFeOx cultures.Abiotic second-order rate constants derived in our study were similar under autotrophic and mixotrophic conditions (0.05 and 0.07 L $mmol^{-1}$ d^{-1}, respectively). In literature, abiotic second-order rate constants are higher (0.23, 0.09 L mol^{-1} d^{-1})[23,26] or lower (0.021 L mol^{-1} d^{-1})[24]. Differences in chemodenitrification rates could be due to differences in EPS secretion, different growth media, substrate concentration or differences in iron(II) phases and should be representative for similar growth conditions.

Under autotrophic conditions, no accumulation of nitrite could be observed nor simulated with the process-based reaction model. Comparing the rates influencing nitrite production ($r_{auto\_bio\_1}$) and consumption ($r_{auto\_bio\_2}$, r_{abio}) reveals that the rates balance each other out, resulting in a net nitrite concentration of zero (Figure A4). In our experiments, nitrite could be detected, yet in only two out of three transfers, which highlights the high variation of nitrite due to its reactivity. Previously, the absence of nitrite in experiments led to the conclusion that abiotic processes play a secondary role, however, our results underline that nitrite is also involved in abiotic processes even without measurable concentrations.

Our results further show that nitrite-driven chemodenitrification can contribute 0.2% to the cumulative Fe(II) oxidation under autotrophic conditions.

Conclusion

By exposing the autotrophic NRFeOx culture HP to acetate we were able to identify by only applying short-read 16S rRNA gene amplicon sequencing analysis microbial community members that are potentially involved in mixotrophic or heterotrophic NRFeOx. By a continuous sampling over three consecutive transfer we were able to conclude that the microbial community adapted quickly to the different growth conditions, but also that the diversity of the microbial community remained stabled over time. Samples for 16S rRNA gene analysis were only taken at the beginning and end of each transfer, however, other studies showed that the relative abundances of individual community members slightly varied over time.[56] To account for this, a continuous sampling for 16S rRNA gene copy numbers and 16S rRNA gene amplicon sequencing over time would be needed in follow up studies.

The analysis of N_2O, a very potent greenhouse gas, allowed us to estimate climate-related impacts from culture HP. By adding acetate, we found that less N_2O-N was produced based on the total reduced NO_3^--N, however, more nitrite was observed as intermediate N-product during nitrate reduction. Therefore, the produced nitrite could further undergo chemodenitrification once exposed to Fe(II) leading to similar N_2O emissions than under autotrophic conditions.

The process-based numerical reaction model allowed us to quantify abiotic Fe(II) oxidation and N_2O emissions in culture HP and provides the basis to also apply the model to other autotrophic NRFeOx cultures, such as KS, BP, or AG.[14,15,32] We found that even in the absence of nitrite, chemodenitrification can contribute up to 2 and 9 % to Fe(II) oxidation and N_2O production, respectively. By adding acetate, we found that even though

the overall (cumulative) contribution of chemodenitrification is similar to autotrophic conditions, chemodenitrification can account for up to 44% of the Fe(II) oxidation or N_2O production. Thus, we conclude that the absence of nitrite is not sufficiently indicative for the absence of chemodenitrification, however, abiotic processes likely play a minor role.

Even though certain simplifications in the process-based reaction model needed to be made, it provides a useful tool for estimating and quantifying different processes in NRFeOx cultures at play. This is especially crucial in mixed cultures, where the interplay of specific microbial community members remains a challenge that needs to be addressed in further research.

Acknowledgements

The authors are thankful to Dr. Shun Li and Prof. Dr. Yong-Guan Zhu for sampling of paddy soil samples. The authors further thank Franziska Schädler for measurements of nitrogen species and for guidance and advice during microbial community analyses and Marie Mollenkopf for HPLC analysis. The authors gratefully acknowledge the Tübingen Structural Microscopy Core Facility (funded by the Excellence Strategy of the German Federal and State Governments) for their support and assistance in this work. NGS sequencing methods were performed at the Institute for Medical Microbiology and Hygiene (MGM) of the University of Tübingen with the support of the DFG-funded NGS Competence Center Tübingen (INST 37/1049-1). We are grateful for financial support from the Deutsche Forschungsgemeinschaft (DFG, German Research Foundation, project ID 431072007) and for infrastructural support by the DFG under Germany's Excellence Strategy, cluster of Excellence EXC2124 (project ID 390838134). Figure 1 was created using BioRender.com.

Data availability statement

Raw sequencing data has been deposited at NCBI in the Sequence Read Archive (SRA) under BioProject accession number PRJNA1189464 (https://www.ncbi.nlm.nih.gov/bioproject/PRJNA1189464).

[FOR REVIEW ONLY: data is currently held private, meanwhile an overview of the deposited data in the repository can be accessed with https://dataview.ncbi.nlm.nih.gov/object/PRJNA1189464?reviewer=5kk43sjmbiem9h2n18ujqnguej]. Underlying experimental data will be made available prior to publication on Zenodo.

Author contributions

A.K. and C.Z. formulated the original hypothesis. H.G. and A.K. designed the experimental project. H.G., P.G. and C.Z. developed the numerical model with the help of M.B.. D.S. processed the amplicon sequencing data and helped with interpretation of the microbial community results. S.F. performed SEM sample preparation and analysis. H.G. performed the main experiment, conducted analyses in the laboratory, data evaluation and wrote the original draft of the manuscript. All authors were responsible for data interpretation. All authors discussed the data, reviewed and edited the manuscript and have read and agreed to the published version of the manuscript.

Declaration of competing interests

The authors declare that they have no known competing financial interests or personal relationships that could have appeared to influence the work reported in this paper.

References

(1) Melton, E. D.; Swanner, E. D.; Behrens, S.; Schmidt, C.; Kappler, A. The Interplay of Microbially Mediated and Abiotic Reactions in the Biogeochemical Fe Cycle. *Nat. Rev. Microbiol.* **2014**, *12* (12), 797–808. https://doi.org/10.1038/nrmicro3347.

(2) Kappler, A.; Bryce, C.; Mansor, M.; Lueder, U.; Byrne, J. M.; Swanner, E. D. An Evolving View on Biogeochemical Cycling of Iron. *Nat. Rev. Microbiol.* **2021**, *19* (6), 360–374. https://doi.org/10.1038/s41579-020-00502-7.

(3) Xiu, W.; Guo, H.; Shen, J.; Liu, S.; Ding, S.; Hou, W.; Ma, J.; Dong, H. Stimulation of Fe(II) Oxidation, Biogenic Lepidocrocite Formation, and Arsenic Immobilization by Pseudogulbenkiania Sp. Strain 2002. *Environ. Sci. Technol.* **2016**, *50* (12), 6449–6458. https://doi.org/10.1021/acs.est.6b00562.

(4) Hohmann, C.; Winkler, E.; Morin, G.; Kappler, A. Anaerobic Fe(II)-Oxidizing Bacteria Show as Resistance and Immobilize as during Fe(III) Mineral Precipitation. *Environ. Sci. Technol.* **2010**, *44* (1), 94–101. https://doi.org/10.1021/es900708s.

(5) Sun, J.; Chillrud, S. N.; Mailloux, B. J.; Stute, M.; Singh, R.; Dong, H.; Lepre, C. J.; Bostick, B. C. Enhanced and Stabilized Arsenic Retention in Microcosms through the Microbial Oxidation of Ferrous Iron by Nitrate. *Chemosphere* **2016**, *144*, 1106–1115. https://doi.org/10.1016/j.chemosphere.2015.09.045.

(6) Jakus, N.; Blackwell, N.; Osenbrück, K.; Straub, D.; Byrne, J. M.; Wang, Z.; Glöckler, D.; Elsner, M.; Lueders, T.; Grathwohl, P.; Kleindienst, S.; Kappler, A. Nitrate Removal by a Novel Lithoautotrophic Nitrate-Reducing, Iron(II)-Oxidizing Culture Enriched from a Pyrite-Rich Limestone Aquifer. *Appl. Environ. Microbiol.* **2021**, *87* (16), e0046021. https://doi.org/10.1128/AEM.00460-21.

(7) Rivett, M. O.; Buss, S. R.; Morgan, P.; Smith, J. W. N.; Bemment, C. D. Nitrate Attenuation in Groundwater: A Review of Biogeochemical Controlling Processes. *Water Res.* **2008**, *42* (16), 4215–4232. https://doi.org/10.1016/j.watres.2008.07.020.

(8) Bryce, C.; Blackwell, N.; Schmidt, C.; Otte, J.; Huang, Y.-M.; Kleindienst, S.; Tomaszewski, E.; Schad, M.; Warter, V.; Peng, C.; Byrne, J. M.; Kappler, A. Microbial Anaerobic Fe(II) Oxidation – Ecology, Mechanisms and Environmental Implications. *Environ. Microbiol.* **2018**, *20* (10), 3462–3483. https://doi.org/10.1111/1462-2920.14328.

(9) Kappler, A.; Schink, B.; Newman, D. K. Fe(III) Mineral Formation and Cell Encrustation by the Nitrate-Dependent Fe(II)-Oxidizer Strain BoFeN1. *Geobiology* **2005**, *3* (4), 235–245. https://doi.org/10.1111/j.1472-4669.2006.00056.x.

(10) Byrne-Bailey, K. G.; Weber, K. A.; Chair, A. H.; Bose, S.; Knox, T.; Spanbauer, T. L.; Chertkov, O.; Coates, J. D. Completed Genome Sequence of the Anaerobic Iron-Oxidizing Bacterium *Acidovorax Ebreus* Strain TPSY. *J. Bacteriol.* **2010**, *192* (5), 1475–1476. https://doi.org/10.1128/JB.01449-09.

(11) Chakraborty, A.; Roden, E. E.; Schieber, J.; Picardal, F. Enhanced Growth of Acidovorax Sp. Strain 2AN during Nitrate-Dependent Fe(II) Oxidation in Batch and Continuous-Flow Systems. *Appl. Environ. Microbiol.* **2011**, *77* (24), 8548–8556. https://doi.org/10.1128/AEM.06214-11.

(12) Chakraborty, A.; Picardal, F. Neutrophilic, Nitrate-Dependent, Fe(II) Oxidation by a Dechloromonas Species. *World J. Microbiol. Biotechnol.* **2013**, *29* (4), 617–623. https://doi.org/10.1007/s11274-012-1217-9.

(13) Coby, A. J.; Picardal, F.; Shelobolina, E.; Xu, H.; Roden, E. E. Repeated Anaerobic Microbial Redox Cycling of Iron. *Appl. Environ. Microbiol.* **2011**, *77* (17), 6036–6042. https://doi.org/10.1128/AEM.00276-11.

(14) Straub, K. L.; Benz, M.; Schink, B.; Widdel, F. Anaerobic, Nitrate-Dependent Microbial Oxidation of Ferrous Iron. *Appl. Environ. Microbiol.* **1996**, *62* (4), 1458–1460. https://doi.org/10.1128/aem.62.4.1458-1460.1996.

(15) Huang, Y.-M.; Straub, D.; Kappler, A.; Smith, N.; Blackwell, N.; Kleindienst, S. A Novel Enrichment Culture Highlights Core Features of Microbial Networks Contributing to Autotrophic Fe(II) Oxidation Coupled to Nitrate Reduction. *Microb. Physiol.* **2021**, *31* (3), 280–295. https://doi.org/10.1159/000517083.

(16) Grimm, H.; Lorenz, J.; Straub, D.; Joshi, P.; Shuster, J.; Zarfl, C.; Muehe, E. M.; Kappler, A. Nitrous Oxide Is the Main Product during Nitrate Reduction by a Novel Lithoautotrophic Iron(II)-Oxidizing Culture from an Organic-Rich Paddy Soil. *Appl. Environ. Microbiol.* **2024**, e01262-24. https://doi.org/10.1128/aem.01262-24.

(17) Tian, H.; Xu, R.; Canadell, J. G.; Thompson, R. L.; Winiwarter, W.; Suntharalingam, P.; Davidson, E. A.; Ciais, P.; Jackson, R. B.; Janssens-Maenhout, G.; Prather, M. J.; Regnier, P.; Pan, N.; Pan, S.; Peters, G. P.; Shi, H.; Tubiello, F. N.; Zaehle, S.;

Zhou, F.; Arneth, A.; Battaglia, G.; Berthet, S.; Bopp, L.; Bouwman, A. F.; Buitenhuis, E. T.; Chang, J.; Chipperfield, M. P.; Dangal, S. R. S.; Dlugokencky, E.; Elkins, J. W.; Eyre, B. D.; Fu, B.; Hall, B.; Ito, A.; Joos, F.; Krummel, P. B.; Landolfi, A.; Laruelle, G. G.; Lauerwald, R.; LI, W.; Lienert, S.; Maavara, T.; MacLeod, M.; Millet, D. B.; Olin, S.; Patra, P. K.; Prinn, R. G.; Raymond, P. A.; Ruiz, D. J.; van der Werf, G. R.; Vuichard, N.; Wang, J.; Weiss, R. F.; Wells, K. C.; Wilson, C.; Yang, J.; Yao, Y. A Comprehensive Quantification of Global Nitrous Oxide Sources and Sinks. *Nature* **2020**, *586* (7828), 248–256. https://doi.org/10.1038/s41586-020-2780-0.

(18) Intergovernmental Panel on Climate Change (IPCC). The Physical Science Basis. Contribution of Working Group I to the Sixth Assessment Report of the Intergovernmental Panel on Climate Change. *Camb. Univ. Press* **2021**, 923–1054. https://doi.org/10.1017/9781009157896.

(19) Klueglein, N.; Kappler, A. Abiotic Oxidation of Fe(II) by Reactive Nitrogen Species in Cultures of the Nitrate-Reducing Fe(II) Oxidizer Acidovorax Sp. BoFeN1 - Questioning the Existence of Enzymatic Fe(II) Oxidation. *Geobiology* **2013**, *11* (2). https://doi.org/10.1111/gbi.12019.

(20) Huang, J.; Mellage, A.; Garcia, J. P.; Glöckler, D.; Mahler, S.; Elsner, M.; Jakus, N.; Mansor, M.; Jiang, H.; Kappler, A. Metabolic Performance and Fate of Electrons during Nitrate-Reducing Fe(II) Oxidation by the Autotrophic Enrichment Culture KS Grown at Different Initial Fe/N Ratios. *Appl. Environ. Microbiol.* **2023**, *89* (3), e00196-23. https://doi.org/10.1128/aem.00196-23.

(21) Jones, L. C.; Peters, B.; Lezama Pacheco, J. S.; Casciotti, K. L.; Fendorf, S. Stable Isotopes and Iron Oxide Mineral Products as Markers of Chemodenitrification. *Environ. Sci. Technol.* **2015**, *49* (6), 3444–3452. https://doi.org/10.1021/es504862x.

(22) Benaiges-Fernandez, R.; Offeddu, F. G.; Margalef-Marti, R.; Palau, J.; Urmeneta, J.; Carrey, R.; Otero, N.; Cama, J. Geochemical and Isotopic Study of Abiotic Nitrite Reduction Coupled to Biologically Produced Fe(II) Oxidation in Marine Environments. *Chemosphere* **2020**, *260*, 127554. https://doi.org/10.1016/j.chemosphere.2020.127554.

(23) Liu, T.; Chen, D.; Luo, X.; Li, X.; Li, F. Microbially Mediated Nitrate-Reducing Fe(II) Oxidation: Quantification of Chemodenitrification and Biological Reactions. *Geochim. Cosmochim. Acta* **2019**, *256*, 97–115. https://doi.org/10.1016/j.gca.2018.06.040.

(24) Jamieson, J.; Prommer, H.; Kaksonen, A. H.; Sun, J.; Siade, A. J.; Yusov, A.; Bostick, B. Identifying and Quantifying the Intermediate Processes during Nitrate-Dependent Iron(II) Oxidation. *Environ. Sci. Technol.* **2018**, *52* (10), 5771–5781. https://doi.org/10.1021/acs.est.8b01122.

(25) Dopffel, N.; Jamieson, J.; Bryce, C.; Joshi, P.; Mansor, M.; Siade, A.; Prommer, H.; Kappler, A. Temperature Dependence of Nitrate-Reducing Fe(II) Oxidation by Acidovorax Strain BoFeN1 - Evaluating the Role of Enzymatic vs. Abiotic Fe(II) Oxidation by Nitrite. *FEMS Microbiol. Ecol.* **2022**, *97* (12). https://doi.org/10.1093/femsec/fiab155.

(26) Kopf, S. H.; Henny, C.; Newman, D. K. Ligand-Enhanced Abiotic Iron Oxidation and the Effects of Chemical versus Biological Iron Cycling in Anoxic Environments. *Environ. Sci. Technol.* **2013**, *47* (6), 2602–2611. https://doi.org/10.1021/es3049459.

(27) Chen, D.; Cheng, K.; Liu, T.; Chen, G.; Kappler, A.; Li, X.; Zeng, R. J.; Yang, Y.; Yue, F.; Hu, S.; Cao, F.; Li, F. Novel Insight into Microbially Mediated Nitrate-Reducing Fe(II) Oxidation by Acidovorax Sp. Strain BoFeN1 Using Dual N–O Isotope Fractionation. *Environ. Sci. Technol.* **2023**, *57* (33), 12546–12555. https://doi.org/10.1021/acs.est.3c02329.

(28) Nordhoff, M.; Tominski, C.; Halama, M.; Byrne, J. M.; Obst, M.; Kleindienst, S.; Behrens, S.; Kappler, A. Insights into Nitrate-Reducing Fe(II) Oxidation Mechanisms through Analysis of Cell-Mineral Associations, Cell Encrustation, and Mineralogy in the Chemolithoautotrophic Enrichment Culture KS. *Appl. Environ. Microbiol.* **2017**, *83* (13), e00752-17. https://doi.org/10.1128/AEM.00752-17.

(29) Tominski, C.; Heyer, H.; Lösekann-Behrens, T.; Behrens, S.; Kappler, A. Growth and Population Dynamics of the Anaerobic Fe(II)-Oxidizing and Nitrate-Reducing Enrichment Culture KS. *Appl. Environ. Microbiol.* **2018**, *84* (9), e02173-17. https://doi.org/10.1128/AEM.02173-17.

(30) Huang, Y.-M.; Straub, D.; Blackwell, N.; Kappler, A.; Kleindienst, S. Meta-Omics Reveal Gallionellaceae and Rhodanobacter Species as Interdependent Key Players

for Fe(II) Oxidation and Nitrate Reduction in the Autotrophic Enrichment Culture KS. *Appl. Environ. Microbiol.* **2021**, *87* (15), e0049621. https://doi.org/10.1128/AEM.00496-21.

(31) Bayer, T.; Tomaszewski, E. J.; Bryce, C.; Kappler, A.; Byrne, J. M. Continuous Cultivation of the Lithoautotrophic Nitrate-Reducing Fe(II)-Oxidizing Culture KS in a Chemostat Bioreactor. *Environ. Microbiol. Rep.* **2023**, *15* (4), 324–334. https://doi.org/10.1111/1758-2229.13149.

(32) Jakus, N.; Blackwell, N.; Osenbrück, K.; Straub, D.; Byrne, J. M.; Wang, Z.; Glöckler, D.; Elsner, M.; Lueders, T.; Grathwohl, P.; Kleindienst, S.; Kappler, A. Nitrate Removal by a Novel Lithoautotrophic Nitrate-Reducing, Iron(II)-Oxidizing Culture Enriched from a Pyrite-Rich Limestone Aquifer. *Appl. Environ. Microbiol.* **2021**, *87* (16), e0046021. https://doi.org/10.1128/AEM.00460-21.

(33) Melton, E. D.; Rudolph, A.; Behrens, S.; Schmidt, C.; Kappler, A. Influence of Nutrient Concentrations on MPN Quantification and Enrichment of Nitrate-Reducing Fe(II)-Oxidizing and Fe(III)-Reducing Bacteria from Littoral Freshwater Lake Sediments. *Geomicrobiol. J.* **2014**, *31* (9), 788–801. https://doi.org/10.1080/01490451.2014.892765.

(34) Notini, L.; Byrne, J. M.; Tomaszewski, E. J.; Latta, D. E.; Zhou, Z.; Scherer, M. M.; Kappler, A. Mineral Defects Enhance Bioavailability of Goethite toward Microbial Fe(III) Reduction. *Environ. Sci. Technol.* **2019**, *53* (15), 8883–8891. https://doi.org/10.1021/acs.est.9b03208.

(35) Schaedler, F.; Kappler, A.; Schmidt, C. A Revised Iron Extraction Protocol for Environmental Samples Rich in Nitrite and Carbonate. *Geomicrobiol. J.* **2018**, *35* (1), 23–30. https://doi.org/10.1080/01490451.2017.1303554.

(36) Stookey, L. L. Ferrozine---a New Spectrophotometric Reagent for Iron. *Anal. Chem.* **1970**, *42* (7), 779–781. https://doi.org/10.1021/ac60289a016.

(37) Caporaso, J. G.; Lauber, C. L.; Walters, W. A.; Berg-Lyons, D.; Lozupone, C. A.; Turnbaugh, P. J.; Fierer, N.; Knight, R. Global Patterns of 16S rRNA Diversity at a Depth of Millions of Sequences per Sample. *Proc. Natl. Acad. Sci.* **2011**, *108 Suppl 1* (Supplement 1), 4516–4522. https://doi.org/10.1073/pnas.1000080107.

(38) Ewels, P. A.; Peltzer, A.; Fillinger, S.; Patel, H.; Alneberg, J.; Wilm, A.; Garcia, M. U.; Di Tommaso, P.; Nahnsen, S. The Nf-Core Framework for Community-Curated Bioinformatics Pipelines. *Nat. Biotechnol.* **2020**, *38* (3), 276–278. https://doi.org/10.1038/s41587-020-0439-x.

(39) Straub, D.; Blackwell, N.; Langarica-Fuentes, A.; Peltzer, A.; Nahnsen, S.; Kleindienst, S. Interpretations of Environmental Microbial Community Studies Are Biased by the Selected 16S rRNA (Gene) Amplicon Sequencing Pipeline. *Front. Microbiol.* **2020**, *11*, 550420. https://doi.org/10.3389/fmicb.2020.550420.

(40) Di Tommaso, P.; Chatzou, M.; Floden, E. W.; Barja, P. P.; Palumbo, E.; Notredame, C. Nextflow Enables Reproducible Computational Workflows. *Nat. Biotechnol.* **2017**, *35* (4), 316–319. https://doi.org/10.1038/nbt.3820.

(41) Kurtzer, G. M.; Sochat, V.; Bauer, M. W. Singularity: Scientific Containers for Mobility of Compute. *PLOS ONE* **2017**, *12* (5), e0177459. https://doi.org/10.1371/journal.pone.0177459.

(42) Martin, M. Cutadapt Removes Adapter Sequences from High-Throughput Sequencing Reads. *EMBnet J.* **2011**, *17* (1), 10–12.

(43) Callahan, B. J.; McMurdie, P. J.; Rosen, M. J.; Han, A. W.; Johnson, A. J. A.; Holmes, S. P. DADA2: High-Resolution Sample Inference from Illumina Amplicon Data. *Nat. Methods* **2016**, *13* (7), 581–583. https://doi.org/10.1038/nmeth.3869.

(44) Quast, C.; Pruesse, E.; Yilmaz, P.; Gerken, J.; Schweer, T.; Yarza, P.; Peplies, J.; Glöckner, F. O. The SILVA Ribosomal RNA Gene Database Project: Improved Data Processing and Web-Based Tools. *Nucleic Acids Res.* **2012**, *41* (D1), D590–D596.

(45) Bolyen, E.; Rideout, J. R.; Dillon, M. R.; Bokulich, N. A.; Abnet, C. C.; Al-Ghalith, G. A.; Alexander, H.; Alm, E. J.; Arumugam, M.; Asnicar, F.; Bai, Y.; Bisanz, J. E.; Bittinger, K.; Brejnrod, A.; Brislawn, C. J.; Brown, C. T.; Callahan, B. J.; Caraballo-Rodríguez, A. M.; Chase, J.; Cope, E. K.; Da Silva, R.; Diener, C.; Dorrestein, P. C.; Douglas, G. M.; Durall, D. M.; Duvallet, C.; Edwardson, C. F.; Ernst, M.; Estaki, M.; Fouquier, J.; Gauglitz, J. M.; Gibbons, S. M.; Gibson, D. L.; Gonzalez, A.; Gorlick, K.; Guo, J.; Hillmann, B.; Holmes, S.; Holste, H.; Huttenhower, C.; Huttley, G. A.; Janssen, S.; Jarmusch, A. K.; Jiang, L.; Kaehler, B. D.; Kang, K. B.; Keefe, C. R.; Keim, P.; Kelley, S. T.; Knights, D.; Koester, I.; Kosciolek, T.; Kreps, J.; Langille, M.

G. I.; Lee, J.; Ley, R.; Liu, Y.-X.; Loftfield, E.; Lozupone, C.; Maher, M.; Marotz, C.; Martin, B. D.; McDonald, D.; McIver, L. J.; Melnik, A. V.; Metcalf, J. L.; Morgan, S. C.; Morton, J. T.; Naimey, A. T.; Navas-Molina, J. A.; Nothias, L. F.; Orchanian, S. B.; Pearson, T.; Peoples, S. L.; Petras, D.; Preuss, M. L.; Pruesse, E.; Rasmussen, L. B.; Rivers, A.; Robeson, M. S.; Rosenthal, P.; Segata, N.; Shaffer, M.; Shiffer, A.; Sinha, R.; Song, S. J.; Spear, J. R.; Swafford, A. D.; Thompson, L. R.; Torres, P. J.; Trinh, P.; Tripathi, A.; Turnbaugh, P. J.; Ul-Hasan, S.; van der Hooft, J. J. J.; Vargas, F.; Vázquez-Baeza, Y.; Vogtmann, E.; Hippel, M.; Walters, W.; Wan, Y.; Wang, M.; Warren, J.; Weber, K. C.; Williamson, C. H. D.; Willis, A. D.; Xu, Z. Z.; Zaneveld, J. R.; Zhang, Y.; Zhu, Q.; Knight, R.; Caporaso, J. G. Reproducible, Interactive, Scalable and Extensible Microbiome Data Science Using QIIME 2. *Nat. Biotechnol.* **2019**, *37* (8), 852–857. https://doi.org/10.1038/s41587-019-0209-9.

(46) Klueglein, N.; Zeitvogel, F.; Stierhof, Y.-D.; Floetenmeyer, M.; Konhauser, K. O.; Kappler, A.; Obst, M. Potential Role of Nitrite for Abiotic Fe(II) Oxidation and Cell Encrustation during Nitrate Reduction by Denitrifying Bacteria. *Appl. Environ. Microbiol.* **2014**, *80* (3), 1051–1061. https://doi.org/10.1128/AEM.03277-13.

(47) Carlson, H. K.; Clark, I. C.; Blazewicz, S. J.; Iavarone, A. T.; Coates, J. D. Fe(II) Oxidation Is an Innate Capability of Nitrate-Reducing Bacteria That Involves Abiotic and Biotic Reactions. *J. Bacteriol.* **2013**, *195* (14), 3260–3268. https://doi.org/10.1128/JB.00058-13.

(48) Li, X.; Zhang, W.; Liu, T.; Chen, L.; Chen, P.; Li, F. Changes in the Composition and Diversity of Microbial Communities during Anaerobic Nitrate Reduction and Fe(II) Oxidation at Circumneutral pH in Paddy Soil. *Soil Biol. Biochem.* **2016**, *94*, 70–79. https://doi.org/10.1016/j.soilbio.2015.11.013.

(49) Blöthe, M.; Roden, E. E. Composition and Activity of an Autotrophic Fe(II)-Oxidizing, Nitrate-Reducing Enrichment Culture. *Appl. Environ. Microbiol.* **2009**, *75* (21), 6937–6940. https://doi.org/10.1128/AEM.01742-09.

(50) Lee, I.-S.; Bae, J.-H.; Yang, Y.; McCarty, P. L. Simulated and Experimental Evaluation of Factors Affecting the Rate and Extent of Reductive Dehalogenation of Chloroethenes with Glucose. *J. Contam. Hydrol.* **2004**, *74* (1), 313–331. https://doi.org/10.1016/j.jconhyd.2004.03.006.

(51) Naher, U. A.; Radziah, O.; Halimi, M. S.; Shamsuddin, Z. H.; Mohd Razi, I. Influence of Root Exudate Carbon Compounds of Three Rice Genotypes on Rhizosphere and Endophytic Diazotrophs. *Pertanika J. Trop. Agric. Sci.* **2009**, *32* (2), 209–223.

(52) Pan, Y.; Fu, Y.-Y.; Zhou, K.; Tian, T.; Li, Y.-S.; Yu, H.-Q. Microbial Mixotrophic Denitrification Using Iron (II) as an Assisted Electron Donor. *Water Res. X* **2023**, *19*, 100176.

(53) Huang, L.; Xing, X.; Zhou, P.; Li Puma, G. Mixotrophic Bacteria for Environmental Detoxification of Contaminated Waste and Wastewater. *Appl. Microbiol. Biotechnol.* **2021**, *105* (18), 6627–6648. https://doi.org/10.1007/s00253-021-11514-5.

(54) Lu, X.; Wan, Y.; Zhong, Z.; Liu, B.; Zan, F.; Zhang, F.; Wu, X. Integrating Sulfur, Iron (II), and Fixed Organic Carbon for Mixotrophic Denitrification in a Composite Filter Bed Reactor for Decentralized Wastewater Treatment: Performance and Microbial Community. *Sci. Total Environ.* **2021**, *795*, 148825.

(55) Buchwald, C.; Grabb, K.; Hansel, C. M.; Wankel, S. D. Constraining the Role of Iron in Environmental Nitrogen Transformations: Dual Stable Isotope Systematics of Abiotic NO2− Reduction by Fe(II) and Its Production of N2O. *Geochim. Cosmochim. Acta* **2016**, *186*, 1–12. https://doi.org/10.1016/j.gca.2016.04.041.

(56) Jakus, N.; Blackwell, N.; Straub, D.; Kappler, A.; Kleindienst, S. Presence of Fe(II) and Nitrate Shapes Aquifer-Originating Communities Leading to an Autotrophic Enrichment Dominated by an Fe(II)-Oxidizing Gallionellaceae Sp. *FEMS Microbiol. Ecol.* **2021**, *97* (11). https://doi.org/10.1093/femsec/fiab145.

Supporting Information

Appendix of

Acetate addition shifts community composition and extent of chemodenitrification in a lithoautotrophic nitrate-reducing microbial culture

Hanna Grimm[1], Paula Gscheidel[1], Matthias Boeckmann[1], Daniel Straub[2], Stefan Fischer[3], Andreas Kappler[1,4], Christiane Zarfl [1,#]

[1]Department of Geosciences, University of Tübingen, Tübingen, Germany

[2]Quantitative Biology Center (QBiC), University of Tübingen, Germany

[3]Tübingen Structural Microscopy Core Facility, University of Tübingen, Tübingen, Germany

[4]Cluster of Excellence: EXC 2124: Controlling Microbes to Fight Infection, Tübingen, Germany

#Address correspondence to Christiane Zarfl, christiane.zarfl@uni-tuebingen.de

Appendix: Methods

For calculating total cell numbers based on 16S rRNA gene copy numbers obtained by qPCR, we estimated the average 16S copies per microbial community member via the ribosomal RNA database (*rrn*DB, accessed on October 7th, 2024). Whenever information was missing on species or genus level, the average 16S copies of the next higher taxonomic level was searched for. For the category “others”, the average 16S copies of bacteria were used. We estimated the following 16S copies relevant in culture HP under different growth conditions on day 0: *Gallionella* sp., 3; *Dechloromonas* sp., 4; *Noviherbaspirillum* sp., 3; *Azospira* sp., 2; *Ramlibacter* sp., 2; *Acidovorax* sp., 3.6; *Parvibaculum* sp., 1; *Defluviimonas* sp., 3.1; *Geothrix* sp., 2; *Zooglea* sp., 3.1; Others, 5.4.

Appendix: Tables

Table A 1. Information related to qPCR and PCR analysis for 16S rRNA gene copy numbers and amplicon sequencing, respectively.

Target gene	Standard	Primer	Primer sequence (5' → 3')	Primer concentration	Thermal program	References
				nM		
16S rRNA gene for qPCR	*Thiomonas* sp.	515F	GTGCCAGCMGCCGCGGTAA	250	95°C -5'; (95°C - 10"; 60°C - 15") x 40; 95°C - 30"; 60-95°C - 5"	Caporaso et al. (2011)[1]
		806R	GGACTACHVGGGTWTCTAAT	250		
16S rRNA gene for amplicon sequencing	*Thiomonas* sp.	515F	TCGTCGGCAGCGTCAGATGTGTATAAGAGACAGGTGYCAGCMGCCGCGGTA	250	94°C - 3'; (94°C - 30"; 55°C - 30") x35; 72°C - 8"; 4°C	Caporaso et al. (2011)[1]
		806R	GTCTCGTGGGCTCGGAGATGTGTATAAGAGACAGGGACTACNVGGGTWTCTAAT	250		

Table A 2. 16S rRNA gene numbers per mL under different growth conditions on day 0 and day 7. A pairwise comparisons using the Wilcoxon signed rank exact test was applied to identify significant differences between day 0 and day 7.

	Day 0	Day 7	Log2FC	n	W	FDR (adjusted p-value)	Effect size
	16S rRNA gene copy no. mL^{-1}						
Autotroph	$2.47\times10^{3}\pm1.82\times10^{3}$	$4.32\times10^{5}\pm4.95\times10^{5}$	7.45	8	-1.15	0.0078	0.67
Mixotroph	$8.72\times10^{3}\pm5.41\times10^{3}$	$9.96\times10^{5}\pm1.14\times10^{6}$	6.84	9	-1.15	0.0039	0.68
Heterotroph	$1.99\times10^{4}\pm2.00\times10^{4}$	$5.80\times10^{6}\pm4.10\times10^{6}$	8.19	9	-1.15	0.0039	0.68

Table A 3. Results of a) Kruskal-Wallis test and b) Wilcoxon rank-sum test with Benjamini-Hochberg-adjusted p-values (FDR, false discovery rate) to identify differences in log_2 fold change of different treatments in *Zoogloea* sp. or *Parvibaculum* sp.. No significant differences were found for other microbial community members of culture HP.

a) Kruskal-Wallis test.

Comparison	χ^2	df	p-value
Treatment vs. *Zoogloea*	7.28	2	0.0263
Treatment vs. *Parvibaculum*	9.09	2	0.0106

b) Wilcoxon rank-sum test, Benjamini-Hochberg adjusted p-values (FDR).

Parameter	Comparison	log2FC	n	W	FDR (adjusted p-value)	Effect size
Zoogloea	Auto vs. Hetero	2.77 vs. 7.88	8 (Auto), 9 (Hetero)	-2.06	0.039	0.50
Parvibaculum	Auto vs. Hetero	4.15 vs. 8.17	9 (Auto), 9 (Hetero)	-2.39	0.017	0.58
	Mixo vs. Hetero	5.88 vs. 8.17	9	-2.09	0.037	0.49

Appendix: Figures

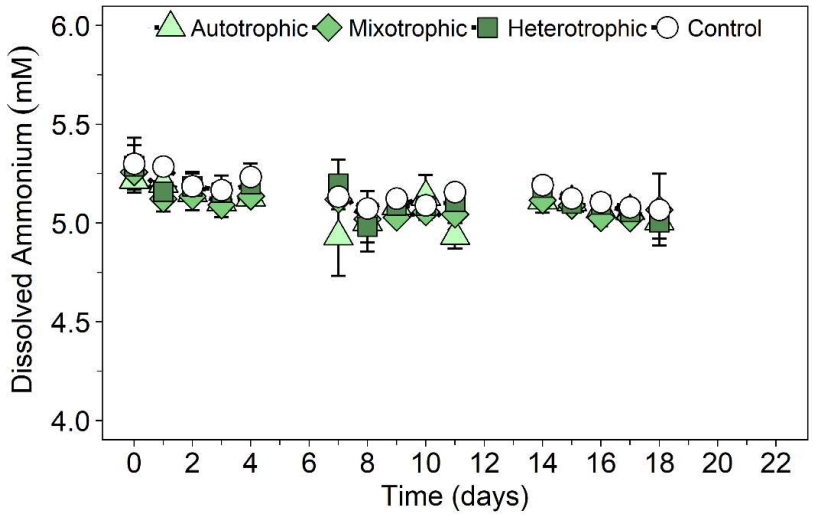

Figure A 1. Ammonium concentrations of culture HP, grown under autotrophic (1 mM nitrate, 2 mM iron(II)), mixotrophic (1 mM nitrate, 2 mM iron(II), 0.2 mM acetate), and heterotrophic (1 mM nitrate, 0.2 mM acetate) conditions, over three consecutive transfers (0 to 4 days). Biotic treatments were inoculated with 10% (v:v) of a microbial pre-culture. The control represents abiotic conditions without a microbial inoculum. Average and standard deviation is shown of three replicates. Note that during transfer 3, the average and range of two replicates is shown under autotrophic conditions.

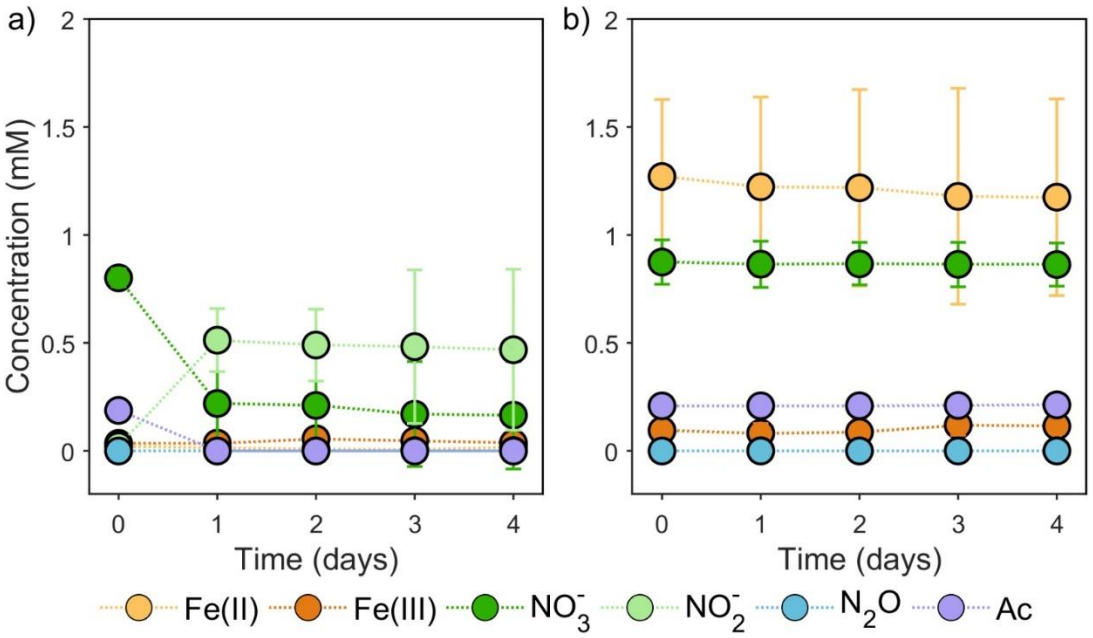

Figure A 2. (a) Heterotrophic and (b) abiotic conditions in the nitrate-reducing, iron(II)-oxidizing culture HP. Ac stands for acetate and the mean±standard deviation is shown for three consecutive transfers of nine replicates. In (b), nitrite and nitrous oxide concentrations are constantly zero and thus, symbols are overlapping.

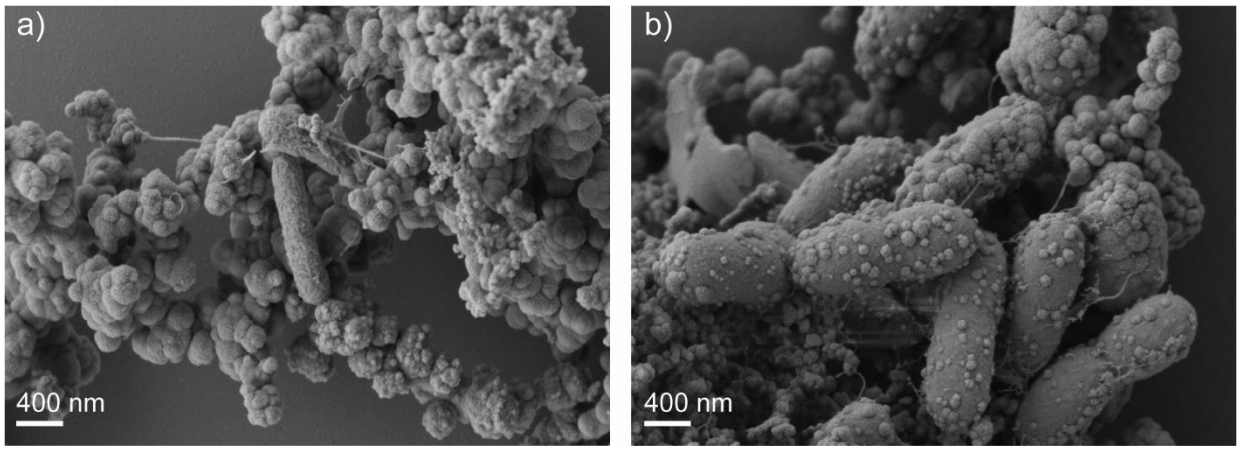

Figure A 3. Scanning electron microscopy of culture HP after 7 days of cultivation under (a) autotrophic and (b) mixotrophic conditions.

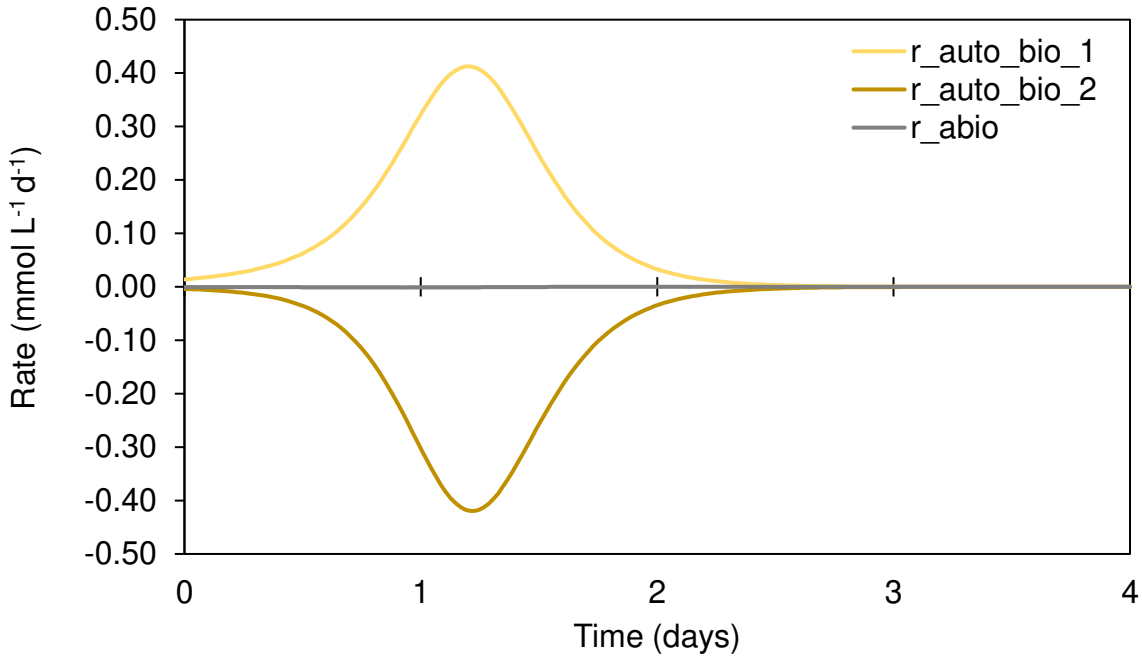

Figure A 4. Rates that are involved in of nitrate reduction and Fe(II) oxidation under autotrophic conditions for culture HP, considering biotic processes – nitrate till nitrite (r_auto_bio_1) and nitrite till nitrous oxide (r_auto_bio_2) – and one abiotic process – chemodenitrification (r_abio).

References

(1) Caporaso, J. G.; Lauber, C. L.; Walters, W. A.; Berg-Lyons, D.; Lozupone, C. A.; Turnbaugh, P. J.; Fierer, N.; Knight, R. Global Patterns of 16S rRNA Diversity at a Depth of Millions of Sequences per Sample. *Proc. Natl. Acad. Sci.* **2011**, *108 Suppl 1* (Supplement 1), 4516–4522. https://doi.org/10.1073/pnas.1000080107.